frontiers | Research Topics

The human lung immuno-inflammatory network: Development, acute and chronic disease, and aging

Edited by
Rabindra Tirouvanziam, Wendy W. J. Unger and Scott James Tebbutt

Published in
Frontiers in Immunology

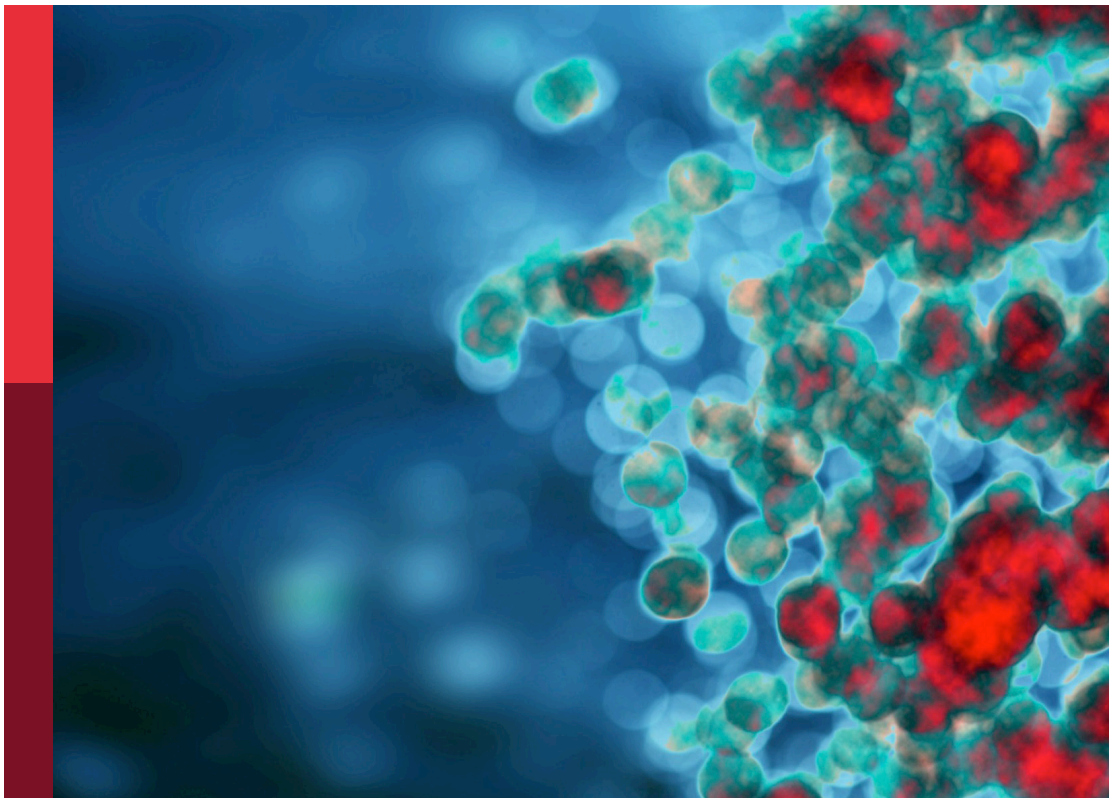

ISSN 1664-8714
ISBN 978-2-8325-2729-0
DOI 10.3389/978-2-8325-2729-0

About Frontiers

Frontiers is more than just an open access publisher of scholarly articles: it is a pioneering approach to the world of academia, radically improving the way scholarly research is managed. The grand vision of Frontiers is a world where all people have an equal opportunity to seek, share and generate knowledge. Frontiers provides immediate and permanent online open access to all its publications, but this alone is not enough to realize our grand goals.

Frontiers journal series

The Frontiers journal series is a multi-tier and interdisciplinary set of open-access, online journals, promising a paradigm shift from the current review, selection and dissemination processes in academic publishing. All Frontiers journals are driven by researchers for researchers; therefore, they constitute a service to the scholarly community. At the same time, the *Frontiers journal series* operates on a revolutionary invention, the tiered publishing system, initially addressing specific communities of scholars, and gradually climbing up to broader public understanding, thus serving the interests of the lay society, too.

Dedication to quality

Each Frontiers article is a landmark of the highest quality, thanks to genuinely collaborative interactions between authors and review editors, who include some of the world's best academicians. Research must be certified by peers before entering a stream of knowledge that may eventually reach the public - and shape society; therefore, Frontiers only applies the most rigorous and unbiased reviews. Frontiers revolutionizes research publishing by freely delivering the most outstanding research, evaluated with no bias from both the academic and social point of view. By applying the most advanced information technologies, Frontiers is catapulting scholarly publishing into a new generation.

What are Frontiers Research Topics?

Frontiers Research Topics are very popular trademarks of the *Frontiers journals series*: they are collections of at least ten articles, all centered on a particular subject. With their unique mix of varied contributions from Original Research to Review Articles, Frontiers Research Topics unify the most influential researchers, the latest key findings and historical advances in a hot research area.

Find out more on how to host your own Frontiers Research Topic or contribute to one as an author by contacting the Frontiers editorial office: frontiersin.org/about/contact

The human lung immuno-inflammatory network: Development, acute and chronic disease, and aging

Topic editors

Rabindra Tirouvanziam — Emory University, United States

Wendy W. J. Unger — Department of General Pediatrics, Sophia Children's Hospital, Erasmus Medical Center, Netherlands

Scott James Tebbutt — University of British Columbia, Canada

Citation

Tirouvanziam, R., Unger, W. W. J., Tebbutt, S. J., eds. (2023). *The human lung immuno-inflammatory network: Development, acute and chronic disease, and aging*. Lausanne: Frontiers Media SA. doi: 10.3389/978-2-8325-2729-0

Table of contents

frontiers in Immunology

ORIGINAL RESEARCH
published: 30 June 2021
doi: 10.3389/fimmu.2021.707355

Dysregulation of the Immune Environment in the Airways During HIV Infection

Rubina Bunjun[1,2], Andreia P. Soares[1,2], Narjis Thawer[1,2], Tracey L. Müller[1,2], Agano Kiravu[1,2], Zekarias Ginbot[1,2], Björn Corleis[3,4], Brandon D. Murugan[1,5], Douglas S. Kwon[3,6], Florian von Groote-Bidlingmaier[7], Catherine Riou[1,2,8], Robert J. Wilkinson[1,8,9,10], Gerhard Walzl[11] and Wendy A. Burgers[1,2]**

[1] Institute of Infectious Disease and Molecular Medicine, University of Cape Town, Cape Town, South Africa, [2] Division of Medical Virology, Department of Pathology, University of Cape Town, Cape Town, South Africa, [3] Ragon Institute of MGH, MIT and Harvard, Cambridge, MA, United States, [4] Institute of Immunology, Friedrich-Loeffler-Institut, Greifswald-Insel Riems, Germany, [5] Division of Chemical and Systems Biology, Department of Integrative Biomedical Sciences, University of Cape Town, Cape Town, South Africa, [6] Division of Infectious Diseases, Massachusetts General Hospital, Boston, MA, United States, [7] Division of Pulmonology, Faculty of Medicine and Health Sciences, Stellenbosch University, Stellenbosch, South Africa, [8] Wellcome Centre for Infectious Diseases Research in Africa, University of Cape Town, Cape Town, South Africa, [9] The Francis Crick Institute, London, United Kingdom, [10] Department of Infectious Disease, Imperial College London, London, United Kingdom, [11] DSI-NRF Centre of Excellence for Biomedical Tuberculosis Research, South African Medical Research Council Centre for Tuberculosis Research, Division of Molecular Biology and Human Genetics, Faculty of Medicine and Health Sciences, Stellenbosch University, Cape Town, South Africa*

OPEN ACCESS

Edited by:
Wendy W. J. Unger, Erasmus MC-Sophia Children's Hospital, Netherlands

Reviewed by:
Megan K. L. MacLeod, University of Glasgow, United Kingdom
Pam Kozlowski, Louisiana State University, United States

***Correspondence:**
Wendy A. Burgers
wendy.burgers@uct.ac.za
Rubina Bunjun
rubina.bunjun@uct.ac.za

Specialty section:
This article was submitted to Mucosal Immunity, a section of the journal Frontiers in Immunology

Received: *09 May 2021*
Accepted: *17 June 2021*
Published: *30 June 2021*

Citation:
Bunjun R, Soares AP, Thawer N, Müller TL, Kiravu A, Ginbot Z, Corleis B, Murugan BD, Kwon DS, von Groote-Bidlingmaier F, Riou C, Wilkinson RJ, Walzl G and Burgers WA (2021) Dysregulation of the Immune Environment in the Airways During HIV Infection. Front. Immunol. 12:707355. doi: 10.3389/fimmu.2021.707355

HIV-1 increases susceptibility to pulmonary infection and disease, suggesting pathogenesis in the lung. However, the lung immune environment during HIV infection remains poorly characterized. This study examined T cell activation and the cytokine milieu in paired bronchoalveolar lavage (BAL) and blood from 36 HIV-uninfected and 32 HIV-infected participants. Concentrations of 27 cytokines were measured by Luminex, and T cells were phenotyped by flow cytometry. Blood and BAL had distinct cytokine profiles (p=0.001). In plasma, concentrations of inflammatory cytokines like IFN-γ (p=0.004) and TNF-α (p=0.004) were elevated during HIV infection, as expected. Conversely, BAL cytokine concentrations were similar in HIV-infected and uninfected individuals, despite high BAL viral loads (VL; median 48,000 copies/ml epithelial lining fluid). HIV-infected individuals had greater numbers of T cells in BAL compared to uninfected individuals (p=0.007); and BAL VL positively associated with CD4+ and CD8+ T cell numbers (p=0.006 and p=0.0002, respectively) and CXCL10 concentrations (p=0.02). BAL T cells were highly activated in HIV-infected individuals, with nearly 2-3 fold greater frequencies of CD4+CD38+ (1.8-fold; p=0.007), CD4+CD38+HLA-DR+ (1.9-fold; p=0.0006), CD8+CD38+ (2.8-fold; p=0.0006), CD8+HLA-DR+ (2-fold; p=0.022) and CD8+CD38+HLA-DR+ (3.6-fold; p<0.0001) cells compared to HIV-uninfected individuals. Overall, this study demonstrates a clear disruption of the pulmonary immune environment during HIV infection, with readily detectable virus and activated T lymphocytes, which may be driven to accumulate by local chemokines.

Keywords: lung, HIV, activation, T cells, inflammation, cytokines

INTRODUCTION

Sub-Saharan Africa has 25.6 million people currently living with HIV and 970,000 new infections a year (1). HIV-infected individuals are highly susceptible to both infectious and non-communicable pulmonary diseases such as tuberculosis [TB], *Pneumocystis* pneumonia, chronic obstructive lung disease [COPD] or pulmonary fibrosis (2–4). Although antiretroviral treatment (ART) has reduced the overall prevalence of HIV-associated lung disease, respiratory diseases still contribute to substantial morbidity and mortality in the HIV-infected population (5–7). This suggests that HIV pathogenesis extends to the lungs, requiring additional strategies to reduce the burden of respiratory diseases in HIV-infected individuals.

HIV infection is characterized by systemic immune hyperactivation and profound damage to mucosal compartments due to viral replication (8–16). Consequently, the demonstrated burden of HIV in the lung has significant implications for local pathology and impaired immunity to respiratory pathogens (17–23). HIV-associated lymphocytic alveolitis, the infiltration of lymphocytes into the airways, is associated with local viral replication (24–28). However, due to the difficulty in studying and sampling the lung compartment, the full extent of HIV-associated pulmonary immune dysfunction is not well understood.

Our previous work established that early HIV infection had a limited effect on *Mycobacterium tuberculosis* (M.tb)-specific T cell responses in BAL (29), warranting a broader investigation of the immune milieu of the lung. Therefore, in this study, we examined viral burden, T cell activation and cytokine concentrations in paired BAL and blood from HIV-uninfected and HIV-infected participants.

METHODS

Study Participants

Participants were recruited from Cape Town, South Africa and grouped according to their HIV status: 32 ART-naive HIV-seropositive persons with CD4+ T-cell counts of >400 cells/mm^3 and 36 HIV-seronegative persons. Participants were not eligible for this study if they had any active respiratory infections. Active TB was excluded on the basis of symptoms, radiological evidence, and BAL fluid culture results. All participants had latent TB infection (LTBI) as confirmed by a positive IFN-γ release assay (IGRA; Quantiferon-TB Gold, Qiagen, Hilden, Germany). This study was approved by the Research Ethics Committees of the University of Cape Town (REF158/2010) and Stellenbosch University (N10/08/275). All participants provided written, informed consent.

Collection and Processing of Samples

BAL samples were collected and processed as previously described (29). Briefly, 160ml of saline was instilled in the middle lobe bronchus and aspirated. After centrifugation, acellular BAL fluid (BALF) was stored at −80°C and the cell pellet was washed and filtered through a 100-μm cell strainer (CellTrics, Partec, Münster, Germany). Cells were then counted using Trypan Blue exclusion and differentially stained in order to count macrophages, lymphocytes and neutrophils (RapidDiff, Clinical Sciences Diagnostics, Johannesburg, South Africa). The absolute number of T lymphocytes in BAL fluid was calculated using differential staining and microscopy, and the frequencies of live CD3+, CD4+, or CD8+ T cells from a flow cytometry phenotyping panel (see below). To correct for epithelial lining fluid (ELF) dilution due to variable fluid volumes recovered, the urea method was used (QuantiChrom, Clonagen, Brussels, Belgium) as described elsewhere (30). BALF viral loads and BAL cell counts were standardized according to the volume of ELF sampled (median, 1 mL; IQR, 0.75–1.64 mL) and are expressed as the number of cells or viral load per ml of ELF.

Blood specimens were collected and processed within 4 hours. Heparinized whole blood was treated with red blood cell lysis buffer without a fixative, and the cell pellet was immediately stained with a panel of antibodies for phenotyping by flow cytometry.

Phenotyping by Multiparameter Flow Cytometry

The staining panel consisted of CCR5 PE (2D7), CD38 APC (HIT2), CD3 PE-Cy7 (SK7), HLA-DR APC-Cy7 (L243; all from BD Biosciences, New Jersey, USA), CD4 PE-Cy5.5 (S3.5), CD8 Qdot-705 (3B5), CD19 Pacific Blue (SJ25-CI), CD14 Pacific Blue (T̈k4; all from Invitrogen, California, USA), CD45RO ECD (UCHL1), CD27 PE-Cy5 (1A4CD27; both from Beckman Coulter, California, USA). Blood and BAL cells were stained with a viability marker (violet fixable viability dye, Invitrogen), followed by CCR5 labelling at 37°C before labelling with antibodies against surface markers. Cells were fixed in 1x CellFix (BD Biosciences) for acquisition a BD Fortessa using FACSDiva software. Data were analysed using FlowJo (TreeStar, Oregon, USA). Gates were set using fluorescence-minus-one (FMO) controls.

Measurement of Soluble Analytes

A total of 27 cytokines and chemokines were measured in paired plasma and concentrated BALF samples using human magnetic bead multiplex kits (Merck Millipore, Massachusetts, USA). The Human Th17 magnetic bead kit was used to measure IL-1β, IL-4, IL-6, IL-10, IL-13, IFN-γ, GM-CSF, TNF-α, IL-21, IL-22, IL-23, IL-15, IL-17 and CCL20. The Human Cytokine/Chemokine magnetic bead kit was used to measure EGF, IL-12p70, IL-7, CXCL8 (IL-8), CXCL10 (IP-10), CCL2 (MCP-1), CCL3 (MIP-1β), CCL4 (MIP-1α), CCL5 (RANTES), CCL7 (MCP-3), CCL11 (eotaxin), CX3CL1 (fractalkine) and sCD40L. Samples were run in duplicate and the mean was calculated. Cytokine concentrations were adjusted for BAL fluid concentration factor. Cytokines that fell below the limit of detection were reported as half the minimum detectable concentration. Analytes were excluded if they fell below the empirical cut-off (either undetectable in 50% or more participants, or with a median of less than twice the minimum detectable concentration for that analyte). These were GM-CSF, IL-22, IL-4, IFN-γ, CCL11

in BAL; and GM-CSF, IL-15, IL-1β, IL-22, IL-4, IL-6 in blood. Analytes were categorized as pro-inflammatory (IL-1β, IL-6, IL-12p70, IL-23, TNF-α, sCD40L), adaptive (IFN-γ, IL-13, IL-17), γ-chain cytokines (IL-7, IL-15, IL-21), regulatory (IL-10), growth factors (EGF) and chemokines (CCL2, CCL3, CCL4, CCL5, CCL7, CCL11, CCL20, CXCL8, CXCL10, CX3CL1) based on function. The relative proportion of each analyte was calculated as a percentage of the sum total of the analyte concentrations in that compartment.

Statistical Analyses

Non-parametric statistical analyses (Mann-Whitney U test, the Wilcoxon matched pairs test, and the Spearman rank test) were performed using Prism 7 (GraphPad). Unsupervised hierarchical clustering, principal component analyses (PCA) and permANOVA were carried out in R (31) using the following packages: pheatmap (32), vegan (33), ggfortify (34), RColourBrewer (35). False discovery rate (FDR) step down procedures were performed to adjust for multiple comparisons as previously described (36). A p value of <0.05 was considered statistically significant. The p values, $p \leq 0.05$, $p \leq 0.01$, $p \leq 0.001$, $p \leq 0.0001$ are reported as *, **, *** and ****, respectively.

RESULTS

Cohort Description

Blood and BAL were collected from HIV-infected (n=32; median age, 31 years; 96% female) and uninfected (n=36; median age, 23 years; 60% female) participants from Cape Town, South Africa (**Table 1** and **Table S1**). HIV-uninfected participants had a median CD4 count of 832 cells/mm^3 (IQR 741-1028 cells/mm^3), while the HIV-infected individuals had a median of 601 cells/mm^3 (IQR 523-782 cells/mm^3; p<0.0001). HIV-infected persons were ART-naïve, however persons with CD4 counts < 400 cells/mm^3 were excluded in order to study the impact of HIV infection prior to severe immunodeficiency. HIV-infected participants had a median HIV viral load in BAL fluid of 48,224 RNA copies/ml ELF (IQR 2,115-27,378 copies/ml ELF) and a median plasma viral load of 6,153 RNA copies/mm^3 (IQR 2,125-17,623 copies/mm^3; p=ns). Consistent with previous reports, there was a significant positive correlation between HIV load in BALF and plasma (p<0.0001; r=0.696; data not shown) (19, 21). These data demonstrate that despite relatively well-preserved CD4 counts, the HIV-infected group had substantial amounts of virus detectable in the airways and in blood.

TABLE 1 | Clinical characteristics of study participants.

	HIV-uninfected (n = 36)	HIV-infected(n = 32)
Blood CD4 count (cells/mm^3)	832 (741-1,028)	601 (523-782)
Plasma viral load (RNA copies/ml)	–	6,153 (2,125-17,623)
BAL viral load (RNA copies/ml ELF)	–	48,224 (2,115-27,378)

Data are median (interquartile range). BAL, bronchoalveolar lavage; ELF, epithelial lining fluid.

Distinct Cytokine Profiles in BAL and Blood

To investigate the immune environment in the airways compared to peripheral blood, soluble cytokines and chemokines were measured in BAL fluid and blood plasma (**Tables S2, S3**). Most cytokines (22/24; 92%) were significantly higher in plasma than BAL fluid, regardless of HIV status (**Figure 1A**). Consequently, principal component analysis (PCA) demonstrated a distinct separation of cytokine profiles by compartment but not HIV status (p=0.001, r^2 = 0.508; **Figure 1B**). We then examined the relative proportion of each cytokine adjusted to represent 100% of the overall milieu in each compartment (**Figure 1C**). Again, we observed divergent cytokine profiles between compartments. In plasma, soluble CD40L was the most abundant and made up 43% of the milieu in HIV-uninfected individuals, but only contributed 3% to the BAL cytokine profile in the same individuals. Likewise, CXCL10 contributed 44% to the milieu in BAL fluid (44%) but only 11% in plasma. Based on these observations, we focused on examining the effect of HIV infection on the airways and blood separately to account for compartmentalisation.

The Cytokine Milieu in BAL Is Less Affected by HIV Infection Than Blood

We first investigated the soluble cytokine milieu to elucidate which immune mediators were elevated during HIV infection. In BAL fluid, there were few differences in the soluble immune milieu between study populations. Compared to uninfected individuals, HIV-infected participants had lower concentrations of EGF (p=0.040, median: 2.02 pg/ml and 0.48 pg/ml, respectively) and CX3CL1 (p=0.044, median: 4.61 pg/ml and 2.24 pg/ml, respectively; **Figure 2A**) after correcting for multiple comparisons. Furthermore, unsupervised hierarchical clustering showed no clear clustering of cytokine profiles between HIV-infected and uninfected individuals (**Figure 2B**). Consistent with this, PCA demonstrated that cytokine profiles of the two groups did not visibly separate according to HIV status, although there was weak but significant variation in cytokine profiles between HIV-infected and uninfected groups (p=0.023, r^2 = 0.04; **Figure 2C**).

In contrast to the airways, the plasma cytokine milieu differed considerably between HIV-infected and uninfected individuals. Compared to uninfected individuals, HIV-infected individuals had notably higher concentrations of inflammatory cytokines IFN-γ (p=0.004, median: 6.32 pg/ml *vs* 12.47 pg/ml), TNF-α (p=0.004, median: 10.18 pg/ml *vs* 25.02 pg/ml) and the chemokine CXCL10 (p=0.002, median: 219.5pg/ml *vs* 487.41 pg/ml), and lower concentrations of IL-7 (p=0.036, median: 2.21 pg/ml *vs* 1.17 pg/ml), IL-12p70 (p=0.007, median: 6.91 pg/ml *vs* 2.43 pg/ml), EGF (p=0.018, median: 15.17 pg/ml *vs* 7.07 pg/ml) and the chemokines CCL3 (p=0.002, median: 49.12 pg/ml *vs* 15 pg/ml), CCL4 (p=0.017, median: 10.4 pg/ml *vs* 1.81 pg/ml), CCL7 (p=0.002, median: 20.3 pg/ml *vs* 9.22 pg/ml), CX3CL1 (p=0.004, median: 169.7 pg/ml *vs* 95.12 pg/ml) and CXCL8 (p=0.004, median: 15.72 pg/ml *vs* 5.25 pg/ml; **Figure 3A**). Indeed, plasma cytokine profiles of HIV-infected and uninfected participants displayed a degree of clustering by unsupervised

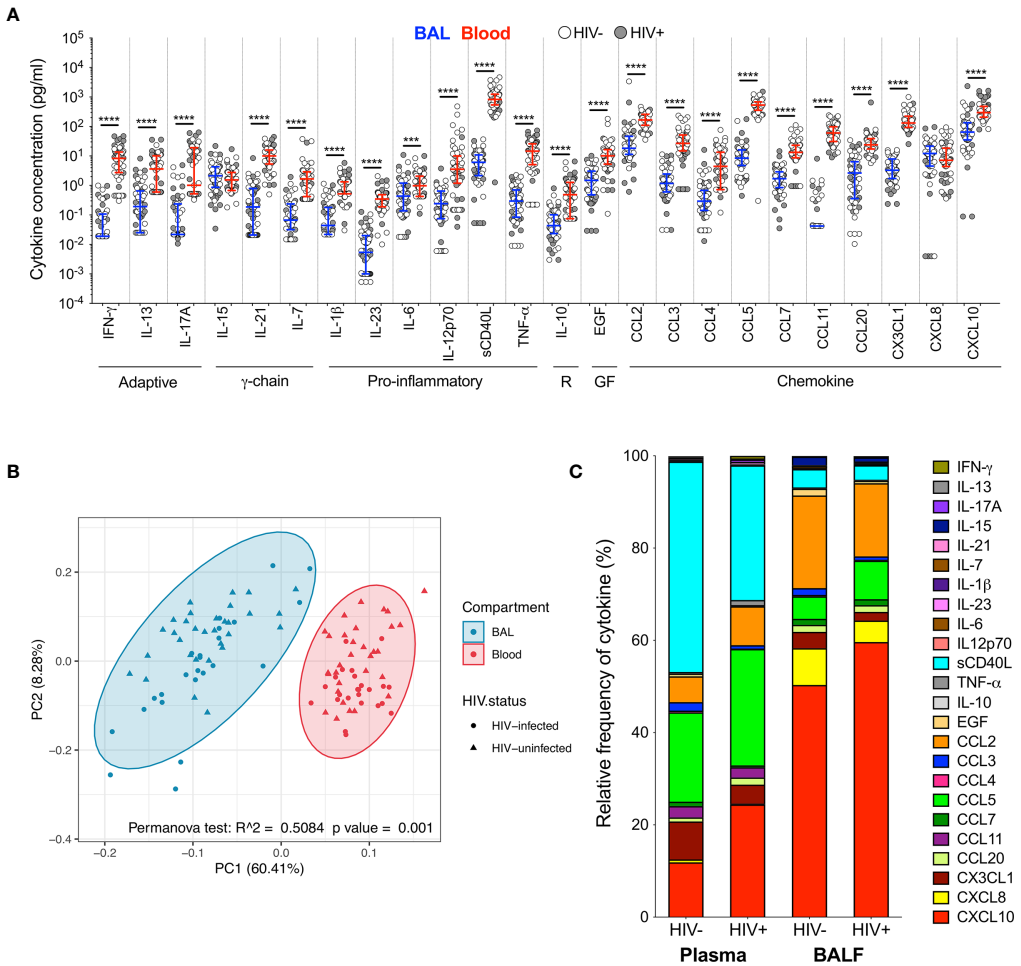

FIGURE 1 | Soluble immune mediators in blood and BAL. **(A)** Comparison of cytokine concentrations in BAL (blue) and blood (red) of HIV-infected (filled circles) and HIV-uninfected (open circles) individuals. "R" refers to regulatory cytokines and "GF" refers to growth factors. The blue and red lines denote the median and interquartile ranges for BAL and blood, respectively. Statistical analyses were performed using a non-parametric Wilcoxon paired test with False Discovery Rate (FDR) step down correction. **(B)** Principal component analysis and permutational multivariate analysis of variance (permANOVA) of cytokine concentrations in BAL (blue) and blood (red). **(C)** Cytokine concentration expressed as a proportion of the total milieu in BAL and plasma. The relative proportion of each analyte was calculated as a percentage of the sum total of the analyte concentrations in that compartment. GM-CSF, IL-22 and IL-4 were excluded altogether as they were below the level of detection in both BAL and blood. Analytes that fell below the limit of detection for some participants were reported as half the minimum detectable concentration. The p values, $p \leq 0.05$, $p \leq 0.01$, $p \leq 0.001$, $p \leq 0.0001$ are reported as *, **, *** and ****, respectively.

hierarchical clustering (**Figure 3B**). Similarly, principal component analysis demonstrated partial separation of cytokine profiles by HIV status (p=0.001, $r^2 = 0.109$; **Figure 3C**). Overall, these results demonstrate that there were larger differences in the cytokine milieu between anatomical compartments than between HIV-infected and uninfected participants, with notably fewer differences observed within BAL compared to plasma, despite high BAL HIV load in these participants.

Chemokine Concentrations Associate With T Cell Numbers and HIV Viral Load in the Airways

As reported previously (29), we found that the absolute numbers of T cells from BAL were significantly higher in HIV-infected participants, and this correlated positively with BAL viral load (**Figure S1**). To examine the interplay between HIV, the cytokine milieu and T cells, we investigated the relationships between cytokine concentrations, absolute T cell numbers and viral load. In plasma, CXCL10 concentration was significantly positively correlated with viral load (p=0.03, r=0.444; **Figure 4A**) but there was no relationship with CD4 count (p=ns; **Figure 4B**). TNF-α and sCD40L were also associated with plasma viral load (p=0.0499, r=0.405) and CD4 count (p=0.032, r=-0.439), respectively (data not shown). In BAL fluid, chemokines were significantly associated with viral load and T cell numbers. Specifically, the concentration of CXCL10 positively correlated with viral load (p=0.02, r=0.471) and the number of CD3+ (p=0.001, r=0.764), CD4+ (p=0.003, r=0.729) and CD8+ T

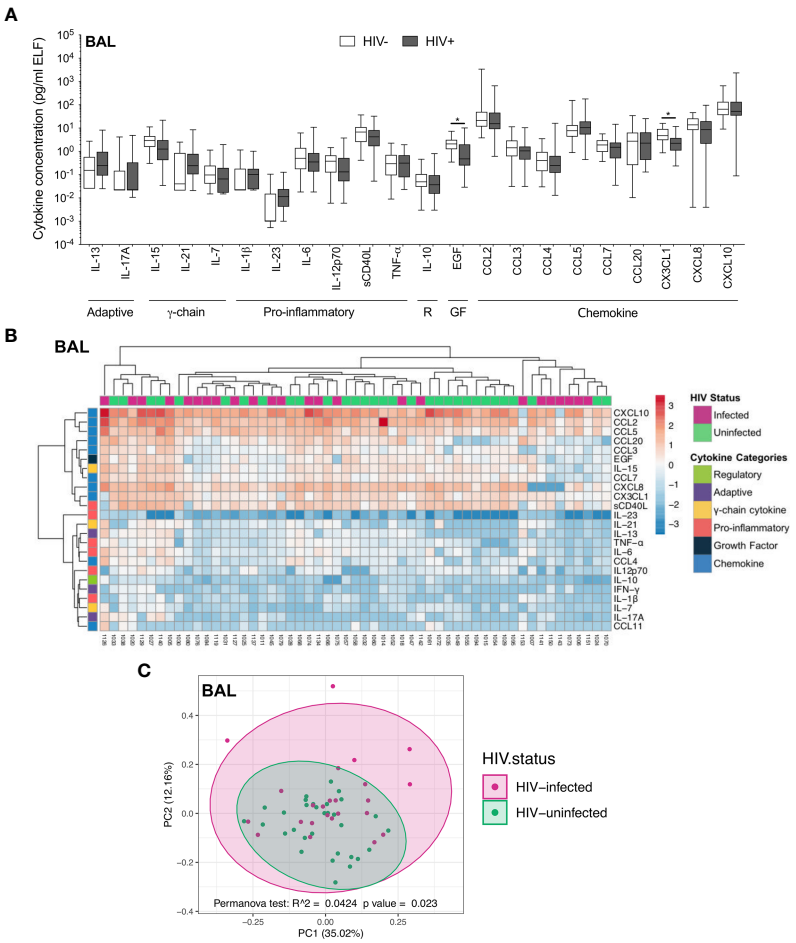

FIGURE 2 | Soluble immune mediators in BAL in HIV-infected and uninfected individuals. **(A)** Box and whisker plots (min-max) comparing cytokine concentrations in BAL according to HIV status. "R" refers to regulatory cytokines and "GF" refers to growth factors. Statistical analyses were performed using a non-parametric Mann-Whitney U test with False Discovery Rate (FDR) step down correction. **(B)** Unsupervised hierarchical clustering of cytokines in BAL. **(C)** Principal component analysis and permutational multivariate analysis of variance (permANOVA) of soluble immune mediators in HIV-infected (pink; n=24) and uninfected (green; n=31) participants. GM-CSF, IL-22, IL-4, IFN-γ and CCL11 were excluded as they were below the level of detection. The p values, $p \leq 0.05$, $p \leq 0.01$, $p \leq 0.001$, $p \leq 0.0001$ are reported as *, **, *** and ****, respectively.

cells (p=0.001, r=0.764) (**Figures 4C–F**). To determine whether outliers drove these correlations, we excluded the two outliers with high CXCL10 concentrations. Apart from viral load (p=0.07), the associations remained statistically significant after the exclusions. Additionally, CCL2 positively associated with BAL fluid viral load (p=0.0496, r=0.405), and CXCL8 was positively associated with numbers of CD3+ (p=0.05, r=0.516) and CD8+ (p=0.0499, r=0.516) T cells (data not shown). These associations suggest that the presence of HIV in the airways may lead to elevated levels of chemokines, and concomitant increases in T cells in the alveolar space.

T Cells From HIV-Infected Participants Are Highly Activated in BAL and Blood

Although widespread immune hyperactivation is well described during HIV infection, little is known about the activation state of lymphocytes in the airways and how this compares to peripheral blood. Thus, we characterized T cell activation, as measured by CD38 and HLA-DR expression (**Figure 5A** and **Figure S2**) and found that in HIV-uninfected individuals, frequencies of activated CD4+ T cells were higher in BAL compared to blood (for HLA-DR+ p<0.0001, median: 22.75% *vs* 5.49%; for CD38+HLA-DR+ p=0.0006, median: 3.32% *vs* 1.22%, respectively; **Figure S3A**). However, in HIV-infected individuals, there were no significant differences in CD4+ T cell activation between compartments (**Figure S3A**). There were also no differences in activated CD8+ T cells between compartments (**Figure S3B**). We observed higher frequencies of CCR5-expressing CD4+ and CD8+ T cells in BAL compared to blood, regardless of HIV status (**Figure S3C**). Furthermore, the frequencies of CD4+CD38+ and CD4+CD38+HLA-DR+ T cells between blood and BAL were positively correlated in both HIV-infected (p=0.018, r=0.537 and p=0.033, r=0.491, respectively) and uninfected individuals (p=0.002, r=0.622 and p=0.049, r=0.424, respectively;

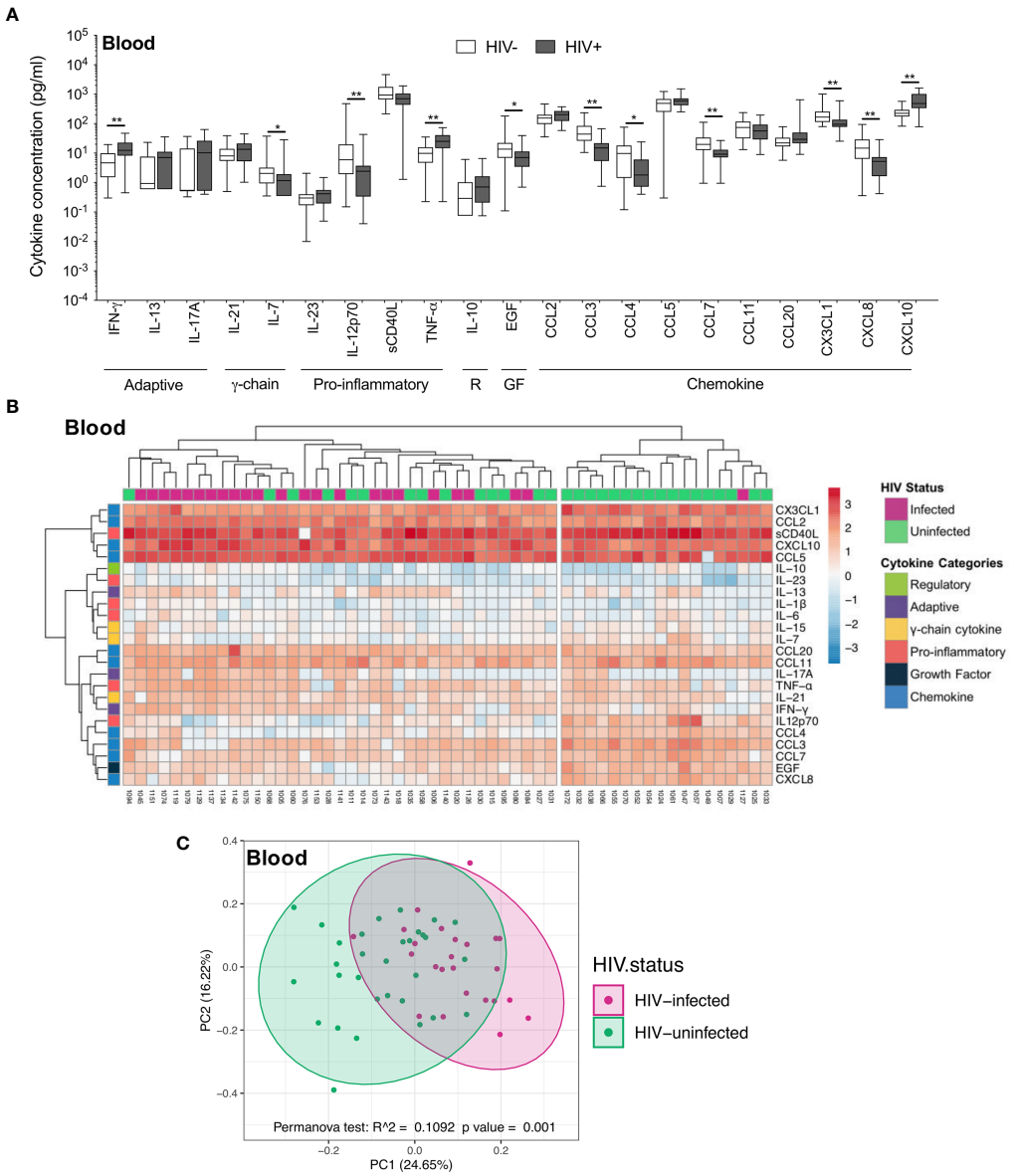

FIGURE 3 | Soluble immune mediators in blood in HIV-infected and uninfected individuals. **(A)** Box and whisker plots (min-max) comparing cytokine concentrations in plasma according to HIV status. "R" refers to regulatory cytokines and "GF" refers to growth factors. Statistical analyses were performed using a non-parametric Mann-Whitney U test with False Discovery Rate (FDR) step down correction. **(B)** Unsupervised hierarchical clustering of cytokines in blood. **(C)** Principal component analysis and permutational multivariate analysis of variance (permANOVA) of soluble immune mediators in HIV-infected (pink; n=24) and uninfected (green; n=31) participants. GM-CSF, IL-15, IL-1β, IL-22, IL-4 and IL-6 were excluded as they were below the level of detection. The p values, $p \leq 0.05$, $p \leq 0.01$, $p \leq 0.001$, $p \leq 0.0001$ are reported as *, **, *** and ****, respectively.

Figure 5B and data not shown). CD8+CD38+ T cells also correlated significantly between compartments, but only in HIV-infected individuals (p=0.002, r=0.762; **Figure 5C**). There was no association between T cell activation and BAL or plasma viral load (data not shown).

Direct comparison of T cell activation according to HIV status demonstrated that compared to uninfected participants, HIV-infected participants had higher frequencies of BAL CD4+ T cells expressing CD38 (p=0.007, medians 9.97% *vs* 17.8%) and co-expressing CD38 and HLA-DR (p=0.0006, medians 3.16% *vs* 6.05%; **Figure 5D**). Consistent with this, there were significantly higher frequencies of activated CD4+ T cells in blood of HIV-infected individuals compared to uninfected individuals (p=0.0002, medians 19.55% *vs* 11.1% for CD4+CD38+; p<0.0001, medians 15.25% *vs* 5.36% for CD4+HLA-DR+; p<0.0001, medians 4.29% *vs* 1.22% for CD4+CD38+HLA-DR+; **Figure 5D**). Higher CD8+ T cell activation was also demonstrated for HIV-infected individuals compared to uninfected individuals

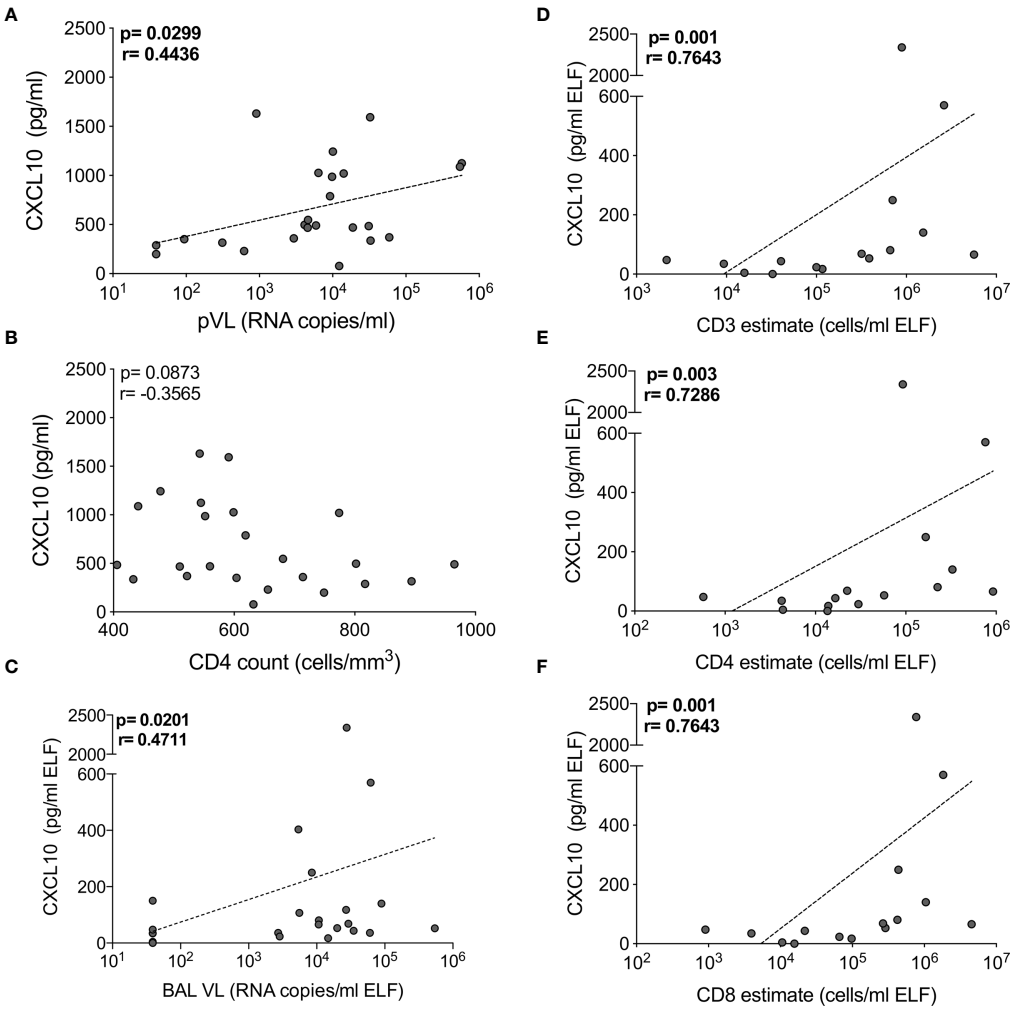

FIGURE 4 | CXCL10 correlates with HIV viral load and T cell numbers in BAL of HIV-infected individuals. The correlation between CXCL10 concentration and **(A)** plasma HIV viral load, **(B)** blood CD4 count in blood, **(C)** BAL HIV viral load (n=24), **(D)** BAL CD3, **(E)** CD4 and **(F)** CD8 T cell estimates (n=16). Each dot represents an individual. Only individuals with absolute BAL cell count data were plotted. The dotted line indicates linear regression for statistically significant correlations. Statistical analyses were performed using a non-parametric Spearman rank correlation.

in both BAL (p=0.0007, medians 22.9% *vs* 8.0%, for CD8+CD38+; p=0.022, medians 21.4% *vs* 10.7% for CD8+HLA-DR+; p<0.0001, medians 6.3% *vs* 1.73% for CD8+CD38+HLA-DR+) and blood (p=0.0002, medians 21.15% *vs* 6.83% for CD8+CD38+; p<0.0001, medians 21.1% *vs* 9.36% for CD8+HLA-DR+; p<0.0001, medians 9.91% *vs* 2.1% for CD8+CD38+HLA-DR+; **Figure 5E**). These observations confirm that T cell activation was consistently higher in HIV-infected individuals in both BAL and blood.

Limited Influence of BAL Cytokines on T Cell Activation

The relationships between cytokines and T cell activation in BAL was examined next. **Figure 6** shows the Spearman rho (r) of each correlation between cytokines and T cells expressing CD38, HLA-DR or CCR5. Overall, more associations between cytokines and activated T cells were observed in HIV-uninfected individuals compared to HIV-infected individuals, which could suggest some regulatory disruptions during HIV infection. However, no significant associations remained after adjusting for multiple comparisons, and linear regression analysis revealed no associations between T cell activation and cytokine concentrations (data not shown).

DISCUSSION

This study investigated HIV-associated immune changes in the airways, to better understand the high incidence of lung disease during HIV infection. We found distinct compartmentalisation of cytokines between BAL and blood in terms of relative cytokine abundance and cytokine concentrations, regardless of HIV status, leading us to examine the effect of HIV on each compartment individually. In BAL of HIV-infected, ART-naïve

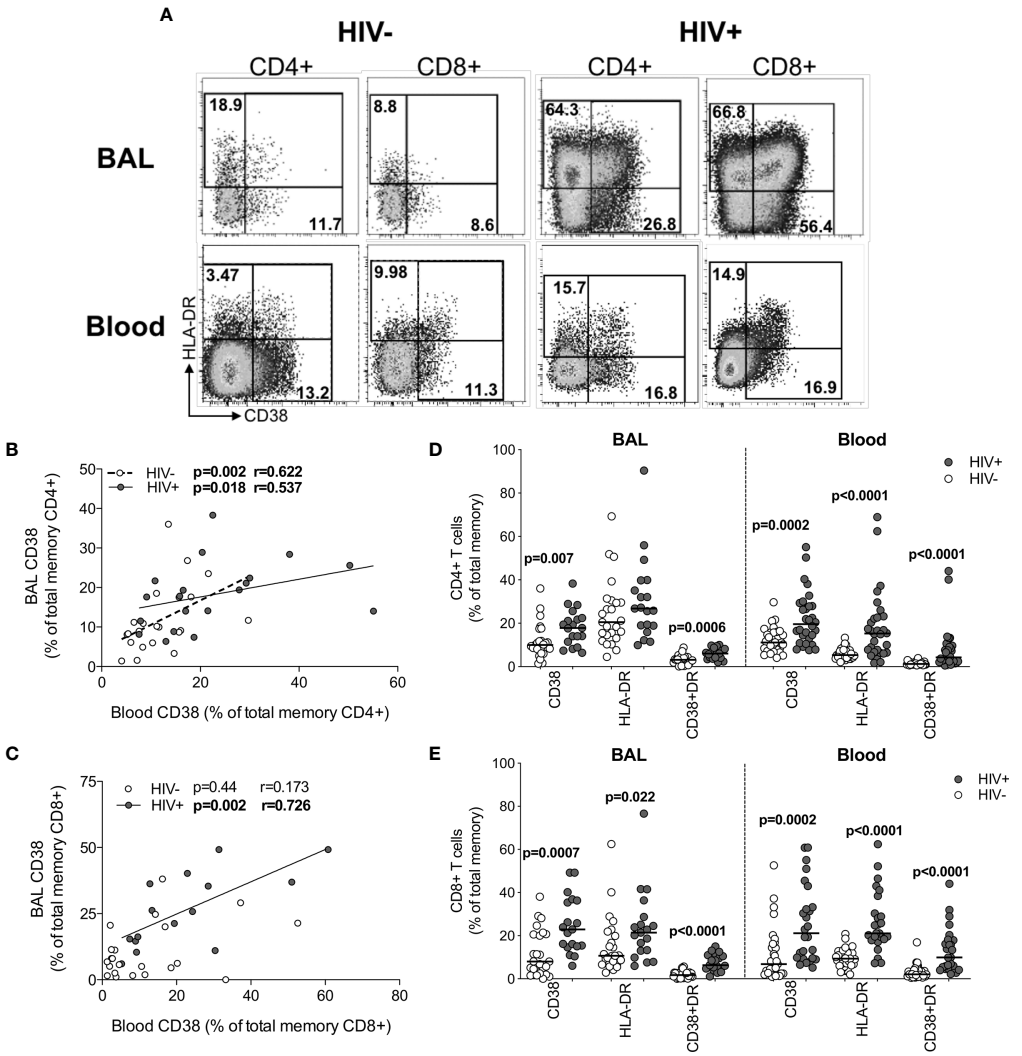

FIGURE 5 | T cell activation in BAL and blood. **(A)** Representative flow cytometry plots of HLA-DR and CD38 expression on T cells in BAL and blood of HIV-infected and uninfected participants. **(B)** The association between CD4+ T cells expressing CD38 in blood and BAL of HIV-uninfected (n=22) and infected (n=15) individuals. **(C)** The association between CD8+ T cells expressing CD38 in blood and BAL of HIV-uninfected (n=22) and infected (n=15) individuals. **(D)** CD38 and HLA-DR expression on CD4+ T cells in blood and BAL of HIV-uninfected (n=31 and n=25, respectively) and infected (n=30 and n=19, respectively) individuals. **(E)** CD38 and HLA-DR expression on CD8+ T cells in blood and BAL of HIV-uninfected and infected individuals. Each dot represents an individual. Open circles represent HIV-uninfected individuals and filled circles represent HIV-infected individuals. Statistical comparisons were performed using the non-parametric Mann Whitney, Wilcoxon matched pairs and Spearman correlation tests.

individuals, we detected a high viral load, and more T cells compared to HIV-uninfected individuals. HIV infection was also associated with increased frequencies of activated T cells. We observed a significant positive correlation between BAL viral load, absolute T cell numbers and the concentration of the chemokine CXCL10.

We detected high concentrations of HIV RNA in BAL fluid, consistent with earlier studies (19–21). The presence of HIV in the lung is likely to contribute to immunopathology and immune dysfunction, increasing susceptibility to respiratory diseases. We report a greater number of lymphocytes in HIV-infected airways, as has previously been described as lymphocytic alveolitis, thought to be predominantly made up of cytotoxic CD8+ T cells (24, 26, 27, 37). On its own, lymphocytic alveolitis causes limited pathology (25), but may contribute to the increased prevalence of pulmonary disease during HIV infection. COPD is associated with an increase in airway CD8+ T cells, particularly when combined with smoking or other risk factors (38–40). Lymphocytic alveolitis may also impair the normal response to pulmonary infections. A CD4+ T cell infiltration to the lungs would be expected in response to bacterial pathogens (41, 42), but this may be skewed towards CD8+ T cells during HIV infection. Indeed, TB-involved lung tissue from co-infected macaques (SIV and active TB) had fewer CD4+ T cells than

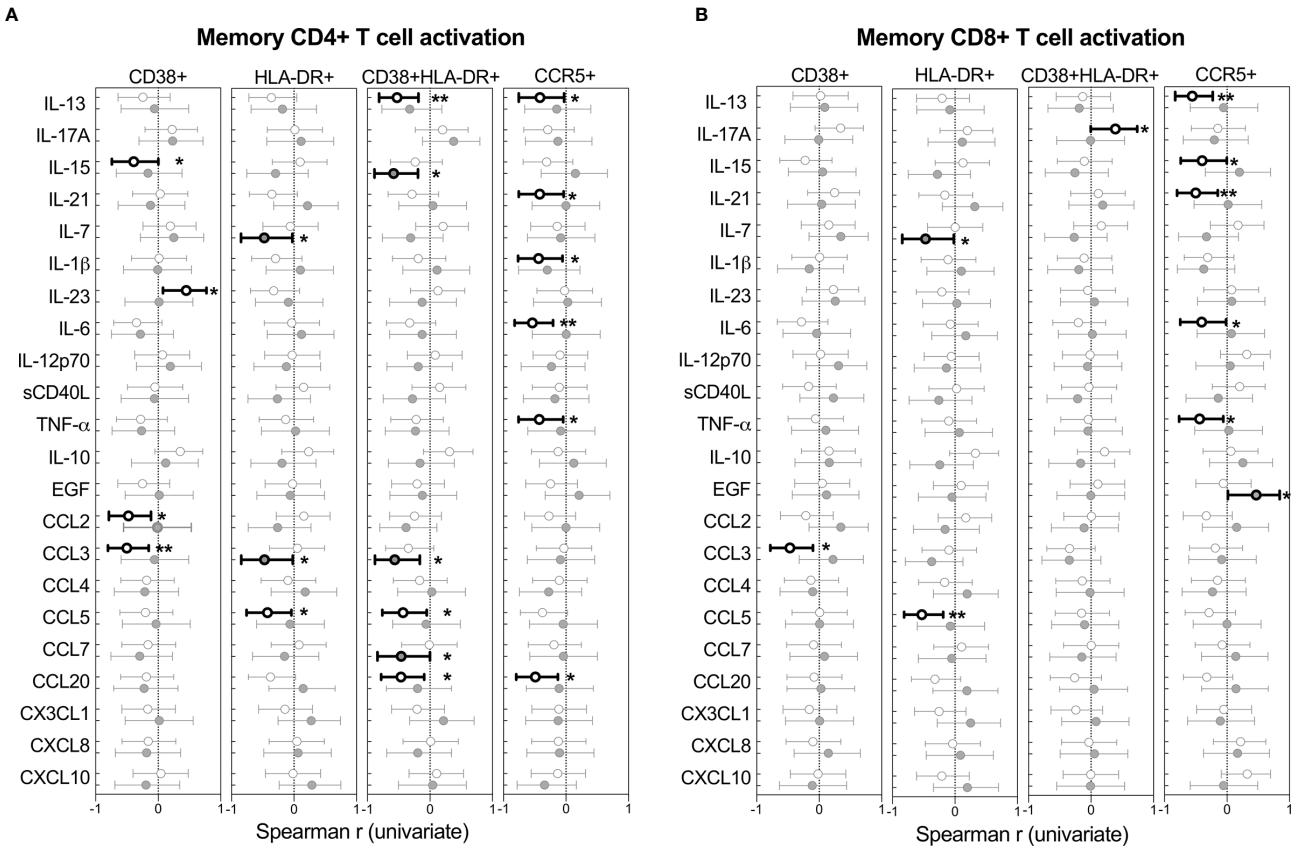

FIGURE 6 | Univariate associations between T cell activation markers and cytokine concentrations in BAL of HIV-infected (n=14) and uninfected (n=21) individuals. Spearman rho (r) of the univariate correlation between each cytokine and the expression of activation markers on **(A)** CD4+ T cells and **(B)** CD8+ T cells. Open circles represent HIV-uninfected individuals and filled circles represent HIV-infected individuals. Statistically significant correlations ($p<0.05$) are indicated in darker lines and symbols. Spearman correlation tests, of which Spearman rho and the 95% confidence intervals are reported here. None of the correlations remained statistically significant after adjusting for multiple comparisons by FDR step down procedures. The p values, $p \leq 0.05$, $p \leq 0.01$, $p \leq 0.001$, $p \leq 0.0001$ are reported as *, **, *** and ****, respectively.

those with active TB alone (43), suggesting SIV may interfere with the recruitment of CD4+ T cells into involved tissue. Furthermore, the infiltration of activated, cytotoxic CD8+ T cells (37), together with local pathology caused by the HIV Nef protein, may also considerably compromise mucosal barrier function via endothelial dysfunction and increased epithelial permeability (44–48). In this study, HIV-infected individuals also had lower concentrations of EGF in BAL fluid. Together, our data and these studies suggest reduced mucosal barrier function and dysregulated migration of T cells, leading to suboptimal control of infection and disease.

In HIV-uninfected individuals, BAL CD4+ T cells were significantly more activated than in blood, which is consistent with a mucosal effector environment (49–51). HIV infection led to similar levels of activated CD4+ and CD8+ T cells in BAL and blood, the likely result of systemically activated cells migrating into the airways.

We found a clear compartmentalisation of cytokine profiles between blood and BAL, with more differences between compartments than between HIV-infected and uninfected individuals. This agrees strongly with a recent study reporting distinct transcriptional profiles between BAL cells and PBMC, regardless of HIV status (37), underscoring the assertion that blood may be a poor surrogate for immune processes in the airways. In BAL, CXCL10 was present at the highest relative proportion. CXCL10 is responsible for T cell chemoattraction and is upregulated in the healthy human lung during pulmonary infection and disease (52, 53). Indeed, the preservation and increase in the BAL T cell population may be driven by the local presence of chemokines, which are elevated during HIV infection (19, 54, 55). We also found that the concentration of CXCL10 positively correlated with BAL viral load and BAL T cell numbers; and the latter two also associated with each other. These data suggest a relationship in which HIV may drive the expression of chemokines from lung cells, which in turn causes an infiltration of lymphocytes, including HIV-specific and M.tb-specific T cells (17, 18, 29, 56). We also observed elevated concentrations of the proinflammatory cytokines TNF-α and IFN-γ in plasma, consistent with previous studies (10, 57–60). In contrast, we did not detect elevated proinflammatory cytokines in BAL, despite high viral loads. Excess inflammation in the lung

may cause tissue damage, which may be especially detrimental to the integrity of alveoli, so an aggressive immune response that would be permissible elsewhere is thought to be tightly controlled and regulated in the lung (61). Indeed, studies have reported that BAL CD8+ T cells have lower cytotoxic potential compared to peripheral blood CD8+ T cells (62).

Although there may be continuous migration of virus between BAL and the circulation (63), local viral replication may also be occurring. HIV target cells in the lung include small alveolar macrophages and resident CD4+ T cells expressing CCR5 (28, 64). Thus, the lung may also act as a reservoir for HIV. Previous studies have shown distinct HIV *env* sequences isolated from the lung, compared to those isolated from peripheral blood in the same individual (65, 66). Whether the lung is an important viral reservoir in the context of viral suppression and cure needs further investigation.

Our study had several limitations. We were only able to phenotype BAL T cells on a limited number of participants, due to the challenge of obtaining sufficient cells from BAL. Although BAL is representative of the bronchus, it may not necessarily reflect the immune environment of lung tissue. Further studies examining lung biopsies or other sources of lung tissue during HIV infection would give a clearer picture of HIV-associated pulmonary dysfunction. Longitudinal studies, perhaps in non-human primate models, are required to fully understand the dynamics of the immune milieu over the course of HIV infection.

In conclusion, this study demonstrates that the immune environment of the airways is disrupted during HIV infection, with readily detectable virus and the accumulation of activated T lymphocytes that may be driven by high levels of chemokines such as CXCL10 at this site. Further mechanistic studies are required to determine whether HIV-associated changes in the airways contribute to the increased susceptibility to pulmonary disease during HIV infection.

DATA AVAILABILITY STATEMENT

The raw data supporting the conclusions of this article will be made available by the authors, without undue reservation.

ETHICS STATEMENT

The studies involving human participants were reviewed and approved by the Human Research Ethics Committee of the University of Cape Town (REF158/2010) and the Research Ethics Committee of Stellenbosch University (N10/08/275). The patients/participants provided their written informed consent to participate in this study.

AUTHOR CONTRIBUTIONS

WB, RB, AS, and RW conceived and designed the experiments. RB, AS, NT, TM, AK, ZG, and BC performed the experiments. RB, AS, BM, CR, and WB analyzed the data. FG-B, GW, DK, and RW contributed reagents, materials, and/or analysis tools. RB and WB wrote the manuscript. All authors contributed to the article and approved the submitted version.

FUNDING

This project is part of the EDCTP2 programme supported by the European Union (EU)'s Horizon 2020 programme (TMA2016SF-1535-CaTCH-22 to WB, TMA2017SF-1951-TB-Spec to CR, TMA2020CDF-3187 to RB). Additional funding came from the Carnegie Corporation; the University of Cape Town; the Canada Africa Prevention Trials Network (all to RB); National Institutes of Health (grant R21AI115977 to CR); Wellcome Trust (203135 and 104803), NIH (U01 AI115940), the Francis Crick Institute (Cancer Research UK, MRC UK and Wellcome FC0010218), and SAMRC (SHIP) (all to RW).

ACKNOWLEDGMENTS

We thank the study participants, for providing samples and for their time and commitment to the study; the clinical staff at the Ubuntu HIV-TB clinic and the bronchoscopy suite at Tygerberg Academic Hospital, for providing essential support; Mrs Kathryn Norman, for administrative assistance; Maximilian Ľcke, for phlebotomy, cataloguing participant radiography findings, and database assistance.

SUPPLEMENTARY MATERIAL

The Supplementary Material for this article can be found online at: https://www.frontiersin.org/articles/10.3389/fimmu.2021.707355/full#supplementary-material

REFERENCES

1. UNAIDS. *Fact Sheet HIV Statistics* (2020). Available at: https://www.unaids.org/en/resources/fact-sheet.
2. Crothers K, Huang L, Goulet JL, Goetz MB, Brown ST, Rodriguez-Barradas MC, et al. HIV Infection and Risk for Incident Pulmonary Diseases in the Combination Antiretroviral Therapy Era. *Am J Respir Crit Care Med* (2011) 183:388–95. doi: 10.1164/rccm.201006-0836OC
3. Meghji J, Miller RF. HIV and the Lung. *Med (Baltimore)* (2013) 41:435–41. doi: 10.1016/j.mpmed.2013.05.015
4. Drummond MB, Kirk GD, Astemborski J, Marshall MM, Mehta SH, McDyer JF, et al. Association Between Obstructive Lung Disease and Markers of HIV Infection in a High-Risk Cohort. *Thorax* (2012) 67:309–14. doi: 10.1136/thoraxjnl-2011-200702
5. Louie JK, Chin Hsu L, Osmond DH, Katz MH, Schwarcz SK. Trends in Causes of Death Among Persons With Acquired Immunodeficiency

Syndrome in the Era of Highly Active Antiretroviral Therapy, San Francisco, 1994-1998. *J Infect Dis* (2002) 186:1023–7. doi: 10.1086/343862
6. Sogaard OS, Lohse N, Gerstoft J, Kronborg G, Ostergaard L, Pedersen C, et al. Hospitalization for Pneumonia Among Individuals With and Without HIV Infection, 1995-2007: A Danish Population-Based, Nationwide Cohort Study. *Clin Infect Dis* (2008) 47:1345–53. doi: 10.1086/592692
7. Segal LN, Methé BA, Nolan A, Hoshino Y, Rom WN, Dawson R, et al. HIV-1 and Bacterial Pneumonia in the Era of Antiretroviral Therapy. *Proc Am Thorac Soc* (2011) 8:282–7. doi: 10.1513/pats.201006-044WR
8. Birx DL, Redfield RR, Tencer K, Fowler A, Burke DS, Tosato G. Induction of Interleukin-6 During Human Immunodeficiency Virus Infection. *Blood* (1990) 76:2303–10. doi: 10.1182/blood.V76.11.2303.bloodjournal76112303
9. Lahdevirta J, Maury CP, Teppo AM, Repo H. Elevated Levels of Circulating Cachectin/Tumor Necrosis Factor in Patients With Acquired Immunodeficiency Syndrome. *Am J Med* (1988) 85:289–91. doi: 10.1016/0002-9343(88)90576-1
10. Liovat A-S, Rey-Cuillé M-A, Lécuroux C, Jacquelin B, Girault I, Petitjean G, et al. Acute Plasma Biomarkers of T Cell Activation Set-Point Levels and of Disease Progression in HIV-1 Infection. *PloS One* (2012) 7:e46143. doi: 10.1371/journal.pone.0046143
11. Liu Z, Cumberland WG, Hultin LE, Kaplan AH, Detels R, Giorgi JV. CD8+ T-Lymphocyte Activation in HIV-1 Disease Reflects an Aspect of Pathogenesis Distinct From Viral Burden and Immunodeficiency. *J Acquir Immune Defic Syndr Hum Retrovirol* (1998) 18:332–40. doi: 10.1097/00042560-199808010-00004
12. Giorgi JV, Liu Z, Hultin LE, Cumberland WG, Hennessey K, Detels R. Elevated Levels of CD38+ CD8+ T Cells in HIV Infection Add to the Prognostic Value of Low CD4+ T Cell Levels: Results of 6 Years of Follow-Up. The Los Angeles Center, Multicenter AIDS Cohort Study. *J Acquir Immune Defic Syndr* (1993) 6:904–12.
13. Hazenberg MD, Otto SA, van Benthem BHB, Roos MTL, Coutinho RA, Lange JMA, et al. Persistent Immune Activation in HIV-1 Infection is Associated With Progression to AIDS. *AIDS* (2003) 17:1881–8. doi: 10.1097/00002030-200309050-00006
14. Roberts L, Passmore JAS, Mlisana K, Williamson C, Little F, Bebell LM, et al. Genital Tract Inflammation During Early HIV-1 Infection Predicts Higher Plasma Viral Load Set Point in Women. *J Infect Dis* (2012) 205:194–203. doi: 10.1093/infdis/jir715
15. Gumbi PP, Jaumdally SZ, Salkinder AL, Burgers WA, Mkhize NN, Hanekom W, et al. CD4 T Cell Depletion at the Cervix During HIV Infection Is Associated With Accumulation of Terminally Differentiated T Cells. *J Virol* (2011) 85:13333–41. doi: 10.1128/JVI.05671-11
16. Brenchley JM, Douek DC. HIV Infection and the Gastrointestinal Immune System. *Mucosal Immunol* (2008) 1:23–30. doi: 10.1038/mi.2007.1
17. Jambo KC, Sepako E, Fullerton DG, Mzinza D, Glennie S, Wright AK, et al. Bronchoalveolar CD4+ T Cell Responses to Respiratory Antigens are Impaired in HIV-Infected Adults. *Thorax* (2011) 66:375–82. doi: 10.1136/thx.2010.153825
18. Kalsdorf B, Scriba T, Wood K, Day CL, Dheda K, Dawson R, et al. HIV-1 Infection Impairs the Bronchoalveolar T-Cell Response to Mycobacteria. *Am J Respir Crit Care Med* (2009) 180:1262–70. doi: 10.1164/rccm.200907-1011OC
19. Kalsdorf B, Skolimowska KH, Scriba TJ, Dawson R, Dheda K, Wood K, et al. Relationship Between Chemokine Receptor Expression, Chemokine Levels and HIV-1 Replication in the Lungs of Persons Exposed to *Mycobacterium Tuberculosis*. *Eur J Immunol* (2013) 43:540–9. doi: 10.1002/eji.201242804
20. Twigg HLIII, Weiden M, Valentine F, Schnizlein-Bick CT, Bassett R, Zheng L, et al. Effect of Highly Active Antiretroviral Therapy on Viral Burden in the Lungs of HIV-Infected Subjects. *J Infect Dis* (2008) 197:109–16. doi: 10.1086/523766
21. Wood KL, Chaiyarit P, Day RB, Wang Y, Schnizlein-Bick CT, Gregory RL, et al. Measurements of HIV Viral Loads From Different Levels of the Respiratory Tract. *Chest* (2003) 124:536–42. doi: 10.1378/chest.124.2.536
22. Dean NC, Golden JA, Evans LA, Warnock ML, Addison TE, Hopewell PC, et al. Human Immunodeficiency Virus Recovery From Bronchoalveolar Lavage Fluid in Patients With AIDS. *Chest* (1988) 93:1176–9. doi: 10.1378/chest.93.6.1176
23. Linnemann CC, Baughman RP, Frame PT, Floyd R. Recovery of Human Immunodeficiency Virus and Detection of P24 Antigen in Bronchoalveolar Lavage Fluid From Adult Patients With AIDS. *Chest* (1989) 96:64–7. doi: 10.1378/chest.96.1.64
24. Agostini C, Poletti V, Zambello R, Trentin L, Siviero F, Spiga L, et al. Phenotypical and Functional Analysis of Bronchoalveolar Lavage Lymphocytes in Patients With HIV Infection. *Am Rev Respir Dis* (1988) 138:1609–15. doi: 10.1164/ajrccm/138.6.1609
25. Guillon JM, Autran B, Denis M, Fouret P, Plata F, Mayaud CM, et al. Human Immunodeficiency Virus-Related Lymphocytic Alveolitis. *Chest* (1988) 94:1264–70. doi: 10.1378/chest.94.6.1264
26. Twigg HLIII, Soliman DM, Day RB, Knox KS, Anderson RJ, Wilkes DS, et al. Lymphocytic Alveolitis, Bronchoalveolar Lavage Viral Load, and Outcome in Human Immunodeficiency Virus Infection. *Am J Respir Crit Care Med* (1999) 159:1439–44. doi: 10.1164/ajrccm.159.5.9808031
27. Young KR, Rankin JA, Naegel GP, Paul ES, Reynolds HY. Bronchoalveolar Lavage Cells and Proteins in Patients With the Acquired Immunodeficiency Syndrome. An Immunologic Analysis. *Ann Intern Med* (1985) 103:522–33. doi: 10.7326/0003-4819-103-4-522
28. Jambo KC, Banda DH, Kankwatira AM, Sukumar N, Allain TJ, Heyderman RS, et al. Small Alveolar Macrophages are Infected Preferentially by HIV and Exhibit Impaired Phagocytic Function. *Mucosal Immunol* (2014) 7:1116–26. doi: 10.1038/mi.2013.127
29. Bunjun R, Riou C, Soares AP, Thawer N, Müller TL, Kiravu A, et al. Effect of HIV on the Frequency and Number of Mycobacterium Tuberculosis-Specific CD4 + T Cells in Blood and Airways During Latent. *M Tuberculosis Infect J Infect Dis* (2017) 216:1550–60. doi: 10.1093/infdis/jix529
30. Rennard SI, Basset G, Lecossier D, O'Donnell KM, Pinkston P, Martin PG, et al. Estimation of Volume of Epithelial Lining Fluid Recovered by Lavage Using Urea as Marker of Dilution. *J Appl Physiol* (1986) 60:532–8. doi: 10.1152/jappl.1986.60.2.532
31. *R: A Language and Environment for Statistical Computing* (2020). Available at: www.R-project.org.
32. Kolde R. Pheatmap: Pretty Heatmaps. *R Package Version 1012* (2019). Available at: https://cran.r-project.org/package=pheatmap.
33. Oksanen J, Blanchet FG, Friendly M, Kindt R, Legendre P, McGlinn D, et al. Vegan: Community Ecology Package. *R Package Version 25-7* (2020). Available at: https://cran.r-project.org/package=vegan.
34. Tang Y, Horikoshi M , Li W. Ggfortify: Unified Interface to Visualise Statistical Result of Popular R Packages. *R J* (2016) 8:474.
35. Neuwirth E. RColorBrewer: ColorBrewer Palettes. *R Package Version 11-2* (2014). Available at: https://cran.r-project.org/package=RColorBrewer.
36. Columb MO, Sagadai S. Multiple Comparisons. *Curr Anaesth Crit Care* (2006) 17:233–6. doi: 10.1016/j.cacc.2006.03.005
37. Muema DM, Mthembu M, Schiff AE, Singh U, Corleis B, Chen D, et al. Contrasting Inflammatory Signatures in Peripheral Blood and Bronchoalveolar Cells Reveal Compartment-Specific Effects of HIV Infection. *Front Immunol* (2020) 11:1–13. doi: 10.3389/fimmu.2020.00864
38. Saetta M, Baraldo S, Corbino L, Turato G, Mapp CE, Maestrelli P, et al. CD8+ve Cells in the Lungs of Smokers With Chronic Obstructive Pulmonary Disease. *Am J Crit Care Med* (1999) 160:711–7. doi: 10.1164/ajrccm.160.2.9812020
39. Williams M, Todd I, Fairclough LC. The Role of CD8 + T Lymphocytes in Chronic Obstructive Pulmonary Disease: A Systematic Review. *Inflamm Res* (2021) 70:11–8. doi: 10.1007/s00011-020-01408-z
40. Di Stefano A, Caramori G, Ricciardolo FLM, Capelli A, Adcock IM, Donner CF. Cellular and Molecular Mechanisms in Chronic Obstructive Pulmonary Disease: An Overview. *Clin Exp Allergy* (2004) 34:1156–67. doi: 10.1111/j.1365-2222.2004.02030.x
41. Hoheisel GB, Tabak L, Teschler H, Erkan F, Kroegel C, Costabel U. Patients With Pulmonary Tuberculosis. *Am J Respir Crit Care Med* (1994) 149:460–3. doi: 10.1164/ajrccm.149.2.8306046
42. Schwander SK, Sada E, Torres M, Escobedo D, Sierra JG, Alt S, et al. and Immature Macrophage Alveolitis in Active Pulmonary Tuberculosis. *J Infect Dis* (1996) 173:1267–72. doi: 10.1093/infdis/173.5.1267
43. Diedrich CR, Mattila JT, Klein E, Janssen C, Phuah J, Sturgeon TJ, et al. Reactivation of Latent Tuberculosis in Cynomolgus Macaques Infected With SIV is Associated With Early Peripheral T Cell Depletion and Not Virus Load. *PloS One* (2010) 5:e9611. doi: 10.1371/journal.pone.0009611
44. Almodovar S, Knight R, Allshouse AA, Roemer S, Lozupone C, McDonald D, et al. Human Immunodeficiency Virus Nef Signature Sequences are Associated With Pulmonary Hypertension. *AIDS Res Hum Retroviruses* (2012) 28:607–18. doi: 10.1089/aid.2011.0021

45. Meignan M, Guillon JM, Denis M, Joly P, Rosso J, Carette MF, et al. Increased Lung Epithelial Permeability in HIV-Infected Patients With Isolated Cytotoxic T-Lymphocytic Alveolitis. *Am Rev Respir Dis* (1990) 141:1241–8. doi: 10.1164/ajrccm/141.5_Pt_1.1241
46. Marecki JC, Cool CD, Parr JE, Beckey VE, Luciw PA, Tarantal AF, et al. HIV-1 Nef is Associated With Complex Pulmonary Vascular Lesions in SHIV-Nef-Infected Macaques. *Am J Respir Crit Care Med* (2006) 174:437–45. doi: 10.1164/rccm.200601-005OC
47. Borchers MT, Wesselkamper SC, Curull V, Ramirez-Sarmiento A, Sánchez-Font A, Garcia-Aymerich J, et al. Sustained CTL Activation by Murine Pulmonary Epithelial Cells Promotes the Development of COPD-Like Disease. *J Clin Invest* (2009) 119:636–49. doi: 10.1172/JCI34462
48. Small BA, Dressel SA, Lawrence CW, Drake DR, Stoler MH, Enelow RI, et al. CD8(+) T Cell-Mediated Injury. *Vivo Progresses Absence Effector T Cells J Exp Med* (2001) 194:1835–46. doi: 10.1084/jem.194.12.1835
49. Galkina E, Thatte J, Dabak V, Williams MB, Ley K, Braciale TJ. Preferential Migration of Effector CD8+ T Cells Into the Interstitium of the Normal Lung. *J Clin Invest* (2005) 115:3473–83. doi: 10.1172/JCI24482
50. Kohlmeier JE, Miller SC, Woodland DL. Cutting Edge: Antigen Is Not Required for the Activation and Maintenance of Virus-Specific Memory CD8 + T Cells in the Lung Airways. *J Immunol* (2007) 178:4721–5. doi: 10.4049/jimmunol.178.8.4721
51. Woodland DL. T Cell Memory in the Lung Airways. *Proc Am Thorac Soc* (2005) 2:126–31. doi: 10.1513/pats.200501-003AW
52. Spurrell JCL, Wiehler S, Zaheer RS, Sanders SP, Proud D. Human Airway Epithelial Cells Produce IP-10 (CXCL10) In Vitro and *In Vivo* Upon Rhinovirus Infections. *Am J Physiol Lung Cell Mol Physiol* (2005) 289:L85–95. doi: 10.1152/ajplung.00397.2004
53. Jiang D, Liang J, Guo R, Xie T, Kelly FL, Martinu T, et al. Long-Term Exposure of Chemokine CXCL10 Causes Bronchiolitis-Like Inflammation. *Am J Respir Cell Mol Biol* (2012) 46:592–8. doi: 10.1165/rcmb.2011-0116OC
54. Brenchley JM, Paiardini M, Knox KS, Asher AI, Cervasi B, Asher TE, et al. Differential Th17 CD4 T-Cell Depletion in Pathogenic and Nonpathogenic Lentiviral Infections. *Blood* (2008) 112:2826–35. doi: 10.1182/blood-2008-05-159301
55. Denis M, Ghadirian E. Alveolar Macrophages From Subjects Infected With HIV-1 Express Macrophage Inflammatory Protein-1 Alpha (MIP-1 Alpha): Contribution to the CD8+ Alveolitis. *Clin Exp Immunol* (1994) 96:187–92. doi: 10.1111/j.1365-2249.1994.tb06540.x
56. Neff CP, Chain JL, MaWhinney S, Martin AK, Linderman DJ, Flores SC, et al. Lymphocytic Alveolitis Is Associated With the Accumulation of Functionally Impaired HIV-Specific T Cells in the Lung of Antiretroviral Therapy–Naive Subjects. *Am J Respir Crit Care Med* (2015) 191:464–73. doi: 10.1164/rccm.201408-1521OC
57. Norris PJ, Pappalardo BL, Custer B, Hecht FM, Busch MP. Elevations in IL-10, TNF-α, and IFN-γ From the Earliest Point of HIV Type 1 Infection. *AIDS Res Hum Retroviruses* (2008) 22:757–62. doi: 10.1089/aid.2006.22.757
58. Roberts L, Passmore JS, Williamson C, Bebell LM, Mlisana K, Burgers WA, et al. Plasma Cytokine Levels During Acute HIV-1 Infection Predict HIV Disease Progression. *Aids* (2010) 24:819–31. doi: 10.1097/QAD.0b013e3283367836
59. Stacey AR, Norris PJ, Qin L, Haygreen EA, Taylor E, Heitman J, et al. Induction of a Striking Systemic Cytokine Cascade Prior to Peak Viremia in Acute Human Immunodeficiency Virus Type 1 Infection, in Contrast to More Modest and Delayed Responses in Acute Hepatitis B and C Virus Infections. *J Virol* (2009) 83:3719–33. doi: 10.1128/JVI.01844-08
60. Wada NI, Jacobson LP, Margolick JB, Breen EC, Macatangay B, Penugonda S, et al. The Effect of HAART-Induced HIV Suppression on Circulating Markers of Inflammation and Immune Activation. *AIDS* (2015) 29:463–71. doi: 10.1097/QAD.0000000000000545
61. Chen K, Kolls JK. T Cell-Mediated Host Immune Defenses in the Lung. *Annu Rev Immunol* (2013) 31:605–33. doi: 10.1146/annurev-immunol-032712-100019
62. Meziane O, Alexandrova Y, Olivenstein R, Dupuy FP, Salahuddin S, Thomson E, et al. Peculiar Phenotypic and Cytotoxic Features of Pulmonary Mucosal CD8 T Cells in People Living With HIV Receiving Long-Term Antiretroviral Therapy. *J Immunol* (2021) 3:641–51. doi: 10.4049/jimmunol.2000916
63. Heath L, Fox A, McClure J, Diem K, van Wout AB, Zhao H, et al. Evidence for Limited Genetic Compartmentalization of HIV-1 Between Lung and Blood. *PloS One* (2009) 4:e6949. doi: 10.1371/journal.pone.0006949
64. Corleis B, Bucsan AN, Deruaz M, Vrbanac VD, Lisanti-Park AC, Gates SJ, et al. HIV-1 and SIV Infection Are Associated With Early Loss of Lung Interstitial CD4+ T Cells and Dissemination of Pulmonary Tuberculosis. *Cell Rep* (2019) 26:1409–18. doi: 10.1016/j.celrep.2019.01.021
65. Nakata K, Weiden M, Harkin T, Ho D, Rom WN. Low Copy Number and Limited Variability of Proviral DNA in Alveolar Macrophages From HIV-1-Infected Patients: Evidence for Genetic Differences in HIV-1 Between Lung and Blood Macrophage Populations. *Mol Med* (1995) 1:744–57. doi: 10.1007/BF03401889
66. Itescu S, Simonelli PF, Winchester RJ, Ginsberg HS. Human Immunodeficiency Virus Type 1 Strains in the Lungs of Infected Individuals Evolve Independently From Those in Peripheral Blood and are Highly Conserved in the C-Terminal Region of the Envelope V3 Loop. *Proc Natl Acad Sci U S A* (1994) 91:11378–82. doi: 10.1073/pnas.91.24.11378

Conflict of Interest: The authors declare that the research was conducted in the absence of any commercial or financial relationships that could be construed as a potential conflict of interest.

frontiers in Immunology

REVIEW
published: 15 November 2021
doi: 10.3389/fimmu.2021.772004

Pulmonary Eosinophils at the Center of the Allergic Space-Time Continuum

Sjoerd T. T. Schetters[1,2*] *and Martijn J. Schuijs*[1,2,3*]

[1] Department of Internal Medicine and Pediatrics, Ghent University, Ghent, Belgium, [2] Laboratory of Immunoregulation and Mucosal Immunology, VIB-UGent Center for Inflammation Research, Ghent, Belgium, [3] Cancer Research Institute Ghent, Ghent, Belgium

Eosinophils are typically a minority population of circulating granulocytes being released from the bone-marrow as terminally differentiated cells. Besides their function in the defense against parasites and in promoting allergic airway inflammation, regulatory functions have now been attributed to eosinophils in various organs. Although eosinophils are involved in the inflammatory response to allergens, it remains unclear whether they are drivers of the asthma pathology or merely recruited effector cells. Recent findings highlight the homeostatic and pro-resolving capacity of eosinophils and raise the question at what point in time their function is regulated. Similarly, eosinophils from different physical locations display phenotypic and functional diversity. However, it remains unclear whether eosinophil plasticity remains as they develop and travel from the bone marrow to the tissue, in homeostasis or during inflammation. In the tissue, eosinophils of different ages and origin along the inflammatory trajectory may exhibit functional diversity as circumstances change. Herein, we outline the inflammatory time line of allergic airway inflammation from acute, late, adaptive to chronic processes. We summarize the function of the eosinophils in regards to their resident localization and time of recruitment to the lung, in all stages of the inflammatory response. In all, we argue that immunological differences in eosinophils are a function of time and space as the allergic inflammatory response is initiated and resolved.

Keywords: eosinophils, immunology, asthma, lung, allergic airway inflammation, innate immunity

OPEN ACCESS

Edited by:
Rabindra Tirouvanziam, Emory University, United States

Reviewed by:
Franz Puttur, Imperial College London, United Kingdom
Eva Sverremark-Ekström, Stockholm University, Sweden

****Correspondence:***
Sjoerd T. T. Schetters
sjoerd.schetters@irc.vib-ugent.be
Martijn J. Schuijs
martijn.schuijs@irc.vib-ugent.be

Specialty section:
This article was submitted to Mucosal Immunity, a section of the journal Frontiers in Immunology

Received: *07 September 2021*
Accepted: *27 October 2021*
Published: *15 November 2021*

Citation:
Schetters STT and Schuijs MJ (2021) Pulmonary Eosinophils at the Center of the Allergic Space-Time Continuum. Front. Immunol. 12:772004. doi: 10.3389/fimmu.2021.772004

INTRODUCTION

Eosinophils represent a minority population of peripheral leukocytes of the innate immune system. They are largely evolutionary conserved and classically considered terminally differentiated end-stage cells (1). Eosinophils develop in the bone marrow from myeloid precursors under the influence of interleukin (IL)-5. Although IL-5 is critical for eosinophil differentiation, priming, and survival, other cytokines, as IL-3 and granulocyte-macrophage colony stimulating factor (GM-CSF) also promote eosinophil differentiation (2). Upon release into the circulation eosinophils are present in the peripheral blood for a few hours; however, they can survive in tissues for several weeks and adopt tissue-specific homeostatic phenotypes (3). The ability of eosinophils to remain in tissues for

extended periods of time suggest they have a necessary role in homeostasis or preventing disease (2). As postulated in the Local Immunity And/or Remodeling/repair (LIAR) hypothesis, by James Lee, eosinophils can be considered intrinsically homeostatic cells that are associated with sites characterized by high cell proliferation/turn-over and cell death (4). Indeed, eosinophils are, under homeostatic conditions, distributed in many organs like the lung, spleen, and gastrointestinal tract, as well as in the blood, lamina propria and adipose tissue (5). As such, these cells are proposed to have a physiological function in each of these different organs, which is strengthened by evidence on the existence of multiple tissue specific subtypes of eosinophils based on distinct surface marker expression and functional characteristics (6, 7). Although they are equipped with an arsenal of pre-formed inflammatory mediators and have the ability to produce several cytokines, eosinophils are most well-recognized for their pivotal role in the inflammatory pathology of a broad range of diseases, including parasitic infections and allergic disease, such as food allergy, asthma, and atopic dermatitis (8). Whether eosinophils are also involved in the resolution phase of these inflammatory afflictions is largely unknown. In general, the immune response after acute inflammation and the accompanying tissue damage is meant to resolve inflammation, repair tissue and re-establish tissue homeostasis.Therefore, it is essential to accurately study the function of immune cells, not only regarding their location, but also include their temporal exposure to different microenvironments at that location. Here we emphasize the need to define eosinophils during acute, late, and chronic inflammatory responses, as well as resolution in lung inflammation in regards to both time and space.

EOSINOPHILS IN MAINTENANCE OF IMMUNOLOGICAL HOMEOSTASIS

At birth very few eosinophils are present in the lungs of mice, however they are recruited by IL-5 from type-2 innate lymphoid cells (ILC2) under the influence of epithelium-derived IL-33 coinciding with the alveolarization phase at post-natal day (PND) 3. After which they rapidly increase in number, peaking on PND14, before the eosinophils decline again after weaning (9). Importantly, eosinophil adopt a type 2 activated immune phenotype during this phase (10). In humans, eosinophils have been shown to be present as early as fetal thymic development (11). From birth onwards the lungs are constantly exposed to a variety of airborne particles and these insults typically result in clearance without acute inflammation, as well as antigenic tolerance. Several studies, in both mice and humans (12, 13), have shown that eosinophils spend between 3 and 24 hours in circulation, however their half-life in the lung is prolonged to about 36 hours (3). Additionally, homeostatic lung eosinophils express several genes, like *Runx3, Serpinb1a*, and *Ldlr*, that are implicated in the maintenance of lung immune homeostasis and negative regulation of T helper cell type 2 (Th2 cell) responses (14). In line with these observations, studies in eosinophil-deficient mice have revealed that sensitivity to house dust mite (HDM) is increased in the absence of eosinophils (14). The unique capability of lung homeostatic eosinophils to prevent Th2-driven allergic airway inflammation has been linked to their ability to inhibit the maturation of allergen-loaded dendritic cells (DCs) (14). However, seeing that eosinophils are central to the alveolarization phase early in life, the widespread use of congenital ΔdblGATA mice and PHIL mice, that both lack eosinophils, may significantly confound experiments performed in adult life. It is still unclear how the absence of eosinophils at birth will impact later respiratory challenges like allergens, bacterial and viral infections.

In the steady state adult lung, Mesnil et al. have identified a small population of tissue-resident eosinophils (rEos). These eosinophils are found to express distinct surface markers like the L-selectin receptor CD62L, that is distinct from "inflammatory" eosinophils (iEos) appearing after allergic inflammation. Even though rEos express the IL-5 receptor, their presence in the lung seem to be IL-5 independent and may promote the development of Th1 immunity by impairing the ability of DCs to induce Th2 immunity (14). In contrast, earlier findings of Nussbaum et al. suggest that basal eosinophilopoiesis and accumulation of eosinophils in tissues is dependent on ILC2-derived IL-5 (15). These apparent contradictions on the role of IL-5 in basal conditions of tissue-eosinophilia highlight the need for a better characterization of the precise role these lung-resident eosinophils have, especially when translating these findings to the human lung (16). Recently, an intra vital microscopy study in mice showed patrolling eosinophils in the lung vasculature, which were differentially activated after stimulation with ovalbumin (OVA)-allergen, suggesting these resident cells to be reactive to allergenic insults (17). Activation of eosinophils to airborne allergens is often studied with purified molecules, like: IL-33, papain, and Aspergillus protease. The use of these type-2 inducing agents allow for a reductionistic experimental system to investigate airway allergy. However, real-life allergens (e.g. HDM) better recapitulate the spatiotemporal interplay between innate and adaptive immunity, including the pleiotropic function of eosinophils epitomized in this review. With new tools becoming available homeostatic- or resident-lung eosinophils can be further characterized and questions on their contribution to the maintenance of homeostasis and tolerance in the lung and the presence of different eosinophil subpopulations can be addressed.

EOSINOPHILS PROMOTE TH2 DIFFERENTIATION DURING SENSITIZATION (PRE-CHALLENGE)

The first encounter with allergens, like; HDM, and the absence of type 1 inflammatory signals in early life ("hygiene hypothesis") – sets the stage for allergic pathology later in life (18). It is now clear that the airway epithelial cells (ECs) play an important role in the induction of allergen-induced inflammatory responses

(19). Not only can epithelial cell damage be seen in all phenotypes of asthma, changes in EC function can be observed at very young age, cumulating to the idea that ECs may play a role in the initiation of asthma in early life (20, 21). The link between epithelial barriers and eosinophils is supported by their preferred association with epithelial barrier tissues, where foreign antigens are most often encountered (6). Amongst these structural barrier cells are pulmonary neuroendocrine cells (PNECs) that are specialized tissue-resident neuroendocrine cells in the airway epithelium (22). PNECs can be innervated by both parasympathetic and sympathetic neuronal fibers (23, 24). With close proximity to steady-state immune cells, like ILC2, PNECs have the ability to amplify allergen-induced immune cell recruitment, including eosinophils (25). Interestingly, eosinophils in turn have been shown to contribute to increased nerve density and airway nerve remodeling which serves as a key mechanism for increased irritant sensitivity and exaggerated airway responsiveness (26).

For the initiation of antigen-specific Th2 responses in the lung, conventional DC2s (cDC2s) need to migrate to the draining lymph nodes, a process augmented by ILC2-derived IL-13, mast cell-derived TNF, epithelial cell-derived GM-CSF, and by type-1 interferon (27–29). Although unclear in the pulmonary setting, in the murine intestine it is proposed that eosinophils play an important role in the activation of DCs and their migration to the draining lymph nodes (30). Eosinophils have also been shown to produce an antimicrobial protein, eosinophil-derived neurotoxin (EDN), that effectively recruits and activates cytokine producing DCs, thereby enhancing Th2 immune responses (31–33). Besides promoting DC activation, murine intestinal and lymph node eosinophils have been reported to express antigen presentation machinery, including; MHC-II, costimulatory molecules CD80 and CD86, and migrate to the draining lymph nodes in a CCR7-dependant manner (34–36). Interestingly, human peripheral blood eosinophils exhibit very low to undetectable levels of MHC-II, whereas class-II expression is observed on airway eosinophils (37, 38). Eosinophils are observed within the T cell zone of the draining lymph nodes, have the ability to present antigen, and express transcripts for IL-4 and IL-13. However, the low number of these cells in the lymph nodes suggest that eosinophils have a minor role as antigen presenting cells and instead may be required for the accumulation of DCs within the lymph nodes and subsequent antigen-specific T effector cell production (39). Interestingly, these effects were independent of MHC-II expression on eosinophils, again proposing an accessory role for eosinophils in the process of T cell stimulation. Moreover, human blood-derived eosinophils have been shown to induce DC maturation by physically interacting with DCs in the presence of bacterial pathogen-associated molecular patterns (PAMPs) (40).

Together, these data demonstrate that eosinophil-derived products can promote Th2 inflammation *via* DC regulation during the sensitization phase to an allergen. At the same time, lymph node eosinophils actively suppress DC-induced Th17 and Th1 responses, thereby promoting Th2 polarization (39). It should be noted that timed depletion of eosinophils using iPHIL mice in the sensitization phase of HDM or OVA allergic airway inflammation did not affect the outcome of type 2 immunity or lung function following allergen challenge, suggesting that eosinophils may have a more subtle effect on downstream adaptive immunity (41). In all, the process of allergic sensitization, aided by eosinophils, results in the proliferation of Th2 cells, the appearance of class-switched plasma cells producing allergen-specific IgE, and the presence of IgE/FcεR1-intraepithelial mast cells in the lung.

PHASES OF ALLERGIC LUNG INFLAMMATION

Any inflammatory response is subject to critical changes through space and time, especially in damage-prone tissues like the lungs (42, 43). The allergic inflammatory response has been classified in terms of three temporal phases of inflammation, the acute, late, and chronic phase (44). Even though this paradigm is now well accepted, surprisingly little is known about the differences in eosinophil functioning during these distinct phases of allergic inflammation. Indeed, complete eosinophil-deficient animals do not distinguish between differential functioning in these phases, significantly hampering understanding of the exact role of eosinophils. For example, *in vitro* exposure of murine blood-derived eosinophils to a certain set of cytokines defines their phenotype in the lung when adoptively transferred *in vivo (*45*)*. Indeed, type 2 cytokines known to affect eosinophils like IL-4, IL-5 and IL-13, chemokines like CCL11 and lipid mediators, like cysteinyl leukotrienes (CysLTs) are produced by different cell types, in different locations and at different time points during the allergic inflammatory process (19). In an effort to holistically address the multi-wave inflammatory response, Walsh and colleagues constructed a network model of allergic airway inflammation that was supported by experimental perturbation experiments (46). They reported early induction of airway hyperresponsiveness (AHR) relied on mast cells in the early phase and on Th2 cells and eosinophils in the late phase. Interestingly, IL-13 seemed to differentially affect AHR in a distinctive manner through time. Other efforts are now being made to conceptualize and visualize these time-dependent inflammatory processes (47). In this review, by visualizing the allergic airway response in space and time in **Figure 1**, we aim to illuminate the heterogeneity of environments and molecular input that govern eosinophil functioning in a spatiotemporal manner.

Acute Phase (Minutes to Hours)

In the lower airways, alveolar macrophages (AMs) are the main immune cell type encountering airborne particles, the lung-resident commensal microbiome and tasked with maintaining homeostasis (48). They actively patrol the alveoli in homeostasis and develop under the influence of epithelial-derived TGFβ and GM-CSF (49–51). As such, it is not surprising that these cell types are found to behave distinctly different in the allergen-

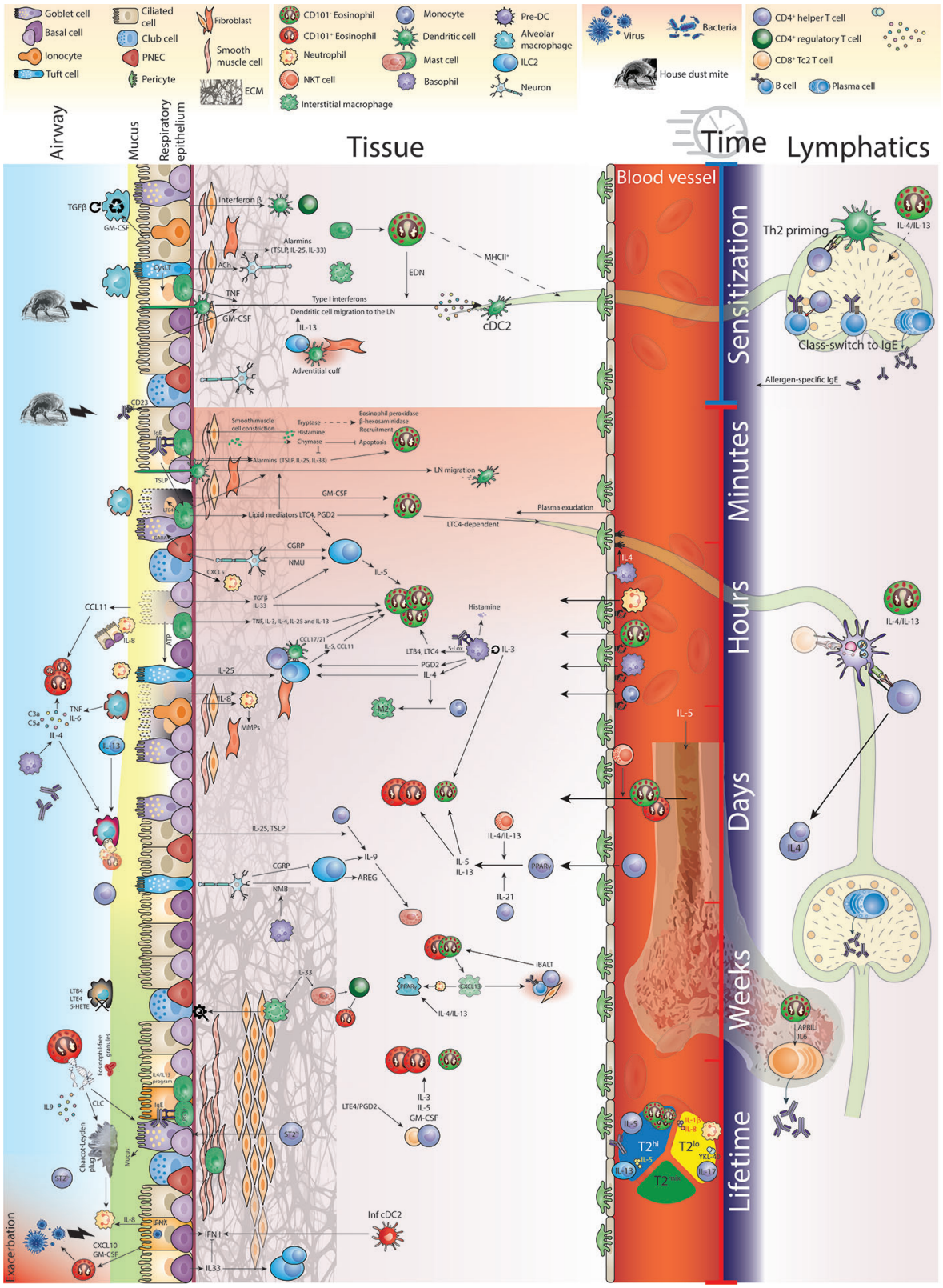

FIGURE 1 | Eosinophil function in time and space during allergic airway inflammation.

challenged lung (52). As the inflammatory response develops and the alveolar space is intruded by other immune cells, like eosinophils, the concerted immune response is highly dynamic. At first, for the AM to initiate and support inflammation, it needs multiple molecular cues to override the TGFβ-driven tolerogenic phenotype (48, 53). Loss of AMs results in exacerbated cellular and humoral type 2 immunity (54). Recognition of HDM by AMs is mediated by Dectin-2 and results in the downstream production of CysLTs (55, 56). Alveolar macrophages readily phagocytose airborne particles and it is now recognized that the phagocytic capacity of these macrophages is dysfunctional in asthmatic patients (52). Interestingly, phagocytosis of apoptotic cells suppressed HDM-induced allergic lung inflammation (57). As the clearing capacity of macrophages is reduced, allergens like HDM can further induce epithelial responses.

Allergen-induced epithelial responses initiate the production of the cytokines IL-33, IL-25, and thymic stromal lymphopoietin (TSLP) that are released upon epithelial activation or damage. In the (naïve) lung, a wide variety of cells respond to these cytokines, including ILC2, DCs, macrophages, mast cells, basophils, and eosinophils (58). Activation of these diverse cell types leads to reciprocal interactions and the release of additional mediators. Especially ILC2 have been shown to coordinate eosinophilia in response to allergen, since they localize and migrate in close proximity to epithelial cells (59). Several cytokines can activate ILC2 in the early stage, epithelial-derived IL33 and TGFβ (60), as well as basophil-derived IL-4 (61), and tuft cell-derived IL-25 and CysLTs (62), of which the end product LTE4 is even detectable in the bronchoalveolar lavage fluid and urine of patients with asthma exacerbations (63). ILC2-derived IL-5 will act as an early mediator of eosinophil differentiation and hematopoiesis. At the same time, ILC2-derived IL-13 enhances the expression of eotaxins that assist with eosinophil recruitment (62). In turn, eosinophils can maintain ILC2 activation through the release of IL-4. Moreover, eosinophils can directly bind IL-33, inducing a wide range of transcripts supporting eosinophil activation (64). Whereas, TSLP has a major role in the recruitment of eosinophil into the respiratory tract (65), it also induces pro-survival mechanisms through direct binding of TSLP by its receptor on eosinophils (66). Besides controlling eosinophil numbers, ILC2 also license DCs to trigger adaptive Th2 cell responses (67). Furthermore, epithelial cells in the allergic lung produce GM-CSF, which controls the recruitment and survival of eosinophils in the lung directly (68). It has further been shown that activation of the NF-κB pathway in the epithelial lineage is crucial for the downstream allergic immune cascade in response to HDM (69) and interference in this cascade early in life can prevent the onset of allergic disease (18).

In recent years it has been demonstrated that large functional heterogeneity exists within the epithelial cell lineage at distinct areas of the respiratory system. Specialized tuft cells contribute to type 2 immune responses and eosinophilia through the production of IL-25 and CysLTs (70, 71). When tuft cells recognize the epithelial stress trigger ATP, they release LTC4, LTD4 and LTE4, which can augment the sensitivity of ILC2 to type 2 inflammatory mediators (72, 73). PNECs are solitary cells in the epithelium of the upper airways and function as chemosensors to respond to changes in oxygen, mechanical- and chemical stimuli by producing neuroactive mediators (22, 74). Mice lacking PNECs have been shown to exhibit reduced allergic inflammation and eosinophilia as ILC2 become less activated (75). In humans, PNECs are found to be increased in number in asthma patients, producing the neuropeptide CGRP and the neurotransmitter GABA increasing ILC2-derived IL-5 and promoting goblet cell hyperplasia, respectively (75). Activation of steady state ILC2 can be further stimulated by the neuron-derived neuromedin U, especially in the presence of IL-25 (76, 77). The specific location of these neuroimmune cell units in the lung and the temporal activation of these early response hubs in allergic inflammation will need further investigation in relation to whether and how they have direct effects on eosinophil activation (78). Importantly, allergen detection may not only be constrained to the apical side of the epithelial layer and its associated cells, as epithelial CD23 (the low-affinity IgE receptor) can bind and transcytose allergen-specific-IgE, resulting in increased allergic inflammation (79).

After the lung is sensitized to the allergen in a type-2 dominant manner, intraepithelial mast cells are primed by expressing FCεR1 binding allergen-specific IgE. Upon allergen stimulation, membrane-bound IgE clusters FCεR1 on mast cells leading to immediate degranulation and the release of pre-formed vesicles filled with histamine and enzymes like tryptase and chymase (80). A reciprocal relationship exists between mast cells and eosinophils, with mast cells supporting eosinophil survival and activation by secreting IL-5. Genetic knockout of mast cells reduced eotaxin levels in the lung of HDM challenged mice and impaired eosinophil recruitment (81). Eosinophil-derived MBP in turn directly activates mast cells and basophils, releasing histamine and TNF (2). It has now been established that mast cell-derived acute phase proteases modulate asthma pathology (reviewed in (82)). Moreover, histamine has multiple direct asthma-related effects in the lung, including; plasma exudation due to increased vascular permeability, release of mucus, and constriction of small respiratory passages (83). Tryptase levels in blood and airway fluid are elevated in asthma patients and correlate with disease severity (84). Interfering with tryptase using antagonistic antibodies reduced mast cell activation and the use of tryptase inhibitors or serine protease inhibitors reduced eosinophil infiltrates (85, 86). Besides, human β-tryptase has been shown to enzymatically inhibit eotaxin and RANTES function, possibly affecting eosinophil recruitment (87). Additionally, human peripheral blood eosinophils respond to enzymatically active tryptase by the release of eosinophil peroxidase and beta-hexosaminidase (88), although it remains to be determined whether the lung resident eosinophils in mice would contribute to the acute phase inflammatory response after release of tryptase. Chymase has been assigned a plethora of asthma-related activities, including increasing mucus production, modification of extracellular matrix and modulation of cytokines like IL-33, IL-4, and IL-1β (89). However,

exploration of chymase (specifically, the direct mouse homologue Mcpt4) in murine models of asthma, suggests a protective role in pathology (90), possibly through the degradation of IL-33 (91). The effect on eosinophils specifically includes the suppression of apoptosis and induction of chemokine production (92).

Secondary to pre-stored granule proteins, mast cells synthesize eicosanoids within minutes and cytokines, chemokines, and growth factors in a matter of hours. Eicosanoids like the arachidonic acid metabolites prostaglandin (PG) D2, LTB4, LTC4, hydroperoxy-eicosatetraenoic acid, and hydroxy-eicosatetraenoic acid (5-HETE) influence eosinophil trafficking and function in asthma and allergic diseases (93, 94). The early CysLTs and PGD2 prime ILC2s by upregulating cytokine receptors that respond to the epithelial cell-derived cytokines IL-33 and IL-25 (62). An intravital microscopy study in mice showed that IL-33 induced $CCR8^+$ ILC2s to patrol the peribronchial and perivascular spaces, possibly localizing eosinophil recruitment to CCL8-rich sites of inflammation (59). Of the prostaglandins, PGD2 can directly bind its receptor DP2/CRTH2 on eosinophils (95, 96), which is robustly expressed on both murine and human eosinophils (97). Exposure of eosinophils to PGD2 induces both activation and chemotaxis (98, 99). Activated mast cells further promote the migration of DCs to the draining LN, contributing to the initiation of adaptive immunity (100). Mast cells further produce cytokines, like IL-3, TNF, IL-4, IL-8, IL-13 and IL-25 (44) and especially, mast cell-derived IL-3 is suggested to play a key role in modulating eosinophil functioning in allergic asthma (101). In fact, IL3 polymorphisms have been associated with decreased risk of asthma (102). In both asthmatic and non-allergic lung eosinophilia, IL-3 production by type 2 $CD8^+$ (Tc2) cells is found to be increased (103, 104). However, it is unclear at which stage in the allergic response $CD8^+$ Tc2 cells are a significant source of IL-3 for eosinophils.

The highly coordinated acute response to allergens at the epithelial barrier seems to set the stage for the downstream allergic inflammatory eosinophilia. However, the immediate response of lung resident eosinophils or the early infiltration of circulating eosinophils upon antigen challenge are poorly investigated, with most studies investigating time points often days after the last antigenic challenge. The early inflammatory landscape is coordinated by epithelial cells, mast cells, ILC2 and neurons, and their products will primarily target resident eosinophils. At the same time, basophil-derived IL-4 and ILC2-derived IL-5, as well as eotaxin, recruit eosinophils from the periphery. However, upon arrival in the lung the inflammatory input for those cells has changed. It is unknown how the lung resident and infiltrating eosinophils coordinate this response. In addition, the type and combination of inflammatory triggers in the lung, may affect the granulocytic composition. For example, early (30 minute) recruitment of CD101- eosinophils after LPS instillation in the lung, suppress neutrophilic lung inflammation (105). However, combined with HDM, LPS induced neutrophil-derived cytoplasts and neutrophil extracellular trap (NET) formation in the broncho-alveolar lavage (BAL) after 24 hours and increased Th17 cells in the lung-draining lymph nodes (106). The acute phase response is mostly "outward-in"; however, some immediate immune reactions can be found in the alveolar space. Within the alveolar space of allergic asthmatic patients' segmental challenge with ragweed showed increases in histamine, PGD2 and thromboxane B2 within 5 minutes of exposure (107). Although, no cellular changes were yet observed at this early timepoint. It will be exciting to see how the division of labor between resident and incoming eosinophils is established and how this shapes the propagation of the allergic response.

Late Phase (Hours to Days)

As local innate inflammation progresses into the late phase, the tissue-contained response is joined by innate cells from the circulation, including neutrophils, eosinophils, basophils and monocytes (44). The lung endothelium is conditioned to allow the tethering, rolling and extravasation of leukocytes into the lung tissue (108). Apart from the chemo-attractants discussed above, endothelial priming is induced by several cell types, like NKT cells and basophils. Whereas mast cells reside in the lung tissue, the majority of basophils are recruited from the periphery into the lung after allergen challenge and affect eosinophil recruitment and function (109, 110). In the late phase of the asthmatic response, basophils are the major IgE bearing granulocyte producing histamine (111). Basophils can, like mast cells, produce IL-3 in response to IgE/FcεR triggering and facilitate an autocrine activation loop (112, 113). However, as reported above, IL-3 actively affects eosinophil function. In addition to their pro-inflammatory function, murine basophils also prime lung ILC2s to respond to the neuropeptide neuromedin B, possibly to inactivate type 2 immune responses and to aid resolution (114). Moreover, through production of lipoxygenases and cyclooxygenases, mast cells and basophils can balance the metabolism of arachidonic acid into leukotrienes and prostaglandins. For example, allergen/IgE-stimulated bone-marrow-derived basophils were found to secrete 5-lipoxygenase (5-Lox) metabolites LTB4 and LTC4 within 30 minutes of exposure (115). In turn, cyclooxygenase (COX)-metabolites like PGD2 and PGE2 were secreted 6 hours after stimulation. This temporal separation adds to their ability to modulate immune responses and the recruitment of immune cells like eosinophils.

Recruitment of circulating eosinophils into the inflamed lung seems to be regulated at several levels. In asthmatic patients, basophil-derived IL-4 is the cardinal cytokine for recruitment of eosinophils into the lung and was found in the bronchoalveolar lavage within 20 hours after segmental allergen challenge (116). The secreted IL-4 could in turn induce a dose and time-dependent increase in the levels of eotaxin mRNA within fibroblasts (117). Additionally, eotaxin-3 expressed by IL-4-stimulated human vascular endothelial cells may contribute to CCR3-dependent eosinophil accumulation in the lung (118). Similarly, human endothelial cells stimulated with IL-4 increased the expression of VCAM-1, which binds to eosinophil VLA-4 contributing to eosinophil extravasation after allergen challenge (119). Otherwise,

Coyle and colleagues reported that IL-4 neutralization just before allergen challenge had little effect on eosinophil infiltration, suggesting that although IL-4 is required for the induction of Th2 immunity, it may be dispensable for eosinophil recruitment in the challenge phase (120). Recently, Felton and colleagues have shown that eosinophil recruitment into tissues is intrinsically dependent on expression of the Ikaros zinc-finger family transcription factor IKZF3 (Aiolos), as Aiolos-deficiency reduced eosinophil CCR3 expression, and subsequent CCL11-induced intracellular ERK1/2 signaling (121). Yi et al. have further shown that it is a network of cDC2s that converge on lung cDC1s, which produce CCL17 and CCL22, directly attracting CCR4-expressing eosinophils (122). Interestingly, the early recruitment within a day was mediated by $CD24^-$ cDC2s producing nitric oxide affecting cDC1 activation, whereas eosinophil recruitment was aborted *via* TGFβ-producing $CD24^+$ cDC2s in later phases of the inflammatory response (122). CCL17 and -22 not only affect eosinophils, as these chemokines are reported to actively recruit T cells to the lungs sustaining type 2 inflammation (123). The need for eosinophils to induce T cell infiltration in allergic airway inflammation was further corroborated (124), although this prerequisite might be less pronounced in BALB/c mice (125, 126). It is likely that the division of labor by DCs in the lung upon inflammation is tightly coordinated in a spatiotemporal manner to allow DC emigration, T cell activation in the lymph node and T cell recruitment to the lung, but also supply the lung parenchyma with the proper inflammatory context. Circulating eosinophils, resident eosinophils, recruited eosinophils, and bone marrow eosinopoiesis should ideally be analyzed independently, since they are likely functionally different or at least different in their susceptibility to external input. *In vivo* challenge studies in mild asthmatic patients have shown eosinophil-specific changes in the BAL transcriptome 48 hours after segmental bronchoprovocation with allergen (127). These changes may well be induced by infiltrating eosinophils receiving different environmental cues. Possibly, tissue damage is sufficient to induce eosinophil recruitment, as is evidenced by intravital microscopy of lung tissue at 12 hours post silica particle-induced acute injury (17). Moreover, radiolabeled eosinophils injected intravenously into asthmatic patients or healthy volunteers also showed lung infiltration within minutes, with asthmatic patients showed higher eosinophil migration to the lung (128).

Neutrophils also play an important role in allergic lung inflammation and their presence has been related to separate endotypes of asthma. For example, the presence of high bronchial neutrophilia with similar levels of eosinophilia was related to increased serum IgE, IL-17 production and clinical corticosteroid dependence (129). The recruitment of neutrophils in the lung is governed by epithelial club cells under the influence of the circadian rhythm, which mode of attraction underlies the anti-inflammatory capacity of dexamethasone (130). Additionally, neutrophil activation in the form of dsDNA-rich NETosis has been implicated in virally-induced asthma exacerbations of type-2 responses in the acute phase of the immune response (131) (discussed in more detail below). Interestingly, neutrophil depletion in the HDM mouse model exacerbated type 2 inflammation and airway pathology (132). This exacerbation was attributed to increased systemic G-CSF, which activated ILC2 and enhanced antigen presentation by monocyte-derived dendritic cells. In addition, a recent study has shown that IL-17a and TNFs stimulation of lung epithelium resulted in local G-CSF (CSF3) production, leading to increased granulopoiesis and both systemic and respiratory neutrophilia (133). However, the prerequisite of IL-17a and TNF would suggest this process to be relevant in the adaptive phase of the inflammatory response, when helper T cell cytokines are abundant. Increased neutrophilia in asthmatics has been shown to be dependent on epithelial cells and IL-8 derived from smooth muscle cells (134, 135). Although IL-8-mediated neutrophilia may beneficially affect immunity to bacterial lung infection, the resulting extensive lung remodeling may lead to impaired lung function in asthmatics (136).

As the lung tissue recruits cells from the circulation, certain immune cells cross the epithelial barrier to the bronchoalveolar space, including eosinophils, basophils and lymphocytes (107). Within 4 hours after segmental allergen challenge in asthmatic patients, eosinophils are recruited to the alveolar space by epithelial-derived eotaxin (137). Another study in humans found increased ILC2 in the BAL at 24 hours after segmental challenge. Moreover, BAL ILC2 expressed higher levels of IL-13 transcript relative to blood ILC2 (138). At the same time, allergen-specific IgE, C3a, C5a and IL-9 accumulates in the BAL (139–141). Allergen-activated macrophages start producing TNF and IL-6 (142). New alveolar macrophages may be partly replenished by monocyte-derived cells attracted by activated epithelial cells (143) and acquire an alternatively-activated phenotype under the influence of basophil-derived IL-4 (144). Besides, asthmatic patients showed increased epithelial-derived MUC5AC levels, at 24 hours after antigen challenge (145).

During the late phase of the immune response, effector cells are mainly structural cells, resident immune cells and infiltrating immune cells from the circulation. In parallel, DCs are activating allergen-specific T cells in the lymph nodes, which expand and travel to the lung tissue to introduce the adaptive phase.

Adaptive Phase (Days to Weeks) and Resolution of Inflammation

Following the initial release of type 2 cytokines in the lung (by ILC2 and NKT cells), activated eosinophils upregulate multiple cell surface receptors, allowing them to become dynamically regulated and in turn drive the production of canonical Th2 cytokines IL-4, IL-5, and IL-13 by T cells (146). A systematic investigation of these cytokines revealed single and synergistic effects on eosinophils and lung inflammatory hallmarks, such as goblet cell metaplasia (147). Over time, plasma cells arise. Meanwhile, in the bone marrow eosinophil-derived APRIL and IL-6 have been shown to sustain the survival of co-localizing plasma cells (148). The adaptive phase of the allergic immune response is further characterized by the influx of Th2 cells. Asthmatic patients who clearly present with allergen-specific Th2 cells, and their associated cytokines, in the bronchoalveolar lavage, as well as with airway and/or blood eosinophilia are

clustered as type 2-high patients (149, 150). On the other side, non- or low-type 2 asthma phenotypes have also been recognized and are defined by the absence of Th2 cytokine signatures and eosinophilia. However, within the type 2-high subtype, circulating Th2 cells appear to be more diverse than initially expected. Circulating allergen-specific Th2 cells have been identified in the lungs of mice and in the blood of allergic asthmatic patients. These Th2 cells have been found to not only produce IL-4, IL-5, IL-6, IL-13, but also IL-9, IL-17, and IL-21 (151, 152). Th2 cells isolated from both humans and mice are characterized by the expression of PPARγ, that seems to be crucial in driving Th2 cell pathogenicity (152, 153). It seems that IL-4 production in the lung is mostly basophil-derived, while IL-4 present in the draining lymph node was T cell-derived (154). Furthermore, Tibbitt and colleagues have shown that while IL-4 may play a more dominant role in the draining lymph node, IL-5 and IL-13 are more prominent T cell cytokines in the lung tissue. This indicates that Th2 cells undergo substantial programming in the lung, making them highly distinct from their lymph node counterparts (152). We found that IL-21 produced by distinct T cell subsets can promote adaptive Th2 cell responses (151). It should be mentioned that the source of IL-13 in allergen-induced airway hyperresponsiveness may depend on the age of first exposure, with IL-13$^+$ CD4$^+$ T cells dominating in neonatal life and IL-13$^+$ ILC2s dominating in adult mice (155). Interestingly, it has also been suggested that pulmonary NKT cells, which are activated by IL-25, IL-33, and TSLP, can license incoming Th2 cells to induce airway hyperresponsiveness, *via* the production of IL-4 and IL-13 (156, 157). Moreover, Vα14-expressing NKT cells, residing in the intravascular space of the lung microvasculature, can recruit eosinophils after binding of αGalCer on CD1d (158). However, it is not clear how precisely NKT cells drive asthma adaptive immune response.

Whereas the classical type 2 cytokines induce the expression of adhesion molecules, such as ICAM-1 and VCAM1, that allow extravasation of eosinophils into the lung, the function of the more enigmatic cytokine IL-9 is largely unknown (159). Besides being produced by highly-differentiated Th2 cells in allergic asthmatic patients (160), also referred to as Th9 cells (161), IL-9 is also produced by human eosinophils and neutrophils (162, 163). Consequently, increased expression of IL-9 has been found in the bronchoalveolar lavage in these patients (141). Additionally, genome-wide expression profiles showed that young asthmatics with a IL-9 polymorphism were more likely to report a severe asthma exacerbation to HDM (164). In murine models IL-9 seems to be critical for the induction of allergic airway inflammation, as the administration of blocking antibodies reduced asthma features (165). Moreover, TSLP and IL-25 signaling was shown to promote Th9 cell differentiation and stimulated IL-9 production by these cells (166, 167). Elevated levels of IL-9 were further reported to increase mast cell numbers in the lungs. Mast cell precursors are attracted to the lung and seem to peak in numbers one day after a seven-day challenge period (168, 169). In fact, it seems that the Th9 cells are critical to the IL-9-mediated recruitment of late phase mast cells (170). The recruited mature mast cells can persist for weeks post allergen challenge, further reinforcing the Th2 environment. In all, incoming T cells produce high-levels of Th2 cytokines and thereby maintaining and propagating asthma features, including the recruitment of eosinophils into the lungs and airways. Samples derived from human asthmatics showed that eosinophils may further sustain Th2 inflammation by maintaining high indoleamine 2,3-dioxygenase (IDO) levels (171). Interestingly, pulmonary eosinophil trafficking into the lung lymphatic compartment is shown to be dependent on LTC4 (172), but independent of eotaxin (34), and has been proposed to be a prerequisite for DC accumulation in the draining lymph nodes and allergen-specific T cell proliferation (39). As mentioned during the sensitization phase, eosinophils can migrate to the draining lymph nodes and localize to the T cell-rich paracortical areas. During the adaptive phase of the allergen-induced immune response, eosinophils have been shown to stimulate antigen-specific T cell proliferation within the lymph nodes (34). Additionally, eosinophils have the ability to influence proliferation and activation of both memory T and B cells, yet have little effect on naïve T and B cells. Interestingly, eosinophilic airway inflammation was unaffected in a chronic HDM model in the absence of B cells or CD40L-dependent B-T cell interactions (173). As the blood-derived eosinophils infiltrate the inflamed lung, the circulation is replenished through increased granulopoiesis in the bone marrow. While the relationship between systemic infection and emergency neutrophil output from the bone marrow is well established (174), it is unclear how acute or chronic allergic lung inflammation affect eosinopoiesis in the bone marrow. IL-5 is clearly the most important factor promoting eosinophil production, differentiation, and in preventing apoptosis (1). Despite the fact that the developmental pathway of eosinophils has been reviewed extensively, its precise trajectory under inflammatory conditions is still a matter of debate (175). Nonetheless, it is worth noting that allergic lung inflammation leads to increased eosinopoiesis *via* systemic IL-5 and further differentiation *via* systemic or local IL-3, GM-CSF and eotaxins (CCL11, CCL24, CCL26) (176).

Although often considered pro-inflammatory, eosinophils have also been suggested to mediate the resolution of inflammation. For example, immune resolution of the airways after allergen exposure is defective in PHIL mice, which lack eosinophils (177). The resolution phase is characterized by apoptosis of various immune cells, and the subsequent uptake by macrophages. Eosinophils can induce macrophage CXCL13 expression in the resolution phase, leading to increased macrophage-dependent phagocytosis and impaired lymphatic drainage (177). Additionally, CXCL13 recruits B cells and CD4$^+$ T cells to the lung, where these may contribute to induced bronchial-associated lymphoid tissue (iBALT). In turn, iBALT structures may facilitate or reduce the accumulation of eosinophils in allergic lung inflammation, depending on the timing and the research model used (178). As the innate inflammatory response needs resolution, several inter-/intracellular negative feedback loops exist to resolve inflammation, remodel damaged tissue and instigate tissue repair (179). Granulocytes are thought to travel into the airways, undergo apoptosis and are removed by macrophage (or epithelial) efferocytosis (180). In the lung, IL-4 and IL-13

together with apoptotic cells programs macrophages to go into a tissue repair phenotype (181, 182). This removal of apoptotic neutrophils is mediated by expression of Gas6 and recognition by its cognate receptors AXL and MERTK (183). A similar MerTK-dependent mechanism of efferocytosis of eosinophils has been described in an ovalbumin-induced allergic inflammation model (184). Moreover, a failure to undergo apoptosis through experimental overexpression of the anti-apoptotic protein Mcl-1 resulted in exacerbated allergic airway inflammation (185). Furthermore, in a murine asthma model phagocytosis of apoptotic cells by alveolar macrophages, resulted in the production of retinoic acid, which promoted regulatory T cell development (57). The notion that apoptosis is the major driver of eosinophil removal from the airways is however contested (186). Eosinophils can undergo a specific type of lytic cell death, which involves the expulsion of DNA-contained eosinophil extracellular traps (EET) and granules (187). Alternatively, eosinophils may undergo ferroptosis-like cell death, which may reduce allergic airway inflammation in mice when therapeutically promoted (188). Nonetheless, how eosinophil death is regulated as part of the resolution phase or during chronic inflammation is unclear. If the clearance of dying cells is impaired, apoptotic cells become necrotic and damage-associated molecular patterns are released, which may actually result in additional inflammation. To aid the clearance of death cells, non-professional phagocytes, such as bronchial epithelial cells, can contribute to apoptotic cell clearance and the restoration of homeostasis (189). Both innate and adaptive immune cells are communicating to ensure resolution of inflammation. For example, IL-33 may stimulate mast cells to produce IL-2, which promotes the expansion of Tregs. These Tregs, in turn, suppress the development of papain- or IL-33-induced eosinophilia in the lung (190). However, the exact time and cellular context of IL-2 production will affect the final outcome (191). IL-33 and IL-13 have also been shown to coordinate macrophage-mediated bronchial epithelial cell repair after lung injury (182, 192), as well as the production of amphiregulin by ILC2 (193). The identification of functional heterogeneity in these immune responses, under the influence of the changing local tissue microenvironment, may reflect their differential roles in regulating proinflammatory versus tissue-protective responses. However, in the case of chronic inflammation, the line between adequate immune activation, immune resolution and tissue regeneration remains even less well defined.

Chronic Phase (Weeks-Years)

Clinical data and investigational reports on mild and severe asthmatic patients provide invaluable information about the chronic phase of the allergic lung. A benchmark study by the groups of Teichmann and Nawijn explored this cellular landscape of the lower airways of healthy and asthmatic lungs by single cell RNA sequencing (194). They revealed a shift in airway structural cell communication to a Th2-dominated interactome in asthmatic lungs compared to healthy lungs. Furthermore, bronchoscopy biopsies from asthmatic patients showed enriched mast cells with high expression of genes involved in downstream biosynthesis of PGD2. Repeated activation of these pulmonary mast cells by allergens in asthma patients can result in lowering their degranulation threshold (195, 196). However, whereas increased mast cell numbers were observed in the bundles of airway smooth muscle from chronic asthmatics, these bundles had a profound absence of T cells or eosinophils (197). Nonetheless, intraepithelial mast cell accumulation is associated with a type 2-high phenotype (198). These mast cells seem to be actively degranulating and may be related to fatal cases of asthma (199). Additionally, in children with severe asthma, mast cells were positively correlated with high numbers of submucosal eosinophils (200). Likewise, a negative correlation was observed between eosinophil counts in atopic individuals and their epithelial barrier integrity (196). Collectively, it seems that the cellular landscape in the lungs of chronic asthmatics is thoroughly affected, resulting in airway dysfunction, as well as mucus- and goblet cell metaplasia.

The relationship between eosinophils and airway dysfunction has been extensively researched. The exact role of eosinophils in common mouse models of allergic airway inflammation likely depends on several factors, including the chronicity of the model, the genetic background, the number of antigenic exposures, the type of allergen, and the mode of antigen delivery (201). Early studies using the OVA protocol with IL-5 knockout mice (202), congenitally eosinophil-deficient mice (203) and eosinophil depleting biologics (204) implicated an important role of eosinophils in airway inflammation. In contrast, Takeda and colleagues showed that an extensive OVA model (2 sensitizations and 7 or 11 challenges over a 50 to 66 day period, respectively) developed airway hyperreactivity reaction (AHR) in both WT and PHIL (eosinophil-deficient) transgenic animals (179). Importantly, eosinophil-deficient animals showed eosinophilic-independent AHR, likely through increased goblet cell numbers after 11 OVA challenges. Jacobsen and colleagues described a genetic mouse model of chronic Th2–driven inflammation by overexpressing IL-5 from T cells and human eotaxin 2 in the lung (*I5/hE2*), which did not show extensive pulmonary histopathology regardless of clear eosinophil activation, type-2 immunity and degranulation (205). Similarly, clinical studies were unable to find an association between reduced eosinophilia by mepolizumab (IL-5 blockade) and airway function/hyperreactivity, although fewer exacerbations were observed (206).

In chronic asthmatics, both prostaglandins and leukotrienes are deregulated and the production of 5-HETE, LTB4 and LTE4 was found to be increased in alveolar macrophages, leading to defective apoptotic cell phagocytosis (207, 208). This may lead to aberrant cell accumulation and increased necroptosis or eosinophil cytolysis. Human eosinophils have also been linked to the deposition of Charcot-Leyden crystals (CLCs), formed after eosinophils undergo cytolysis and form extracellular traps (EET) (209, 210). In severe asthmatics peripheral EET-forming eosinophils are elevated and can stimulate IL-33 and TSLP production by lung epithelial cells (211). Moreover, CLC formation leads to the production of IL-1β, IL-6, and TNF, as

well as the recruitment of several innate and adaptive immune cells and the induction of mucus production by epithelial cells (209, 212). CLC crystals are found more abundantly in asthmatic patients, where they are located within the mucus plugs potentially changing their rheology and rigidity, making it harder to cough them up (209, 213). CLC are amply found in patients with chronic rhinosinusitis with nasal polyps (CRSwNP), a condition of type 2 inflammation of the nose and paranasal sinuses. Here, crystals promote neutrophil recruitment and neutrophil NETosis, creating a favorable niche for persistent type 2 immune cells (214). In a recent study in mice EETs were shown to activate PNECs to produce CGRP and GABA, contributing to asthma pathology (215). Finally, EETosis also involves the release of intact granules that retain granule proteins and can still be activated by CCL11 (187). It has been proposed that these bioactive cell-free granules remain pathogenic in the tissue after IL-5/IL-5R blockade, possibly explaining sustained pathology regardless of significant reductions in eosinophil counts.

In both murine experimental asthma models, as well as in patients with eosinophilic asthma, a population of $CD4^+$ resident memory T (Trm) cells was observed (194, 216). Trm cells express the IL-33 receptor ST2, suggesting they could be directly activated by epithelial-derived IL-33 and contribute to the chronicity of the asthma pathogenesis (217). Indeed, higher levels of ST2 were found on allergen-specific $CD4^+$ T cells in the BAL of asthmatics after segmental allergen challenge (145). In murine models, allergen-specific Trm cells produced more Th2 cytokines than circulating Th2 cells. Interestingly, the functional difference between the pool of lung Trm and circulating memory cells could be further explained by their localization. Whereas circulating Th2 cells preferentially localized in the lung parenchyma, controlling eosinophil and T cell recruitment, Trm cells localized primarily near the airways and induced eosinophil activation, mucus production, and AHR (218). In human tissue samples from CRSwNP, there was a notable expansion of basal cells at the expense of epithelial cell diversity. This process was not only driven by type-2 cytokines (IL-4 and IL-13), but also induced a possible memory-like phenotype in the basal cell population (219). When comparing allergic asthmatics with allergic nonasthmatic controls, both groups developed allergic airway inflammation in response to allergen. However, in the asthmatic patients type-2 cytokine levels and mucin levels were substantially higher compared to controls (145). Interestingly, type-2 cytokine levels only correlated with mucin production in the asthmatic subjects, but not in the controls, suggesting differences in the airway epithelial responses to inflammation (145). Besides, chronic exposure of the lung to IL-33 seems to drive the allergic immune response beyond the typical type 2 phenotype towards aberrant remodeling of lung epithelium and lung parenchyma (220).

Importantly, not only adaptive antigen-specific immune cells like T and B cells are educated by previous inflammatory insults. This suggests that alveolar macrophages, ILC2, and lung epithelial (stem) cells may be functionally and epigenetically reprogrammed by an inflammatory insult or inflammatory microenvironment. However, it remains to be determined whether it is the same alveolar macrophage lineage or newly recruited monocyte-derived alveolar macrophages, that are subject to this environmental imprinting. In settings of allergic airway inflammation, papain and IL-33 have been shown to induce long-term changes in lung ILC2, with some persisting up to two months in the lung and even 4 months in the mLN. Exposure of these 'conditioned' ILC2 to a second unrelated allergen resulted in exaggerated cytokine responses and increased type 2 immune response (221). Interestingly, ILC memory resembles adaptive T cell memory even in absence of antigen-specificity. A novel finding is the presence of inflammatory memory in basal cells from allergic nasal polyp samples (222). Basal cells were found to expand at the expense of differentiated epithelial cells and displayed IL-4/IL-13 responsive genes that remained fixed *ex vivo*. It is unknown whether eosinophils or granulocyte progenitors display such immunological memory as a result of chronic allergic airway inflammation. However, it is clear that chronic asthma patients are immunologically predisposed to airway insults that result in repeated acute and adaptive immune responses aimed at antigen clearing and tissue repair.

Like all chronically ill individuals, asthmatic patients inevitably enter the clinic with an extensive inflammatory history involving chronic eosinophilia. Experimental eradication of eosinophils in animal models before onset of chronic inflammation severely compound the conclusions that can be extrapolated in relation to eosinophil functioning in asthmatics. Another observation of interest is the shortening of telomere length in peripheral leukocytes of asthmatics (223, 224), suggesting extensive leukocyte proliferation and found to correlate with eotaxin 1 expression (225). However, telomerase-deficient mice showed debilitating eosinophil responses in the lung and reduced eosinopoiesis, although eosinophil-independent effects of telomerase cannot be excluded (226). Whether constant eosinopoiesis in long-term severe asthmatics induces inflammaging phenotypes in eosinophils remains unknown.

EOSINOPHILS IN ASTHMA EXACERBATIONS

Chronic asthmatics are commonly hospitalized for asthma exacerbations and these account for roughly one-third of all asthma-related deaths in the US (227). Exacerbations of asthma can be induced by various different stimuli, including allergens, pollution, cold air, microbes, and viruses. Amongst the latter, respiratory viruses and especially respiratory syncytial virus (RSV) and rhinovirus (RV) are major drivers of asthma exacerbations in children and adults, respectively (228). Respiratory viruses most frequently infect lung epithelial cells (229). Remarkably, asthma exacerbations are mainly induced in patients with high eosinophil numbers (type 2 high phenotype) (230). Recent studies have shown that during viral-induced asthma exacerbations, high levels of IL-33 were produced by airway epithelial cells,

consequently suppressing type-I IFN production and leaving the epithelium more vulnerable to repeated infections (231–233). Likewise, epithelial cells from asthmatics showed defective interferon λ production after infection with rhinovirus (234). Importantly, a recent study suggests that the response of the lung epithelium to rhinovirus infection is not qualitatively changed, but is delayed (235). The epithelium of healthy patients showed a peak in the anti-viral response at 48 hours post-infection, whereas lung epithelial cells from asthma of COPD patients peaked at 96 hours post-infection (235). As exposure to respiratory viruses increased the levels of IL-33 and TSLP produced by lung ECs, it comes to no surprise that children hospitalized with severe respiratory infection had increased ILC2 numbers in the lungs (236). Equivalently, in murine models of influenza infections, increased numbers of ILC2 were found in the lungs. Although influenza is rarely involved in asthma exacerbations, these data may suggest a division of labor between Th2 cells contributing early in the response and ILC2-derived cytokines that contribute at a later stage to lung repair *via* the production of amphiregulin (237). Recent studies have also identified a specific population of SIRPα$^+$IFNAR$^+$ conventional DC2 with strong capacities to activate antiviral CD4$^+$ and CD8$^+$ T cell responses (238). Such DC responses are dependent on type-I interferons, which are high during antiviral responses and are known to inhibit ILC2 functions (239). However, within the Th2 environment, the levels of type-I interferons may be lower and this may impact the function of SIRPα$^+$IFNAR$^+$ DC2s and the subsequent antiviral response. It is still unclear how exactly type-I interferons, SIRPα$^+$IFNAR$^+$ DC2s, and virus-induced asthma exacerbations are linked. Nonetheless, it is tempting to speculate that increased levels of IL-33, produced by airway epithelial cells upon respiratory viral infection, and stronger activation of Th2 cells and ILC2, would enhance asthmic features, including BHR and eosinophilia.

A common feature of the asthmatic lung is the disruption of the airway epithelium (240). An increase of epithelial cells in the sputum (sometimes referred to as Creola bodies) of pediatric asthma patients was found during acute exacerbations (241, 242). These exacerbations were related to increased IL-8, which recruits neutrophils and in turn eosinophils to the lungs (243). Similar findings were reported in a model of rhinoviral-induced asthma exacerbation (244), with type 2 cytokines potentially enhancing the epithelial production of CXCL10, IL-8 and GM-CSF (245). Of note is the observation that the immune response to RV is changed by mepolizumab, without directly affecting eosinophil functioning (246). Taken together, it is clear that both neutrophils and eosinophils enhance RV exacerbations in asthmatics (243).

Human eosinophils express several functional Toll-like receptors (TLRs), including TLR1, 2, 3, 4, 5, 6, 7, and 9, with some heterogeneity associated with atopic status (247, 248). Besides, supporting a potential role for eosinophils in PAMP recognition, TLR expression can provide a mechanism by which bacterial or viral infections exacerbate allergic disease (249). However, to complicate things, eosinophils may play an important role in the protection against viral and bacterial pathogens. Mouse studies with the murine equivalent of RSV, pneumonia virus of mice indicated that eosinophil degranulation was associated with a more favourable outcome in infected mice (250). Although, in human rhinovirus infection, eosinophils were found to lower epithelial interferon production, thereby increasing viral load (251). In patients with RSV infection, eosinophil degranulation products, such as ECP and EDN, have been isolated from the bronchoalveolar lavage of the lower airways (252). More recently, it has been shown that EDN can enter viral capsids and degrade RNA from RSV (253). Eosinophils have even been shown to quickly internalize and inactivate RSV and influenza virus *in vitro*; a characteristic that was defective in eosinophils from asthmatics (254). From murine studies, it is clear that mice overexpressing both IL-5 and eotaxin-2 were protected against lethal pneumovirus infection (250). Eosinophil-driven antiviral activity has further been demonstrated for other respiratory viruses, including influenza, parainfluenza, and HIV, although the exact mechanisms by which eosinophils protect from viral infections have still to be elucidated (253, 255, 256). Taken together, there is a complexity within eosinophil function in viral infection and it is unclear how eosinophil-viral interactions are regulated. As the majority of the eosinophil-viral interactions comes from RSV research, the investigation of other viruses, like rotavirus or SARS-CoV2, may provide further insights regarding eosinophil-viral interactions.

CONCLUDING REMARKS AND FUTURE DIRECTIONS

Our perspective on the lung has changed dramatically over the last decades, culminating in the view of the lung as a place where epithelial cells, stromal cells, and immune cells support a multifaceted frontline defense system focused on inducing tolerance, supporting highly-efficient injury-repair responses, as well as (destructive) inflammatory responses, like asthma. Indeed, not a single cell seems to be left out of the inflammatory response to airborne allergens. Over the last years, mouse models of asthma have evolved from primarily focusing on the role of eosinophils as proinflammatory cells, to a consensus that eosinophils have a divers set of functions ranging from proinflammatory to immune modulating. In these nuanced disease settings, it can be questioned whether, where, and when eosinophils are contributing cells, rather than primary mediators. Shifting the focus of eosinophils being the primary promotors of the inflammatory cascade, towards a view where eosinophils play multiple defined roles along the disease progression trajectory. This may explain the mixed results of eosinophil-depleting therapies in asthma and other inflammatory diseases. The traditional view of eosinophils as being released into circulation as terminally differentiated cells led us to ask the question at which level within the developmental pathway functional differentiation and plasticity is arranged. Recent findings on other granulocytes like neutrophils have addressed similar questions on plasticity in the overarching

developmental trajectory and into inflammatory situations. For example, certain combinations of transcription factors govern specific parts of the neutrophil inflammatory response (257). Interestingly, neutrophils are released into circulation in a circadian rhythm and a recent study showed that this chronicity (termed "neutrotime") largely determines the core transcriptional profile of neutrophils (258), with limited transcriptional change inducible by external input. Whereas these significant advances are made possible using scRNA sequencing, the eosinophil is notoriously difficult to capture in single cell transcriptomics. Hypotheses that are currently entertained include the possibility that RNAses are abundant present in eosinophils and may break down mRNA before it can be amplified, and the terminally differentiated status that simple excludes active transcriptional plasticity. A recent study using the 10X scRNAseq platform showed that the transcriptome of circulating eosinophils is very low, even though eosinophils can be readily detected by RNA-barcoded antibodies in the same setup (CITEseq) (259). Even if transcriptional changes can be found in eosinophils between conditions of *in vivo* allergen challenge in asthmatics, it is unclear whether the readout arises from transcriptional changes in resident eosinophils or the transcriptionally pre-activated circulating eosinophils infiltrating the inflamed lung. The study from Mesnil and colleagues support the latter option, where "inflammatory" eosinophils are proposed to accumulate independent of resident eosinophils. This raises the question at which level local adaptation can occur; are eosinophils victims of predetermined signaling cascades or can they still change their core programs upon receiving environmental cues?

The modulation of eosinophils in the allergic lung, and beyond, may otherwise entail post-transcriptional changes like metabolic switches or translational modifications. We have recently shown that eosinophils participate in the competition for glucose in the tumor microenvironment of lung metastases, inhibiting anti-tumor NK cells (260). Interestingly, eosinophils appear to display greater metabolic flexibility compared to neutrophils, and can switch metabolic programming during *in vitro* differentiation. Hence, eosinophil swarming in the allergic lung will undoubtedly affect local immunometabolism (261, 262).

Current eosinophil depleting strategies may pose, currently unknown, pre-dispositions to other diseases. Thus warranting a more sophisticated approach to modulating their function. If we are to understand eosinophil functioning in space and time, we will undoubtedly need to resort to new and more refined modes of measuring eosinophil states along the developmental trajectory. As the last frontier in myeloid developmental understanding on the single cell level, the eosinophil may yet prove to be a new dimension.

AUTHOR CONTRIBUTIONS

SS and MS conceptualized and wrote the manuscript. All authors contributed to the article and approved the submitted version.

FUNDING

We acknowledge the following funding sources for SS; Dutch Research Council Rubicon (452019321), Fonds Wetenschappelijk Onderzoek Vlaanderen/F.R.S.-F.N.R.S. EOS consortium U-HEAD, and for MS; Fonds Wetenschappelijk Onderzoek Vlaanderen (12Y5322N), Fund Suzanne Duchesne (managed by the King Baudouin Foundation), and Fondation ACTERIA.

REFERENCES

1. Rothenberg ME, Hogan SP. The Eosinophil. *Annu Rev Immunol* (2006) 24:147–74. doi: 10.1146/annurev.immunol.24.021605.090720
2. Jacobsen EA, Jackson DJ, Heffler E, Mathur SK, Bredenoord AJ, Pavord ID, et al. Eosinophil Knockout Humans: Uncovering the Role of Eosinophils Through Eosinophil-Directed Biological Therapies. *Annu Rev Immunol* (2021) 39:719–57. doi: 10.1146/annurev-immunol-093019-125918
3. Carlens J, Wahl B, Ballmaier M, Bulfone-Paus S, Forster R, Pabst O. Common Gamma-Chain- Dependent Signals Confer Selective Survival of Eosinophils in the Murine Small Intestine. *J Immunol* (2009) 183(9):5600–7. doi: 10.4049/jimmunol.0801581
4. Lee JJ, Jacobsen EA, McGarry MP, Schleimer RP, Lee NA. Eosinophils in Health and Disease: The LIAR Hypothesis. *Clin Exp Allergy* (2010) 40 (4):563–75. doi: 10.1111/j.1365-2222.2010.03484.x
5. Weller PF, Spencer LA. Functions of Tissue-Resident Eosinophils. *Nat Rev Immunol* (2017) 17:746–60. doi: 10.1038/nri.2017.95
6. Abdala-Valencia H, Coden ME, Chiarella SE, Jacobsen EA, Bochner BS, Lee JJ, et al. Shaping Eosinophil Identity in the Tissue Contexts of Development, Homeostasis, and Disease. *J Leukoc Biol* (2018) 104(1):95–108. doi: 10.1002/jlb.1mr1117-442rr
7. Marichal T, Mesnil C, Bureau F. Homeostatic Eosinophils: Characteristics and Functions. *Front Med (Lausanne)* (2017) 4:101. doi: 10.3389/fmed.2017.00101
8. Shomali W, Gotlib J. World Health Organization-Defined Eosinophilic Disorders: 2019 Update on Diagnosis, Risk Stratification, and Management. *Am J Hematol* (2019) 94(10):1149–67. doi: 10.1002/ajh.25617
9. de Kleer IM, Kool M, de Bruijn MJW, Willart M, van Moorleghem J, Schuijs MJ, et al. Perinatal Activation of the Interleukin-33 Pathway Promotes Type 2 Immunity in the Developing Lung. *Immunity* (2016) 45(6):1285–98. doi: 10.1016/j.immuni.2016.10.031
10. Loffredo LF, Coden ME, Jeong BM, Walker MT, Anekalla KR, Doan TC, et al. Eosinophil Accumulation in Postnatal Lung Is Specific to the Primary Septation Phase of Development. *Sci Rep* (2020) 10(1):4425. doi: 10.1038/s41598-020-61420-5
11. Müller E. Localization of Eosinophils in the Thymus by the Peroxidase Reaction. *Histochemistry* (1977) 52(3):273–9. doi: 10.1007/bf00495862
12. Farahi N, Singh NR, Heard S, Loutsios C, Summers C, Solanki CK, et al. Use of 111-Indium- Labeled Autologous Eosinophils to Establish the *In Vivo* Kinetics of Human Eosinophils in Healthy Subjects. *Blood* (2012) 120 (19):4068–71. doi: 10.1182/blood-2012-07-443424
13. Wen T, Besse JA, Mingler MK, Fulkerson PC, Rothenberg ME. Eosinophil Adoptive Transfer System to Directly Evaluate Pulmonary Eosinophil Trafficking *In Vivo*. *Proc Natl Acad Sci* (2013) 110(15):6067. doi: 10.1073/pnas.1220572110
14. Mesnil C, Raulier S, Paulissen G, Xiao X, Birrell MA, Pirottin D, et al. Lung-Resident Eosinophils Represent a Distinct Regulatory Eosinophil Subset. *J Clin Invest* (2016) 126(9):3279–95. doi: 10.1172/JCI85664

15. Nussbaum JC, Van Dyken SJ, von Moltke J, Cheng LE, Mohapatra A, Molofsky AB, et al. Type 2 Innate Lymphoid Cells Control Eosinophil Homeostasis. *Nature* (2013) 502(7470):245–8. doi: 10.1038/nature12526
16. Rothenberg ME. A Hidden Residential Cell in the Lung. *J Clin Invest* (2016) 126(9):3185–7. doi: 10.1172/jci89768
17. Chojnacki A, Wojcik K, Petri B, Aulakh G, Jacobsen EA, LeSuer WE, et al. Intravital Imaging Allows Real-Time Characterization of Tissue Resident Eosinophils. *Commun Biol* (2019) 2(1):181. doi: 10.1038/s42003-019-0425-3
18. Schuijs MJ, Willart MA, Vergote K, Gras D, Deswarte K, Ege MJ, et al. Farm Dust and Endotoxin Protect Against Allergy Through A20 Induction in Lung Epithelial Cells. *Science* (2015) 349(6252):1106–10. doi: 10.1126/science.aac6623
19. Hammad H, Lambrecht BN. The Basic Immunology of Asthma. *Cell* (2021) 184(6):1469–85. doi: 10.1016/j.cell.2021.02.016
20. Papi A, Brightling C, Pedersen SE, Reddel HK. Asthma. *Lancet* (2018) 391 (10122):783–800. doi: 10.1016/S0140-6736(17)33311-1
21. Carsin A, Mazenq J, Ilstad A, Dubus J-C, Chanez P, Gras D. Bronchial Epithelium in Children: A Key Player in Asthma. *Eur Respir Rev* (2016) 25 (140):158. doi: 10.1183/16000617.0101-2015
22. Xu J, Yu H, Sun X. Less Is More: Rare Pulmonary Neuroendocrine Cells Function as Critical Sensors in Lung. *Dev Cell* (2020) 55(2):123–32. doi: 10.1016/j.devcel.2020.09.024
23. Liu T, Yang L, Han X, Ding X, Li J, Yang J. Local Sympathetic Innervations Modulate the Lung Innate Immune Responses. *Sci Adv* (2020) 6(20): eaay1497. doi: 10.1126/sciadv.aay1497
24. Huh JR, Veiga-Fernandes H. Neuroimmune Circuits in Inter-Organ Communication. *Nat Rev Immunol* (2020) 20(4):217–28. doi: 10.1038/s41577-019-0247-z
25. Barrios J, Patel KR, Aven L, Achey R, Minns MS, Lee Y, et al. Early Life Allergen-Induced Mucus Overproduction Requires Augmented Neural Stimulation of Pulmonary Neuroendocrine Cell Secretion. *FASEB J* (2017) 31(9):4117–28. doi: 10.1096/fj.201700115R
26. Drake MG, Scott GD, Blum ED, Lebold KM, Nie Z, Lee JJ, et al. Eosinophils Increase Airway Sensory Nerve Density in Mice and in Human Asthma. *Sci Transl Med* (2018) 10(457). doi: 10.1126/scitranslmed.aar8477
27. Halim T, Steer CA, Mathä L, Gold MJ, Martinez-Gonzalez I, McNagny KM, et al. Group 2 Innate Lymphoid Cells Are Critical for the Initiation of Adaptive T Helper 2 Cell-Mediated Allergic Lung Inflammation. *Immunity* (2014) 40(3):425–35. doi: 10.1016/j.immuni.2014.01.011
28. Webb LM, Lundie RJ, Borger JG, Brown SL, Connor LM, Cartwright AN, et al. Type I Interferon Is Required for T Helper (Th) 2 Induction by Dendritic Cells. *EMBO J* (2017) 36(16):2404–18. doi: 10.15252/embj.201695345
29. Nobs SP, Pohlmeier L, Li F, Kayhan M, Becher B, Kopf M. GM-CSF Instigates a Dendritic Cell–T- Cell Inflammatory Circuit That Drives Chronic Asthma Development. *J Allergy Clin Immunol* (2021) 147 (6):2118–33.e3. doi: 10.1016/j.jaci.2020.12.638
30. Chu DK, Jimenez-Saiz R, Verschoor CP, Walker TD, Goncharova S, Llop-Guevara A, et al. Indigenous Enteric Eosinophils Control DCs to Initiate a Primary Th2 Immune Response *In Vivo*. *J Exp Med* (2014) 211(8):1657–72. doi: 10.1084/jem.20131800
31. Yang D, Chen Q, Su SB, Zhang P, Kurosaka K, Caspi RR, et al. Eosinophil-Derived Neurotoxin Acts as an Alarmin to Activate the TLR2-MyD88 Signal Pathway in Dendritic Cells and Enhances Th2 Immune Responses. *J Exp Med* (2008) 205(1):79–90. doi: 10.1084/jem.20062027
32. Yang D, Rosenberg HF, Chen Q, Dyer KD, Kurosaka K, Oppenheim JJ. Eosinophil-Derived Neurotoxin (EDN), an Antimicrobial Protein With Chemotactic Activities for Dendritic Cells. *Blood* (2003) 102(9):3396–403. doi: 10.1182/blood-2003-01-0151
33. Yang D, Chen Q, Rosenberg HF, Rybak SM, Newton DL, Wang ZY, et al. Human Ribonuclease A Superfamily Members, Eosinophil-Derived Neurotoxin and Pancreatic Ribonuclease, Induce Dendritic Cell Maturation and Activation. *J Immunol* (2004) 173(10):6134–42. doi: 10.4049/jimmunol.173.10.6134
34. Shi HZ, Humbles A, Gerard C, Jin Z, Weller PF. Lymph Node Trafficking and Antigen Presentation by Endobronchial Eosinophils. *J Clin Invest* (2000) 105:945–53. doi: 10.1172/JCI8945
35. Xenakis Jason J, Howard Emily D, Smith Kalmia M, Olbrich Courtney L, Huang Y, Anketell D, et al. Resident Intestinal Eosinophils Constitutively Express Antigen Presentation Markers and Include Two Phenotypically Distinct Subsets of Eosinophils. *Immunology* (2017) 154(2):298–308. doi: 10.1111/imm.12885
36. Wang HB, Ghiran I, Matthaei K, Weller PF. Airway Eosinophils: Allergic Inflammation Recruited Professional Antigen-Presenting Cells. *J Immunol* (2007) 179(11):7585–92.
37. Mengelers HJ, Maikoe T, Brinkman L, Hooibrink B, Lammers JW, Koenderman L. Immunophenotyping of Eosinophils Recovered From Blood and BAL of Allergic Asthmatics. *Am J Respir Crit Care Med* (1994) 149(2 Pt 1):345–51. doi: 10.1164/ajrccm.149.2.8306028
38. Sedgwick JB, Calhoun WJ, Vrtis RF, Bates ME, McAllister PK, Busse WW. Comparison of Airway and Blood Eosinophil Function After *In Vivo* Antigen Challenge. *J Immunol* (1992) 149(11):3710–8.
39. Jacobsen EA, Zellner KR, Colbert D, Lee NA, Lee JJ. Eosinophils Regulate Dendritic Cells and Th2 Pulmonary Immune Responses Following Allergen Provocation. *J Immunol* (2011) 187(11):6059–68. doi: 10.4049/jimmunol.1102299
40. Lotfi R, Lotze MT. Eosinophils Induce DC Maturation, Regulating Immunity. *J Leukoc Biol* (2008) 83(3):456–60. doi: 10.1189/jlb.0607366
41. Jacobsen EA, LeSuer WE, Willetts L, Zellner KR, Mazzolini K, Antonios N, et al. Eosinophil Activities Modulate the Immune/Inflammatory Character of Allergic Respiratory Responses in Mice. *Allergy* (2014) 69(3):315–27. doi: 10.1111/all.12321
42. Iwasaki A, Foxman EF, Molony RD. Early Local Immune Defences in the Respiratory Tract. *Nat Rev Immunol* (2017) 17(1):7–20. doi: 10.1038/nri.2016.117
43. Bordag N, Biasin V, Schnoegl D, Valzano F, Jandl K, Nagy BM, et al. Machine Learning Analysis of the Bleomycin Mouse Model Reveals the Compartmental and Temporal Inflammatory Pulmonary Fingerprint. *iScience* (2020) 23(12):101819. doi: 10.1016/j.isci.2020.101819
44. Galli SJ, Tsai M, Piliponsky AM. The Development of Allergic Inflammation. *Nature* (2008) 454(7203):445–54. doi: 10.1038/nature07204
45. Jacobsen EA, Doyle AD, Colbert DC, Zellner KR, Protheroe CA, LeSuer WE, et al. Differential Activation of Airway Eosinophils Induces IL-13-Mediated Allergic Th2 Pulmonary Responses in Mice. *Allergy* (2015) 70(9):1148–59. doi: 10.1111/all.12655
46. Walsh ER, Thakar J, Stokes K, Huang F, Albert R, August A. Computational and Experimental Analysis Reveals a Requirement for Eosinophil-Derived IL-13 for the Development of Allergic Airway Responses in C57BL/6 Mice. *J Immunol* (2011) 186(5):2936–49. doi: 10.4049/jimmunol.1001148
47. Serhan CN, Gupta SK, Perretti M, Godson C, Brennan E, Li Y, et al. The Atlas of Inflammation Resolution (AIR). *Mol Aspects Med* (2020) 74:100894. doi: 10.1016/j.mam.2020.100894
48. Hussell T, Bell TJ. Alveolar Macrophages: Plasticity in a Tissue-Specific Context. *Nat Rev Immunol* (2014) 14(2):81–93. doi: 10.1038/nri3600
49. Neupane AS, Willson M, Chojnacki AK, Vargas E, Silva Castanheira F, Morehouse C, et al. Patrolling Alveolar Macrophages Conceal Bacteria From the Immune System to Maintain Homeostasis. *Cell* (2020) 183(1):110–25.e11. doi: 10.1016/j.cell.2020.08.020
50. McCowan J, Kirkwood PM, Fercoq F, T'Jonck W, Mawer CM, Cunningham R, et al. The Transcription Factor EGR2 is Indispensable for Tissue-Specific Imprinting of Alveolar Macrophages in Health and Tissue Repair. *bioRxiv* (2021). doi: 10.1101/2021.05.06.442095. 2021.05.06.442095.
51. Gschwend J, Sherman S, Ridder F, Feng X, Liang H-E, Locksley RM, et al. Alveolar Macrophages Strictly Rely on GM-CSF From Alveolar Epithelial Type 2 Cells Before and After Birth. *bioRxiv* (2021). doi: 10.1101/2021.04.01.438051. 2021.04.01.438051.
52. Fricker M, Gibson PG. Macrophage Dysfunction in the Pathogenesis and Treatment of Asthma. *Eur Respir J* (2017) 50(3). doi: 10.1183/13993003.00196-2017
53. Yu X, Buttgereit A, Lelios I, Utz SG, Cansever D, Becher B, et al. The Cytokine TGF-β Promotes the Development and Homeostasis of Alveolar Macrophages. *Immunity* (2017) 47(5):903–12.e4. doi: 10.1016/j.immuni.2017.10.007
54. Mathie SA, Dixon KL, Walker SA, Tyrrell V, Mondhe M, O'Donnell VB, et al. Alveolar Macrophages Are Sentinels of Murine Pulmonary

Homeostasis Following Inhaled Antigen Challenge. *Allergy* (2015) 70(1):80–9. doi: 10.1111/all.12536
55. Barrett NA, Rahman OM, Fernandez JM, Parsons MW, Xing W, Austen KF, et al. Dectin-2 Mediates Th2 Immunity Through the Generation of Cysteinyl Leukotrienes. *J Exp Med* (2011) 208(3):593–604. doi: 10.1084/jem.20100793
56. Clarke DL, Davis NHE, Campion CL, Foster ML, Heasman SC, Lewis AR, et al. Dectin-2 Sensing of House Dust Mite is Critical for the Initiation of Airway Inflammation. *Mucosal Immunol* (2014) 7(3):558–67. doi: 10.1038/mi.2013.74
57. Miki H, Pei H, Gracias DT, Linden J, Croft M. Clearance of Apoptotic Cells by Lung Alveolar Macrophages Prevents Development of House Dust Mite-Induced Asthmatic Lung Inflammation. *J Allergy Clin Immunol* (2021) 147(3):1087–92.e3. doi: 10.1016/j.jaci.2020.10.005
58. Hammad H, Lambrecht BN. Barrier Epithelial Cells and the Control of Type 2 Immunity. *Immunity* (2015) 43(1):29–40. doi: 10.1016/j.immuni.2015.07.007
59. Puttur F, Denney L, Gregory LG, Vuononvirta J, Oliver R, Entwistle LJ, et al. Pulmonary Environmental Cues Drive Group 2 Innate Lymphoid Cell Dynamics in Mice and Human. *Sci Immunol* (2019) 4(36):eaav7638. doi: 10.1126/sciimmunol.aav7638
60. Denney L, Byrne Adam J, Shea Thomas J, Buckley James S, Pease James E, Herledan Gaelle MF, et al. Pulmonary Epithelial Cell-Derived Cytokine TGF-β1 Is a Critical Cofactor for Enhanced Innate Lymphoid Cell Function. *Immunity* (2015) 43(5):945–58. doi: 10.1016/j.immuni.2015.10.012
61. Motomura Y, Morita H, Moro K, Nakae S, Artis D, Endo Takaho A, et al. Basophil-Derived Interleukin-4 Controls the Function of Natural Helper Cells, a Member of ILC2s, in Lung Inflammation. *Immunity* (2014) 40(5):758–71. doi: 10.1016/j.immuni.2014.04.013
62. Schuijs MJ, Halim TYF. Group 2 Innate Lymphocytes at the Interface Between Innate and Adaptive Immunity. *Ann New Y Acad Sci* (2018) 1417(1):87–103. doi: 10.1111/nyas.13604
63. Austen KF, Maekawa A, Kanaoka Y, Boyce JA. The Leukotriene E4 Puzzle: Finding the Missing Pieces and Revealing the Pathobiologic Implications. *J Allergy Clin Immunol* (2009) 124(3):406–14; quiz 15-6. doi: 10.1016/j.jaci.2009.05.046
64. Bouffi C, Rochman M, Zust CB, Stucke EM, Kartashov A, Fulkerson PC, et al. IL-33 Markedly Activates Murine Eosinophils by an NF-κb-Dependent Mechanism Differentially Dependent Upon an IL-4-Driven Autoinflammatory Loop. *J Immunol* (2013) 191(8):4317–25. doi: 10.4049/jimmunol.1301465
65. Hui CC, Yu A, Heroux D, Akhabir L, Sandford AJ, Neighbour H, et al. Thymic Stromal Lymphopoietin (TSLP) Secretion From Human Nasal Epithelium is a Function of TSLP Genotype. *Mucosal Immunol* (2015) 8(5):993–9. doi: 10.1038/mi.2014.126
66. Wong CK, Hu S, Cheung PF, Lam CW. Thymic Stromal Lymphopoietin Induces Chemotactic and Prosurvival Effects in Eosinophils: Implications in Allergic Inflammation. *Am J Respir Cell Mol Biol* (2010) 43(3):305–15. doi: 10.1165/rcmb.2009-0168OC
67. Halim TYF, Hwang Y, Scanlon ST, Zaghouani H, Garbi N, Fallon PG, et al. Group 2 Innate Lymphoid Cells License Dendritic Cells to Potentiate Memory TH2 Cell Responses. *Nat Immunol* (2016) 17(1):57–64. doi: 10.1038/ni.3294
68. Nobs SP, Kayhan M, Kopf M. GM-CSF Intrinsically Controls Eosinophil Accumulation in the Setting of Allergic Airway Inflammation. *J Allergy Clin Immunol* (2019) 143(4):1513–24.e2. doi: 10.1016/j.jaci.2018.08.044
69. Tully JE, Hoffman SM, Lahue KG, Nolin JD, Anathy V, Lundblad LKA, et al. Epithelial NF-κb Orchestrates House Dust Mite–Induced Airway Inflammation, Hyperresponsiveness, and Fibrotic Remodeling. *J Immunol* (2013) 191(12):5811–21. doi: 10.4049/jimmunol.1301329
70. McGinty JW, Ting H-A, Billipp TE, Nadjsombati MS, Khan DM, Barrett NA, et al. Tuft-Cell- Derived Leukotrienes Drive Rapid Anti-Helminth Immunity in the Small Intestine But Are Dispensable for Anti-Protist Immunity. *Immunity* (2020) 52(3):528–41.e7. doi: 10.1016/j.immuni.2020.02.005
71. Bankova LG, Dwyer DF, Yoshimoto E, Ualiyeva S, McGinty JW, Raff H, et al. The Cysteinyl Leukotriene 3 Receptor Regulates Expansion of IL-25–Producing Airway Brush Cells Leading to Type 2 Inflammation. *Sci Immunol* (2018) 3(28):eaat9453. doi: 10.1126/sciimmunol.aat9453
72. Ualiyeva S, Hallen N, Kanaoka Y, Ledderose C, Matsumoto I, Junger WG, et al. Airway Brush Cells Generate Cysteinyl Leukotrienes Through the ATP Sensor P2Y2. *Sci Immunol* (2020) 5(43):eaax7224. doi: 10.1126/sciimmunol.aax7224
73. von Moltke J, O'Leary CE, Barrett NA, Kanaoka Y, Austen KF, Locksley RM. Leukotrienes Provide an NFAT-Dependent Signal That Synergizes With IL-33 to Activate ILC2s. *J Exp Med* (2017) 214(1):27–37. doi: 10.1084/jem.20161274
74. Branchfield K, Nantie L, Verheyden JM, Sui P, Wienhold MD, Sun X. Pulmonary Neuroendocrine Cells Function as Airway Sensors to Control Lung Immune Response. *Science* (2016) 351(6274):707–10. doi: 10.1126/science.aad7969
75. Sui P, Wiesner DL, Xu J, Zhang Y, Lee J, Van Dyken S, et al. Pulmonary Neuroendocrine Cells Amplify Allergic Asthma Responses. *Science* (2018) 360(6393):eaan8546. doi: 10.1126/science.aan8546
76. Cardoso V, Chesné J, Ribeiro H, García-Cassani B, Carvalho T, Bouchery T, et al. Neuronal Regulation of Type 2 Innate Lymphoid Cells *via* Neuromedin U. *Nature* (2017) 549(7671):277–81. doi: 10.1038/nature23469
77. Wallrapp A, Riesenfeld SJ, Burkett PR, Abdulnour R-EE, Nyman J, Dionne D, et al. The Neuropeptide NMU Amplifies ILC2-Driven Allergic Lung Inflammation. *Nature* (2017) 549(7672):351–6. doi: 10.1038/nature24029
78. Motomura Y, Kobayashi T, Moro K. The Neuropeptide CGRP Induces Bipolar Syndrome in Group 2 Innate Lymphoid Cells. *Immunity* (2019) 51(4):598–600. doi: 10.1016/j.immuni.2019.09.015
79. Palaniyandi S, Liu X, Periasamy S, Ma A, Tang J, Jenkins M, et al. Inhibition of CD23-Mediated IgE Transcytosis Suppresses the Initiation and Development of Allergic Airway Inflammation. *Mucosal Immunol* (2015) 8(6):1262–74. doi: 10.1038/mi.2015.16
80. Abraham SN, St John AL. Mast Cell-Orchestrated Immunity to Pathogens. *Nat Rev Immunol* (2010) 10(6):440–52. doi: 10.1038/nri2782
81. de Boer JD, Yang J, van den Boogaard FE, Hoogendijk AJ, de Beer R, van der Zee JS, et al. Mast Cell-Deficient Kit Mice Develop House Dust Mite-Induced Lung Inflammation Despite Impaired Eosinophil Recruitment. *J Innate Immun* (2014) 6(2):219–26. doi: 10.1159/000354984
82. Pejler G. The Emerging Role of Mast Cell Proteases in Asthma. *Eur Respir J* (2019) 54(4):1900685. doi: 10.1183/13993003.00685-2019
83. Persson C. Airways Exudation of Plasma Macromolecules: Innate Defense, Epithelial Regeneration, and Asthma. *J Allergy Clin Immunol* (2019) 143(4):1271–86. doi: 10.1016/j.jaci.2018.07.037
84. Maun HR, Jackman JK, Choy DF, Loyet KM, Staton TL, Jia G, et al. An Allosteric Anti-Tryptase Antibody for the Treatment of Mast Cell-Mediated Severe Asthma. *Cell* (2019) 179(2):417–31.e19. doi: 10.1016/j.cell.2019.09.009
85. Oh S-W, Pae CI, Lee D-K, Jones F, Chiang GKS, Kim H-O, et al. Tryptase Inhibition Blocks Airway Inflammation in a Mouse Asthma Model. *J Immunol* (2002) 168(4):1992. doi: 10.4049/jimmunol.168.4.1992
86. Chen CL, Wang SD, Zeng ZY, Lin KJ, Kao ST, Tani T, et al. Serine Protease Inhibitors Nafamostat Mesilate and Gabexate Mesilate Attenuate Allergen-Induced Airway Inflammation and Eosinophilia in a Murine Model of Asthma. *J Allergy Clin Immunol* (2006) 118(1):105–12. doi: 10.1016/j.jaci.2006.02.047
87. Pang L, Nie M, Corbett L, Sutcliffe A, Knox AJ. Mast Cell β-Tryptase Selectively Cleaves Eotaxin and RANTES and Abrogates Their Eosinophil Chemotactic Activities. *J Immunol* (2006) 176(6):3788. doi: 10.4049/jimmunol.176.6.3788
88. Vliagoftis H, Lacy P, Luy B, Adamko D, Hollenberg M, Befus D, et al. Mast Cell Tryptase Activates Peripheral Blood Eosinophils to Release Granule-Associated Enzymes. *Int Arch Allergy Immunol* (2004) 135(3):196–204. doi: 10.1159/000081304
89. Bradding P, Arthur G. Mast Cells in Asthma – State of the Art. *Clin Exp Allergy* (2016) 46(2):194–263. doi: 10.1111/cea.12675
90. Waern I, Jonasson S, Hjoberg J, Bucht A, Abrink M, Pejler G, et al. Mouse Mast Cell Protease 4 Is the Major Chymase in Murine Airways and has a Protective Role in Allergic Airway Inflammation. *J Immunol* (2009) 183(10):6369–76. doi: 10.4049/jimmunol.0900180
91. Waern I, Lundequist A, Pejler G, Wernersson S. Mast Cell Chymase Modulates IL-33 Levels and Controls Allergic Sensitization in Dust-Mite

Induced Airway Inflammation. *Mucosal Immunol* (2013) 6(5):911–20. doi: 10.1038/mi.2012.129
92. Wong CK, Ng SSM, Lun SWM, Cao J, Lam CWK. Signalling Mechanisms Regulating the Activation of Human Eosinophils by Mast-Cell-Derived Chymase: Implications for Mast Cell–Eosinophil Interaction in Allergic Inflammation. *Immunology* (2009) 126(4):579–87. doi: 10.1111/j.1365-2567.2008.02916.x
93. Thompson-Souza GA, Gropillo I, Neves JS. Cysteinyl Leukotrienes in Eosinophil Biology: Functional Roles and Therapeutic Perspectives in Eosinophilic Disorders. *Front Med* (2017) 4:106(106). doi: 10.3389/fmed.2017.00106
94. Wenzel SE, Westcott JY, Larsen GL. Bronchoalveolar Lavage Fluid Mediator Levels 5 Minutes After Allergen Challenge in Atopic Subjects With Asthma: Relationship to the Development of Late Asthmatic Responses. *J Allergy Clin Immunol* (1991) 87(2):540–8. doi: 10.1016/0091-6749(91)90013-E
95. Hirai H, Tanaka K, Yoshie O, Ogawa K, Kenmotsu K, Takamori Y, et al. Prostaglandin D2 Selectively Induces Chemotaxis in T Helper Type 2 Cells, Eosinophils, and Basophils *via* Seven- Transmembrane Receptor CRTH2. *J Exp Med* (2001) 193(2):255–61.
96. Nagata K, Hirai H, Tanaka K, Ogawa K, Aso T, Sugamura K, et al. CRTH2, an Orphan Receptor of T-Helper-2-Cells, Is Expressed on Basophils and Eosinophils and Responds to Mast Cell-Derived Factor(s). *FEBS Lett* (1999) 459(2):195–9.
97. Konya V, Mjösberg J. Lipid Mediators as Regulators of Human ILC2 Function in Allergic Diseases. *Immunol Lett* (2016) 179:36–42. doi: 10.1016/j.imlet.2016.07.006
98. Kagawa S, Fukunaga K, Oguma T, Suzuki Y, Shiomi T, Sayama K, et al. Role of Prostaglandin D2 Receptor CRTH2 in Sustained Eosinophil Accumulation in the Airways of Mice With Chronic Asthma. *Int Arch Allergy Immunol* (2011) 155 Suppl 1:6–11. doi: 10.1159/000327257
99. Kataoka N, Satoh T, Hirai A, Saeki K, Yokozeki H. Indomethacin Inhibits Eosinophil Migration to Prostaglandin D2 : Therapeutic Potential of CRTH2 Desensitization for Eosinophilic Pustular Folliculitis. *Immunology* (2013) 140(1):78–86. doi: 10.1111/imm.12112
100. Reuter S, Dehzad N, Martin H, Heinz A, Castor T, Sudowe S, et al. Mast Cells Induce Migration of Dendritic Cells in a Murine Model of Acute Allergic Airway Disease. *Int Arch Allergy Immunol* (2010) 151(3):214–22. doi: 10.1159/000242359
101. Esnault S, Kelly EA. Essential Mechanisms of Differential Activation of Eosinophils by IL-3 Compared to GM-CSF and IL-5. *Crit Rev Immunol* (2016) 36(5):429–44. doi: 10.1615/CritRevImmunol.2017020172
102. Park BL, Kim LH, Choi YH, Lee J-H, Rhim T, Lee YM, et al. Interleukin 3 (IL3) Polymorphisms Associated With Decreased Risk of Asthma and Atopy. *J Hum Genet* (2004) 49(10):517–27. doi: 10.1007/s10038-004-0184-x
103. Hinks TSC, Hoyle RD, Gelfand EW. CD8+ Tc2 Cells: Underappreciated Contributors to Severe Asthma. *Eur Respir Rev* (2019) 28(154):190092. doi: 10.1183/16000617.0092-2019
104. Stoeckle C, Simon HU. CD8(+) T Cells Producing IL-3 and IL-5 in Non-IgE-Mediated Eosinophilic Diseases. *Allergy* (2013) 68(12):1622–5. doi: 10.1111/all.12311
105. Zhu C, Weng QY, Zhou LR, Cao C, Li F, Wu YF, et al. Homeostatic and Early-Recruited CD101(-) Eosinophils Suppress Endotoxin-Induced Acute Lung Injury. *Eur Respir J* (2020) 56(5):1902354. doi: 10.1183/13993003.02354-2019
106. Krishnamoorthy N, Douda DN, Brüggemann TR, Ricklefs I, Duvall MG, Abdulnour RE, et al. Neutrophil Cytoplasts Induce T(H)17 Differentiation and Skew Inflammation Toward Neutrophilia in Severe Asthma. *Sci Immunol* (2018) 3(26):eaao4747. doi: 10.1126/sciimmunol.aao4747
107. Liu MC, Hubbard WC, Proud D, Stealey BA, Galli SJ, Kagey-Sobotka A, et al. Immediate and Late Inflammatory Responses to Ragweed Antigen Challenge of the Peripheral Airways in Allergic Asthmatics. Cellular, Mediator, and Permeability Changes. *Am Rev Respir Dis* (1991) 144(1):51–8. doi: 10.1164/ajrccm/144.1.51
108. Alon R, Sportiello M, Kozlovski S, Kumar A, Reilly EC, Zarbock A, et al. Leukocyte Trafficking to the Lungs and Beyond: Lessons From Influenza for COVID-19. *Nat Rev Immunol* (2021) 21(1):49–64. doi: 10.1038/s41577-020-00470-2
109. Iype J, Fux M. Basophils Orchestrating Eosinophils' Chemotaxis and Function in Allergic Inflammation. *Cells* (2021) 10(4):895. doi: 10.3390/cells10040895
110. Gauvreau GM, Lee JM, Watson RM, Irani AM, Schwartz LB, O'Byrne PM. Increased Numbers of Both Airway Basophils and Mast Cells in Sputum After Allergen Inhalation Challenge of Atopic Asthmatics. *Am J Respir Crit Care Med* (2000) 161(5):1473–8. doi: 10.1164/ajrccm.161.5.9908090
111. Outh R, Boutin C, Gueudet P, Suzuki M, Saada M, Aumaître H. Eosinopenia <100/µl as a Marker of Active COVID-19: An Observational Prospective Study. *J Microbiol Immunol Infect* (2021) 54(1):61–8. doi: 10.1016/j.jmii.2020.12.005
112. Zellweger F, Buschor P, Hobi G, Brigger D, Dahinden CA, Villiger PM, et al. IL-3 But Not Monomeric IgE Regulates Fcεri Levels and Cell Survival in Primary Human Basophils. *Cell Death Dis* (2018) 9(5):510. doi: 10.1038/s41419-018-0526-9
113. Schroeder JT, Chichester KL, Bieneman AP. Human Basophils Secrete IL-3: Evidence of Autocrine Priming for Phenotypic and Functional Responses in Allergic Disease. *J Immunol* (2009) 182(4):2432–8. doi: 10.4049/jimmunol.0801782
114. Inclan-Rico JM, Ponessa JJ, Valero-Pacheco N, Hernandez CM, Sy CB, Lemenze AD, et al. Basophils Prime Group 2 Innate Lymphoid Cells for Neuropeptide-Mediated Inhibition. *Nat Immunol* (2020) 21(10):1181–93. doi: 10.1038/s41590-020-0753-y
115. Bando T, Fujita S, Nagano N, Yoshikawa S, Yamanishi Y, Minami M, et al. Differential Usage of COX-1 and COX-2 in Prostaglandin Production by Mast Cells and Basophils. *Biochem Biophys Rep* (2017) 10:82–7. doi: 10.1016/j.bbrep.2017.03.004
116. Schroeder JT, Lichtenstein LM, Roche EM, Xiao H, Liu MC. IL-4 Production by Human Basophils Found in the Lung Following Segmental Allergen Challenge. *J Allergy Clin Immunol* (2001) 107(2):265–71. doi: 10.1067/mai.2001.112846
117. Mochizuki M, Bartels J, Mallet AI, Christophers E, Schröder J-M. IL-4 Induces Eotaxin: A Possible Mechanism of Selective Eosinophil Recruitment in Helminth Infection and Atopy. *J Immunol* (1998) 160(1):60–8.
118. Shinkai A, Yoshisue H, Koike M, Shoji E, Nakagawa S, Saito A, et al. A Novel Human CC Chemokine, Eotaxin-3, Which Is Expressed in IL-4-Stimulated Vascular Endothelial Cells, Exhibits Potent Activity Toward Eosinophils. *J Immunol* (1999) 163(3):1602–10.
119. Schleimer RP, Sterbinsky SA, Kaiser J, Bickel CA, Klunk DA, Tomioka K, et al. IL-4 Induces Adherence of Human Eosinophils and Basophils But Not Neutrophils to Endothelium. Association With Expression of VCAM-1. *J Immunol* (1992) 148(4):1086–92.
120. Coyle AJ, Gros GL, Bertrand C, Tsuyuki S, Heusser CH, Kopf M, et al. Interleukin-4 is Required for the Induction of Lung Th2 Mucosal Immunity. *Am J Respir Cell Mol Biol* (1995) 13(1):54–9. doi: 10.1165/ajrcmb.13.1.7598937
121. Felton JM, Bouffi C, Schwartz JT, Schollaert KL, Malik A, Vallabh S, et al. Aiolos Regulates Eosinophil Migration Into Tissues. *Mucosal Immunol* (2021) 14(6):1271–81. doi: 10.1038/s41385-021-00416-4
122. Yi S, Zhai J, Niu R, Zhu G, Wang M, Liu J, et al. Eosinophil Recruitment is Dynamically Regulated by Interplay Among Lung Dendritic Cell Subsets After Allergen Challenge. *Nat Commun* (2018) 9(1):3879. doi: 10.1038/s41467-018-06316-9
123. Jacobsen EA, Ochkur SI, Pero RS, Taranova AG, Protheroe CA, Colbert DC, et al. Allergic Pulmonary Inflammation in Mice is Dependent on Eosinophil-Induced Recruitment of Effector T Cells. *J Exp Med* (2008) 205(3):699–710. doi: 10.1084/jem.20071840
124. Walsh ER, Sahu N, Kearley J, Benjamin E, Kang BH, Humbles A, et al. Strain-Specific Requirement for Eosinophils in the Recruitment of T Cells to the Lung During the Development of Allergic Asthma. *J Exp Med* (2008) 205(6):1285–92. doi: 10.1084/jem.20071836
125. Fulkerson PC, Fischetti CA, McBride ML, Hassman LM, Hogan SP, Rothenberg ME. A Central Regulatory Role for Eosinophils and the Eotaxin/CCR3 Axis in Chronic Experimental Allergic Airway Inflammation. *Proc Natl Acad Sci USA* (2006) 103(44):16418–23. doi: 10.1073/pnas.0607863103
126. Voehringer D, Reese TA, Huang X, Shinkai K, Locksley RM. Type 2 Immunity Is Controlled by IL-4/IL-13 Expression in Hematopoietic non-

Eosinophil Cells of the Innate Immune System. *J Exp Med* (2006) 203 (6):1435–46. doi: 10.1084/jem.20052448
127. Esnault S, Kelly EA, Schwantes EA, Liu LY, DeLain LP, Hauer JA, et al. Identification of Genes Expressed by Human Airway Eosinophils After an *In Vivo* Allergen Challenge. *PloS One* (2013) 8(7):e67560. doi: 10.1371/journal.pone.0067560
128. Farahi N, Loutsios C, Tregay N, Wright AKA, Berair R, Lok LSC, et al. *In Vivo* Imaging Reveals Increased Eosinophil Uptake in the Lungs of Obese Asthmatic Patients. *J Allergy Clin Immunol* (2018) 142(5):1659–62.e8. doi: 10.1016/j.jaci.2018.07.011
129. Bullone M, Carriero V, Bertolini F, Folino A, Mannelli A, Di Stefano A, et al. Elevated Serum IgE, Oral Corticosteroid Dependence and IL-17/22 Expression in Highly Neutrophilic Asthma. *Eur Respir J* (2019) 54 (5):1900068. doi: 10.1183/13993003.00068-2019
130. Gibbs J, Ince L, Matthews L, Mei J, Bell T, Yang N, et al. An Epithelial Circadian Clock Controls Pulmonary Inflammation and Glucocorticoid Action. *Nat Med* (2014) 20(8):919–26. doi: 10.1038/nm.3599
131. Toussaint M, Jackson DJ, Swieboda D, Guedán A, Tsourouktsoglou T-D, Ching YM, et al. Host DNA Released by NETosis Promotes Rhinovirus-Induced Type-2 Allergic Asthma Exacerbation. *Nat Med* (2017) 23(6):681–91. doi: 10.1038/nm.4332
132. Patel DF, Peiró T, Bruno N, Vuononvirta J, Akthar S, Puttur F, et al. Neutrophils Restrain Allergic Airway Inflammation by Limiting ILC2 Function and Monocyte–Dendritic Cell Antigen Presentation. *Sci Immunol* (2019) 4(41):eaax7006. doi: 10.1126/sciimmunol.aax7006
133. Kim Y-M, Kim H, Lee S, Kim S, Lee J-U, Choi Y, et al. Airway G-CSF Identifies Neutrophilic Inflammation and Contributes to Asthma Progression. *Eur Respir J* (2020) 55(2):1900827. doi: 10.1183/13993003.00827-2019
134. Wood LG, Baines KJ, Fu J, Scott HA, Gibson PG. The Neutrophilic Inflammatory Phenotype Is Associated With Systemic Inflammation in Asthma. *Chest* (2012) 142(1):86–93. doi: 10.1378/chest.11-1838
135. Lilly CM, Tateno H, Oguma T, Israel E, Sonna LA. Effects of Allergen Challenge on Airway Epithelial Cell Gene Expression. *Am J Respir Crit Care Med* (2005) 171(6):579–86. doi: 10.1164/rccm.200404-532OC
136. Reynolds CJ, Quigley K, Cheng X, Suresh A, Tahir S, Ahmed-Jushuf F, et al. Lung Defense Through IL-8 Carries a Cost of Chronic Lung Remodeling and Impaired Function. *Am J Respir Cell Mol Biol* (2018) 59(5):557–71. doi: 10.1165/rcmb.2018-0007OC
137. Lilly CM, Nakamura H, Belostotsky OI, Haley KJ, Garcia-Zepeda EA, Luster AD, et al. Eotaxin Expression After Segmental Allergen Challenge in Subjects With Atopic Asthma. *Am J Respir Crit Care Med* (2001) 163(7):1669–75. doi: 10.1164/ajrccm.163.7.9812044
138. Winkler C, Hochdörfer T, Israelsson E, Hasselberg A, Cavallin A, Thörn K, et al. Activation of Group 2 Innate Lymphoid Cells After Allergen Challenge in Asthmatic Patients. *J Allergy Clin Immunol* (2019) 144(1):61–9.e7. doi: 10.1016/j.jaci.2019.01.027
139. Wilson DR, Merrett TG, Varga EM, Smurthwaite L, Gould HJ, Kemp M, et al. Increases in Allergen-Specific IgE in BAL After Segmental Allergen Challenge in Atopic Asthmatics. *Am J Respir Crit Care Med* (2002) 165 (1):22–6. doi: 10.1164/ajrccm.165.1.2010112
140. Krug N, Tschernig T, Erpenbeck VJ, Hohlfeld JM, Köhl. Complement Factors C3a and C5a Are Increased in Bronchoalveolar Lavage Fluid After Segmental Allergen Provocation in Subjects With Asthma. *Am J Respir Crit Care Med* (2001) 164(10):1841–3. doi: 10.1164/ajrccm.164.10.2010096
141. Erpenbeck VJ, Hohlfeld JM, Volkmann B, Hagenberg A, Geldmacher H, Braun A, et al. Segmental Allergen Challenge in Patients With Atopic Asthma Leads to Increased IL-9 Expression in Bronchoalveolar Lavage Fluid Lymphocytes. *J Allergy Clin Immunol* (2003) 111(6):1319–27. doi: 10.1067/mai.2003.1485
142. Gosset P, Tsicopoulos A, Wallaert B, Vannimenus C, Joseph M, Tonnel AB, et al. Increased Secretion of Tumor Necrosis Factor Alpha and Interleukin-6 by Alveolar Macrophages Consecutive to the Development of the Late Asthmatic Reaction. *J Allergy Clin Immunol* (1991) 88(4):561–71.
143. Lee YG, Jeong JJ, Nyenhuis S, Berdyshev E, Chung S, Ranjan R, et al. Recruited Alveolar Macrophages, in Response to Airway Epithelial–Derived Monocyte Chemoattractant Protein 1/CCL2, Regulate Airway Inflammation and Remodeling in Allergic Asthma. *Am J Respir Cell Mol Biol* (2015) 52 (6):772–84. doi: 10.1165/rcmb.2014-0255OC
144. Van Dyken SJ, Locksley RM. Interleukin-4- and Interleukin-13-Mediated Alternatively Activated Macrophages: Roles in Homeostasis and Disease. *Annu Rev Immunol* (2013) 31:317–43. doi: 10.1146/annurev-immunol-032712-095906
145. Cho JL, Ling MF, Adams DC, Faustino L, Islam SA, Afshar R, et al. Allergic Asthma is Distinguished by Sensitivity of Allergen-Specific CD4+ T Cells and Airway Structural Cells to Type 2 Inflammation. *Sci Transl Med* (2016) 8 (359):359ra132. doi: 10.1126/scitranslmed.aag1370
146. Spencer LA, Szela CT, Perez SA, Kirchhoffer CL, Neves JS, Radke AL, et al. Human Eosinophils Constitutively Express Multiple Th1, Th2, and Immunoregulatory Cytokines That Are Secreted Rapidly and Differentially. *J Leukoc Biol* (2009) 85(1):117–23. doi: 10.1189/jlb.0108058
147. Beckert H, Meyer-Martin H, Buhl R, Taube C, Reuter S. Single and Synergistic Effects of Type 2 Cytokines on Eosinophils and Asthma Hallmarks. *J Immunol* (2020) 204(3):550–8. doi: 10.4049/jimmunol.1901116
148. Chu VT, Fröhlich A, Steinhauser G, Scheel T, Roch T, Fillatreau S, et al. Eosinophils are Required for the Maintenance of Plasma Cells in the Bone Marrow. *Nat Immunol* (2011) 12(2):151–9. doi: 10.1038/ni.1981
149. Peters MC, Ringel L, Dyjack N, Herrin R, Woodruff PG, Rios C, et al. A Transcriptomic Method to Determine Airway Immune Dysfunction in T2-High and T2-Low Asthma. *Am J Respir Crit Care Med* (2019) 199(4):465–77. doi: 10.1164/rccm.201807-1291OC
150. Robinson DR, Hamid Q, Ying S, Tsicopoulos A, Barkans J, Bentley AM, et al. Predominant Th2- Like Bronchoalveolar T Lymphocyte Population in Atopic Asthma. *NEnglJMed* (1992) 326:298–304.
151. Coquet Jonathan M, Schuijs Martijn J, Smyth Mark J, Deswarte K, Beyaert R, Braun H, et al. Interleukin-21-Producing CD4+ T Cells Promote Type 2 Immunity to House Dust Mites. *Immunity* (2015) 43(2):318–30. doi: 10.1016/j.immuni.2015.07.015
152. Tibbitt CA, Stark JM, Martens L, Ma J, Mold JE, Deswarte K, et al. Single-Cell RNA Sequencing of the T Helper Cell Response to House Dust Mites Defines a Distinct Gene Expression Signature in Airway Th2 Cells. *Immunity* (2019) 51(1):169–84.e5. doi: 10.1016/j.immuni.2019.05.014
153. Chen T, Tibbitt CA, Feng X, Stark JM, Rohrbeck L, Rausch L, et al. PPAR-γ Promotes Type 2 Immune Responses in Allergy and Nematode Infection. *Sci Immunol* (2017) 2(9):eaal5196. doi: 10.1126/sciimmunol.aal5196
154. Liang H-E, Reinhardt RL, Bando JK, Sullivan BM, Ho IC, Locksley RM. Divergent Expression Patterns of IL-4 and IL-13 Define Unique Functions in Allergic Immunity. *Nat Immunol* (2012) 13(1):58–66. doi: 10.1038/ni.2182
155. Saglani S, Gregory LG, Manghera AK, Branchett WJ, Uwadiae F, Entwistle LJ, et al. Inception of Early-Life Allergen–Induced Airway Hyperresponsiveness is Reliant on IL-13+CD4+ T Cells. *Sci Immunol* (2018) 3(27):eaan4128. doi: 10.1126/sciimmunol.aan4128
156. Akbari O, Stock P, Meyer E, Kronenberg M, Sidobre S, Nakayama T, et al. Essential Role of NKT Cells Producing IL-4 and IL-13 in the Development of Allergen-Induced Airway Hyperreactivity. *Nat Med* (2003) 9(5):582–8. doi: 10.1038/nm851
157. Terashima A, Watarai H, Inoue S, Sekine E, Nakagawa R, Hase K, et al. A Novel Subset of Mouse NKT Cells Bearing the IL-17 Receptor B Responds to IL-25 and Contributes to Airway Hyperreactivity. *J Exp Med* (2008) 205 (12):2727–33. doi: 10.1084/jem.20080698
158. Scanlon ST, Thomas SY, Ferreira CM, Bai L, Krausz T, Savage PB, et al. Airborne Lipid Antigens Mobilize Resident Intravascular NKT Cells to Induce Allergic Airway Inflammation. *J Exp Med* (2011) 208(10):2113–24. doi: 10.1084/jem.20110522
159. Godar M, Deswarte K, Vergote K, Saunders M, de Haard H, Hammad H, et al. A Bispecific Antibody Strategy to Target Multiple Type 2 Cytokines in Asthma. *J Allergy Clin Immunol* (2018) 142(4):1185–93. doi: 10.1016/j.jaci.2018.06.002
160. Seumois G, Ramírez-Suástegui C, Schmiedel BJ, Liang S, Peters B, Sette A, et al. Single-Cell Transcriptomic Analysis of Allergen-Specific T Cells in Allergy and Asthma. *Sci Immunol* (2020) 5(48):eaba6087. doi: 10.1126/sciimmunol.aba6087
161. Veldhoen M, Uyttenhove C, van Snick J, Helmby H, Westendorf A, Buer J, et al. Transforming Growth Factor-Beta 'Reprograms' the Differentiation of

T Helper 2 Cells and Promotes an Interleukin 9- Producing Subset. *Nat Immunol* (2008) 9(12):1341–6. doi: 10.1038/ni.1659
162. Gounni AS, Nutku E, Koussih L, Aris F, Louahed J, Levitt RC, et al. IL-9 Expression by Human Eosinophils: Regulation by IL-1β and TNF-α. *J Allergy Clin Immunol* (2000) 106(3):460–6. doi: 10.1067/mai.2000.109172
163. Sun B, Zhu L, Tao Y, Sun H-X, Li Y, Wang P, et al. Characterization and Allergic Role of IL-33- Induced Neutrophil Polarization. *Cell Mol Immunol* (2018) 15(8):782–93. doi: 10.1038/cmi.2017.163
164. Sordillo JE, Kelly R, Bunyavanich S, McGeachie M, Qiu W, Croteau-Chonka DC, et al. Genome- Wide Expression Profiles Identify Potential Targets for Gene-Environment Interactions in Asthma Severity. *J Allergy Clin Immunol* (2015) 136(4):885–92.e2. doi: 10.1016/j.jaci.2015.02.035
165. Du X, Li C, Wang W, Huang Q, Wang J, Tong Z, et al. IL-33 Induced Airways Inflammation Is Partially Dependent on IL-9. *Cell Immunol* (2020) 352:104098.
166. Yao W, Zhang Y, Jabeen R, Nguyen Evelyn T, Wilkes David S, Tepper Robert S, et al. Interleukin-9 Is Required for Allergic Airway Inflammation Mediated by the Cytokine TSLP. *Immunity* (2013) 38(2):360–72. doi: 10.1016/j.immuni.2013.01.007
167. Angkasekwinai P, Chang SH, Thapa M, Watarai H, Dong C. Regulation of IL-9 Expression by IL-25 Signaling. *Nat Immunol* (2010) 11(3):250–6. doi: 10.1038/ni.1846
168. Bankova LG, Dwyer DF, Liu AY, Austen KF, Gurish MF. Maturation of Mast Cell Progenitors to Mucosal Mast Cells During Allergic Pulmonary Inflammation in Mice. *Mucosal Immunol* (2015) 8(3):596–606. doi: 10.1038/mi.2014.91
169. Kearley J, Erjefalt JS, Andersson C, Benjamin E, Jones CP, Robichaud A, et al. IL-9 Governs Allergen-Induced Mast Cell Numbers in the Lung and Chronic Remodeling of the Airways. *Am J Respir Crit Care Med* (2011) 183(7):865–75. doi: 10.1164/rccm.200909-1462OC
170. Sehra S, Yao W, Nguyen ET, Glosson-Byers NL, Akhtar N, Zhou B, et al. TH9 Cells Are Required for Tissue Mast Cell Accumulation During Allergic Inflammation. *J Allergy Clin Immunol* (2015) 136(2):433–40.e1. doi: 10.1016/j.jaci.2015.01.021
171. Odemuyiwa SO, Ghahary A, Li Y, Puttagunta L, Lee JE, Musat-Marcu S, et al. Cutting Edge: Human Eosinophils Regulate T Cell Subset Selection Through Indoleamine 2,3-Dioxygenase. *J Immunol* (2004) 173(10):5909–13. doi: 10.4049/jimmunol.173.10.5909
172. Wang HB, Akuthota P, Kanaoka Y, Weller PF. Airway Eosinophil Migration Into Lymph Nodes in Mice Depends on Leukotriene C4. *Allergy* (2017) 72 (6):927–36. doi: 10.1111/all.13094
173. Vroman H, Bergen IM, Li BW, van Hulst JA, Lukkes M, van Uden D, et al. Development of Eosinophilic Inflammation Is Independent of B-T Cell Interaction in a Chronic House Dust Mite-Driven Asthma Model. *Clin Exp Allergy* (2017) 47(4):551–64. doi: 10.1111/cea.12834
174. Manz MG, Boettcher S. Emergency Granulopoiesis. *Nat Rev Immunol* (2014) 14(5):302–14. doi: 10.1038/nri3660
175. Berdnikovs S. The Twilight Zone: Plasticity and Mixed Ontogeny of Neutrophil and Eosinophil Granulocyte Subsets. *Semin Immunopathol* (2021) 43(3):337–46. doi: 10.1007/s00281-021-00862-z
176. Klion AD, Ackerman SJ, Bochner BS. Contributions of Eosinophils to Human Health and Disease. *Annu Rev Pathol: Mech Dis* (2020) 15(1):179–209. doi: 10.1146/annurev-pathmechdis-012419-032756
177. Tani Y, Isobe Y, Imoto Y, Segi-Nishida E, Sugimoto Y, Arai H, et al. Eosinophils Control the Resolution of Inflammation and Draining Lymph Node Hypertrophy Through the Proresolving Mediators and CXCL13 Pathway in Mice. *FASEB J Off Publ Fed Am Soc Exp Biol* (2014) 28 (9):4036–43. doi: 10.1096/fj.14-251132
178. Hwang JY, Randall TD, Silva-Sanchez A. Inducible Bronchus-Associated Lymphoid Tissue: Taming Inflammation in the Lung. *Front Immunol* (2016) 7:258(258). doi: 10.3389/fimmu.2016.00258
179. Takeda K, Shiraishi Y, Ashino S, Han J, Jia Y, Wang M, et al. Eosinophils Contribute to the Resolution of Lung-Allergic Responses Following Repeated Allergen Challenge. *J Allergy Clin Immunol* (2015) 135(2):451–60. doi: 10.1016/j.jaci.2014.08.014
180. Leitch AE, Duffin R, Haslett C, Rossi AG. Relevance of Granulocyte Apoptosis to Resolution of Inflammation at the Respiratory Mucosa. *Mucosal Immunol* (2008) 1(5):350–63. doi: 10.1038/mi.2008.31
181. Bosurgi L, Cao YG, Cabeza-Cabrerizo M, Tucci A, Hughes LD, Kong Y, et al. Macrophage Function in Tissue Repair and Remodeling Requires IL-4 or IL-13 With Apoptotic Cells. *Science* (2017) 356(6342):1072–6. doi: 10.1126/science.aai8132
182. Lechner AJ, Driver IH, Lee J, Conroy CM, Nagle A, Locksley RM, et al. Recruited Monocytes and Type 2 Immunity Promote Lung Regeneration Following Pneumonectomy. *Cell Stem Cell* (2017) 21(1):120–34.e7. doi: 10.1016/j.stem.2017.03.024
183. Nepal S, Tiruppathi C, Tsukasaki Y, Farahany J, Mittal M, Rehman J, et al. STAT6 Induces Expression of Gas6 in Macrophages to Clear Apoptotic Neutrophils and Resolve Inflammation. *Proc Natl Acad Sci* (2019) 116 (33):16513–8. doi: 10.1073/pnas.1821601116
184. Felton JM, Lucas CD, Dorward DA, Duffin R, Kipari T, Vermeren S, et al. Mer-Mediated Eosinophil Efferocytosis Regulates Resolution of Allergic Airway Inflammation. *J Allergy Clin Immunol* (2018) 142(6):1884–93.e6. doi: 10.1016/j.jaci.2018.01.029
185. Felton JM, Dorward DA, Cartwright JA, Potey PM, Robb CT, Gui J, et al. Mcl-1 Protects Eosinophils From Apoptosis and Exacerbates Allergic Airway Inflammation. *Thorax* (2020) 75(7):600–5. doi: 10.1136/thoraxjnl-2019-213204
186. Persson C. *In Vivo* Observations Provide Insight Into Roles of Eosinophils and Epithelial Cells in Asthma. *Eur Respir J* (2019) 54(4):1900470. doi: 10.1183/13993003.00470-2019
187. Ueki S, Melo RC, Ghiran I, Spencer LA, Dvorak AM, Weller PF. Eosinophil Extracellular DNA Trap Cell Death Mediates Lytic Release of Free Secretion-Competent Eosinophil Granules in Humans. *Blood* (2013) 121(11):2074–83. doi: 10.1182/blood-2012-05-432088
188. Wu Y, Chen H, Xuan N, Zhou L, Wu Y, Zhu C, et al. Induction of Ferroptosis-Like Cell Death of Eosinophils Exerts Synergistic Effects With Glucocorticoids in Allergic Airway Inflammation. *Thorax* (2020) 75 (11):918–27. doi: 10.1136/thoraxjnl-2020-214764
189. Boada-Romero E, Martinez J, Heckmann BL, Green DR. The Clearance of Dead Cells by Efferocytosis. *Nat Rev Mol Cell Biol* (2020) 21(7):398–414. doi: 10.1038/s41580-020-0232-1
190. Morita H, Arae K, Unno H, Miyauchi K, Toyama S, Nambu A, et al. An Interleukin-33-Mast Cell- Interleukin-2 Axis Suppresses Papain-Induced Allergic Inflammation by Promoting Regulatory T Cell Numbers. *Immunity* (2015) 43(1):175–86. doi: 10.1016/j.immuni.2015.06.021
191. Whyte CE, Singh K, Burton OT, Aloulou M, Moudra A, Roca CP, et al. Context-Dependent Effects of IL-2 Rewire Immunity Into Distinct Cellular Circuits. *bioRxiv* (2020). doi: 10.1101/2020.12.18.423431. 2020.12.18.423431.
192. Dagher R, Copenhaver AM, Besnard V, Berlin A, Hamidi F, Maret M, et al. IL-33-ST2 Axis Regulates Myeloid Cell Differentiation and Activation Enabling Effective Club Cell Regeneration. *Nat Commun* (2020) 11 (1):4786. doi: 10.1038/s41467-020-18466-w
193. Monticelli LA, Osborne LC, Noti M, Tran SV, Zaiss DMW, Artis D. IL-33 Promotes an Innate Immune Pathway of Intestinal Tissue Protection Dependent on Amphiregulin-EGFR Interactions. *Proc Natl Acad Sci USA* (2015) 112(34):10762–7. doi: 10.1073/pnas.1509070112
194. Vieira Braga FA, Kar G, Berg M, Carpaij OA, Polanski K, Simon LM, et al. A Cellular Census of Human Lungs Identifies Novel Cell States in Health and in Asthma. *Nat Med* (2019) 25(7):1153–63. doi: 10.1038/s41591-019-0468-5
195. Djukanovic R, Lai C, Wilson J, Britten K, Wilson S, Roche W, et al. Bronchial Mucosal Manifestations of Atopy: A Comparison of Markers of Inflammation Between Atopic Asthmatics, Atopic Nonasthmatics and Healthy Controls. *Eur Respir J* (1992) 5(5):538–44.
196. Amin K, Lúdvíksdóttir D, Janson C, Nettelbladt O, Björnsson E, Roomans GM, et al. Inflammation and Structural Changes in the Airways of Patients With Atopic and Nonatopic Asthma. *Am J Respir Crit Care Med* (2000) 162 (6):2295–301. doi: 10.1164/ajrccm.162.6.9912001
197. Brightling CE, Bradding P, Symon FA, Holgate ST, Wardlaw AJ, Pavord ID. Mast-Cell Infiltration of Airway Smooth Muscle in Asthma. *N Engl J Med* (2002) 346(22):1699–705. doi: 10.1056/NEJMoa012705
198. Dougherty RH, Sidhu SS, Raman K, Solon M, Solberg OD, Caughey GH, et al. Accumulation of Intraepithelial Mast Cells With a Unique Protease Phenotype in T(H)2-High Asthma. *J Allergy Clin Immunol* (2010) 125 (5):1046–53.e8. doi: 10.1016/j.jaci.2010.03.003
199. Carroll NG, Mutavdzic S, James AL. Increased Mast Cells and Neutrophils in Submucosal Mucous Glands and Mucus Plugging in Patients With Asthma. *Thorax* (2002) 57(8):677–82. doi: 10.1136/thorax.57.8.677

200. Lezmi G, Galmiche-Rolland L, Rioux S, Jaubert F, Tillie-Leblond I, Scheinmann P, et al. Mast Cells are Associated With Exacerbations and Eosinophilia in Children With Severe Asthma. *Eur Respir J* (2016) 48 (5):1320–8. doi: 10.1183/13993003.00947-2016
201. Debeuf N, Haspeslagh E, van Helden M, Hammad H, Lambrecht BN. Mouse Models of Asthma. *Curr Protoc Mouse Biol* (2016) 6(2):169–84. doi: 10.1002/cpmo.4
202. Foster PS, Hogan SP, Ramsay AJ, Matthaei KI, Young KI. Interleukin 5 Deficiency Abolishes Eosinophilia, Airways Hyperreactivity and Lung Damage in a Mouse Asthma Model. *J Exp Med* (1996) 183:195–201. doi: 10.1084/jem.183.1.195
203. Lee JJ, Dimina D, Macias MP, Ochkur SI, McGarry MP, O'Neill KR, et al. Defining a Link With Asthma in Mice Congenitally Deficient in Eosinophils. *Science* (2004) 305(5691):1773–6. doi: 10.1126/science.1099472
204. Justice JP, Borchers MT, Crosby JR, Hines EM, Shen HH, Ochkur SI, et al. Ablation of Eosinophils Leads to a Reduction of Allergen-Induced Pulmonary Pathology. *Am J Physiology-Lung Cell Mol Physiol* (2003) 284 (1):L169–78. doi: 10.1152/ajplung.00260.2002
205. Jacobsen EA, Ochkur SI, Doyle AD, LeSuer WE, Li W, Protheroe CA, et al. Lung Pathologies in a Chronic Inflammation Mouse Model Are Independent of Eosinophil Degranulation. *Am J Respir Crit Care Med* (2017) 195 (10):1321–32. doi: 10.1164/rccm.201606-1129OC
206. Haldar P, Brightling CE, Hargadon B, Gupta S, Monteiro W, Sousa A, et al. Mepolizumab and Exacerbations of Refractory Eosinophilic Asthma. *N Engl J Med* (2009) 360(10):973–84. doi: 10.1056/NEJMoa0808991
207. Damon M, Chavis C, Daures J, Crastes de Paulet A, Michel F, Godard P. Increased Generation of the Arachidonic Metabolites LTB4 and 5-HETE by Human Alveolar Macrophages in Patients With Asthma: Effect *In Vitro* Nedocromil Sodium. *Eur Respir J* (1989) 2(3):202–9.
208. Huynh M-LN, Malcolm KC, Kotaru C, Tilstra JA, Westcott JY, Fadok VA, et al. Defective Apoptotic Cell Phagocytosis Attenuates Prostaglandin E2 and 15-Hydroxyeicosatetraenoic Acid in Severe Asthma Alveolar Macrophages. *Am J Respir Crit Care Med* (2005) 172(8):972–9. doi: 10.1164/rccm.200501-035OC
209. Persson EK, Verstraete K, Heyndrickx I, Gevaert E, Aegerter H, Percier JM, et al. Protein Crystallization Promotes Type 2 Immunity and Is Reversible by Antibody Treatment. *Science* (2019) 364(6442). doi: 10.1126/science.aaw4295
210. Aegerter H, Smole U, Heyndrickx I, Verstraete K, Savvides SN, Hammad H, et al. Charcot- Leyden Crystals and Other Protein Crystals Driving Type 2 Immunity and Allergy. *Curr Opin Immunol* (2021) 72:72–8. doi: 10.1016/j.coi.2021.03.013
211. Choi Y, Kim YM, Lee HR, Mun J, Sim S, Lee DH, et al. Eosinophil Extracellular Traps Activate Type 2 Innate Lymphoid Cells Through Stimulating Airway Epithelium in Severe Asthma. *Allergy* (2020) 75(1):95–103.
212. Ueki S, Tokunaga T, Melo RCN, Saito H, Honda K, Fukuchi M, et al. Charcot-Leyden Crystal Formation Is Closely Associated With Eosinophil Extracellular Trap Cell Death. *Blood* (2018) 132(20):2183–7. doi: 10.1182/blood-2018-04-842260
213. Nyenhuis SM, Alumkal P, Du J, Maybruck BT, Vinicky M, Ackerman SJ. Charcot–Leyden Crystal Protein/Galectin-10 Is a Surrogate Biomarker of Eosinophilic Airway Inflammation in Asthma. *Biomarkers Med* (2019) 13 (9):715–24.
214. Gevaert E, Delemarre T, De Volder J, Zhang N, Holtappels G, De Ruyck N, et al. Charcot-Leyden Crystals Promote Neutrophilic Inflammation in Patients With Nasal Polyposis. *J Allergy Clin Immunol* (2020) 145(1):427–30.e4.
215. Lu Y, Huang Y, Li J, Huang J, Zhang L, Feng J, et al. Eosinophil Extracellular Traps Drive Asthma Progression Through Neuro-Immune Signals. *Nat Cell Biol* (2021) 23(10):1060–72. doi: 10.1038/s41556-021-00762-2
216. Hondowicz Brian D, An D, Schenkel Jason M, Kim Karen S, Steach Holly R, Krishnamurty Akshay T, et al. Interleukin-2-Dependent Allergen-Specific Tissue-Resident Memory Cells Drive Asthma. *Immunity* (2016) 44(1):155–66. doi: 10.1016/j.immuni.2015.11.004
217. Bošnjak B, Kazemi S, Altenburger LM, Mokrović G, Epstein MM. Th2-TRMs Maintain Life-Long Allergic Memory in Experimental Asthma in Mice. *Front Immunol* (2019) 10:840. doi: 10.3389/fimmu.2019.00840
218. Rahimi RA, Nepal K, Cetinbas M, Sadreyev RI, Luster AD. Distinct Functions of Tissue-Resident and Circulating Memory Th2 Cells in Allergic Airway Disease. *J Exp Med* (2020) 217(9):e20190865. doi: 10.1084/jem.20190865
219. Hewitt RJ, Lloyd CM. Regulation of Immune Responses by the Airway Epithelial Cell Landscape. *Nat Rev Immunol* (2021) 21(6):347–62. doi: 10.1038/s41577-020-00477-9
220. Allinne J, Scott G, Lim WK, Birchard D, Erjefält JS, Sandén C, et al. IL-33 Blockade Affects Mediators of Persistence and Exacerbation in a Model of Chronic Airway Inflammation. *J Allergy Clin Immunol* (2019) 144(6):1624–37.e10. doi: 10.1016/j.jaci.2019.08.039
221. Martinez-Gonzalez I, Mathä L, Steer Catherine A, Ghaedi M, Poon Grace FT, Takei F. Allergen- Experienced Group 2 Innate Lymphoid Cells Acquire Memory-Like Properties and Enhance Allergic Lung Inflammation. *Immunity* (2016) 45(1):198–208. doi: 10.1016/j.immuni.2016.06.017
222. Ordovas-Montanes J, Dwyer DF, Nyquist SK, Buchheit KM, Vukovic M, Deb C, et al. Allergic Inflammatory Memory in Human Respiratory Epithelial Progenitor Cells. *Nature* (2018) 560(7720):649–54. doi: 10.1038/s41586-018-0449-8
223. Kyoh S, Venkatesan N, Poon AH, Nishioka M, Lin T-Y, Baglole CJ, et al. Are Leukocytes in Asthmatic Patients Aging Faster? A Study of Telomere Length and Disease Severity. *J Allergy Clin Immunol* (2013) 132(2):480–2.e2. doi: 10.1016/j.jaci.2013.02.010
224. Belsky DW, Shalev I, Sears MR, Hancox RJ, Harrington HL, Houts R, et al. Is Chronic Asthma Associated With Shorter Leukocyte Telomere Length at Midlife? *Am J Respir Crit Care Med* (2014) 190(4):384–91. doi: 10.1164/rccm.201402-0370OC
225. Barbé-Tuana FM, Grun LK, Pierdoná V, Parisi MM, Friedrich F, Guma FTCR, et al. Shorter Telomeres in Children With Severe Asthma, an Indicative of Accelerated Aging. *Aging* (2021) 13(2):1686–91. doi: 10.18632/aging.202527
226. Piñeiro-Hermida S, Martínez P, Blasco MA. Short and Dysfunctional Telomeres Protect From Allergen-Induced Airway Inflammation. *Aging Cell* (2021) 20(5):e13352. doi: 10.1111/acel.13352
227. Krishnan V, Diette GB, Rand CS, Bilderback AL, Merriman B, Hansel NN, et al. Mortality in Patients Hospitalized for Asthma Exacerbations in the United States. *Am J Respir Crit Care Med* (2006) 174(6):633–8. doi: 10.1164/rccm.200601-007OC
228. Jartti T, Gern JE. Role of Viral Infections in the Development and Exacerbation of Asthma in Children. *J Allergy Clin Immunol* (2017) 140 (4):895–906. doi: 10.1016/j.jaci.2017.08.003
229. Busse WW, Lemanske RF Jr, Gern JE. Role of Viral Respiratory Infections in Asthma and Asthma Exacerbations. *Lancet* (2010) 376(9743):826–34. doi: 10.1016/S0140-6736(10)61380-3
230. Denlinger LC, Phillips BR, Ramratnam S, Ross K, Bhakta NR, Cardet JC, et al. Inflammatory and Comorbid Features of Patients With Severe Asthma and Frequent Exacerbations. *Am J Respir Crit Care Med* (2017) 195(3):302–13. doi: 10.1164/rccm.201602-0419OC
231. Lynch JP, Werder RB, Simpson J, Loh Z, Zhang V, Haque A, et al. Aeroallergen-Induced IL-33 Predisposes to Respiratory Virus–Induced Asthma by Dampening Antiviral Immunity. *J Allergy Clin Immunol* (2016) 138(5):1326–37. doi: 10.1016/j.jaci.2016.02.039
232. Altman MC, Gill MA, Whalen E, Babineau DC, Shao B, Liu AH, et al. Transcriptome Networks Identify Mechanisms of Viral and Nonviral Asthma Exacerbations in Children. *Nat Immunol* (2019) 20(5):637–51. doi: 10.1038/s41590-019-0347-8
233. Zhu J, Message SD, Mallia P, Kebadze T, Contoli M, Ward CK, et al. Bronchial Mucosal IFN-α/β and Pattern Recognition Receptor Expression in Patients With Experimental Rhinovirus-Induced Asthma Exacerbations. *J Allergy Clin Immunol* (2019) 143(1):114–25.e4. doi: 10.1016/j.jaci.2018.04.003
234. Contoli M, Message SD, Laza-Stanca V, Edwards MR, Wark PA, Bartlett NW, et al. Role of Deficient Type III Interferon-Lambda Production in Asthma Exacerbations. *Nat Med* (2006) 12(9):1023–6. doi: 10.1038/nm1462
235. Veerati PC, Troy NM, Reid AT, Li NF, Nichol KS, Kaur P, et al. Airway Epithelial Cell Immunity Is Delayed During Rhinovirus Infection in Asthma and COPD. *Front Immunol* (2020) 11:974(974). doi: 10.3389/fimmu.2020.00974
236. Vu LD, Siefker D, Jones TL, You D, Taylor R, DeVincenzo J, et al. Elevated Levels of Type 2 Respiratory Innate Lymphoid Cells in Human Infants With

Severe Respiratory Syncytial Virus Bronchiolitis. *Am J Respir Crit Care Med* (2019) 200(11):1414–23. doi: 10.1164/rccm.201812-2366OC
237. Li BW, de Bruijn MJ, Lukkes M, van Nimwegen M, Bergen IM, KleinJan A, et al. T Cells and ILC2s Are Major Effector Cells in Influenza-Induced Exacerbation of Allergic Airway Inflammation in Mice. *Eur J Immunol* (2019) 49(1):144–56. doi: 10.1002/eji.201747421
238. Bosteels C, Neyt K, Vanheerswynghels M, van Helden MJ, Sichien D, Debeuf N, et al. Inflammatory Type 2 cDCs Acquire Features of Cdc1s and Macrophages to Orchestrate Immunity to Respiratory Virus Infection. *Immunity* (2020) 52(6):1039–56. doi: 10.1016/j.immuni.2020.04.005
239. Duerr CU, McCarthy CDA, Mindt BC, Rubio M, Meli AP, Pothlichet J, et al. Type I Interferon Restricts Type 2 Immunopathology Through the Regulation of Group 2 Innate Lymphoid Cells. *Nat Immunol* (2015) 17:65. doi: 10.1038/ni.3308
240. Heijink IH, Nawijn MC, Hackett T-L. Airway Epithelial Barrier Function Regulates the Pathogenesis of Allergic Asthma. *Clin Exp Allergy* (2014) 44 (5):620–30. doi: 10.1111/cea.12296
241. Yoshihara S, Yamada Y, Abe T, Lindén A, Arisaka O. Association of Epithelial Damage and Signs of Neutrophil Mobilization in the Airways During Acute Exacerbations of Paediatric Asthma. *Clin Exp Immunol* (2006) 144(2):212–6. doi: 10.1111/j.1365-2249.2006.03058.x
242. Norzila MZ, Fakes K, Henry RL, Simpson J, Gibson PG. Interleukin-8 Secretion and Neutrophil Recruitment Accompanies Induced Sputum Eosinophil Activation in Children With Acute Asthma. *Am J Respir Crit Care Med* (2000) 161(3 Pt 1):769–74. doi: 10.1164/ajrccm.161.3.9809071
243. Nakagome K, Nagata M. Involvement and Possible Role of Eosinophils in Asthma Exacerbation. *Front Immunol* (2018) 9:2220. doi: 10.3389/fimmu.2018.02220
244. Johnston SL, Papi A, Bates PJ, Mastronarde JG, Monick MM, Hunninghake GW. Low Grade Rhinovirus Infection Induces a Prolonged Release of IL-8 in Pulmonary Epithelium. *J Immunol* (1998) 160(12):6172–81.
245. Cakebread JA, Haitchi HM, Xu Y, Holgate ST, Roberts G, Davies DE. Rhinovirus-16 Induced Release of IP-10 and IL-8 Is Augmented by Th2 Cytokines in a Pediatric Bronchial Epithelial Cell Model. *PloS One* (2014) 9 (4):e94010. doi: 10.1371/journal.pone.0094010
246. Piñeros YSS, Bal SM, Pol M, Dierdorp BS, Dekker T, Dijkhuis A, et al. Anti–IL-5 in Mild Asthma Alters Rhinovirus-Induced Macrophage, B-Cell, and Neutrophil Responses (MATERIAL). A Placebo-Controlled, Double-Blind Study. *Am J Respir Crit Care Med* (2019) 199(4):508–17. doi: 10.1164/rccm.201803-0461OC
247. Månsson A, Cardell LO. Role of Atopic Status in Toll-Like Receptor (TLR)7- and TLR9-Mediated Activation of Human Eosinophils. *J Leukoc Biol* (2009) 85(4):719–27. doi: 10.1189/jlb.0808494
248. Ferreira DS, Annoni R, Silva LF, Buttignol M, Santos AB, Medeiros MC, et al. Toll-Like Receptors 2, 3 and 4 and Thymic Stromal Lymphopoietin Expression in Fatal Asthma. *Clin Exp Allergy* (2012) 42(10):1459–71. doi: 10.1111/j.1365-2222.2012.04047.x
249. Kim CK, Callaway Z, Gern JE. Viral Infections and Associated Factors That Promote Acute Exacerbations of Asthma. *Allergy Asthma Immunol Res* (2018) 10(1):12–7. doi: 10.4168/aair.2018.10.1.12
250. Percopo CM, Dyer KD, Ochkur SI, Luo JL, Fischer ER, Lee JJ, et al. Activated Mouse Eosinophils Protect Against Lethal Respiratory Virus Infection. *Blood* (2014) 123(5):743–52. doi: 10.1182/blood-2013-05-502443
251. Mathur SK, Fichtinger PS, Kelly JT, Lee WM, Gern JE, Jarjour NN. Interaction Between Allergy and Innate Immunity: Model for Eosinophil Regulation of Epithelial Cell Interferon Expression. *Ann Allergy Asthma Immunol* (2013) 111(1):25–31. doi: 10.1016/j.anai.2013.05.010
252. Jayaram L, Pizzichini MM, Cook RJ, Boulet LP, Lemière C, Pizzichini E, et al. Determining Asthma Treatment by Monitoring Sputum Cell Counts: Effect on Exacerbations. *Eur Respir J* (2006) 27(3):483. doi: 10.1183/09031936.06.00137704
253. Samarasinghe AE, Melo RC, Duan S, LeMessurier KS, Liedmann S, Surman SL, et al. Eosinophils Promote Antiviral Immunity in Mice Infected With Influenza A Virus. *J Immunol* (2017) 198(8):3214–26. doi: 10.4049/jimmunol.1600787
254. Sabogal Piñeros YS, Bal SM, Dijkhuis A, Majoor CJ, Dierdorp BS, Dekker T, et al. Eosinophils Capture Viruses, a Capacity That Is Defective in Asthma. *Allergy* (2019) 74(10):1898–909. doi: 10.1111/all.13802
255. Ramirez GA, Yacoub MR, Ripa M, Mannina D, Cariddi A, Saporiti N, et al. Eosinophils From Physiology to Disease: A Comprehensive Review. *BioMed Res Int* (2018) 2018:9095275. doi: 10.1155/2018/9095275
256. Drake MG, Bivins-Smith ER, Proskocil BJ, Nie Z, Scott GD, Lee JJ, et al. Human and Mouse Eosinophils Have Antiviral Activity Against Parainfluenza Virus. *Am J Respir Cell Mol Biol* (2016) 55(3):387–94. doi: 10.1165/rcmb.2015-0405OC
257. Khoyratty TE, Ai Z, Ballesteros I, Eames HL, Mathie S, Martín-Salamanca S, et al. Distinct Transcription Factor Networks Control Neutrophil-Driven Inflammation. *Nat Immunol* (2021) 22(9):1093–106. doi: 10.1038/s41590-021-00968-4
258. Grieshaber-Bouyer R, Radtke FA, Cunin P, Stifano G, Levescot A, Vijaykumar B, et al. The Neutrotime Transcriptional Signature Defines a Single Continuum of Neutrophils Across Biological Compartments. *Nat Commun* (2021) 12(1):2856. doi: 10.1038/s41467-021-22973-9
259. Qi J, D'Souza D, Dawson T, Geanon D, Stefanos H, Marvin R, et al. Multimodal Single-Cell Characterization of the Human Granulocyte Lineage. *bioRxiv* (2021). doi: 10.1101/2021.06.12.448210. 2021.06.12.448210.
260. Schuijs MJ, Png S, Richard AC, Tsyben A, Hamm G, Stockis J, et al. ILC2-Driven Innate Immune Checkpoint Mechanism Antagonizes NK Cell Antimetastatic Function in the Lung. *Nat Immunol* (2020). doi: 10.1038/s41590-020-0745-y
261. Coden ME, Walker MT, Jeong BM, Connelly AR, Nagasaka R, Berdnikovs S. Beyond Il-5: Metabolic Reprogramming and Stromal Support Are Prerequisite for Generation and Survival of Long- Lived Eosinophil. *Cells* (2021) 10(4):815. doi: 10.3390/cells10040815
262. Porter L, Toepfner N, Bashant KR, Guck J, Ashcroft M, Farahi N, et al. Metabolic Profiling of Human Eosinophils. *Front Immunol* (2018) 9:1404 (1404). doi: 10.3389/fimmu.2018.01404

Conflict of Interest: The authors declare that the research was conducted in the absence of any commercial or financial relationships that could be construed as a potential conflict of interest.

Publisher's Note: All claims expressed in this article are solely those of the authors and do not necessarily represent those of their affiliated organizations, or those of the publisher, the editors and the reviewers. Any product that may be evaluated in this article, or claim that may be made by its manufacturer, is not guaranteed or endorsed by the publisher.

frontiers in Immunology

ORIGINAL RESEARCH
published: 23 November 2021
doi: 10.3389/fimmu.2021.740933

Major Neutrophil-Derived Soluble Mediators Associate With Baseline Lung Pathology and Post-Treatment Recovery in Tuberculosis Patients

Caleb Nwongbouwoh Muefong[1,2], Olumuyiwa Owolabi[1], Simon Donkor[1], Salome Charalambous[3], Joseph Mendy[1], Isatou C. M. Sey[1], Abhishek Bakuli[2,4], Andrea Rachow[2,4], Christof Geldmacher[2,4] and Jayne S. Sutherland[1]*

[1] Vaccines and Immunity Theme, Medical Research Council (MRC) Unit The Gambia at London School of Hygiene and Tropical Medicine (LSHTM), Fajara, Gambia, [2] Division of Infectious Diseases and Tropical Medicine, University Hospital, Ludwig Maximilian University (LMU) Munich, Munich, Germany, [3] School of Public Health, Aurum Institute, Johannesburg, South Africa, [4] International Clinical Trials Unit, German Centre for Infection Research (DZIF), Partner Site Munich, Munich, Germany

OPEN ACCESS

Edited by:
Rabindra Tirouvanziam,
Emory University, United States

Reviewed by:
Nathalie Winter,
Institut National de Recherche pour l'Agriculture, l'Alimentation et l'Environnement (INRAE), France
Dhiraj Kumar Singh,
Southwest National Primate Research Center (SNPRC), United States

***Correspondence:**
Caleb Nwongbouwoh Muefong
Caleb.Muefong@lshtm.ac.uk

Specialty section:
This article was submitted to Mucosal Immunity, a section of the journal Frontiers in Immunology

Received: 13 July 2021
Accepted: 01 November 2021
Published: 23 November 2021

Citation:
Muefong CN, Owolabi O, Donkor S, Charalambous S, Mendy J, Sey ICM, Bakuli A, Rachow A, Geldmacher C and Sutherland JS (2021) Major Neutrophil-Derived Soluble Mediators Associate With Baseline Lung Pathology and Post-Treatment Recovery in Tuberculosis Patients. Front. Immunol. 12:740933. doi: 10.3389/fimmu.2021.740933

Background: The inflammatory response to *Mycobacterium tuberculosis* results in variable degrees of lung pathology during active TB (ATB) with central involvement of neutrophils. Little is known about neutrophil-derived mediators and their role in disease severity at baseline and recovery upon TB treatment initiation.

Methods: 107 adults with confirmed pulmonary TB were categorised based on lung pathology at baseline and following successful therapy using chest X-ray scores (Ralph scores) and GeneXpert bacterial load (Ct values). Plasma, sputum, and antigen-stimulated levels of MMP1, MMP3, MMP8, MMP9, MPO, S100A8/9, IL8, IL10, IL12/23(p40), GM-CSF, IFNγ, and TNF were analysed using multiplex cytokine arrays.

Results: At baseline, neutrophil counts correlated with plasma levels of MMP8 (rho = 0.45, p = 2.80E–06), S100A8 (rho = 0.52, p = 3.00E–08) and GM-CSF (rho = 0.43, p = 7.90E–06). Levels of MMP8 (p = 3.00E–03), MMP1 (p = 1.40E–02), S100A8 (p = 1.80E–02) and IL12/23(p40) (p = 1.00E–02) were associated with severe lung damage, while sputum MPO levels were directly linked to lung damage (p = 1.80E–03), Mtb load (p = 2.10E–02) and lung recovery (p = 2.40E–02). Six months of TB therapy significantly decreased levels of major neutrophil-derived pro-inflammatory mediators: MMP1 (p = 4.90E–12 and p = 2.20E–07), MMP8 (p = 3.40E–14 and p = 1.30E–05) and MMP9 (p = 1.60E–04 and p = 1.50E–03) in plasma and sputum, respectively. Interestingly, following H37Rv whole cell lysate stimulation, S100A8 (p = 2.80E–02), MMP9 (p = 3.60E–02) and MPO (p = 9.10E–03) levels at month 6 were significantly higher compared to baseline. Sputum MMP1 (p = 1.50E–03), MMP3 (p = 7.58E–04), MMP9 (p = 2.60E–02) and TNF (p = 3.80E–02) levels were lower at month 6 compared to baseline in patients with good lung recovery.

Conclusion: In this study, patients with severe lung pathology at baseline and persistent lung damage after treatment were associated with higher plasma and sputum levels of major pro-inflammatory neutrophil-derived mediators. Interestingly, low sputum MPO

levels were associated with severe lung damage, higher Mtb burden and low recovery. Our data suggest that therapeutic agents which target these mediators should be considered for future studies on biomarkers and host-directed therapeutic approaches against TB-related lung pathology and/or lung recovery.

Keywords: tuberculosis, neutrophils, myeloperoxidase, S100A8/9, MMP8, lung pathology

INTRODUCTION

Tuberculosis (TB) caused 1.2 million deaths from HIV-negative individuals in 2019 (1). While treatment is available, former patients are more likely to experience long-term pulmonary disability (2) and only about 50% of patients achieve full recovery from lung damage (3). It has been suggested that higher initial inflammatory responses against *Mycobacterium tuberculosis* (Mtb) lead to more severe lung damage prior to treatment initiation (4) and thus reduced of recovery following treatment.

Inflammatory mediators generated during the natural immune response to Mtb (5) are linked to increased disease severity, bacterial burden and delayed culture conversion. However, the overall inflammatory response depends on the interplay between pro- and anti-inflammatory mediators (6). Interestingly, reports show that severe inflammation and lung damage following *Mycoplasma pneumoniae* infection in mice may be a result of oxidant–antioxidant imbalances which can be reduced by immunosuppression (6). Similarly, certain neutrophil sub-types have been shown to express immunosuppressive functions including: $CD16^{bright}CD62L^{low}$ neutrophils (7) and granulocytic myeloid-derived suppressor cells (G-MDSCs) (8, 9). These support the idea that an equilibrium between neutrophilic pro- and anti-inflammatory functions (10–14) determines the extend of inflammation and lung damage in TB patients.

Previous studies have investigated a broad range of biomarkers for TB disease progression and lung damage severity in humans (15–19), recently reviewed (20–22). While some neutrophilic activities have been tested, major neutrophil-derived mediators have not been the main focus. Neutrophils are mainly pro-inflammatory but recent studies reveal that different subtypes also display anti-inflammatory functions (11, 14, 23, 24) depending on the type and quantity of inflammatory mediators produced. A current challenge is to elucidate which neutrophil subtypes and mediators are predominantly pro- or anti-inflammatory during active TB and to determine the underlying immunological mechanisms involved in protective outcomes. Muefong and Sutherland reviewed (12) promising neutrophil-derived targets for developing host directed therapies (HDTs) against TB-induced lung pathology. We also recently showed, in a smaller group of participants from this Gambian cohort, that immature (banded) neutrophils and IL10-expressing $CD16^{dim}CD62L^{low}$ neutrophils are associated with reduced lung damage in active TB patients pre-treatment (13). Additionally, MDSCs are currently considered in the development of HDTs against TB progression and Mtb control (9, 25, 26) due to their role as effectors of Mtb pathogenesis and their modulatory role on T-cell function.

Studies in mice (27), macaques (28, 29) and humans (30, 31) suggest that heightened neutrophil function correlates with tissue injury. For example, during hypoxic conditions, human neutrophils have been shown to drive tissue destruction during ATB by secreting matrix metalloproteinases (MMPs) like MMP8 and MMP9 (32). Sputum MMP levels have also been associated with disease severity in ATB patients pre-treatment (33) and excess MMP activity enhances tissue injury in clinical studies and preclinical models of pulmonary pathology (34). S100A8/9 is another neutrophil-derived mediator known to exacerbate the inflammatory response to Mtb infection and it is currently targeted in Mtb control studies (28, 35).

On the other hand, recent studies highlight an immunoregulatory effect of granulocytes (36). In mice exposed to zymosan, deficiency in myeloperoxidase (MPO)—a major constituent of neutrophil granules—results in severe lung inflammation (37), suggesting that MPO could play immunomodulatory functions; an observation which has not been made in TB. Hence, different neutrophil-related mediators could differentially influence ATB-related lung pathology.

We contribute to the field of TB biomarkers by focusing on major neutrophil-derived inflammatory mediator levels in ATB patients and relate this to chest X-ray (CXR) based lung pathology scores and bacterial load before and after TB therapy. We address gaps in our understanding of TB pathogenesis by monitoring the impact of neutrophil-derived mediators on the severity of TB-induced lung pathology to inform future experiments in controlled animal models investigating TB HDTs.

METHODS

Ethics Approval

Ethical approval was obtained from the Medical Research Council/Gambia government joint ethics committee (SCC1523). All study participants provided written informed consent prior to collection of samples.

Participants

Adult, TB patients with positive GeneXpert (Cepheid, USA) results were recruited from the TB clinic at the MRC Unit The Gambia at LSHTM between April 2018 and October 2019 as part of a parent study, TB Sequel (3). This study was conducted on a sub-cohort of TB Sequel and patients were selected based on their lung recovery outcome post-treatment. All participants

were later confirmed to have a positive mycobacteria growth indicator tube (MGIT) culture result at baseline, were drug sensitive and had not previously received anti-TB therapy (ATT). They were given standard TB therapy consisting of 2 months intensive phase and 4 months continuation phase. Sputum liquid MGIT culture was performed at baseline (BL), 2 months (2M) and 6 months (6M) after ATT initiation. Heparinised blood and sputum samples were collected and processed at BL, 2M and 6M of standard treatment. All patients were culture negative by 6M and HIV positive patients were excluded from analysis.

Scoring of Chest Radiographs

Chest radiographs were analysed based on the Ralph score (RS) (38). Briefly, posteroanterior chest radiographs were assessed for the percentage of the lung fields affected by known ATB features. When at least one cavity could be identified, 40 points were added to the value of percentage lung affected. The median [interquartile range (IQR)] RS score at baseline (RS_{Med}) of all participants in our cohort was determined, 65 [29–80]. Lung damage severity (pre- and post-treatment) groupings were defined as follows: "mild pathology" ($RS < RS_{Med}$) and "severe pathology" ($RS \geq RS_{Med}$).

GeneXpert MTB/RIF Results

The GeneXpert® machine (Cepheid, USA) was used to determine cycle threshold (Ct) values at baseline. The lowest Ct value generated among the five rpoB probes of Xpert MTB/RIF (or of the four rpoB probes in the nested-PCR stage for GeneXpert Ultra) was taken as a measure of the Mtb cell number (39). The median [interquartile range (IQR)] Ct value (Ct_{Med}) of all participants was computed, 17.4 [17.1–18.4]. Patients were grouped into: "high Mtb load" ($Ct < Ct_{Med}$) and "low Mtb load" ($Ct > Ct_{Med}$) groups.

Recovery from Severe Lung Pathology After Treatment

For each patient, RS changes (ΔRS) from BL to 6M (ΔRS = RS at BL/RS at 6M) and median change [IQR] in RS of the entire cohort (ΔRS_{Med}) were computed, 6.5 [1.6–14]. Patients were grouped into: "Good" ($\Delta RS \geq \Delta RS_{Med}$) and "Poor" ($\Delta RS < \Delta RS_{Med}$) lung recovery groups. Nine participants had a ΔRS equal to the ΔRS_{Med}.

Sputum Sample Supernatant Collection

Aliquots of sputum were digested with an equal volume of Sputolysin (MerckMillipore, USA) for 15 min and centrifuged. The supernatant was harvested and stored at −80°C until use.

Whole Blood Processing, Storage and Stimulation

Plasma was obtained from blood vials by centrifugation at 2,500 rpm and stored at −80°C prior to use. Approximately 500 µl of whole blood was stimulated with either ESAT-6/CFP-10 peptide pool (EC; at 2.5 µg/ml/peptide), purified protein derivative (PPD at 10 µg/ml; Staten Serum Institute, Denmark), H37Rv whole cell lysate (WCL; at 10 µg/ml; BEI Resources, USA) or phorbol 12-myristate 13-acetate (PMA; positive control; 10 µg/ml) along with co-stimulatory antibodies (anti-CD28, anti-CD49d; Becton Dickinson, USA); or unstimulated/cultured with medium alone (NIL; negative control). Following overnight incubation at 37°C, 5% CO_2, plates were spun (1,500 rpm, 5 min) and 200–250 µl of supernatant was harvested from each well into 0.5 ml Sarstedt tubes prior to storage at −80°C for multiplex cytokine assays.

Multiplex Cytokine Arrays

Multiplex cytokine arrays were performed using a customised 13-plex inflammatory marker panel (R&D Systems, USA) according to the manufacturer's instructions. The 13 analytes measured were GM-CSF, IL8/CXCL8, IL12/23(p40), MMP3, MMP9, S100A8, S100A9, TNF, IFNγ, IL10, MMP1, MMP8, and MPO. The minimum levels of detection for these were: 11.52, 2.96, 383.13, 78.48, 128.31, 74.86, 8.44, 42.35, 3.70, 40.95, 241.11, 113.00, and 26.87 pg/ml, respectively. Briefly, lyophilised standards were reconstituted and serial dilutions performed. Coupled beads were diluted in assay buffer and 50 µl were added to each well of the assay plate. Approximately 50 µl of diluted standards, blanks, samples (plasma, ag-stimulated supernatants or *ex vivo* sputum) and controls were added per well. Plates were then incubated at room temperature (RT), with shaking (350 rpm, 2 h) followed by three washes in wash buffer. Detection antibodies were diluted in detection antibody diluent as recommended and 50 µl added to each well followed by another 1 h incubation period. Following three washes, 100× streptavidin-PE was diluted in wash buffer (one in 100) and 50 µl added to each well. Plates were then incubated for 30 min and washed three times. Approximately 100 µl of assay buffer were then added to each well, plates were shaken for 2 min and read using Bioplex 200 plate reader with Bio-Plex Manager Software (version 6.1; Bio-Rad, Belgium).

Data Analysis

All statistical analyses were performed using R version 3.5.2 (40). For antigen-specific blood responses, background was subtracted using the unstimulated (NIL) samples. Non-parametric tests were used for all comparisons. Differences between BL, 2M and 6M samples within each group were analysed using a Kruskal–Wallis test with Dunn's post-test comparison. For comparisons between severity, treatment response and recovery groups, a Wilcoxon rank sum test was performed. The Benjamini–Hochberg test (41) was used to adjust for multiple comparisons throughout. Adjusted p values (q values) of less than 0.05 were considered statistically significant. Linear regression models were used to determine significant differences after adjusting for sex.

RESULTS

Patient Demographics

We analysed pre-selected plasma and sputum samples from 107 adult HIV negative, pulmonary TB patients of which 77% were males (**Table 1**). The median [interquartile range (IQR)] CXR score at baseline was 65 [29–80] with 46 patients in the mild (RS <65) and 61 patients in the severe group (RS ≥65). The median [IQR] CXR

TABLE 1 | Patient demographics.

	Total	CXR-defined		GeneXpert-defined			Lung Recovery	
		Mild N = 46	Severe N = 61	Low N = 53	High N = 45	NA N = 9	Good N = 30	Poor N = 22
Age	32 [23–40]	29.5 [21–39]	32 [26–41]	29 [22–40]	31 [25–40]	32 [30–34]	32 [24–41]	32 [26–37]
Male n (%)	82 (77)	29 (63)	53 (87)	34 (64)	40 (89)	8 (89)	26 (87)	19 (86)
		p = 3.90E–03			p = 4.50E–03		ns	

ns, not significant; CXR, chest X-ray; age = median [interquartile range].

score for the mild and severe groups at baseline was 25 [16.2–51.5] and 75 [65–90] respectively. For patients with severe damage at baseline, the median [IQR] change in CXR scores (ΔRS) from baseline to 6 months was 6.5 [1.6–14] with 30 patients in the good recovery (ΔRS ≥6.5) and 22 in the poor recovery group (ΔRS <6.5). Within the good and poor recovery groups, the median [IQR] ΔRS was 14 [9.5–18] and 1.5 [1.3–2.6], respectively. Nine of the patients with severe damage at BL could not be classified into either good or poor recovery groups due to missing month 6 CXR scores (NA). At the end of treatment (6M) the median [IQR] CXR for the mild and severe groups was 5 [0–10] and 5 [5–13.5], respectively. For bacterial load calculations, we analysed the Xpert Ct values for all participants. The median [IQR] Ct value was 17.4 [17.1–18.4] with 45 patients in the high bacterial load group (Ct <17.4) and 53 patients in the low bacterial low group (Ct >17.4). The median [IQR] Ct values for the high and low bacterial load groups were 17.0 [16.8–17.1] and 18.4 [17.8–19.6], respectively. CXR-derived Ralph scores and Xpert MTB/RIF cycle threshold weakly correlated (rho = −0.24, p = 1.40E−02) at baseline. No differences in age were observed in the mild *vs.* severe lung damage, low *vs.* high Mtb load and good *vs.* poor recovery groups (**Table 1**). Male sex was associated with higher levels of lung damage (p = 3.90E−03) and Mtb loads (p = 4.50E−03) but not with reduced lung recovery (ns).

Analysis of ATB Severity

The two measures of ATB severity that we used were sputum GeneXpert Ct values and CXR Ralph scores. There was a weak negative correlation between patient Ct values and Ralph scores at baseline (rho = −0.24, p = 1.40E−02) (**Supplementary Figure 1A**) as previously reported (42). We also observed a weak positive correlation between baseline Ralph scores and neutrophil counts (rho = 0.22, p = 2.50E−02) but not between baseline Ct values and baseline percentage neutrophil counts (**Supplementary Figures 1B, C**).

Neutrophil levels are associated with higher risk of lung damage (10) and death in TB patients (30) and we recently showed that neutrophil activation and function vary in ATB patients based on the severity of the lung pathology (43). Hence, we monitored the impact of neutrophil counts and neutrophilic inflammatory mediator levels on lung damage severity or Mtb burden.

Association Between Neutrophil Count and Analyte Concentrations in Plasma at Baseline

At baseline, plasma concentrations of all inflammatory mediators, excluding MPO and MMP9, correlated with absolute neutrophil counts (**Table 2**). The strongest correlations were observed for MMP8 (rho = 0.45, p = 2.80E−06), S100A8 (rho = 0.52, p = 3.00E−08), S100A9 (rho = 0.33, p = 6.30E−04) and GM-CSF (rho = 0.43, p = 7.90E−06). Analysis within groups showed that plasma MPO was associated with neutrophil counts in patients with high Mtb load only (rho = 0.37, p = 1.50E−02) and MMP9 was associated with neutrophil counts in patients with severe lung damage only (rho = 0.26, p = 4.10E−02) (**Table 3**). S100A8, MMP8, S100A9, IL10, GM-CSF, TNF, and IFNγ correlated with neutrophil count in patients with both severe lung damage and high Mtb load at baseline (**Table 3**).

For patients with mild lung damage at baseline, correlations were weaker and only significant for MMP8, S100A8, and S100A9 (**Table 3**). Likewise, within the low Mtb load group, significant correlations were only observed for S100A8, TNF, and GM-CSF (**Table 3**). These values reveal that while most plasma neutrophilic inflammatory marker levels are generally associated with neutrophil counts irrespective of the severity of lung pathology, MPO and MMP9 are only associated with neutrophil counts in patients with a severe form of lung pathology.

Analysis of Neutrophil Mediators in Relation to Lung Pathology and Sex at Baseline

Plasma concentrations of MMP8, MMP1, S100A8, IL12/23(p40), IFNγ, IL8, and TNF were significantly elevated in patients with severe lung damage at baseline compared to those with mild damage (p = 9.00E−04, p = 9.30E−03, p = 2.50E−03,

TABLE 2 | Correlation between neutrophil count and analyte concentrations at baseline.

	rho	p-value
MMP1	0.20	ns
MMP3	0.23	2.20E−02
MMP8	0.45	2.80E−06
MMP9	0.16	ns
MPO	0.021	ns
S1000A8	0.52	3.00E−08
S100A9	0.33	6.30E−04
IL8	0.22	3.00E−02
IL10	0.32	1.30E−03
IL12/23(p40)	0.32	1.10E−03
GM-CSF	0.43	7.90E−06
TNF	0.38	1.00E−05
IFNγ	0.36	2.40E−04

ns, not significant; rho, spearman's rank correlation coefficient.

TABLE 3 | Correlation between neutrophil count and analyte concentrations in plasma for patients with different degree of lung damage (CXR) and Mtb load (GeneXpert) at baseline.

Analyte	Lung damage				Mtb load			
	Mild		Severe		Low		High	
	rho	p-value	rho	p-value	rho	p-value	rho	p-value
MMP1	0.16	ns	0.16	ns	0.20	ns	0.18	ns
MMP3	0.13	ns	0.26	ns	0.26	ns	0.11	ns
MMP8	0.46	2.00E−03	0.40	2.10E−03	0.27	ns	0.65	2.80E−06
MMP9	−0.13	ns	0.26	4.10E−02	0.04	ns	0.29	ns
MPO	−0.13	ns	0.10	ns	−0.18	ns	0.37	1.50E−02
S1000A8	0.39	9.70E−03	0.49	8.20E−05	0.41	3.50E−03	0.59	2.60E−05
S100A9	0.39	1.00E−02	0.27	4.00E−02	0.26	ns	0.47	1.40E−03
IL8	0.06	ns	0.26	4.70E−02	0.09	ns	0.30	ns
IL10	0.28	ns	0.38	3.80E−03	0.20	ns	0.42	6.40E−03
IL12/23(p40)	0.18	ns	0.35	6.40E−03	0.13	ns	0.50	7.20E−04
GM-CSF	0.27	ns	0.50	5.40E−05	0.34	1.50E−02	0.51	5.50E−04
TNF	0.18	ns	0.45	4.10E−04	0.38	7.30E−03	0.37	1.50E−02
IFNγ	0.18	ns	0.43	8.20E−04	0.21	ns	0.46	1.90E−03

ns, not significant; rho, spearman's rank coefficient.

p = 3.50E−03, p = 7.70E−03, p = 2.10E−02, and p = 4.20E−02, respectively; **Figure 1A**).

Severe lung damage was associated with plasma MMP8, MMP1, S100A8, IL12/23(p40), and IFNγ (p = 3.00E−03, p = 1.40E−02, p = 1.80E−02, p = 1.00E−02, and p = 1.90E−02, respectively) even after adjusting for sex (**Supplementary Table 5** and **Supplementary Figure 2A**). With respect to Mtb burden at baseline, the only difference in plasma inflammatory mediator levels between high Mtb and low Mtb load groups was observed for S100A9 (p = 4.60E−02, adjusted for sex) (**Supplementary Table 5**).

In sputum, MMP8 (p = 7.40E−03) levels were higher in patients with severe lung damage at baseline (**Figure 1B**) however, this was not significant after adjusting for sex. TNF levels were associated with lung damage severity only after adjusting for sex (p = 5.70E−02 and p = 4.50E−02; unadjusted

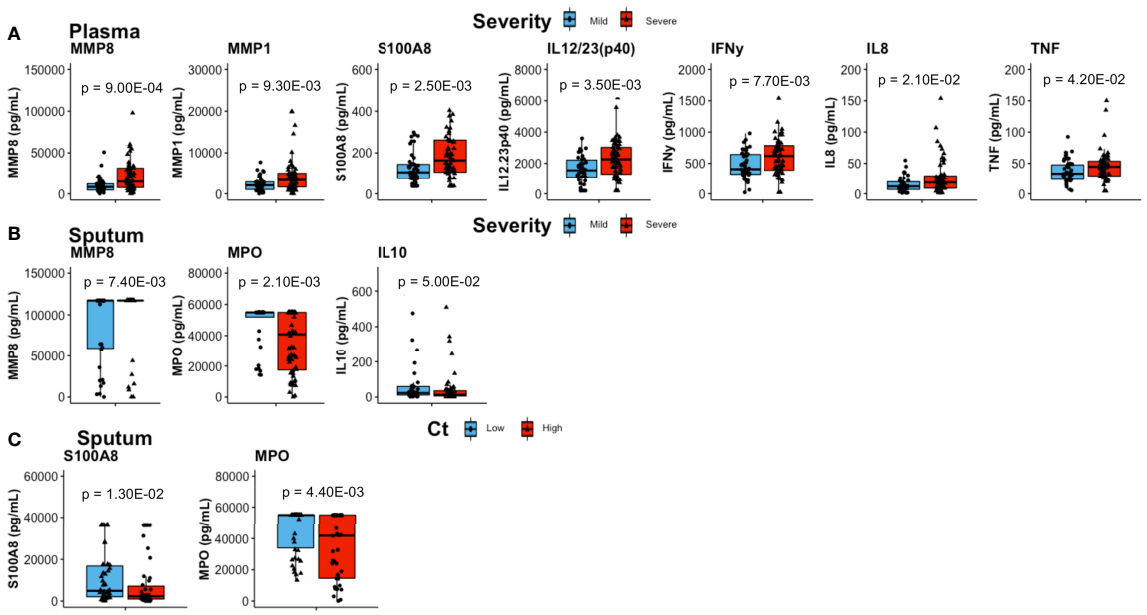

FIGURE 1 | Comparisons of inflammatory mediator concentrations at baseline. **(A)** In plasma, patients with severe lung damage (n = 61) had higher levels of proinflammatory mediators than those with mild lung damage (n = 46). **(B)** Sputum levels of mmp8 were higher whilst MPO and IL10 were lower in patients with severe (n = 60) compared to mild lung (n = 36) damage. **(C)** Whereas sputum S100A8 was higher and MPO was lower in patients with high Mtb loads (n = 45) compared to low Mtb loads (n = 53). Boxes represent the first and third quartiles and horizontal bars within indicate median concentration. Whiskers indicate minimum and maximum values. Each dot represents one individual patient. P-values were obtained using the Wilcoxon signed rank test.

and adjusted for sex, respectively) (**Supplementary Table 6**). In contrast, baseline sputum levels of IL10 (p = 5.00E−02) and MPO (p = 1.20E−03) were significantly lower in severe lung damage compared to mild lung damage group (**Figure 1B**). For MPO, the association with lung damage was significant (p = 1.80E−02) even after adjusting for sex (**Supplementary Table 6** and **Supplementary Figure 2B**). Additionally, sputum MPO (p = 4.40E−03) and S100A8 (p = 1.30E−02) concentrations were significantly lower and higher, respectively in patients with high Mtb load compared to those with low Mtb load (**Figure 1C**). This association between MPO levels and Mtb load was significant (p = 2.10E−02) even after adjusting for sex (**Supplementary Table 6**). For whole blood stimulated samples (EC, PPD, WCL, and PMA), there was no significant difference in baseline inflammatory mediator levels between either severe and mild lung damage or high and low Mtb loads (not shown).

We also observed that sputum MMP1 (p = 2.70E−02) and plasma concentrations of MMP3, IL8, IL10, IL12/23(p40), GM-CSF, and TNF (p = 3.00E−03, p = 3.76E−02, p = 4.03E−02, p = 3.30E−02, p = 2.65E−02, and p = 3.36E−02, respectively) were higher in males compared to females (**Supplementary Table 1**). Interestingly, sputum MPO concentrations were higher females (p = 1.85E−02) (**Supplementary Table 1**).

Changes in Neutrophil Mediator Concentrations Post-Treatment

The majority of pro-inflammatory mediators in plasma decreased during TB treatment except for MMP3, MPO, and IL8 (**Supplementary Table 2**). Compared to baseline, plasma levels were lower at month 2 and month 6, respectively for MMP1, MMP8, MMP9, S100A8, S100A9, TNF, IFNγ, GM-CSF, IL10, and IL12/23(p40) (**Supplementary Table 2**). In sputum, concentrations of MMP1, MMP3, MMP8, MMP9, and TNF were significantly lower at both month 2 and month 6, when compared with baseline (**Supplementary Table 2**).

Additionally, sputum GM-CSF (p = 5.50E−07), TNF (p = 2.10E−05), IFNγ (ns), S100A8 (ns), and MPO (ns) were higher at month 6 compared to baseline (**Supplementary Table 2**). Interestingly, the concentrations of these specific mediators in whole blood stimulated samples were also higher after treatment compared to baseline. Notably, this increase was significant at month 6 for GM-CSF [EC, p = 2.70E−02; PPD, p = 1.50E−09; WCL, p = 2.80E−05, and PMA, p = 6.70E−11], TNF [EC, p = 2.80E−02; PPD, p = 2.00E−03; WCL, p = 2.00E−04 and PMA, p = 2.00E−02], IFNγ [EC, (ns); PPD, p = 3.20E−08; WCL, p = 6.30E−03 and PMA, p = 1.00E−11], S100A8 [EC, (ns); PPD, (ns); WCL, p = 2.80E−02 and PMA, (ns)), MPO (EC, (ns); PPD, (ns); WCL, p = 9.10E−03 and PMA (ns)] and MMP9 [EC, (ns); PPD, p = 1.90E−08; WCL, p = 3.60E−02 and PMA, p = 5.40E−07] (**Supplementary Table 2**).

The decrease in plasma and sputum concentrations of these mediators at month 6 compared to baseline was more pronounced in patients with initially (at baseline) severe lung damage (**Supplementary Table 3**) or initially high Mtb loads (**Supplementary Table 4**). Interestingly, this decrease in concentrations was exclusive to the initially severe lung damage group for S100A8 (p = 4.61E−09), MMP9 (p = 1.26E−02), IL10 (p = 3.86E−04), TNF (p = 3.77E−06), IFNγ (p = 3.84E−07) and GM-CSF (p = 4.54E−05) levels in plasma; and for MMP1 (p = 1.90E−05), MMP8 (p = 4.99E−05) and TNF (p = 1.31E−03) levels in sputum (**Supplementary Table 3**). No such analogy was observed when groups defined by Mtb burden were considered (**Supplementary Table 4**).

Patients with good lung recovery had higher baseline sputum MPO (p = 4.70E−02) and IL10 (p = 2.70E−02) levels compared to patients with poor recovery (**Figure 2A**). For MPO, the association with lung recovery was significant (p = 2.40E−02) after adjusting for sex (**Supplementary Table 6**). Additionally, logistic regression revealed significant associations between and lung recovery and levels of plasma MMP8 (**Supplementary Table 5**) and sputum TNF (**Supplementary Table 6**) after adjusting for sex (p = 3.90E−02 and p = 3.80E−02, respectively).

Additionally, sputum MMP1, MMP3, MMP9, and TNF levels decreased significantly (p = 1.50E−03, p = 7.58E−04, p = 2.06E−02, and p = 3.81E−02, respectively) from baseline to month 6 in patients with good lung recovery but not in those with poor recovery (**Figure 2B**). We also saw significantly higher levels of MMP1 (p = 4.40E−02), MMP9 (p = 2.90E−02) and IL8 (p = 3.50E−02) in sputum from patients with poor lung recovery compared to good lung recovery at month 6 (**Figure 2C**).

In whole blood stimulated supernatants, with the exception of IFNγ (WCL at BL; p = 1.60E−02), IL12/23(p40) (WCL at 6M; p = 4.80E−02) and S100A8 (EC at BL; p = 3.00E−02) concentrations which were higher in mild compared to severe lung damage; MMP1 (PPD at BL; p = 5.00E−03) which was higher in high compared to low Mtb load and; S100A8 (EC at BL; p = 3.00E−02) which was higher in low compared to high Mtb load, there were no other significant differences in inflammatory mediator levels of whole blood stimulated samples (EC, PPD and WCL) from patients in severe *vs* mild lung damage or high *vs* low Mtb loads at any time point (not shown).

Finally, S100A9 concentrations at month 6 were significantly higher in severe lung damage and high Mtb load groups compared to mild damage and low Mtb load groups, respectively (p = 3.00E−02, and p = 2.10E−02, respectively) at month 6 (**Figures 3A, B**). Additionally, sputum levels of MMP9 declined significantly from baseline to month 6 in patients with low Mtb load (p = 3.20E−03) but not in patients with high Mtb load (**Figure 3C**). Moreover, these sputum concentrations of MMP9 remained significantly higher in the high Mtb load compared to the low Mtb load group at month 6 (p = 2.00E−02) (**Figure 3C**).

DISCUSSION

The aim of this study was to analyse neutrophil-associated soluble mediators in lung and blood samples from patients with different levels of lung pathology at baseline and recovery following treatment. We report stronger correlations between neutrophil counts and primarily neutrophil-derived mediators like MMP8, S100A8/A9, TNF, and GM-CSF as compared to

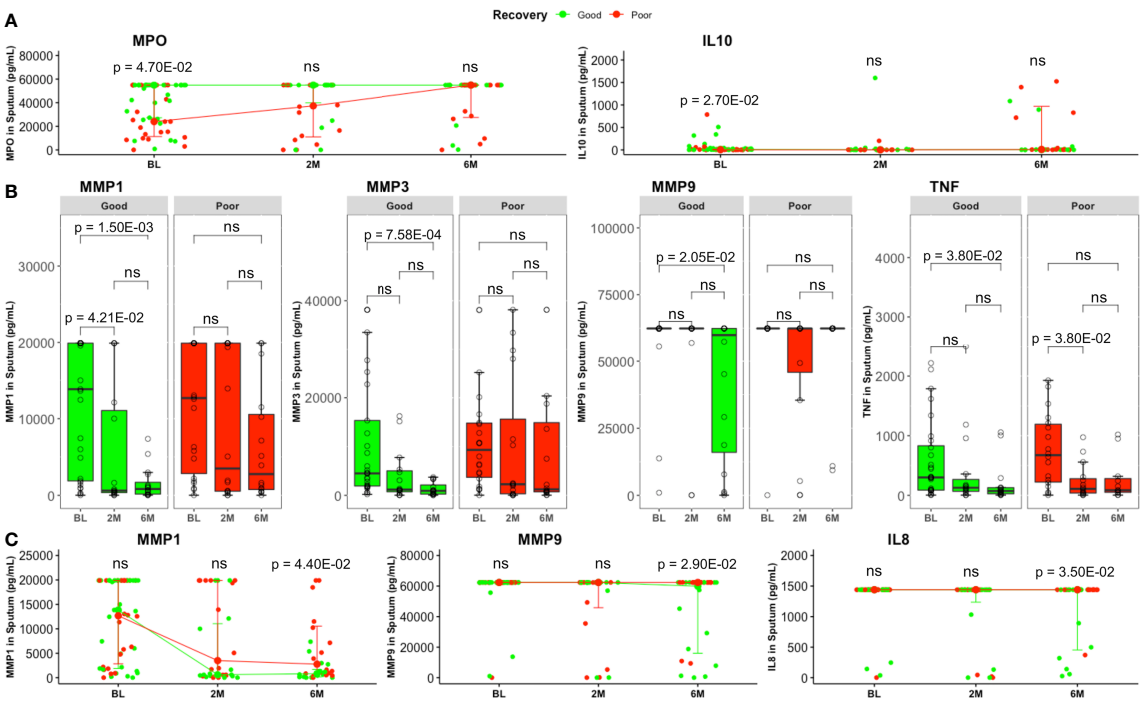

FIGURE 2 | Comparison of sputum inflammatory mediator levels between good and poor lung recovery groups with treatment time. **(A)** MPO and IL10 were higher in good (BL, n = 29; 2M, n = 16; 6M, n = 16) compared to poor (BL, n = 22; 2M, n = 16; 6M, n = 16) lung recovery groups at baseline. Data represent median [IQR]. Differences between lung pathology groups at any given time point were compared using the Wilcoxon signed rank test. **(B)** Most MMP1, 3, 9, and TNF levels were significantly lower at month 6 compared to baseline in patients with good lung recovery but not in those with poor lung recovery. Boxes represent the first and third quartiles and horizontal bars within indicate median concentration. Whiskers indicate minimum and maximum values. Each dot represents one individual patient. Kruskal–Wallis test with Dunn's post-test comparison was performed to analyse differences between time points. **(C)** At the end of standard TB treatment, MMP1, MMP9 and IL8 concentrations were still higher in patients with poor lung recovery compared to those with poor lung recovery. Groups were compared using the Wilcoxon signed rank test. Data represent median [IQR]. ns, not significant.

other known TB-related inflammatory markers like IFNγ, IL10 or IL12/23(p40), for which neutrophils are not necessarily the major sources.

GM-CSF is a known neutrophil primer and MMP8 concentrations have previously been linked to clinical and radiological TB severity (44, 45), while S100A8/9 regulates CD11b expression and accumulation in chronic TB mouse models (28, 35). Our data supports these previous observations. We show that pre-treatment plasma levels of S100A8/9, MMP8 and GM-CSF correlate strongly with neutrophil counts and lung damage severity. Interestingly, while sputum levels of MMP8 correlate positively, MPO correlates negatively with lung damage and Mtb burden at baseline. This suggest that lung pathology results from increased systemic and pulmonary inflammation. It also hints that MPO could dampen the inflammatory response in ATB, thereby preventing excessive bacterial load and lung damage. We recently revealed that neutrophil subsets are associated with protective or detrimental effects on the severity of TB-linked lung pathology (13). Gideon and collaborators also showed pro-(IFNγ) and anti-inflammatory (IL10) cytokine expression by different neutrophil subsets in granulomas from Mtb-infected cynomolgus macaques (24), suggesting an immunoregulatory function of neutrophils in TB granulomas. Also, neutrophil elastase dissociation is triggered by reactive oxygen species (ROS) in an MPO-dependent manner during NETosis (46, 47), suggesting that NETs are involved in an MPO-related protective mechanism. Additionally, Mtb control by HIV-coinfected macrophages is enhanced by apoptotic neutrophils in *via* an MPO-dependent process (48). Whilst MPO inhibition is reported to block Mtb-induced necrotic cell death (49), MPO-deficient mice develop severe lung inflammation following exposure to zymosan (37). In fact, a recent review details the numerous protective and harmful functions of MPO in human disease (50). Whilst IL10 is released by several immune cell types during TB and monocytes/macrophages also produce MPO, neutrophil granules are the main source of MPO (48). This to our knowledge, is the first report of an MPO-related beneficial role in TB-related lung pathology and recovery.

The current literature overwhelmingly supports a detrimental effect of neutrophils on lung pathology in TB patients, however, some neutrophil subsets are protective. Specific neutrophil subsets were associated with protective outcomes against TB lung pathology suggesting that the variations observed in disease outcomes may be driven by different immunomodulatory mediators or interactions with other immunocytes (13).

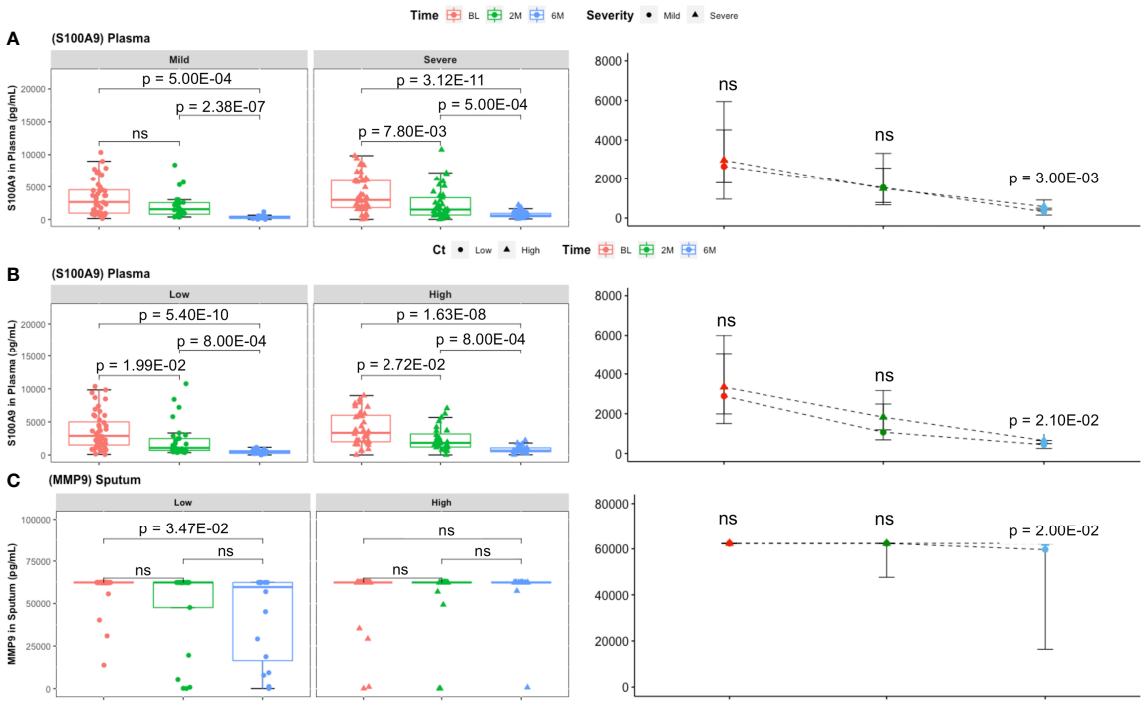

FIGURE 3 | Comparison of inflammatory mediator levels between lung damage and Mtb burden defined groups with treatment time. **(A)** In plasma, the decrease in S100A9 concentrations was comparable between lung damage groups (mild: BL, n = 46; 2M, n = 25; 6M, n = 14 and severe: BL, n = 61; 2M, n = 42; 6M, n = 43) over time. However, at month 6, S100A9 was significantly higher in patients with initially severe lung damage compared to mild lung damage. **(B)** The same observation made between initially high Mtb and low Mtb loads with S100A9 levels being higher in the former at month 6. Boxes represent the first and third quartiles and horizontal bars within indicate median concentration. Whiskers indicate minimum and maximum values. Each dot represents one individual patient. Kruskal–Wallis test with Dunn's post-test comparison was performed to analyse differences between time points. Differences between lung pathology groups at any given time point were compared using the Wilcoxon signed rank test. Data represent median [IQR]. **(C)** Sputum (low: BL, n = 46; 2M, n = 21; 6M, n = 16 and high: BL, n = 42; 2M, n = 22; 6M, n = 17) MMP9 levels were significantly lower at month 6 compared to baseline in patients with low but not in those with high Mtb loads. Additionally, S100A9 concentration at month 6 was significantly higher in patients with high Mtb compared to low Mtb load. ns, not significant.

Additionally, a neutrophil-driven regulatory effect is not unheard of. In fact, neutrophils (*via* CD11b-dependent responses) and endothelial cells have been shown to cooperate in detection and capture of pathogens in lung capillaries (51). Also, neutrophils play a central role in controlling human metapneumovirus-induced inflammation by regulating γδ T cell recruitment to the lung (52). Meanwhile, neutrophils were found to suppress of lymphocyte function by secreting MPO and hydrogen peroxide (53) and Mtb-specific stimulation of neutrophils inhibits antigen-specific T-cell production of IFNγ (24). More recently, this neutrophil-related immunosuppressive function on lymphocytes has been attributed to hyper-segmented subsets (7) and to the neutrophil-like MDSCs (54, 55) (in cancer (56, 57), leukaemia (58) and lately TB (9, 59). While the immunosuppressive roles of MDSCs on Mtb pathogenesis are still under investigation, recent experimental models show benefits in limiting their accumulation during TB HDTs (25, 60). We suggest that MPO could be protective against TB progression and lung damage.

We understand that functional analysis of neutrophils is technically difficult considering that they are short-lived, easily activated by laboratory processing methods and cannot be cryopreserved. Nevertheless, we support future investigation of mechanistical pathways that promote the secretion of these mediators or increased production of neutrophil subsets that produce them to achieve desirable outcomes during ATB. We could not confirm the link between MPO and bacterial burden using Mtb killing assays *in-vitro*. However, prospective studies within the TB sequel project are being designed to achieve that by assessing the levels of these mediators in the presence/absence of TB-targeted HDTs. We also recommend studies using isolated neutrophils from patients within these different lung pathology and gender groups to address this gap in knowledge (potentially also in animal models).

Variability in immune responses between genders have been linked to: specific immune cell types, age, levels of sex hormones, environmental factors (e.g., nutritional status or microbiome composition) and disease states (61). In accordance with previous studies (62, 63), ATB prevalence in our Gambian cohort is higher in males. Also similar to previous studies on chronic inflammatory diseases (64, 65), we observe that the pro-inflammatory response in males is higher than that in females. We report higher plasma levels of notoriously pro-inflammatory mediators like TNF, MMP3, GM-CSF, and IL8 in males

compared to females. This is in accordance with the observation that male neutrophils are more responsive to LPS and IFNγ stimulation than female neutrophils; with the former expressing higher levels of toll-like receptor 4 (TLR4) and producing more TNF (66). Meanwhile, we also observe higher sputum MPO levels in females, supporting the idea that increased MPO concentration is linked to suppressed inflammation.

Moreover, patients showing good lung recovery had higher sputum MPO concentrations at baseline. In contrast, MMP8 and sputum TNF levels were positively associated with poor recovery after adjusting for sex. These suggest that MPO, MMP8, and TNF play a considerable role in determining the degree of recovery from severe TB-related lung damage after treatment. It also supports future investigation of these mediators as proxies for predicting lung recovery following injury.

As treatment progresses, sputum and plasma concentrations of MMP1, 8, 9 and plasma levels of S100A8/9 and MMP3 decrease rapidly, suggesting that the neutrophil-related inflammatory response and matrix-degrading activity are not only fuelled by MMPs ((32, 33, 67)) and calprotectin (28) activity but also potentially resolved by variations in levels of these mediators with treatment. In contrast, sputum levels of IL8 and MPO remain fairly constant, suggesting that variations in neutrophil (and potentially monocyte) recruitment and overall activity during ATB treatment may be more complexly regulated. This is supported by our other observation that the decrease in concentrations of S100A8, MMP9, IL10, TNF, IFNγ, and GM-CSF in plasma and MMP1, MMP8, and TNF in sputum are exclusive to the severe lung damage group; suggesting that these inflammatory mediators are major contributors to severe TB-related lung pathology pre-treatment. The fact that no such analogy was observed when groups defined by Mtb burden were considered also supports the idea that high Mtb loads are not necessarily ascribed to severe lung damage outcomes (42).

Post-therapy, we observed high plasma S100A8 levels in severe compared to mild lung damage group, meanwhile plasma S100A8 and sputum MMP9 were significantly higher in patients with initially high Mtb load compared to the initially low Mtb load group. S100A9 and MMP9 are neutrophil-derived mediators, suggesting that severe lung damage at presentation may contribute to heightened residual neutrophil activity after treatment. Also, post-treatment levels of sputum MMP1, MMP9, and IL8 were higher in patients with poor lung recovery compared to those with good lung recovery. This suggests that unresolved lung damage is linked to continuous neutrophil activity and persistent leucocyte infiltration in the lungs post-treatment. While, previous studies suggested that for patients with severe lung damage, recovery may only begin many months after the end of standard ATT (68, 69), a possible reason for this was not provided. This, to our knowledge is the first report of several major neutrophil-derived mediators (in plasma and sputum) being directly linked to TB lung pathology and unresolved lung damage. Furthermore, higher levels of MMP1, MMP9, and IL8 in sputum from patients with poor compared to good lung recovery at month 6 suggest that poor lung recovery results from continuous neutrophil activity and persistent leucocyte infiltration in the lungs even after treatment completion.

For whole blood stimulated supernatants (notably with H37Rv whole cell lysate), the increased levels of GM-CSF (also increased in sputum), TNF (also increased in sputum), IFNγ, S100A8, MPO and MMP9 after treatment compared to baseline hint at an enhanced sensitivity of immune cells to pathogen stimulation. Previous studies have reported lower cytokine production by T-cells pre-treatment, suggesting that continual pathogen stimulation results in T-cell exhaustion which is then restored after treatment (reviewed in (70). To our knowledge, this is the first report of increased concentrations of major neutrophil-derived mediator levels in ATB post-treatment compared with pre-treatment levels. These suggest that chronic TB could directly (or indirectly, *via* T-cell exhaustion which leads to either higher levels of immune-inhibitory molecules like PD-1 (71, 72) and TIM3 (73) or reduced release of innate immune cell activators like IFNγ and TNF) result in reduced neutrophil activity pre-treatment. It also highlights the need to monitor the impact of neutrophil interactions with other immunocytes on TB pathogenesis. Finally, we suggest that toll-like receptor (TLR)-mediated pathogen sensing by lung epithelial/innate immune cells, MPO-regulated NET formation, neutrophil migration/activation following increased secretion of inflammatory mediators (e.g., S100A8/9, MMP8, GM-CSF, TNF, IFNγ and potentially IL17/IL17R, RANTES, IL6, ICAM1, etc.) and ROS release/NADPH-dependent leucocyte recruitment (74–76) are immune pathways potentially involved in balancing the neutrophilic inflammatory response during ATB.

CONCLUSION

We show that S100A8/9 and MMP8 contribute to increased lung damage and that MPO acts as an anti-inflammatory agent which potentially regulates TB-related lung pathology and promotes lung recovery. We also suggest that increased MPO-mediated immunosuppression could limit lung pathology in females. Treatment results in decreased inflammation characterised by lower sputum and plasma concentrations of neutrophil-derived pro-inflammatory mediators especially in patients with severe lung pathology (but not High Mtb load) at presentation. We hereby highlight the relationship between neutrophil-derived inflammatory mediator levels and radiological disease severity irrespective of Mtb burden. We also report that S100A8/9 and other neutrophilic mediators like MMP9 and IL8 may be responsible for unresolving lung damage in patients with poor lung recovery. Finally, we recommend targeting S100A8/9, MMP8, and MPO for developing host-directed therapies against TB-induced lung pathology and to promote recovery.

DATA AVAILABILITY STATEMENT

The raw data supporting the conclusions of this article will be made available by the authors, without undue reservation.

ETHICS STATEMENT

The studies involving human participants were reviewed and approved by the Medical Research Council/Gambia government joint ethics committee (SCC1523). The patients/participants provided their written informed consent to participate in this study.

AUTHOR CONTRIBUTIONS

CN: Conceptualisation, Data curation, Formal analysis, Investigation, Methodology and writing of manuscript. OO: Patient recruitment and follow-up, clinical data, and review of manuscript. SD: Data Management. JM: Assisted with wet-lab experiments. IS: Assisted with wet-lab experiments. SC: Funding acquisition and review of manuscript. AB: Data curation and Formal analysis. AR: Conceptualisation, Funding acquisition, data analysis, and review of manuscript. CG: Supervision, Methodology, and manuscript review. JS: Supervision, Conceptualisation, Data curation, Methodology, Funding acquisition, and review of manuscript. All authors contributed to the article and approved the submitted version.

FUNDING

This work was supported by a PhD student stipend from TB Sequel (grant number 66.3010.7-002.00) funded by the German Ministry for Education and Research (BMBF).

ACKNOWLEDGMENTS

We thank the patients and their families who volunteered for this study and The MRC Unit The Gambia at LSHTM for facilitating access to laboratory, clinical and other facilities. We are thankful to all the staff at The MRC Unit The Gambia at LSHTM's TB research group for technical support.

SUPPLEMENTARY MATERIAL

The Supplementary Material for this article can be found online at: https://www.frontiersin.org/articles/10.3389/fimmu.2021.740933/full#supplementary-material

REFERENCES

1. WHO. *Global Tuberculosis Report 2020* Vol. 66. Geneva: World Health Organization (2020) p. 37–9.
2. Ralph AP, Kenangalem E, Waramori G, Pontororing GJ, Sandjaja, Tjitra E, et al. High Morbidity During Treatment and Residual Pulmonary Disability in Pulmonary Tuberculosis: Under-Recognised Phenomena. *PloS One* (2013) 8(11):1–11. doi: 10.1371/journal.pone.0080302
3. Rachow A, Ivanova O, Wallis R, Charalambous S, Jani I, Bhatt N, et al. TB Sequel: Incidence, Pathogenesis and Risk Factors of Long-Term Medical and Social Sequelae of Pulmonary TB - A Study Protocol. *BMC Pulm Med* (2019) 19(1):1–9. doi: 10.1186/s12890-018-0777-3
4. Cadena AM, Fortune SM, Flynn JL. Heterogeneity in Tuberculosis. *Nat Rev Immunol* (2017) 17(11):691–702. doi: 10.1038/nri.2017.69
5. O'Garra A, Redford PS, McNab FW, Bloom CI, Wilkinson RJ, Berry MPR. The Immune Response in Tuberculosis. *Annu Rev Immunol* (2013) 31 (1):475–527. doi: 10.1146/annurev-immunol-032712-095939
6. Shi S, Zhang X, Zhou Y, Tang H, Zhao D, Liu F. Immunosuppression Reduces Lung Injury Caused by Mycoplasma Pneumoniae Infection. *Sci Rep* (2019) 9 (1):1–8. doi: 10.1038/s41598-019-43451-9
7. Pillay J, Kamp VM, Van Hoffen E, Visser T, Tak T, Lammers J, et al. A Subset of Neutrophils in Human Systemic Inflammation Inhibits T Cell Responses Through Mac-1. *J Clin Invest* (2012) 122(1):327–36. doi: 10.1172/JCI57990
8. Pillay J, Tak T, Kamp VM, Koenderman L. Immune Suppression by Neutrophils and Granulocytic Myeloid-Derived Suppressor Cells: Similarities and Differences. *Cell Mol Life Sci* (2013) 70(20):3813–27. doi: 10.1007/s00018-013-1286-4
9. Dorhoi A, Kotzé LA, Berzofsky JA, Sui Y, Gabrilovich DI, Garg A, et al. Therapies for Tuberculosis and AIDS: Myeloid-Derived Suppressor Cells in Focus. *J Clin Invest* (2020) 130(6):2789–99. doi: 10.1172/JCI136288
10. De Melo MGM, Mesquita EDD, Oliveira MM, Da Silva-Monteiro C, Silveira AKA, Malaquias TS, et al. Imbalance of NET and Alpha-1-Antitrypsin in Tuberculosis Patients is Related With Hyper Inflammation and Severe Lung Tissue Damage. *Front Immunol* (2019) 10(JAN):1–17. doi: 10.3389/fimmu.2018.03147
11. Lyadova IV. Neutrophils in Tuberculosis: Heterogeneity Shapes the Way? *Mediators Inflamm* (2017) 2017:8619307. doi: 10.1155/2017/8619307
12. Muefong CN, Sutherland JS. Neutrophils in Tuberculosis-Associated Inflammation and Lung Pathology. *Front Immunol* (2020) 11(May):1–9. doi: 10.3389/fimmu.2020.00962
13. Nwongbouwoh Muefong C, Owolabi O, Donkor S, Charalambous S, Bakuli A, Rachow A, et al. Neutrophils Contribute to Severity of Tuberculosis Pathology and Recovery From Lung Damage Pre- and Post-Treatment. *Clin Infect Dis* (2021) ciab729:962. doi: 10.1093/cid/ciab729
14. Borkute RR, Woelke S, Pei G, Dorhoi A. Neutrophils in Tuberculosis: Cell Biology, Cellular Networking and Multitasking in Host Defense. *Int J Mol Sci* (2021) 22(9):4801. doi: 10.3390/ijms22094801
15. Kumar NP, Moideen K, Nancy A, Viswanathan V, Shruthi BS, Sivakumar S, et al. Plasma Chemokines are Biomarkers of Disease Severity, Higher Bacterial Burden and Delayed Sputum Culture Conversion in Pulmonary Tuberculosis. *Sci Rep* (2019) 9(1):1–8. doi: 10.1038/s41598-019-54803-w
16. Riou C, Du Bruyn E, Ruzive S, Goliath RT, Lindestam Arlehamn CS, Sette A, et al. Disease Extent and Anti-Tubercular Treatment Response Correlates With *Mycobacterium Tuberculosis*-Specific CD4 T-Cell Phenotype Regardless of HIV-1 Status. *Clin Transl Immunol* (2020) 9(9):e1176. doi: 10.1002/cti2.1176
17. Khosa C, Bhatt N, Massango I, Azam K, Saathoff E, Bakuli A, et al. Development of Chronic Lung Impairment in Mozambican TB Patients and Associated Risks. *BMC Pulm Med* (2020) 20(1):1–11. doi: 10.1186/s12890-020-1167-1
18. Leem AY, Song JH, Lee EH, Lee H, Sim B, Kim SY, et al. Changes in Cytokine Responses to TB Antigens ESAT-6, CFP-10 and TB 7.7 and inflammatory markers in peripheral blood during therapy. *Sci Rep* (2018) 8(1):4–11. doi: 10.1038/s41598-018-19523-7
19. Cho Y, Park Y, Sim B, Kim J, Lee H, Cho SN, et al. Identification of Serum Biomarkers for Active Pulmonary Tuberculosis Using a Targeted Metabolomics Approach. *Sci Rep* (2020) 10(1):1–11. doi: 10.1038/s41598-020-60669-0
20. MacLean E, Broger T, Yerlikaya S, Fernandez-Carballo BL, Pai M, Denkinger CM. A Systematic Review of Biomarkers to Detect Active Tuberculosis. *Nat Microbiol* (2019) 4(5):748–58. doi: 10.1038/s41564-019-0380-2
21. Yong YK, Tan HY, Saeidi A, Wong WF, Vignesh R, Velu V, et al. Immune Biomarkers for Diagnosis and Treatment Monitoring of Tuberculosis: Current Developments and Future Prospects. *Front Microbiol* (2019) 10 (December). doi: 10.3389/fmicb.2019.02789
22. Morrison H, McShane H. Local Pulmonary Immunological Biomarkers in Tuberculosis. *Front Immunol* (2021) 12(March):5–10. doi: 10.3389/fimmu.2021.640916
23. Kroon EE, Coussens AK, Kinnear C, Orlova M, Möller M, Seeger A, et al. Neutrophils: Innate Effectors of TB Resistance? *Front Immunol* (2018) 9 (NOV):1–12. doi: 10.3389/fimmu.2018.02637

24. Gideon HP, Phuah J, Junecko BA, Mattila JT. Neutrophils Express Pro- and Anti-Inflammatory Cytokines in Granulomas From Mycobacterium Tuberculosis-Infected Cynomolgus Macaques. *Mucosal Immunol* (2019) 12 (6):1370–81. doi: 10.1038/s41385-019-0195-8
25. Parveen S, Lun S, Urbanowski ME, Cardin M, Shen J, Murphy JR, et al. Effective Host-Directed Therapy for Tuberculosis by Depletion of Myeloid-Derived Suppressor Cells and Related Cells Using a Diphtheria Toxin Fusion Protein. *J Infect Dis* (2021) jiab235. doi: 10.1093/infdis/jiab235
26. Young C, Walzl G, Du Plessis N. Therapeutic Host-Directed Strategies to Improve Outcome in Tuberculosis. *Mucosal Immunol* (2020) 13(2):190–204. doi: 10.1038/s41385-019-0226-5
27. Mishra BB, Lovewell RR, Olive AJ, Zhang G, Wang W, Eugenin E, et al. Nitric Oxide Prevents a Pathogen Permissive Granulocytic Inflammation During Tuberculosis. *Nat Microbiol* (2017) 2:17072. doi: 10.1038/nmicrobiol.2017.72
28. Gopal R, Monin L, Torres D, Slight S, Mehra S, McKenna KC, et al. S100A8/A9 Proteins Mediate Neutrophilic Inflammation and Lung Pathology During Tuberculosis. *Am J Respir Crit Care Med* (2013) 188(9):1137–46. doi: 10.1164/rccm.201304-0803OC
29. Mattila JT, Maiello P, Sun T, Via LE, Flynn JL. Granzyme B-Expressing Neutrophils Correlate With Bacterial Load in Granulomas From Mycobacterium Tuberculosis-Infected Cynomolgus Macaques. *Cell Microbiol* (2015) 17(8):1085–97. doi: 10.1111/cmi.12428
30. Lowe DM, Bandara AK, Packe GE, Barker RD, Robert J. Neutrophilia Independently Predicts Death in Tuberculosis. *Eur Respir J* (2014) 42 (6):1752–7. doi: 10.1183/09031936.00140913
31. Berry MPR, Graham CM, McNab FW, Xu Z, Bloch SAA, Oni T, et al. An Interferon-Inducible Neutrophil-Driven Blood Transcriptional Signature in Human Tuberculosis. *Nature* (2010) 466(7309):973–7. doi: 10.1038/nature09247
32. Ong CWM, Elkington PT, Brilha S, Ugarte-Gil C, Tome-Esteban MT, Tezera LB, et al. Neutrophil-Derived MMP-8 Drives AMPK-Dependent Matrix Destruction in Human Pulmonary Tuberculosis. *PloS Pathog* (2015) 11 (5):1–21. doi: 10.1371/journal.ppat.1004917
33. Ugarte-Gil CA, Elkington P, Gilman RH, Coronel J, Tezera LB, Bernabe-Ortiz A, et al. Induced Sputum MMP-1, -3 & -8 Concentrations During Treatment of Tuberculosis. *PloS One* (2013) 8(4):2–9. doi: 10.1371/journal.pone.0061333
34. Elkington PTG, Friedland JS. Matrix Metalloproteinases in Destructive Pulmonary Pathology. *Thorax* (2006) 61(3):259–66. doi: 10.1136/thx.2005.051979
35. Scott NR, Swanson RV, Al-Hammadi N, Domingo-Gonzalez R, Rangel-Moreno J, Kriel BA, et al. S100A8/A9 Regulates CD11b Expression and Neutrophil Recruitment During Chronic Tuberculosis. *J Clin Invest* (2020) 130(6):3098–112. doi: 10.1172/JCI130546
36. Munder M, Schneider H, Luckner C, Giese T, Langhans CD, Fuentes JM, et al. Suppression of T-Cell Functions by Human Granulocyte Arginase. *Blood* (2006) 108(5):1627–34. doi: 10.1182/blood-2006-11-010389
37. Takeuchi K, Umeki Y, Matsumoto N, Yamamoto K, Yoshida M, Suzuki K, et al. Severe Neutrophil-Mediated Lung Inflammation in Myeloperoxidase-Deficient Mice Exposed to Zymosan. *Inflamm Res* (2012) 61(3):197–205. doi: 10.1007/s00011-011-0401-y
38. Ralph AP, Ardian M, Wiguna A, Maguire GP, Becker NG, Drogumuller G, et al. A Simple, Valid, Numerical Score for Grading Chest X-Ray Severity in Adult Smear-Positive Pulmonary Tuberculosis. *Thorax* (2010) 65(10):863–9. doi: 10.1136/thx.2010.136242
39. Chakravorty S, Simmons AM, Rowneki M, Parmar H, Cao Y, Ryan J, et al. The New Xpert MTB/RIF Ultra: Improving Detection of Mycobacterium Tuberculosis and Resistance to Rifampin in an Assay Suitable for Point-of-Care Testing. *MBio* (2017) 8(4):1–12. doi: 10.1128/mBio.00812-17
40. Team RC. R: A Language and Environment for Statistical Computing. In: *R Foundation for Statistical Computing*. Vienna, Austria: R Foundation for Statistical Computing (2018). Available at: https://www.R-project.org/https://www.r-project.org/.
41. Benjamini Y, Hochberg Y. Controlling the False Discovery Rate : A Practical and Powerful Approach to Multiple Testing. *J R Stat Soc Ser B Methodol* (1995) 57(1):289–300. Publi. J R Stat Soc. doi: 10.1111/j.2517-6161.1995.tb02031.x
42. Murthy SE, Chatterjee F, Crook A, Dawson R, Mendel C, Murphy ME, et al. Pretreatment Chest X-Ray Severity and Its Relation to Bacterial Burden in Smear Positive Pulmonary Tuberculosis. *BMC Med* (2018) 16(1):1–11. doi: 10.1186/s12916-018-1053-3
43. Nwongbouwoh Muefong C, Owolabi O, Donkor S, Charalambous S, Bakuli A, Rachow A, et al. Neutrophils Contribute to Severity of Tuberculosis Pathology and Recovery From Lung Damage Pre- and Posttreatment. *Clin Infect Dis* (2021) 2021:1–10. doi: 10.1093/cid/ciab729
44. Sigal GB, Segal MR, Mathew A, Jarlsberg L, Wang M, Barbero S, et al. Biomarkers of Tuberculosis Severity and Treatment Effect: A Directed Screen of 70 Host Markers in a Randomized Clinical Trial. *EBioMedicine* (2017) 25:112–21. doi: 10.1016/j.ebiom.2017.10.018
45. Ong CWM, Fox K, Ettorre A, Elkington PT, Friedland JS. Hypoxia Increases Neutrophil-Driven Matrix Destruction After Exposure to Mycobacterium Tuberculosis. *Sci Rep* (2018) 8(1):1–11. doi: 10.1038/s41598-018-29659-1
46. Metzler KD, Goosmann C, Lubojemska A, Zychlinsky A, Papayannopoulos V. Myeloperoxidase-Containing Complex Regulates Neutrophil Elastase Release and Actin Dynamics During NETosis. *Cell Rep* (2014) 8(3):883–96. doi: 10.1016/j.celrep.2014.06.044
47. Papayannopoulos V, Metzler KD, Hakkim A, Zychlinsky A. Neutrophil Elastase and Myeloperoxidase Regulate the Formation of Neutrophil Extracellular Traps. *J Cell Biol* (2010) 191(3):677–91. doi: 10.1083/jcb.201006052
48. Andersson AM, Larsson M, Stendahl O, Blomgran R. Efferocytosis of Apoptotic Neutrophils Enhances Control of Mycobacterium Tuberculosis in HIV-Coinfected Macrophages in a Myeloperoxidase-Dependent Manner. *J Innate Immun* (2020) 12(3):235–47. doi: 10.1159/000500861
49. Corleis B, Korbel D, Wilson R, Bylund J, Chee R, Schaible UE. Escape of Mycobacterium Tuberculosis From Oxidative Killing by Neutrophils. *Cell Microbiol* (2012) 14(7):1109–21. doi: 10.1111/j.1462-5822.2012.01783.x
50. Arnhold J. The Dual Role of Myeloperoxidase in Immune Response. *Int J Mol Sci* (2020) 21(21):8057. doi: 10.3390/ijms21218057
51. Yipp BG, Kim JH, Lima R, Zbytnuik LD, Petri B, Swanlund N, et al. The Lung is a Host Defense Niche for Immediate Neutrophil-Mediated Vascular Protection. *Sci Immunol* (2017) 2(10):1–14. doi: 10.1126/sciimmunol.aam8929
52. Cheemarla NR, Baños-Lara MDR, Naidu S, Guerrero-Plata A. Neutrophils Regulate the Lung Inflammatory Response *via* γδ T Cell Infiltration in an Experimental Mouse Model of Human Metapneumovirus Infection. *J Leukoc Biol* (2017) 101(6):1383–92. doi: 10.1189/jlb.4A1216-519RR
53. el-Hag A, Clark RA. Immunosuppression by Activated Human Neutrophils. Dependence on the Myeloperoxidase System. *J Immunol* (1987) 139(7):2406–13.
54. Yang P, Li Y, Xie Y, Liu Y. Different Faces for Different Places: Heterogeneity of Neutrophil Phenotype and Function. *J Immunol Res* (2019) 2019:8016254. doi: 10.1155/2019/8016254
55. Sagiv JY, Michaeli J, Assi S, Mishalian I, Kisos H, Levy L, et al. Phenotypic Diversity and Plasticity in Circulating Neutrophil Subpopulations in Cancer. *Cell Rep* (2015) 10(4):562–74. doi: 10.1016/j.celrep.2014.12.039
56. Cassetta L, Bruderek K, Skrzeczynska-Moncznik J, Osiecka O, Hu X, Rundgren IM, et al. Differential Expansion of Circulating Human MDSC Subsets in Patients With Cancer, Infection and Inflammation. *J Immunother Cancer* (2020) 8(2):e001223. doi: 10.1136/jitc-2020-001223
57. Yang Y, Li C, Liu T, Dai X, Bazhin AV. Myeloid-Derived Suppressor Cells in Tumors: From Mechanisms to Antigen Specificity and Microenvironmental Regulation. *Front Immunol* (2020) 11(July):1–22. doi: 10.3389/fimmu.2020.01371
58. Ferrer G, Jung B, Chiu PY, Aslam R, Palacios F, Mazzarello AN, et al. Myeloid-Derived Suppressor Cell Subtypes Differentially Influence T-Cell Function, T-Helper Subset Differentiation, and Clinical Course in CLL. *Leukemia* (2021) 35(11):3163–75. doi: 10.1038/s41375-021-01249-7
59. Magcwebeba T, Dorhoi A, Du Plessis N. The Emerging Role of Myeloid-Derived Suppressor Cells in Tuberculosis. *Front Immunol* (2019) 10(APR). doi: 10.3389/fimmu.2019.00917
60. Leukes V, Walzl G, du Plessis N. Myeloid-Derived Suppressor Cells as Target of Phosphodiesterase-5 Inhibitors in Host-Directed Therapeutics for Tuberculosis. *Front Immunol* (2020) 11(March):1–7. doi: 10.3389/fimmu.2020.00451
61. Klein SL, Flanagan KL. Sex Differences in Immune Responses. *Nat Rev Immunol* (2016) 16(10):626–38. doi: 10.1038/nri.2016.90
62. Neyrolles O, Quintana-Murci L. Sexual Inequality in Tuberculosis. *PloS Med* (2009) 6(12):e1000199. doi: 10.1371/journal.pmed.1000199

63. Horton KC, MacPherson P, Houben RMGJ, White RG, Corbett EL. Sex Differences in Tuberculosis Burden and Notifications in Low- and Middle-Income Countries: A Systematic Review and Meta-Analysis. *PloS Med* (2016) 13(9):1–23. doi: 10.1371/journal.pmed.1002119
64. Gemmati D, Bramanti B, Serino ML, Secchiero P. COVID-19 and Individual Genetic Susceptibility/Receptivity: Role of ACE1/ACE2 Genes, Immunity, Inflammation and Coagulation. Might the Double X-Chromosome in Females Be Protective Against SARS-CoV-2 Compared to the Single X-Chromosome in Males? *Int J Mol Sci* (2020) 21(3474):1–23. doi: 10.3390/ijms21103474
65. Doss PMIA, Umair M, Baillargeon J, Fazazi R, Fudge N, Akbar I, et al. Male Sex Chromosomal Complement Exacerbates the Pathogenicity of Th17 Cells in a Chronic Model of Central Nervous System Autoimmunity. *Cell Rep* (2021) 34(10):108833. doi: 10.1016/j.celrep.2021.108833
66. Aomatsu M, Kato T, Kasahara E, Kitagawa S. Gender Difference in Tumor Necrosis Factor-α Production in Human Neutrophils Stimulated by Lipopolysaccharide and Interferon-γ. *Biochem Biophys Res Commun* (2013) 441(1):220–5. doi: 10.1016/j.bbrc.2013.10.042
67. Kumar NP, Moideen K, Viswanathan V, Shruthi BS, Sivakumar S, Menon PA, et al. Elevated Levels of Matrix Metalloproteinases Reflect Severity and Extent of Disease in Tuberculosis-Diabetes Co-Morbidity and are Predominantly Reversed Following Standard Anti-Tuberculosis or Metformin Treatment. *BMC Infect Dis* (2018) 18(1):1–10. doi: 10.1186/s12879-018-3246-y
68. Hnizdo E, Singh T, Churchyard G. Chronic Pulmonary Function Impairment Caused by Initial and Recurrent Pulmonary Tuberculosis Following Treatment. *Thorax* (2000) 55(1):32–8. doi: 10.1136/thorax.55.1.32
69. Long R, Maycher B, Dhar A, Manfreda J, Hershfield E, Anthonisen N. Pulmonary Tuberculosis Treated With Directly Observed Therapy: Serial Changes in Lung Structure and Function. *Chest* (1998) 113(4):933–43. doi: 10.1378/chest.113.4.933
70. Khan N, Vidyarthi A, Amir M, Mushtaq K, Agrewala JN. T-Cell Exhaustion in Tuberculosis: Pitfalls and Prospects. *Crit Rev Microbiol* (2017) 43(2):133–41. doi: 10.1080/1040841X.2016.1185603
71. Day CL, Moshi ND, Abrahams DA, Van Rooyen M, O'Rie T, De Kock M, et al. Patients With Tuberculosis Disease Have Mycobacterium Tuberculosis-Specific CD8 T Cells With a Pro-Apoptotic Phenotype and Impaired Proliferative Capacity, Which is Not Restored Following Treatment. *PloS One* (2014) 9(4):1–12. doi: 10.1371/journal.pone.0094949
72. Day CL, Abrahams DA, Lerumo L, Janse van Rensburg E, Stone L, O'rie T, et al. Functional Capacity of Mycobacterium Tuberculosis -Specific T Cell Responses in Humans Is Associated With Mycobacterial Load. *J Immunol* (2011) 187(5):2222–32. doi: 10.4049/jimmunol.1101122
73. Jayaraman P, Jacques MK, Zhu C, Steblenko KM, Stowell BL, Madi A, et al. TIM3 Mediates T Cell Exhaustion During Mycobacterium Tuberculosis Infection. *PloS Pathog* (2016) 12(3):1–21. doi: 10.1371/journal.ppat.1005490
74. Greene CM, Hiemstra PS. Innate Immunity of the Lung. *J Innate Immun* (2020) 12(1):1–3. doi: 10.1159/000504621
75. Kumar V. Pulmonary Innate Immune Response Determines the Outcome of Inflammation During Pneumonia and Sepsis-Associated Acute Lung Injury. *Front Immunol* (2020) 11(August):1722. doi: 10.3389/fimmu.2020.01722
76. Galeas-Pena M, McLaughlin N, Pociask D. The Role of the Innate Immune System on Pulmonary Infections. *Biol Chem* (2019) 400(4):443–56. doi: 10.1515/hsz-2018-0304

Conflict of Interest: The authors declare that the research was conducted in the absence of any commercial or financial relationships that could be construed as a potential conflict of interest.

frontiers in Immunology

ORIGINAL RESEARCH
published: 07 December 2021
doi: 10.3389/fimmu.2021.714027

Flagellin From *Pseudomonas aeruginosa* Modulates SARS-CoV-2 Infectivity in Cystic Fibrosis Airway Epithelial Cells by Increasing TMPRSS2 Expression

Manon Ruffin[1†], Jeanne Bigot[1,2†], Claire Calmel[1], Julia Mercier[1], Maëlle Givelet[1], Justine Oliva[3], Andrés Pizzorno[3], Manuel Rosa-Calatrava[3], Harriet Corvol[1,4], Viviane Balloy[1], Olivier Terrier[3] and Loïc Guillot[1]*

[1] Sorbonne Université, Inserm, Centre de Recherche Saint-Antoine (CRSA), Paris, France, [2] Laboratoire de Parasitologie-Mycologie, APHP, Hôpital Saint-Antoine, Paris, France, [3] CIRI, Centre International de Recherche en Infectiologie, Team VirPath, Université de Lyon, Inserm U1111, Université Claude Bernard Lyon 1, CNRS, UMR5308, ENS de Lyon, Lyon, France, [4] Pneumologie Pédiatrique, APHP, Hôpital Trousseau, Paris, France

In the coronavirus disease 2019 (COVID-19) health crisis, one major challenge is to identify the susceptibility factors of severe acute respiratory syndrome-coronavirus-2 (SARS-CoV-2) in order to adapt the recommendations for populations, as well as to reduce the risk of COVID-19 development in the most vulnerable people, especially patients with chronic respiratory diseases such as cystic fibrosis (CF). Airway epithelial cells (AECs) play a critical role in the modulation of both immune responses and COVID-19 severity. SARS-CoV-2 infects the airway through the receptor angiotensin-converting enzyme 2, and a host protease, transmembrane serine protease 2 (TMPRSS2), plays a major role in SARS-CoV-2 infectivity. Here, we show that *Pseudomonas aeruginosa* increases TMPRSS2 expression, notably in primary AECs with deficiency of the ion channel CF transmembrane conductance regulator (CFTR). Further, we show that the main component of *P. aeruginosa* flagella, the protein flagellin, increases TMPRSS2 expression in primary AECs and Calu-3 cells, through activation of Toll-like receptor-5 and p38 MAPK. This increase is particularly seen in Calu-3 cells deficient for CFTR and is associated with an intracellular increased level of SARS-CoV-2 infection, however, with no effect on the amount of virus particles released. Considering the urgency of the COVID-19 health crisis, this result may be of clinical significance for CF patients, who are frequently infected with and colonized by *P. aeruginosa* during the course of CF and might develop COVID-19.

Keywords: cystic fibrosis, infection, COVID19, *Pseudomonas aeruginosa*, SARS-CoV-2, TLR5, protease

OPEN ACCESS

Edited by:
Rabindra Tirouvanziam, Emory University, United States

Reviewed by:
James Harker, Imperial College London, United Kingdom
Luke Wisely Garratt, University of Western Australia, Australia

***Correspondence:**
Loïc Guillot
loic.guillot@inserm.fr

†These authors have contributed equally to this work and share first authorship

Specialty section:
This article was submitted to Mucosal Immunity, a section of the journal Frontiers in Immunology

Received: *24 May 2021*
Accepted: *05 November 2021*
Published: *07 December 2021*

Citation:
Ruffin M, Bigot J, Calmel C, Mercier J, Givelet M, Oliva J, Pizzorno A, Rosa-Calatrava M, Corvol H, Balloy V, Terrier O and Guillot L (2021) Flagellin From Pseudomonas aeruginosa Modulates SARS-CoV-2 Infectivity in Cystic Fibrosis Airway Epithelial Cells by Increasing TMPRSS2 Expression. Front. Immunol. 12:714027. doi: 10.3389/fimmu.2021.714027

INTRODUCTION

As of October 30, 2021, the coronavirus disease 2019 (COVID-19) pandemic, caused by severe acute respiratory syndrome (SARS)-coronavirus (CoV)-2, has infected nearly 245 million people globally and led to >4.9 million deaths (https://covid19.who.int). In this health crisis, one of the major challenges is to identify the susceptibility factors of the infecting virus in order to adapt public health recommendations and to reduce the risk of getting COVID-19, particularly in the case of the most vulnerable people: patients with common chronic respiratory diseases such as asthma and chronic obstructive pulmonary disease, and patients with less common or rare chronic respiratory diseases such as cystic fibrosis (CF). Given their lung impairments, patients with chronic respiratory diseases can reasonably be expected to face an elevated risk of developing severe COVID-19, but the magnitude of this risk remains uncertain (1). Together with clinical follow-up studies conducted to more accurately estimate the disease risk of these patients, basic research on the pathophysiology of SARS-CoV-2 infection should provide critical insights into how COVID-19 affects patients with respiratory diseases.

The aforementioned COVID-19 development in patients is particularly relevant in the case of people with CF (pwCF). CF is caused by variants in the gene *CFTR* (CF transmembrane conductance regulator), with the most frequent variant being F508del, which leads to aberrant function of airway epithelial cells (AECs). During the course of CF, the lungs of the patients are inflamed and chronically infected by various pathogens, including *Pseudomonas aeruginosa*, the most prevalent pathogen (2). The most recent multinational report identified 181 cases of pwCF infected by SARS-CoV-2, and recorded 7 deaths (3); among the 181 pwCF, 82% were symptomatic, 47% were hospitalized, and 51% showed airway infection by *P. aeruginosa*.

AECs play a critical role in the regulation of both the immune response and the severity of COVID-19 (4). Notably, several studies examining SARS-CoV-2 cellular tropism have demonstrated that ciliated and secretory cells are the major targets of infection (4–8). SARS-CoV-2 infects the airway mainly through the cell-surface receptor angiotensin-converting enzyme-2 (ACE2), and two specific host proteases, TMPRSS2 (transmembrane serine protease 2) and FURIN, have been shown to play a major role in SARS-CoV-2 infectivity (9–13).

Here, we show that the main component of *P. aeruginosa* flagella, the protein flagellin (*Pa*-F), upregulates TMPRSS2 expression in AECs, especially in patients' cells deficient for *CFTR*, through Toll-like receptor-5 (TLR5) and p38 activation. Importantly, this enhanced TMPRSS2 expression is associated with an increase in the level of SARS-CoV-2 infection.

MATERIAL AND METHODS

Reagents

Ultrapure flagellin from *P. aeruginosa* (tlrl-pafla) and ultrapure (tlrl-epstfla), recombinant (tlrl-flic), and vaccigrade (vac-fla) flagellin from *Salmonella enterica* serovar Typhimurium were from InvivoGen (San Diego, CA, USA). Anti-TLR5 antibody and NF-κB inhibitor (BAY 11-7082) were from InvivoGen. DMSO and p38 inhibitor (SB203580) were from Sigma-Aldrich (Saint-Louis, MO, USA).

Cell Culture

Calu-3 cells (ATCC HTB-55™/Lot: 62657853) and Calu-3-*CFTR*-WT and Calu-3-*CFTR*-KD cells (generously provided by Prof. Marc Chanson, University of Geneva, Switzerland) were cultured in MEM-Glutamax (Gibco, Paisley, UK) supplemented with 10% fetal calf serum (FCS; Eurobio, Les Ulis, France) and 1% non-essential amino acids, 10 mmol/L HEPES (pH 7.2-7.5), 1% sodium pyruvate, and 1% antibiotics (all from Gibco). They grow at the air-liquid interface, in Transwell® dishes (12 mm; 3460, Corning, Kennebunk, ME, USA), to obtain polarized cells as previously described (14). Primary human bronchial epithelial cells (source characteristics listed in **Table 1**) were cultured as recommended by the manufacturer by using hAEC complete culture medium (Epithelix, Geneva, Switzerland). Beas-2B cells (CRL-9609™/Lot: 59227035) were cultured in F12 medium supplemented with 10% FCS, 10 mmol/L HEPES, and 1% antibiotics. 16HBE14o- cells were generously supplied by Pr. Dieter Gruenert (originator) and Dr. Beate Illek (provider) from the University of California San Francisco (UCSF); the cells were cultured in MEM-Glutamax supplemented with 10% FCS and 1% antibiotics, as recommended by the provider. Caco-2/TC7 cell line, a clonal population established from human colon carcinoma Caco-2 cells at late passage (15), were generously provided by Dr. Véronique Carrière (Sorbonne Université/Centre de recherche St-Antoine); the cells were cultured in high-glucose DMEM-Glutamax (Gibco) supplemented with 20% FCS, 1% non-essential amino acids, and 1% antibiotics.

Reverse Transcription-qPCR

Human RNA was isolated using a NucleoSpin RNA/miRNA kit (Macherey Nagel, Duren, Germany). RT was performed using a high-capacity cDNA kit (Applied Biosystems, Foster City, CA, USA). Real-time qPCR was performed by using an ABI QS3 with a Sensifast Probe Lo-Rox Kit (Bio-technofix, Guibeville, France), TaqMan probes for *ACE2* (Hs01085333_m1), *TMPRSS2* (Hs00237175_m1), *FURIN* (Hs00965485_g1), and *GAPDH* (Hs02786624_g1), and a cDNA template. For relative quantification, the expression level of target genes was normalized to the expression of *GAPDH* relative to the reference group (specified in the figure legends) used as a calibrator and was calculated using the $2^{-\Delta\Delta Ct}$ method.

SARS-CoV-2 Infection and Viral Quantification

Fully polarized Calu-3 cells grown at the air-liquid interface were infected with SARS-CoV-2 (strain BetaCoV/France/IDF0571/2020; accession ID EPI_ISL_411218) at a multiplicity of infection of 1, as previously described (1 h of contact with the virus followed by a change of the medium, and analysis at 24h) (16). Viral quantification through RT-qPCR targeting of ORF1b-nsp14 was performed as described (16).

TABLE 1 | Characteristics of donors of bronchial epithelial cells.

Group	Reference	Origin	Sex	Age	CFTR variant	Smoker	Used in
WT	02AB077201F2	Caucasian	Male	63	–	No	**Figure 1C**
	02AB068001F2	Caucasian	Female	71	–	No	**Figure 1C**
	02AB067101	Caucasian	Male	72	–	No	**Figure 1C**
	02AB0839.01	Caucasian	Male	54	–	No	**Figure 1C**
CF	CFAB043703	Unknown	Male	27	F508del/F508del	No	**Figure 1C**
	CFAB060901	Unknown	Female	21	F508del/F508del	No	**Figure 1C**
	CFAB045202	Unknown	Male	32	F508del/F508del	No	**Figure 1C**
	CFAB064901	Unknown	Female	37	F508del/1717-1G>A	No	**Figures 1C**, **3D, E**

Western Blotting

Total proteins were extracted using RIPA buffer (Euromedex, Souffelweyersheim, France), and then equal amounts of proteins were reduced, size-separated on 12% stain-free precast SDS-polyacrylamide gels (Bio-Rad, Hercules, CA, USA), and transferred to nitrocellulose membranes by using an iBlot2 apparatus (Thermo Fisher Scientific). The membranes were blocked in 5% milk in TBS-Tween 0.1% and incubated with specific primary antibodies overnight at 4°C; the antibodies were against ACE2 (AF933, R&D Systems, Minneapolis, MN, USA; 1:200), phospho- and total p38 (9211 and 9212, Cell Signaling Technology, Danvers, MA, USA; 1:2,000), phospho- and total NF-κB p65 (3039 and 8242, Cell Signaling Technology; 1:2,000), and β-actin (A2228, Sigma-Aldrich; 1:5,000). The blots were exposed to horseradish peroxidase-conjugated anti-rabbit (Cell Signaling Technology, 7074; 1:10,000) and anti-goat (A27104, Thermo Fisher Scientific; 1:2,000) secondary antibodies, and bound antibodies were detected using Clarity chemiluminescent substrate (Bio-Rad). Images were recorded using a Fujifilm LAS-3000 bioimaging system (Stamford, CT, USA).

Immunofluorescence

After various treatments, Calu-3 grown at the air-liquid interface were rinsed with PBS and fixed with ice-cold 4% paraformaldehyde for 20 min, permeabilized for 10 min with 0.1% Triton X-100 in PBS, and then washed with PBS and incubated in a blocking solution (PBS + 5% BSA) for 1 h. Next, the cells were incubated overnight at 4°C with primary antibodies against TMPRSS2 (14437-1-AP, Thermo Fisher Scientific; 1:100) or ACE2 (AF933, R&D Systems; 1:60) in PBS supplemented with 1% BSA, and on the following day, the cells were washed (3 × 5 min) with PBS and incubated for 1 h at room temperature with secondary antibodies, anti-rabbit Alexa 488 (4412, Cell Signaling Technology, 1:2,000) or anti-goat Alexa 488 (A11078, Thermo Fisher Scientific, 1:2,000). After staining with 4,6-diamidino-2-phenylindole (DAPI), coverslips were mounted and sealed with ProLong diamond mounting medium (Thermo Fisher Scientific). Fluorescent images were obtained using an Olympus BX43 microscope (Hamburg, Germany).

ELISA

Concentrations of human IL-8, IL-6, IFN-β, IFN-λ in cell supernatants were measured using ELISA kits (DY208, DY206, DY814 and DY1598B, R&D Systems), according to the manufacturer's instructions. The substrate 3,3′,5,5′-tetramethylbenzidine was from Cell Signaling Technology.

Statistical Analysis

Differences among groups were assessed for statistical significance by using Prism 9.00 software (GraphPad Software, La Jolla, CA, USA), as indicated in the figure legends. $P < 0.05$ was considered statistically significant.

Ethics

This project was approved (Opinion number 20-688) by the Inserm Institutional Review Board (IRB00003888, IORG0003254, FWA00005831).

Data Availability

RNAseq data used here are from a transcriptomic study (17) which RNAseq raw datafiles are available in the European Nucleotide Archive (ENA) (primary accession number PRJEB9292). http://www.ebi.ac.uk/ena/data/view/PRJEB9292.

RESULTS

ACE2, *FURIN*, and *TMPRSS2* Expression In CF and Non-CF Primary Human AECs Upon *P. aeruginosa* Infection

We first examined *ACE2*, *FURIN*, and *TMPRSS2* expression from a previous transcriptomic study performed using primary hAECs; the cells were isolated from control (non-CF) donors and pwCF homozygous for the *CFTR* F508del variant, and were infected by *P. aeruginosa* (17). At baseline (time 0 h), similar *ACE2* and *FURIN* mRNA expression levels were observed in non-CF and CF primary hAECs (**Figure 1A**), whereas *TMPRSS2* expression was significantly higher in CF primary hAECs (**Figures 1A, B**). Importantly, *P. aeruginosa* infection increased *TMPRSS2* mRNA expression over time in CF but not in non-CF primary hAECs (**Figures 1A, B**), whereas the infection did not affect *ACE2* and *FURIN* expression (**Figure 1A**).

Because the most critical proinflammatory factor from *P. aeruginosa* present in the sputum of pwCF is flagellin (18), we next exposed CF primary hAECs to flagellin. Treatment with flagellin increased the mRNA level of *TMPRSS2* without increasing that of *ACE2* (**Figure 1C**) or *FURIN* (not illustrated). This effect was observed in both non-CF and CF

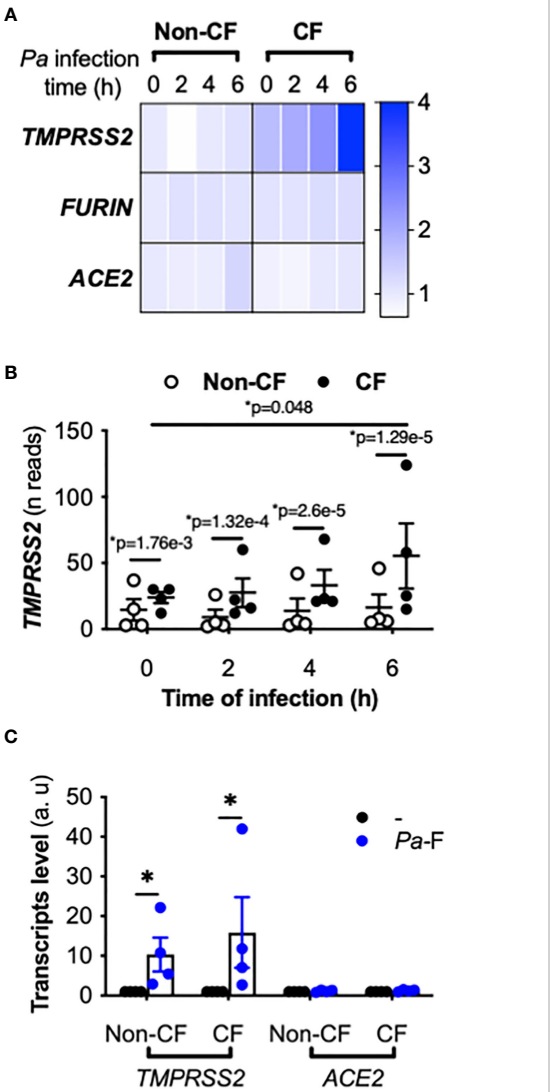

FIGURE 1 | Effect of *P. aeruginosa* infection on *ACE2*, *TMPRSS2*, and *FURIN* expression in primary hAECs. Heatmap of *ACE2*, *TMPRSS2*, and *FURIN* expression (fold-change) **(A)** and kinetics of *TMPRSS2* expression (shown in reads) **(B)** in primary hAECs isolated from non-CF and CF patients and infected with *P. aeruginosa* (multiplicity of infection = 0.25) [RNA-seq data extracted from a previous study (17), Benjamini-Hochberg adjusted p value (*p)]. **(C)** *ACE2* and *TMPRSS2* mRNA expression (in arbitrary units, a.u.) in submerged non-CF (n=4) and CF (n=4) primary hAECs stimulated with control medium (reference group) or *Pa*-F (50 ng/mL) for 6 h (ANOVA with Bonferroni's multiple-comparison test, $*P < 0.05$).

primary hAECs, although in both groups, the level of induction varied considerably between individuals.

ACE2, *FURIN*, and *TMPRSS2* Expression in *CFTR*-Sufficient and -Deficient Calu-3 Cells Exposed to *P. aeruginosa Flagellin*

To investigate the mechanism underlying the aforementioned increase in TMPRSS2 expression and to eliminate the interindividual variability, we sought to identify AEC lines expressing detectable levels of ACE2 and TMPRSS2 mRNA and protein. Thus, we measured ACE2 and TMPRSS2 expression in the AEC lines Calu-3, Beas-2B, and 16HBE (**Figure 2A**), which revealed that Calu-3 cells expressed higher mRNA levels of *ACE2* and *TMPRSS2* relative to the other cell lines, and that ACE2 protein was detected only in Calu-3 cells. These results agree with the documented higher ability of SARS-CoV-2 to replicate in Calu-3 cells than in Beas-2B cells (10). Thus, we hereafter used the Calu-3 cell line, specifically isogenic *CFTR*-sufficient (Calu-3-*CFTR*-WT) and *CFTR*-deficient Calu-3 (Calu-3-*CFTR*-KD) cells.

In accord with what was observed in CF primary hAECs, we found that exposure of Calu-3 cells to *P. aeruginosa* flagellin significantly increased *TMPRSS2* mRNA expression (**Figure 2B**) in a dose-dependent manner (**Supplementary Figure 1**) without affecting the transcripts levels of *ACE2* (**Figure 2C**) and *FURIN* (not illustrated). This increase in *TMPRSS2* expression was more notable in Calu-3-*CFTR*-KD than in Calu-3-*CFTR*-WT (**Figure 2B**), and the TMPRSS2 upregulation was also detected at the protein level (**Figure 2D**). As expected, flagellin induced the synthesis of the proinflammatory cytokines interleukin (IL)-8 and IL-6 (**Supplementary Figure 2A, B**) both in Calu-3-*CFTR*-WT and Calu-3-*CFTR*-KD cells, and this inflammatory response was relatively higher in the Calu-3-*CFTR*-KD cells, which agrees with previous work showing that CF epithelial cells from human (19) or porcine (20) origin exhibit an enhanced inflammatory response to flagellin.

To ascertain whether the observed effect of flagellin is specific to the bacterial source of the protein, we used ultrapure flagellin isolated from *S. Typhimurium* serovar Typhimurium (*St*-F) in our assays, which revealed that *St*-F induced similar *TMPRSS2* expression in Calu-3 cells as did flagellin isolated from *P. aeruginosa* (**Figure 3A**). By contrast, recombinant flagellins (standard or vaccigrade™) from *S.* Typhimurium did not affect the expression (**Figure 3A**).

Flagellin is known to activate TLR5 and the downstream p38 mitogen-activated protein kinase (MAPK) signaling pathway (21); thus, we tested the involvement of this pathway in the observed *TMPRSS2* induction. We showed that the upregulation of *TMPRSS2* expression depended on TLR5 signaling (**Figure 3B**). When a p38 inhibitor was used, flagellin-induced *TMPRSS2* expression was diminished in Calu-3-*CFTR*-KD cells (**Figure 3C**) and primary CF hAECs (**Figure 3D**). Furthermore, an inhibitor of nuclear factor-kappa B (NF-κB) also reduced the *TMPRSS2* induction by flagellin. Accordingly, the results of western blotting confirmed that flagellin stimulated p38 phosphorylation as well as NF-κB activation (**Figure 3E**). Moreover, as shown previously (21), we further observed that this NF-κB activation depended on p38 activity (**Figure 3E**).

To determine whether *TMPRSS2* induction was restricted to the lung epithelium, we examined the flagellin effect in an intestinal cell line, Caco-2/TC7. Our results showed that flagellins from *P. aeruginosa* and S. Typhimurium, which were able to induce IL-8 production (**Supplementary Figure 3A**), exerted no effect on *TMPRSS2* expression in these cells (**Supplementary Figure 3B**).

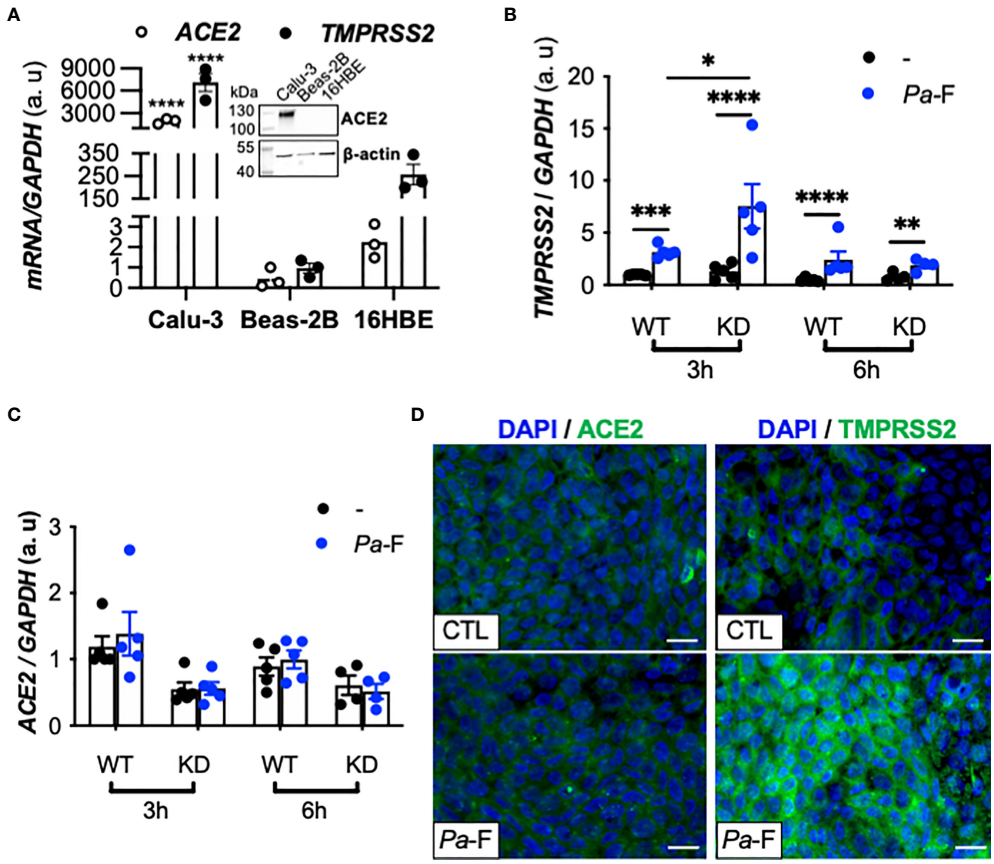

FIGURE 2 | Effect of *P. aeruginosa* flagellin on ACE2, FURIN, and TMPRSS2 expression in *CFTR*-deficient Calu-3 cells. **(A)** *ACE2* and *TMPRSS2* mRNA expression in submerged cultures of Calu-3, Beas-2B (reference), and 16HBE14o- cell lines (n = 3, ANOVA with Dunnett's multiple-comparison test, control group: Calu-3, ****P < 0.0001). *GAPDH*, housekeeping gene. Representative western blot (with 20 µg of protein) showing ACE2 and β-actin protein expression in submerged cultures of Calu-3, Beas-2B, and 16HBE14o- cell lines. *TMPRSS2* **(B)** and *ACE2* **(C)** mRNA expression (relative to that of housekeeping gene *GAPDH*) in Calu-3-*CFTR*-WT (reference group) and -*CFTR*-KD cells grown at the air-liquid interface and either not stimulated (–) or stimulated for 3 or 6 h with *P. aeruginosa* flagellin (*Pa*-F, 50 ng/mL) (n = 5, ANOVA with Bonferroni's multiple-comparison test, *P < 0.05, **P < 0.01, ***P < 0.001, ****P < 0.0001). **(D)** Immunofluorescence analysis of TMPRSS2 and ACE2 protein expression in Calu-3 cells (ATCC) grown at the air-liquid interface and stimulated with *Pa*-F for 18 h; scale bar, 20 µm.

Influence of TMPRSS2 Induction by *P. aeruginosa* Flagellin on SARS-CoV-2 Infectivity in *CFTR*-Sufficient and -Deficient Calu-3 Cells

Lastly, we investigated whether TMPRSS2 induction by flagellin influences SARS-CoV-2 infectivity. After infection with SARS-CoV-2, the intracellular *nsp14* viral mRNA level was increased, and this level was significantly higher in Calu-3-*CFTR*-KD than -*CFTR*-WT cells and was even more notably elevated when the cells were pre-stimulated with flagellin (**Figure 4A**). By contrast, the extracellular *nsp14* viral mRNA level, measured in the apical supernatant of AECs as a surrogate for viral production, was significantly lower in Calu-3-*CFTR*-KD cells than in Calu-3-*CFTR*-WT cells (**Figure 4B**). Whereas pre-stimulation with flagellin did not affect viral-particle release in Calu-3-*CFTR*-WT cells, a lower, albeit not statistically significant, level of *nsp14* mRNA was measured at the apical side of Calu-3-*CFTR*-KD cells pre-stimulated with flagellin. To ensure that viral particles release was not due to an increase in the permeability of the epithelial barrier by flagellin, we measured TEER and observed that flagellin treatment was not associated with a loss of epithelial integrity (**Supplementary Figure 4**). Lastly, IFN-β and IFN-λ measurements in basal supernatants were not induced either by the virus or the flagellin in the different conditions tested (not illustrated).

DISCUSSION

In this study, we showed that exposure of AECs to flagellin from *P. aeruginosa* induces an increase in TMPRSS2 expression, which is dependent on TLR5 and p38 MAPK activation. Notably, prior exposure of AECs to flagellin results in increased infectivity of SARS-CoV-2 (illustrated in **Figure 5**).

We found that *TMPRSS2* is more expressed in hAECs from pwCF as compared with the level in controls. Although the

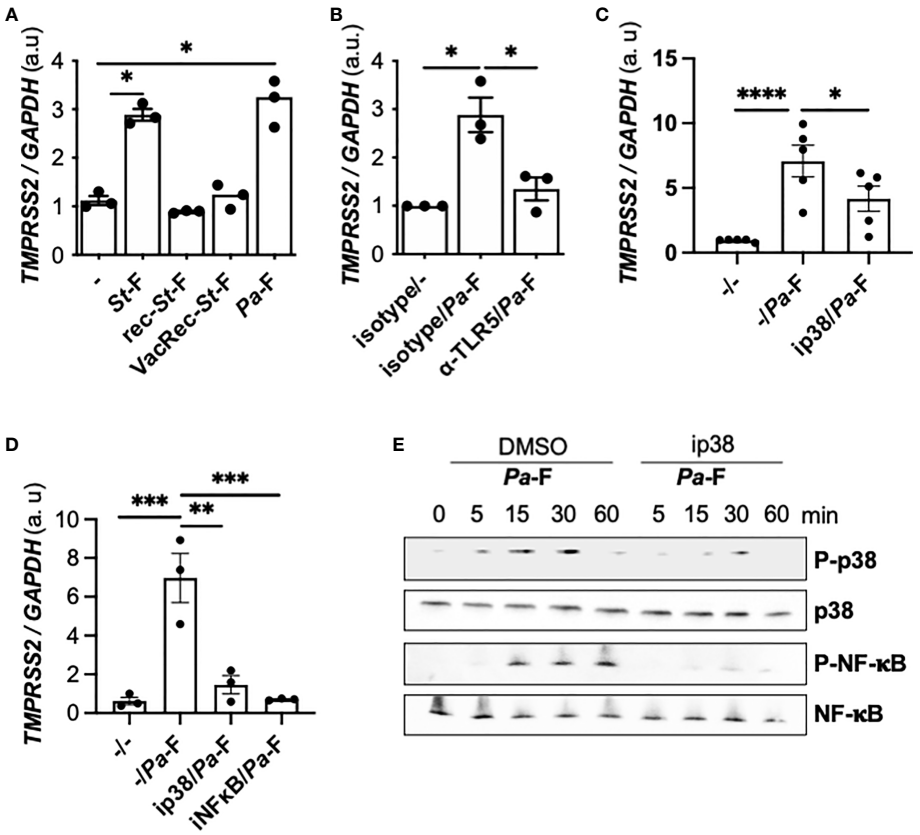

FIGURE 3 | Effect of TLR5 and p38 inhibition on flagellin induced-TMPRSS2 expression in *CFTR*-deficient cells. **(A)** *TMPRSS2* mRNA expression in Calu-3-*CFTR*-KD grown at the air-liquid interface and either not stimulated or stimulated for 6 h with 50 ng/mL ultrapure flagellin from S. Typhimurium (*St*)-F, recombinant *St*-F, vaccigrade *St*-F, or *Pa*-F (n = 3, ANOVA with Dunnett's multiple-comparison test, $^{*}P < 0.05$). **(B)** *TMPRSS2* mRNA expression in Calu-3-*CFTR*-KD cells grown at the air-liquid interface and incubated for 1 h with isotype control (reference) or anti-TLR5 antibody (10 µg/mL) and then either not stimulated or stimulated for 6 h with *Pa*-F (50 ng/mL) (n = 3, ANOVA with Dunnett's multiple-comparison test, control group: Isotype/*Pa*-F, $^{*}P < 0.05$). *TMPRSS2* mRNA expression in Calu-3-*CFTR*-KD cells grown at the air-liquid interface **(C)** or in primary CF hAECs **(D)** that were preincubated for 1 h with 20 µmol/L p38 or 20 µmol/L NF-κB inhibitors and then stimulated for 6 h with 50 ng/mL *Pa*-F in the presence of the inhibitor. ANOVA with Dunnett's multiple-comparison test, control group: -/*Pa*-F, $^{*}P < 0.05$, $^{**}P < 0.01$, $^{***}P < 0.001$, $^{****}P < 0.0001$. **(E)** Western blot (with 10 µg of protein) of phospho- and total p38 and phospho- and total NF-κB in primary hAECs stimulated with 50 ng/mL *Pa*-F.

hAECs were isolated from a limited number of pwCF, this observation agrees with previous results obtained using excised lungs, where RNA *in situ* hybridization revealed that TMPRSS2 expression was higher in pwCF than in non-CF patients (7). We also observed that flagellin from *P. aeruginosa* increases TMPRSS2 expression in primary bronchial epithelial cells from both pwCF and controls. The variability of the flagellin-elicited response in the two groups is likely due to the effect of several donor-related factors, such as sex, age, and CF clinical history in the case of pwCF. An age-related increase in TLR5 expression and sensing has been observed in human monocytes (22). Moreover, the single-nucleotide polymorphism *TLR5* c.1174C>T, which is common in the general population (23) and generates a variant that acts as a modifier gene in CF (24), might also contribute to this variability. Unfortunately, it was not possible to have age-matched donors which constitutes a limitation in our study.

To elucidate the specific contribution of CFTR in the level of TMPRSS2 induction by flagellin, we used isogenic Calu-3-*CFTR*-WT and Calu-3-*CFTR*-KD cells. We found that TMPRSS2 is highly induced in Calu-3-*CFTR*-KD cells, and we further confirmed previous observations indicating that *CFTR*-deficient bronchial cells show an elevated inflammatory response to flagellin, characterized by increased levels of IL-6 and IL-8 (19). Flagellin is known to activate TLR5 and downstream p38 and NF-κB in Calu-3 cells (21). Confirming these results, TMPRSS2 induction by flagellin was found here to depend on p38 and NF-κB, both in Calu-3 cells and primary CF hAECs. Interestingly, a recent phosphoproteomic study in Vero-6 cells revealed that SARS-CoV-2 stimulates the p38 pathway, and that pharmacological inhibition of p38 shows antiviral efficacy (25). Thus, this study and our results here suggest that inhibiting the p38 pathway could represent a potential COVID-19 therapy.

The increase in intracellular viral mRNA levels in CF cells exposed to flagellin, which indicates an elevated level of infection, is likely the result of the upregulated expression of TMPRSS2. Accordingly, TMPRSS2 inhibition by using the serine-protease

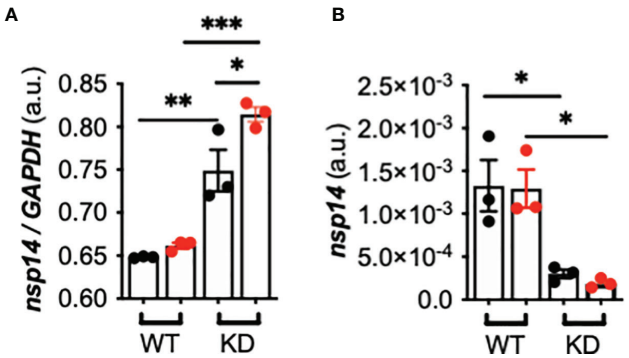

FIGURE 4 | Effect of TMPRSS2 induction by *P. aeruginosa* flagellin on SARS-CoV-2 infectivity in *CFTR*-deficient Calu-3 cells. **(A)** Intracellular *nsp14/GAPDH* and **(B)** apical (supernatant) *nsp14* mRNA expression in Calu-3-*CFTR*-WT (reference group) and -*CFTR*-KD cells grown at the air-liquid interface and either not stimulated (black circle) or stimulated (red circle) for 16 h with *Pa*-F 50 ng/mL), and then infected for 24 h with SARS-CoV-2 (multiplicity of infection = 1) (n = 3, ANOVA with Bonferroni's multiple-comparison test, $^{*}P < 0.05$, $^{**}P < 0.01$, $^{***}P < 0.001$).

inhibitor camostat mesylate is sufficient for preventing infection with SARS-CoV-2 (10). Intriguingly, we observed a lower level of viral particles at the apical side of CF cells as compared with the levels in non-CF cells; this could be the result of an increased host-defense capacity of CF cells against viral infection, or a delay in the kinetics of virus release. Interestingly, a recent transcriptomic study shows that despite the fact that influenza virus (IAV) replication in Calu3-*CFTR*-WT and Calu-3-*CFTR*-KD cells is similar, a specific immune gene profile is observed in Calu-3-*CFTR*-KD before and after infection with IAV. It is also shown by RNAseq analysis that flagellin stimulation revealed potential dysregulation of pathways involved in viral infection. Importantly, by stimulating cells with IFNs and using a transcription network analysis, they also demonstrated that IFN signaling is altered in *CFTR* deficient cells (26) which could explain in part our results. Future studies specifically investigating infection kinetics, viral-particle release, and the resulting antiviral response including the production of IL-6 and Type I/III interferons should facilitate definitive assessment of whether prior exposure to flagellin induces either a protective or damaging effect after SARS-CoV-2 infection of CF cells. The non-detection of IFN-β and IFN-λ in our viral infection conditions is probably related to the very short infection time chosen, which if it allows to study the initiation of the viral

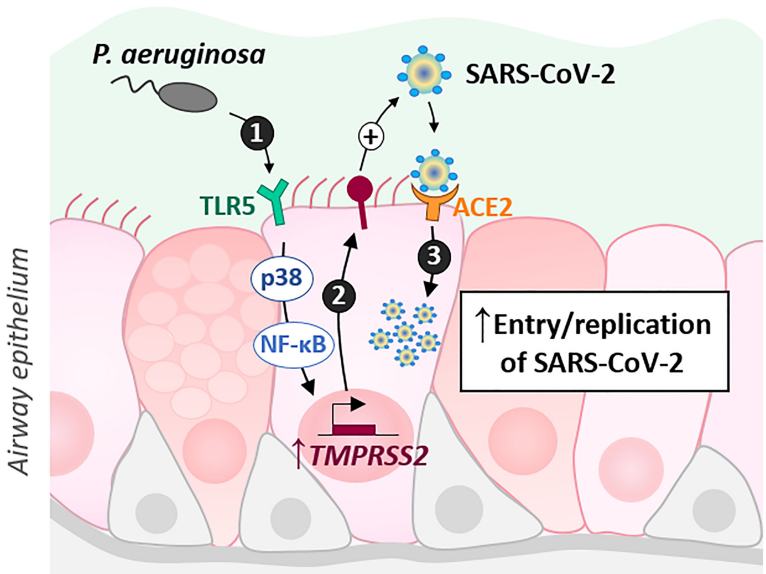

FIGURE 5 | Schematic illustrating the results. *P. aeruginosa* interacts with the airway epithelial cells of pwCF, notably by activating the TLR5 signaling pathway through its virulence factor, flagellin. This activation, dependent on p38 MAPK and NF-kB, leads to an increase in TMPRSS2 which could regulate SARS-CoV-2 infectivity.

infection process does not allow to study at best the resulting inflammatory response. Indeed, it was shown in Calu-3 cells that SARS-CoV-2 induces a significant but delayed IFN-β in comparison to Sendaï virus or synthetic dsRNA (poly I:C) (27).

Further investigations conducted using primary cells differentiated at the air-liquid interface will be necessary to specifically characterize the response of CF bronchial epithelial cells. Nevertheless, the model used here is relevant. As noted in the introduction section, secretory cells are infected by SARS-CoV-2; this was demonstrated in previous studies conducted using single-cell RNA-seq, either ex vivo with lung biopsies of patients infected with SARS-CoV-2 (4), or *in vitro* with a reconstituted epithelium at the air-liquid interface (6, 8). Calu-3 cells polarized at the air-liquid interface present the characteristics of secretory cells (mucus production) and express naturally (i.e., without exogenous overexpression) the required proteins (ACE2, TMPRSS2) for infection by SARS-CoV-2, which is not the case with the other epithelial cell lines tested in this study.

Several studies have delineated the antiviral capacity endowed by flagellin against other respiratory viruses, including influenza A (28). Furthermore, flagellin was recently suggested to be capable of modulating the innate immune response and thereby eliminating SARS-CoV-2 and resolving COVID-19 (29). Accordingly, the use of recombinant flagellin as an adjuvant in vaccine development has been considered (30). However, we observed here that recombinant flagellin (standard or vaccigrade™) from *S.* Typhimurium did not affect *TMPRSS2* expression. Thus, although these data were obtained *in vitro*, it is likely based on the aforementioned finding that pathogen-targeting vaccines developed using recombinant flagellin as an adjuvant will not produce negative effects in the case of concomitant exposure to SARS-CoV-2. Moreover, the observed upregulation of TMPRSS2 expression induced by flagellin appears specific to the lung epithelium, because the effect was not replicated in Caco-2/TC7 cells, which are epithelial cells of intestinal origin. During their lifetime, pwCF are also infected with other flagellated bacteria including *Burkholderia cenocepacia* and *Stenotrophomonas maltophilia* (31). In particular, flagellin from *Burkholderia cenocepacia* also known to activate TLR5 (32, 33), could also modulate TMPRSS2 expression.

The question of whether CF patients face an increased risk of developing a severe form of COVID-19 is a topical one and a source of discussion (34). Clinical follow-up results obtained to date indicate that pwCF, both adults (3, 35) and children (36), do not show an elevated risk of developing severe COVID-19 as compared with the general population. However, pwCF with advanced CF disease (associated with older age, CF-related diabetes, lower lung function, having received an organ transplant) might develop a severe clinical course (3, 35).

In a recent French study, we compared the baseline clinical characteristics of 31 pwCF infected by SARS-CoV-2 during the first wave of the pandemic to that of the overall French CF population (n = 6,913; >90% of all French CF cases) (37). The pwCF with COVID-19 were found to be older and more frequently chronically colonized with *P. aeruginosa* (37). However, considering the small number of patients, these results must be interpreted with caution. Thus, whether the risk of developing severe COVID-19 is increased in pwCF because of their *P. aeruginosa* infection remains unresolved and will require further meta-analysis performed using international cohorts. Moreover, a recent study including 874 individuals with COVID-19 showed that carriers of CF-causing variants (N=40) may be more likely to develop severe COVID-19 (38). This reinforces the interest in studying the specific role of CFTR in the pathogenesis of COVID-19.

In conclusion, we have shown that exposure of CF AECs to flagellin from *P. aeruginosa* can enhance SARS-CoV-2 infectivity. Further clinical follow-up studies and *in vitro* experimental investigations into the mechanisms associated with the specific host response of primary CF cells to SARS-CoV-2 infection should help elucidate this matter and provide insights for future clinical care.

DATA AVAILABILITY STATEMENT

The datasets presented in this study can be found in online repositories. The names of the repository/repositories and accession number(s) can be found below: https://www.ebi.ac.uk/ena, PRJEB9292.

AUTHOR CONTRIBUTIONS

LG, MR, and OT, designed experiments. MR, JB, CC, VB, OT, AP, JM, MG, JO, conducted the experiments. LG wrote the manuscript. MR, JB, VB, MR-C, HC and OT critically revised the manuscript. All authors contributed to the article and approved the submitted version.

FUNDING

LG received a grant from the Faculté de Médecine Sorbonne Université (AAP COVID19).

ACKNOWLEDGMENTS

We thank Prof. Marc Chanson (University of Geneva) for generously providing Calu-3-*CFTR*-WT and Calu-3-*CFTR*-KD cells (14), Prof. Dieter Gruenert and Dr. Beate Illek (University of California San Francisco (UCSF)) for 16HBE14o- cells, and Dr. Véronique Carrière (Sorbonne Université/Centre de recherche St-Antoine) for Caco-2/TC7 cell line. This manuscript has been released as a pre-print (39).

SUPPLEMENTARY MATERIAL

The Supplementary Material for this article can be found online at: https://www.frontiersin.org/articles/10.3389/fimmu.2021.714027/full#supplementary-material

REFERENCES

1. To T, Viegi G, Cruz A, Taborda-Barata L, Asher M, Behera D, et al. A Global Respiratory Perspective on the COVID-19 Pandemic: Commentary and Action Proposals. *Eur Respir J* (2020) 56(1):2001704. doi: 10.1183/13993003.01704-2020
2. Elborn JS. Cystic Fibrosis. *Lancet* (2016) 388(10059):2519–31. doi: 10.1016/S0140-6736(16)00576-6
3. McClenaghan E, Cosgriff R, Brownlee K, Ahern S, Burgel PR, Byrnes CA, et al. The Global Impact of SARS-CoV-2 in 181 People With Cystic Fibrosis. *J Cyst Fibros* (2020) 19(6):868–71. doi: 10.1016/j.jcf.2020.10.003
4. Chua RL, Lukassen S, Trump S, Hennig BP, Wendisch D, Pott F, et al. COVID-19 Severity Correlates With Airway Epithelium-Immune Cell Interactions Identified by Single-Cell Analysis. *Nat Biotechnol* (2020) 38 (8):970–9. doi: 10.1038/s41587-020-0602-4
5. Zhu N, Wang W, Liu Z, Liang C, Wang W, Ye F, et al. Morphogenesis and Cytopathic Effect of SARS-CoV-2 Infection in Human Airway Epithelial Cells. *Nat Commun* (2020) 11(1):3910. doi: 10.1038/s41467-020-17796-z
6. Ravindra NG, Alfajaro MM, Gasque V, Huston NC, Wan H, Szigeti-Buck K, et al. Single-Cell Longitudinal Analysis of SARS-CoV-2 Infection in Human Airway Epithelium Identifies Target Cells, Alterations in Gene Expression, and Cell State Changes. *PloS Biol* (2021) 19(3):e3001143. doi: 10.1371/journal.pbio.3001143
7. Hou YJ, Okuda K, Edwards CE, Martinez DR, Asakura T, Dinnon KH3rd, et al. SARS-CoV-2 Reverse Genetics Reveals a Variable Infection Gradient in the Respiratory Tract. *Cell* (2020) 182(2):429–446 e14. doi: 10.1016/j.cell.2020.05.042
8. Fiege JK, Thiede JM, Nanda HA, Matchett WE, Moore PJ, Montanari NR, et al. Single Cell Resolution of SARS-CoV-2 Tropism, Antiviral Responses, and Susceptibility to Therapies in Primary Human Airway Epithelium. *PloS Pathog* (2021) 17(1):e1009292. doi: 10.1371/journal.ppat.1009292
9. Coutard B, Valle C, de Lamballerie X, Canard B, Seidah NG, Decroly E. The Spike Glycoprotein of the New Coronavirus 2019-Ncov Contains a Furin-Like Cleavage Site Absent in CoV of the Same Clade. *Antiviral Res* (2020) 176:104742. doi: 10.1016/j.antiviral.2020.104742
10. Hoffmann M, Kleine-Weber H, Schroeder S, Kruger N, Herrler T, Erichsen S, et al. SARS-CoV-2 Cell Entry Depends on ACE2 and TMPRSS2 and Is Blocked by a Clinically Proven Protease Inhibitor. *Cell* (2020) 181(2):271–80.e8. doi: 10.1016/j.cell.2020.02.052
11. Walls AC, Park YJ, Tortorici MA, Wall A, McGuire AT, Veesler D. Structure, Function, and Antigenicity of the SARS-CoV-2 Spike Glycoprotein. *Cell* (2020) 183(6):1735. doi: 10.1101/2020.02.19.956581
12. Yan R, Zhang Y, Li Y, Xia L, Guo Y, Zhou Q. Structural Basis for the Recognition of the SARS-CoV-2 by Full-Length Human ACE2. *Science* (2020) 367(6485):1444–8. doi: 10.1101/2020.02.19.956946
13. Zhou P, Yang XL, Wang XG, Hu B, Zhang L, Zhang W, et al. A Pneumonia Outbreak Associated With a New Coronavirus of Probable Bat Origin. *Nature* (2020) 579(7798):270–3. doi: 10.1038/s41586-020-2012-7
14. Bellec J, Bacchetta M, Losa D, Anegon I, Chanson M, Nguyen TH. CFTR Inactivation by Lentiviral Vector-Mediated RNA Interference and CRISPR-Cas9 Genome Editing in Human Airway Epithelial Cells. *Curr Gene Ther* (2015) 15(5):447–59. doi: 10.2174/1566523215666150812115939
15. Chantret I, Rodolosse A, Barbat A, Dussaulx E, Brot-Laroche E, Zweibaum A, et al. Differential Expression of Sucrase-Isomaltase in Clones Isolated From Early and Late Passages of the Cell Line Caco-2: Evidence for Glucose-Dependent Negative Regulation. *J Cell Sci* (1994) 107(Pt 1):213–25. doi: 10.1242/jcs.107.1.213
16. Pizzorno A, Padey B, Julien T, Trouillet-Assant S, Traversier A, Errazuriz-Cerda E, et al. Characterization and Treatment of SARS-CoV-2 in Nasal and Bronchial Human Airway Epithelia. *Cell Rep Med* (2020) 1(4):100059. doi: 10.1016/j.xcrm.2020.100059
17. Balloy V, Varet H, Dillies MA, Proux C, Jagla B, Coppee JY, et al. Normal and Cystic Fibrosis Human Bronchial Epithelial Cells Infected With Pseudomonas Aeruginosa Exhibit Distinct Gene Activation Patterns. *PloS One* (2015) 10 (10):e0140979. doi: 10.1371/journal.pone.0140979
18. Balloy V, Thevenot G, Bienvenu T, Morand P, Corvol H, Clement A, et al. Flagellin Concentrations in Expectorations From Cystic Fibrosis Patients. *BMC Pulm Med* (2014) 14:100. doi: 10.1186/1471-2466-14-100
19. Blohmke CJ, Victor RE, Hirschfeld AF, Elias IM, Hancock DG, Lane CR, et al. Innate Immunity Mediated by TLR5 as a Novel Antiinflammatory Target for Cystic Fibrosis Lung Disease. *J Immunol* (2008) 180(11):7764–73. doi: 10.4049/jimmunol.180.11.7764
20. Fleurot I, Lopez-Galvez R, Barbry P, Guillon A, Si-Tahar M, Bahr A, et al. TLR5 Signalling is Hyper-Responsive in Porcine Cystic Fibrosis Airways Epithelium. *J Cyst Fibros* (2021). doi: 10.1016/j.jcf.2021.08.002
21. Illek B, Fu Z, Schwarzer C, Banzon T, Jalickee S, Miller SS, et al. Flagellin-Stimulated Cl- Secretion and Innate Immune Responses in Airway Epithelia: Role for P38. *Am J Physiol Lung Cell Mol Physiol* (2008) 295(4):L531–42. doi: 10.1152/ajplung.90292.2008
22. Qian F, Wang X, Zhang L, Chen S, Piecychna M, Allore H, et al. Age-Associated Elevation in TLR5 Leads to Increased Inflammatory Responses in the Elderly. *Aging Cell* (2012) 11(1):104–10. doi: 10.1111/j.1474-9726.2011.00759.x
23. Hawn TR, Verbon A, Lettinga KD, Zhao LP, Li SS, Laws RJ, et al. A Common Dominant TLR5 Stop Codon Polymorphism Abolishes Flagellin Signaling and is Associated With Susceptibility to Legionnaires' Disease. *J Exp Med* (2003) 198(10):1563–72. doi: 10.1084/jem.20031220
24. Blohmke CJ, Park J, Hirschfeld AF, Victor RE, Schneiderman J, Stefanowicz D, et al. TLR5 as an Anti-Inflammatory Target and Modifier Gene in Cystic Fibrosis. *J Immunol* (2010) 185(12):7731–8. doi: 10.4049/jimmunol.1001513
25. Bouhaddou M, Memon D, Meyer B, White KM, Rezelj VV, Correa Marrero M, et al. The Global Phosphorylation Landscape of SARS-CoV-2 Infection. *Cell* (2020) 182(3):685–712 e19. doi: 10.1016/j.cell.2020.06.034
26. Sofoluwe A, Zoso A, Bacchetta M, Lemeille S, Chanson M. Immune Response of Polarized Cystic Fibrosis Airway Epithelial Cells Infected With Influenza A Virus. *J Cyst Fibros* (2020) 20(4):655–63. doi: 10.1016/j.jcf.2020.08.012
27. Lei X, Dong X, Ma R, Wang W, Xiao X, Tian Z, et al. Activation and Evasion of Type I Interferon Responses by SARS-CoV-2. *Nat Commun* (2020) 11 (1):3810. doi: 10.1038/s41467-020-17665-9
28. Georgel AF, Cayet D, Pizzorno A, Rosa-Calatrava M, Paget C, Sencio V, et al. Toll-Like Receptor 5 Agonist Flagellin Reduces Influenza A Virus Replication Independently of Type I Interferon and Interleukin 22 and Improves Antiviral Efficacy of Oseltamivir. *Antiviral Res* (2019) 168:28–35. doi: 10.1016/j.antiviral.2019.05.002
29. Golonka RM, Saha P, Yeoh BS, Chattopadhyay S, Gewirtz AT, Joe B, et al. Harnessing Innate Immunity to Eliminate SARS-CoV-2 and Ameliorate COVID-19 Disease. *Physiol Genomics* (2020) 52(5):217–21. doi: 10.1152/physiolgenomics.00033.2020
30. Cui B, Liu X, Fang Y, Zhou P, Zhang Y, Wang Y. Flagellin as a Vaccine Adjuvant. *Expert Rev Vaccines* (2018) 17(4):335–49. doi: 10.1080/14760584.2018.1457443
31. Blanchard AC, Waters VJ. Microbiology of Cystic Fibrosis Airway Disease. *Semin Respir Crit Care Med* (2019) 40(6):727–36. doi: 10.1055/s-0039-1698464
32. Urban TA, Griffith A, Torok AM, Smolkin ME, Burns JL, Goldberg JB. Contribution of Burkholderia Cenocepacia Flagella to Infectivity and Inflammation. *Infect Immun* (2004) 72(9):5126–34. doi: 10.1128/IAI.72.9.5126-5134.2004
33. de CVGM, Le Goffic R, Balloy V, Plotkowski MC, Chignard M, Si-Tahar M. TLR 5, But Neither TLR2 Nor TLR4, is Involved in Lung Epithelial Cell Response to Burkholderia Cenocepacia. *FEMS Immunol Med Microbiol* (2008) 54(1):37–44. doi: 10.1111/j.1574-695X.2008.00453.x
34. Peckham D, McDermott MF, Savic S, Mehta A. COVID-19 Meets Cystic Fibrosis: For Better or Worse? *Genes Immun* (2020) 21(4):260–2. doi: 10.1038/s41435-020-0103-y
35. Cosgriff R, Ahern S, Bell SC, Brownlee K, Burgel PR, Byrnes C, et al. A Multinational Report to Characterise SARS-CoV-2 Infection in People With Cystic Fibrosis. *J Cyst Fibros* (2020) 19(3):355–8. doi: 10.1016/j.jcf.2020.04.012
36. Bain R, Cosgriff R, Zampoli M, Elbert A, Burgel PR, Carr SB, et al. Clinical Characteristics of SARS-CoV-2 Infection in Children With Cystic Fibrosis: An International Observational Study. *J Cyst Fibros* (2021) 20(1):25–30. doi: 10.1016/j.jcf.2020.11.021
37. Corvol H, de Miranda S, Lemonnier L, Kemgang A, Reynaud Gaubert M, Chiron R, et al. First Wave of COVID-19 in French Patients With Cystic Fibrosis. *J Clin Med* (2020) 9(11). doi: 10.3390/jcm9113624
38. Baldassarri M, Fava F, Fallerini C, Daga S, Benetti E, Zguro K, et al. Severe COVID-19 in Hospitalized Carriers of Single CFTR Pathogenic Variants. *J Pers Med* (2021) 11(6). doi: 10.3390/jpm11060558

39. Ruffin M, Bigot J, Calmel C, Mercier J, Pizzorno A, Rosa-Calatrava M, et al. Flagellin From Pseudomonas Aeruginosa Modulates SARS-CoV-2 Infectivity in CF Airway Epithelial Cells by Increasing TMPRSS2 Expression. *bioRxiv* (2020). 2020.08.24.264564. doi: 10.1101/2020.08.24.264564

Conflict of Interest: The authors declare that the research was conducted in the absence of any commercial or financial relationships that could be construed as a potential conflict of interest.

Publisher's Note: All claims expressed in this article are solely those of the authors and do not necessarily represent those of their affiliated organizations, or those of the publisher, the editors and the reviewers. Any product that may be evaluated in this article, or claim that may be made by its manufacturer, is not guaranteed or endorsed by the publisher.

frontiers in Immunology

METHODS
published: 22 December 2021
doi: 10.3389/fimmu.2021.788705

DNA Methylation Profiles of Purified Cell Types in Bronchoalveolar Lavage: Applications for Mixed Cell Paediatric Pulmonary Studies

Shivanthan Shanthikumar[1,2,3]*, *Melanie R. Neeland*[2,4], *Richard Saffery*[2,4], *Sarath C. Ranganathan*[1,2,3], *Alicia Oshlack*[5,6,7] and *Jovana Maksimovic*[2,3,5]

[1] Respiratory and Sleep Medicine, Royal Children's Hospital, Parkville, VIC, Australia, [2] Department of Paediatrics, University of Melbourne, Parkville, VIC, Australia, [3] Respiratory Diseases, Murdoch Children's Research Institute, Parkville, VIC, Australia, [4] Molecular Immunity, Murdoch Children's Research Institute, Parkville, VIC, Australia, [5] Computational Biology Program, Peter MacCallum Cancer Centre, Parkville, VIC, Australia, [6] Sir Peter MacCallum Department of Oncology, University of Melbourne, Parkville, VIC, Australia, [7] School of BioScience, University of Melbourne, Parkville, VIC, Australia

OPEN ACCESS

Edited by:
Scott James Tebbutt,
University of British Columbia, Canada

Reviewed by:
Yaqiang Cao,
National Institutes of Health (NIH), United States
Michael Volkmar,
German Cancer Research Center (DKFZ), Germany

***Correspondence:**
Shivanthan Shanthikumar
Shivanthan.shanthikumar@rch.org.au

Specialty section:
This article was submitted to Mucosal Immunity, a section of the journal Frontiers in Immunology

Received: 03 October 2021
Accepted: 03 December 2021
Published: 22 December 2021

Citation:
Shanthikumar S, Neeland MR, Saffery R, Ranganathan SC, Oshlack A and Maksimovic J (2021) DNA Methylation Profiles of Purified Cell Types in Bronchoalveolar Lavage: Applications for Mixed Cell Paediatric Pulmonary Studies. Front. Immunol. 12:788705. doi: 10.3389/fimmu.2021.788705

In epigenome-wide association studies analysing DNA methylation from samples containing multiple cell types, it is essential to adjust the analysis for cell type composition. One well established strategy for achieving this is reference-based cell type deconvolution, which relies on knowledge of the DNA methylation profiles of purified constituent cell types. These are then used to estimate the cell type proportions of each sample, which can then be incorporated to adjust the association analysis. Bronchoalveolar lavage is commonly used to sample the lung in clinical practice and contains a mixture of different cell types that can vary in proportion across samples, affecting the overall methylation profile. A current barrier to the use of bronchoalveolar lavage in DNA methylation-based research is the lack of reference DNA methylation profiles for each of the constituent cell types, thus making reference-based cell composition estimation difficult. Herein, we use bronchoalveolar lavage samples collected from children with cystic fibrosis to define DNA methylation profiles for the four most common and clinically relevant cell types: alveolar macrophages, granulocytes, lymphocytes and alveolar epithelial cells. We then demonstrate the use of these methylation profiles in conjunction with an established reference-based methylation deconvolution method to estimate the cell type composition of two different tissue types; a publicly available dataset derived from artificial blood-based cell mixtures and further bronchoalveolar lavage samples. The reference DNA methylation profiles developed in this work can be used for future reference-based cell type composition estimation of bronchoalveolar lavage. This will facilitate the use of this tissue in studies examining the role of DNA methylation in lung health and disease.

Keywords: DNA methylation, bronchoalveolar lavage, paediatrics, cystic fibrosis, pulmonary disease, epigenetics

INTRODUCTION

DNA methylation (DNAm) is the most widely studied epigenetic mark and is important in both development and disease (1). It has been studied in numerous diseases to improve understanding of pathophysiology and to identify novel therapeutic targets and disease biomarkers (2). The advent of genome-wide DNAm arrays has enabled large, epigenome-wide association studies (EWAS). Specifically, the Illumina HumanMethylation450 (450k) and HumanMethylationEPIC (EPIC) BeadChips, which interrogate over 450,000 and 850,000 CpGs, respectively, have allowed researchers to interrogate human DNAm at an unprecedented scale.

The DNAm profile of each tissue and cell type is unique and can therefore differentiate cells from different organs (e.g., brain vs. lung), as well as different cell types within an organ (e.g., grey matter and white matter tissue in the brain have unique profiles) (3). As such, the biological sample used for EWAS should ideally be from a relevant organ/tissue (4). However, this is generally not possible in living humans. Furthermore, in samples which consist of multiple cell types, the outcome of interest may be confounded by differences in cell type composition (5). To address this, previous work has shown that the unique DNAm signature of individual cell types can be leveraged to estimate their relative proportions in mixed-cell samples such as blood (6). These cell type proportions can then be accounted for in downstream statistical analysis (6). However, as was demonstrated by Bakulski et al (7), reference DNAm signatures of cell types from one source (e.g., adult blood) may not be perfectly representative of similar cell types from a different source (e.g., cord blood).

Clinical research of pulmonary diseases is currently limited by a lack of data from tissue and cell type specific samples. According to the EWAS Atlas, an online repository of published EWAS studies, there are 19 published EWAS studies in non-cancer lung diseases such as asthma, cystic fibrosis (CF), chronic obstructive pulmonary disease, acute respiratory distress syndrome and granulomatous lung disease (8). The majority have utilised samples from adult participants (13/19). Blood was the most commonly used biological sample in these studies (8/19 studies), followed by nasal and airway epithelial cells (6/19). The majority of these sample types do not contain immune cells, which are an integral part of the cellular milieu of the lung and are relevant to many lung diseases (9).

Bronchoalveolar lavage (BAL) is commonly collected as part of clinical care of lung disease. Particularly in young children, who cannot expectorate sputum, it is considered the gold-standard method of sampling the lung. BAL fluid permits assessment a variety of cells in the lung, including both circulating and resident immune cells, as well as respiratory epithelial cells (10). The predominant cell types in BAL are alveolar macrophages, granulocytes, lymphocytes and alveolar epithelial cells (AEC) (10–12). A current barrier to the widespread use of BAL samples in EWAS is the lack of a BAL-derived set of reference DNAm profiles for constituent cell types. Only three prior EWAS have utilised BAL samples, with varying approaches for adjustment of cell composition. One study, involving 8 participants (18-33years old), investigated only BAL macrophages, and used a reference-free approach to estimate and adjust for alveolar macrophage subtype composition (8). Another study, involving 48 adult participants, used microscopy derived lymphocyte cell counts to estimate the proportion of lymphocytes in the sample and adjust their analysis (13). This approach is limited by the resolution of microscopy and only accounts for lymphocytes in BAL, omitting other cell types (14, 15). A final study (16), involving 35 adult participants (median age 25.0, range: 22.0–29.0), used the publicly available eFORGE tool (17) to adjust for cell type composition. This tool was developed using a number of biological specimens such as fetal lung tissue and purified immune cell subsets. However, lung resident macrophages, which are the most common cell type in BAL, were not assessed. At present, there are no studies that have profiled the genome-wide DNAm of the cell types found in BAL, particularly from paediatric samples.

Here, we collected and purified individual cell populations from BAL collected from children with CF and generated cell-specific DNA methylation profiles with the aim of creating a BAL-derived DNAm reference panel of constituent cell types. Genome-wide DNAm profiles for 4 clinically-relevant BAL cell types (lymphocytes, granulocytes, alveolar macrophages, AECs) were measured using the Illumina EPIC array. We then used our BAL-derived reference panel in conjunction with a well-established deconvolution method to demonstrate its utility in the estimation of cell type proportions of BAL DNAm data. This BAL-specific reference panel will be useful for epigenetic studies of paediatric pulmonary disease.

MATERIALS AND METHODS

A summary of the experimental workflow is shown in **Figure 1**. All analysis code presented in this manuscript can be found at https://jovmaksimovic.github.io/paed-BAL-meth-ref/index.html. The analysis website was created using the *workflowr* (1.6.2) R package (18). The GitHub repository associated with the analysis website is at: https://github.com/JovMaksimovic/paed-BAL-meth-ref.

Sample Population and Biospecimen Collection

The 17 BAL samples used to establish the methylation reference panel of constituent cell types were obtained as part of the AREST CF study, with ethics approval (HREC #25054). We utilised excess BAL taken at the time of a clinically indicated procedures in children with CF (age 0 – 6 years). Flexible bronchoscopy was conducted by a respiratory physician under general anaesthesia. BAL was performed by instillation of sterile 0.9% normal saline in aliquots of one ml/kg (maximum 20ml). The aliquots used in this study were the second wash in the same bronchial tree location, which samples the distal airways this increasing the chances of sampling alveolar macrophages (19, 20). Samples were kept on ice after collection and cryopreserved within one hour, using previously described methods (10).

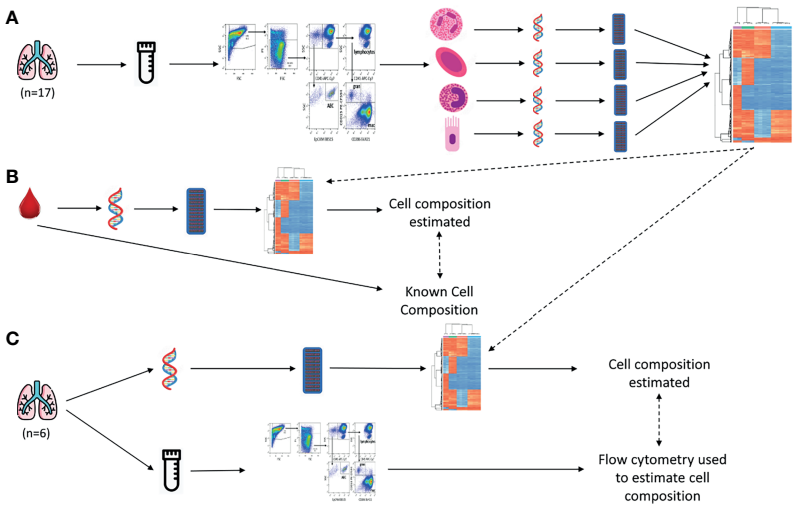

FIGURE 1 | Study outline. **(A)** BAL samples were collected, cryopreserved and sorted using fluorescence-activated single cell sorting, resulting in 4 purified cell populations (Alveolar Epithelial Cells, Alveolar Macrophages, Granulocytes, and Lymphocytes). Their DNA was extracted and pooled and DNAm profiled on EPIC arrays. Unique DNAm profiles for constituent cell types were identified. These DNAm profiles were then used to estimate cell type compositions in subsequent validation experiments. **(B)** Data from a publicly available blood-derived artificial cell mixture with known cell composition, and matching DNAm data, was used to validate our BAL-derived reference panel. The BAL-derived DNAm profiles we developed were used in conjunction with a reference-based deconvolution method to estimate cell composition from the DNAm data of the artificial cell mixtures. This was then compared to the known cell composition. **(C)** BAL samples were collected and divided into a raw fraction and a cryopreserved fraction. DNA was extracted from the raw fraction, DNAm profiled, and our BAL-derived DNAm profiles used in conjunction with a reference-based deconvolution method to estimate cell composition. The cryopreserved fraction was profiled using flow cytometry, and cell composition estimated. The methylation-based estimates were compared to the flow-cytometry cell composition measurements.

For estimation of constituent cell type proportions, BAL was collected from a further 6 subjects involved in the AREST CF study, as described above. Prior to processing, 1 mL of raw lavage was collected and stored at -80°C. The remaining BAL was cryopreserved as described. The cryopreserved fraction was then thawed and cell composition determined *via* flow cytometry using previously described methods (see "*Cell selection and Purification*" section for brief description) (10).

Cell Selection and Purification

Cryopreserved samples were thawed and then fluorescence activated cell sorting was used to isolate alveolar macrophages, granulocytes, lymphocytes and AEC using previously described methods (10). Briefly the following markers were used to identify cell types: alveolar macrophages: CD45+, CD206+, granulocytes: CD45+, CD206-, CD15+, lymphocytes: CD45+, CD206-, CD15-, low forward scatter/side scatter, and AEC: CD45-, EpCAM+. Purified cell pellets were resuspended in 350uL of RLT buffer (Qiagen, Venlo, Netherlands) with 1% ß-mercaptoethanol (Gibco, New York, USA), and stored at -80°C until DNA extraction.

DNA Extraction and Methylation Profiling

DNA was extracted from samples using the QIAamp DNA Micro Kit (Qiagen, Venlo, Netherlands). Aside from initial storage of the sample in RLT buffer with 1% ß-mercaptoethanol, the standard protocol for DNA extraction was used. DNA quantity and quality were assessed using a QUBIT<sp>® fluorometer and Nanodrop™ spectrophotometer respectively.

For purified cell type samples, the yield from an individual BAL was found to be insufficient for downstream whole genome methylation analysis. Thus, to avoid potential biases resulting from whole genome amplification (21, 22), DNA extracted from purified cell populations from the 17 individuals were pooled. This produced 5 macrophage pools (4 pools comprised of cells from 3 individuals, 1 comprised of cells from 2 individuals), 4 granulocyte pools (3 pools comprised of cells from 3 individuals, 1 pool comprised of cells from 5 individuals), 3 lymphocyte pools (2 pools comprised of cells from 6 individuals, 1 pool comprised of cells from 5 individuals) and 2 AEC pools (1 pool comprised of cells from 12 individuals, 1 pool comprised of cells from 5 individuals). To assess the impact of our pooling strategy, we examined the relationship between the number of individuals contributing to a pool and the variance across CpGs in the sample (**Supplementary Figure 1**). Regression analysis showed no statistically significant association between the number of individuals contributing to a pool and variance across CpGs (Adj. R^2 = -0.02; p-value = 0.43), indicating that the sample pools were representative of the sorted cell types. Following extraction and pooling, DNA was stored at -30°C until further analysis.

The raw BAL samples, from 6 individuals, intended for cell composition estimation were thawed, and DNA was extracted and assessed for quality as previously described.

Genome-wide methylation profiling was performed for all samples using the Infinium MethylationEPIC array (EPIC array, Ilumina, San Diego, USA) at either GenomeScan (Leiden, Netherlands) or Erasmus Medical Centre (Rotterdam, Netherlands).

All of the data is available from the Gene Expression Omnibus: https://www.ncbi.nlm.nih.gov/geo/query/acc.cgi?acc=GSE185556.

DNAm Data Pre-Processing

The EPIC array data were analysed using the R programming language (23) (Version 4.0.3) according to best practices for methylation array analysis (24). Raw IDAT files were imported using *minfi* (25, 26), followed by quality control. Firstly, as a measure of the quality of the array data, the detection p-value was calculated for each probe and any poor-quality samples with a mean detection p-value > 0.01 were excluded from subsequent analysis. The data was then normalised, using subset quantile normalisation (SQN) (27). Poor performing probes with detection p-value > 0.01 in one or more samples were excluded. In addition, probes known to have a single nucleotide polymorphism at the CpG site, probes that map to sex chromosomes, and cross-reactive probes that have been shown map to multiple places in the genome, were also excluded (28).

Identification DNAm Cell Type Signature Probes

A modified version of the estimateCellCounts2 function from the *FlowSorted.Blood.EPIC* package (29), estimateCellCounts2Mod, was used to identify DNAm profiles unique to each cell type, and then estimate cell type proportions. This function implements the Houseman (6) deconvolution algorithm, but unlike the original *minfi* implementation, allows the use of a custom panel of reference epigenomes. Our estimateCellCounts2Mod function was specifically modified (https://github.com/JovMaksimovic/paed-BAL-meth-ref/blob/main/code/functions.R) to allow for the removal of probes excluded during quality control, prior to identification of DNAm cell type signature probes and cell proportion estimation.

We explored two *probeSelect* parameter options for DNAm cell type signature probe selection; *"both"* and *"any"*. Using *"both"*selects the top 50 hypermethylated and 50 hypomethylated probes (F-stat p-value < 1E-8) with the greatest methylation difference between each cell type compared to all the others. Using *"any"* selects the top 100 probes (F-stat p-value < 1E-8) with the greatest methylation difference between each cell type compared to all the others, regardless of direction of effect. The *processMethod* parameter, which determines how data will be normalised, was set to SQN (27).

Gene set enrichment analysis of probes selected using either the *"any"* or *"both"* options, and the probes that are in common and different between them was performed using the gometh function from the *missMethyl* (30) R Bioconductor package to account for known biases in gene set testing of methylation array data (31).

Cell Type Proportion Estimation of Artificial Cell Mixtures

To assess the accuracy of cell proportions estimated using our BAL-derived reference panel in conjunction with the Houseman (6) algorithm, we utilised 12 publicly available artificial DNA mixtures profiled using Illumina Infinium HumanMethylationEPIC BeadChips (GSE110554). The mixtures were generated by combining known proportions of flow-sorted neutrophils, monocytes, B-lymphocytes, CD4+ T cells, CD8+ T cells, and natural killer cells (29). The data was downloaded using the *ExperimentHub* Bioconductor package (29). The known proportions of T, B and NK cells were summed to allow for comparison to the lymphocyte proportion estimated from the DNAm data using our BAL-derived reference panel, which only profiled total lymphocytes.

RESULTS

Generation of a Methylation Reference Panel for BAL Derived Purified Cell Populations

Seventeen BAL samples obtained from children with CF were used for development of the BAL-specific reference panel. The median (range) age of the children was 36 months (14-70 months), and 11/17 (64.7%) were female. One child was of South-Asian ethnicity, and all other children were of European ethnicity. On average six mL of BAL was used. The median (range) cell composition of samples, determined by flow cytometry, was alveolar macrophages 63.7% (5.2%-95.9%), granulocytes 23.7% (2.9%-86.1%), lymphocytes 8.1% (0.7%-26.5%), and AEC 1.5% (0.2%-8.3%).

DNAm of pooled purified BAL-derived macrophage, granulocyte, lymphocyte and AEC samples was profiled on EPIC arrays in 2 batches; 9 arrays were run at Erasmus MC and 11 arrays at GenomeScan. Following quality control, there were 732,778 probes remaining for further analysis. Multidimensional scaling (MDS) plots show strong clustering of the samples by cell type (**Figure 2**). A scree plot (**Supplementary Figure 2**) of the sources of variation in the data shows that the vast majority of the variation is explained by the first 4 principal components.

The Houseman (6) deconvolution algorithm, as implemented in the *estimateCellCounts2* function from the *FlowSorted.Blood.EPIC* Bioconductor package (29), was used to identify DNA methylation profiles unique to each cell type. Briefly, the Houseman (6) algorithm is a type of regression calibration, originally developed using white blood cells, where a methylation pattern is considered to be a high-dimensional multivariate surrogate for the proportion of constituent cell in a sample of mixed cell types. It essentially leverages the DNAm profiles of purified cell types to estimate their relative proportions in a mixture. These estimates can subsequently be incorporated into statistical models to adjust for cell type composition in an EWAS (6, 32, 33), or independently investigated for their association with disease or environmental exposures (34–36). Cell composition was estimated with the *probeSelect* parameter set to "*both*" and then repeated with the "*any*" option. As shown in **Figure 3**, the probes selected using either option were able to clearly delineate the 4 cell types using hierarchical clustering. The selected probes are primarily associated

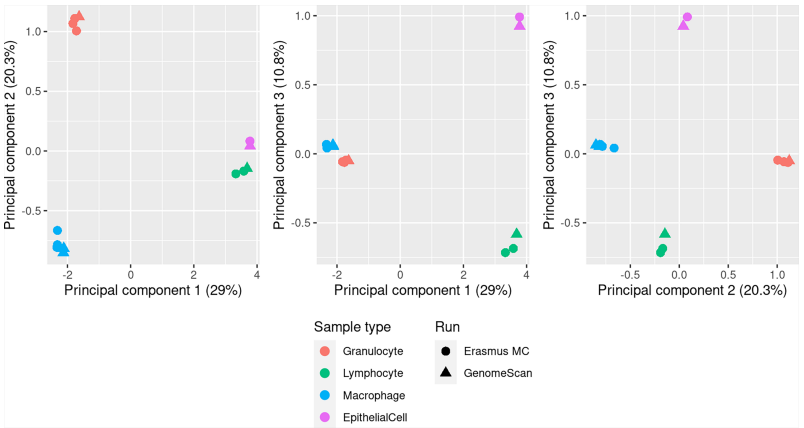

FIGURE 2 | MDS plots showing the first 3 principal components of methylation data from pooled BAL macrophage (n=5), granulocyte (n=4), lymphocyte (n=3) and AEC (n=2) samples. Each pool contained purified cells from multiple individuals (see *Methods*). Clear separation of the different cell populations is seen in the first 3 principal components, which account for 60.1% of the total variation, and there is no evidence of a significant batch affect related to samples run at different service providers (Erasmus MC or GenomeScan).

with genes and overlap DNase hypersensitivity sites but most are not within CpG islands or in close proximity to the transcription start site (**Supplementary Figure 3**). Although there were no statistically significant terms at a false discovery rate less than 0.05, gene set enrichment analysis (GSEA) of probes selected using either option suggests that they are enriched for immune related-genes, which is unsurprising as ¾ of the contributing cell types were immune cells. Using the *"any"* option, the top 5 ranked Gene Ontology (GO) terms were "leukocyte activation", "T cell activation", "immune response" and "leukocyte cell-cell adhesion" (**Supplementary Table 1**). Similarly, using the *"both"* option, the top ranked GO terms were "leukocyte cell-cell adhesion", "T cell activation", leukocyte activation", "lymphocyte activation" and "regulation of leukocyte cell-cell adhesion" (**Supplementary Table 2**). Of the 400 probes selected by each option, 221 (55.25%) were the same. GSEA of the overlapping probes also ranked various immune-related terms highly (**Supplementary Table 3**). The probes that differed between the *"any"* and *"both"* options also ranked some immune-specific terms highly, however, the top ranked terms were dominated by processes related to the JNK, JUN and MAPK cascades (**Supplementary Table 4**).

Methylation-Based Cell Type Proportions Validated Using Artificial Cell Mixtures

We initially assessed cell proportion estimates underpinned by our BAL-specific cell reference panel using a publicly available dataset

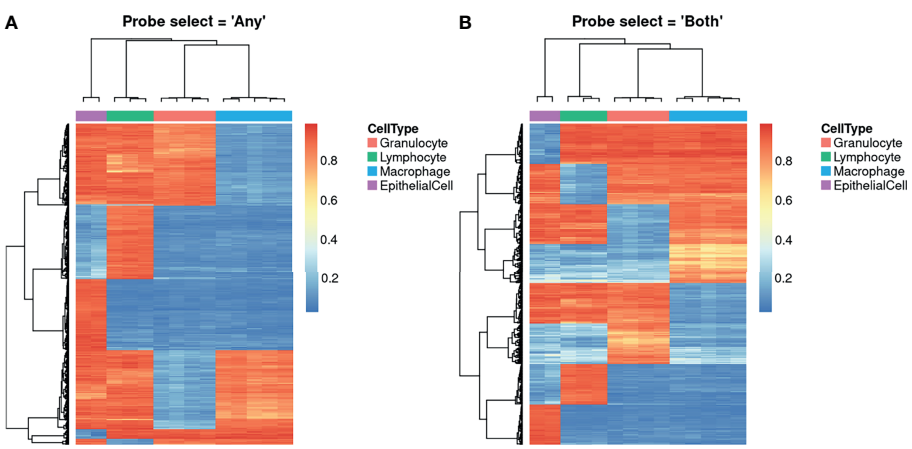

FIGURE 3 | Heatmaps showing unique DNA methylation profiles for constituent cell types. The probes shown were algorithmically selected based on their ability to discriminate between the different cell types. The heatmaps demonstrate the different probe set selected when the *probeSelect* parameter is set to **(A)** *"any"* or **(B)** *"both"*. *"Both"* selects the top 50 hypermethylated and 50 hypomethylated probes (F-stat p-value < 1E-8) with the greatest methylation difference between each cell type compared to all the others. *"Any"* selects the top 100 probes (F-stat p-value < 1E-8) with the greatest methylation difference between each cell type compared to all the others, regardless of direction of effect.

(29) of twelve artificially created cell mixtures. This allowed for validation of the accuracy of methylation-based estimates of BAL lymphocyte and granulocyte proportions. The results are summarised in **Figure 4**. For the cell types with available reference epigenomes (lymphocytes and granulocytes), there is a tight correlation between the true cell proportion and the methylation-based cell proportion estimated using our reference (**Figure 4A**). As expected, the sum of the estimated cell proportions was close to one (6). The methylation-based estimates include a proportion of alveolar macrophages not contained in the artificial cell mixture (**Figure 4A**). We expect that this is due to the presence of monocytes in the artificial cell mixture, which are macrophage precursor cells and are likely to share some similarity in their methylation patterns (37, 38). Furthermore, a fraction of alveolar macrophages is made up of circulating monocytes that migrate to the lungs and become a resident population (39, 40).

Overall, the mean squared error (MSE) (**Figures 4B, C**) between the true proportions and methylation-based estimates was close to zero for both lymphocytes and granulocytes, using either the "*any*" or "*both*" *probeSelect* option, indicating very high performance. However, the MSE for granulocytes was slightly higher than for lymphocytes, for both *probeSelect* options.

Methylation-Based Cell Type Proportions in Paediatric BAL Samples

Six BAL samples were obtained for comparing cell type proportions determined by flow cytometry to methylation-based estimates generated using the Houseman method (6), in conjunction with our BAL-specific reference epigenomes. Five BALs were from children with CF, and one was from a "control" subject. Four of the six children (66.7%) were female. The median (range) age of the children was 57 months (23-89 months), which is slightly older than those used to derive the reference panel (median age 36 months, range 14-70 months). Five children were of European ethnicity and one was of South Asian ethnicity. All BAL samples had sufficient DNA extracted for methylation analysis.

The cell composition of all samples was determined using flow cytometry on cryopreserved BAL fractions (**Table 1**). For flow cytometry data, the proportion of cells identified ranged between 46.2% - 89.0%. The majority of the unidentified cells were CD45 –ve and EpCAM –ve indicating they were likely red blood cells. As red blood cells do not contain DNA, they do not contribute a DNA methylation signature. To support this, we identified 3479 CpG probes with mean ß values that were either ≥0.95 or ≤0.05 in all the sorted cell types, which should also be either fully methylated or unmethylated in the raw BAL samples if no other nucleated cell types are present. As shown in **Supplementary Figure 4**, these probes have consistent methylation levels across all the sorted cell types and the raw BAL samples, suggesting that cells not identified by flow cytometry were indeed red blood cells. Consequently, analysis was conducted including both the unknown cells (referred to as "original") in the cell proportions and excluding them (referred to as "scaled"). The cell composition of most samples was as expected; however, two samples (CF1, CF5) had a CD45-, EpCAM- fraction in excess of 30% which is higher than expected and may relate to a traumatic blood-stained BAL.

As for the artificial cell mixture data, methylation-based cell proportion estimates using the *"any"* or *"both"* probe selection methods were highly consistent across all cell types (**Figure 5A**). An MDS plot of the 6 BAL samples in the context of the purified cell type samples show them positioned centrally relative to the sorted cell samples (**Supplementary Figure 5**), with one BAL sample closer to the granulocyte cluster, suggesting a higher granulocyte proportion (**Supplementary Figure 5**). Cell proportions estimated using the methylation data and flow cytometry are compared in **Table 1** and **Figure 5**. The MSE between the "original" and "scaled" flow and methylation-based estimates was generally close to zero for all cell types and both *probeSelect* options, indicating reasonable concordance between the technologies (**Figures 5B, C**). The AEC and lymphocyte methylation-based estimates were the most concordant with the flow cytometry data. The alveolar macrophage and granulocyte proportions were more variable; in certain subjects (CF1 and control) there was a larger discrepancy between flow cytometry and DNAm estimated cell composition, reflected by a larger MSE of ~0.06, relative to the "original" flow estimates. Comparison to the "scaled" flow values markedly reduced the MSE for subjects CF1, CF4 and CF5 but had a negligible effect on the others.

DISCUSSION

We used the EPIC array to generate a reference panel of DNAm profiles for the four most common and clinically-relevant cell types in paediatric BAL: alveolar macrophages, granulocytes, lymphocytes and alveolar epithelial cells. The DNAm reference panel was then used to demonstrate estimation of cell composition of samples in two different datasets. Strengths of the work include purification of individual cell populations using FACS which was undertaken using previously validated, high-quality methods (10). The DNA methylation analysis and, in particular, the methods used for identifying cell-specific methylation probes have been well-established and widely used (6, 24, 29).

We compared known proportions of lymphocytes and granulocytes in an artificial cell mixture to estimates using DNAm with our BAL-specific reference panel in conjunction with the Houseman (6) deconvolution method. The known and estimated lymphocyte and granulocyte proportions were highly correlated, with MSE close to zero for cell types in all samples. In a subset of samples, the granulocyte proportion was slightly overestimated. This may be because the reference sample contains eosinophils as well as neutrophils and thus is therefore not a direct reflection of the cellular composition of the artificial cell mixture. Furthermore, in their original study, Houseman et al (6) also observed the most significant discrepancy between the true and estimated proportion for granulocytes.

We also estimated the cell type proportions of six paediatric BAL samples using our BAL-specific DNAm reference panel with the Houseman (6) deconvolution method and compared them to proportions measured using flow-cytometry. Two of the six subjects showed the greatest divergence between the flow-cytometry and DNAm estimates largely driven by differences

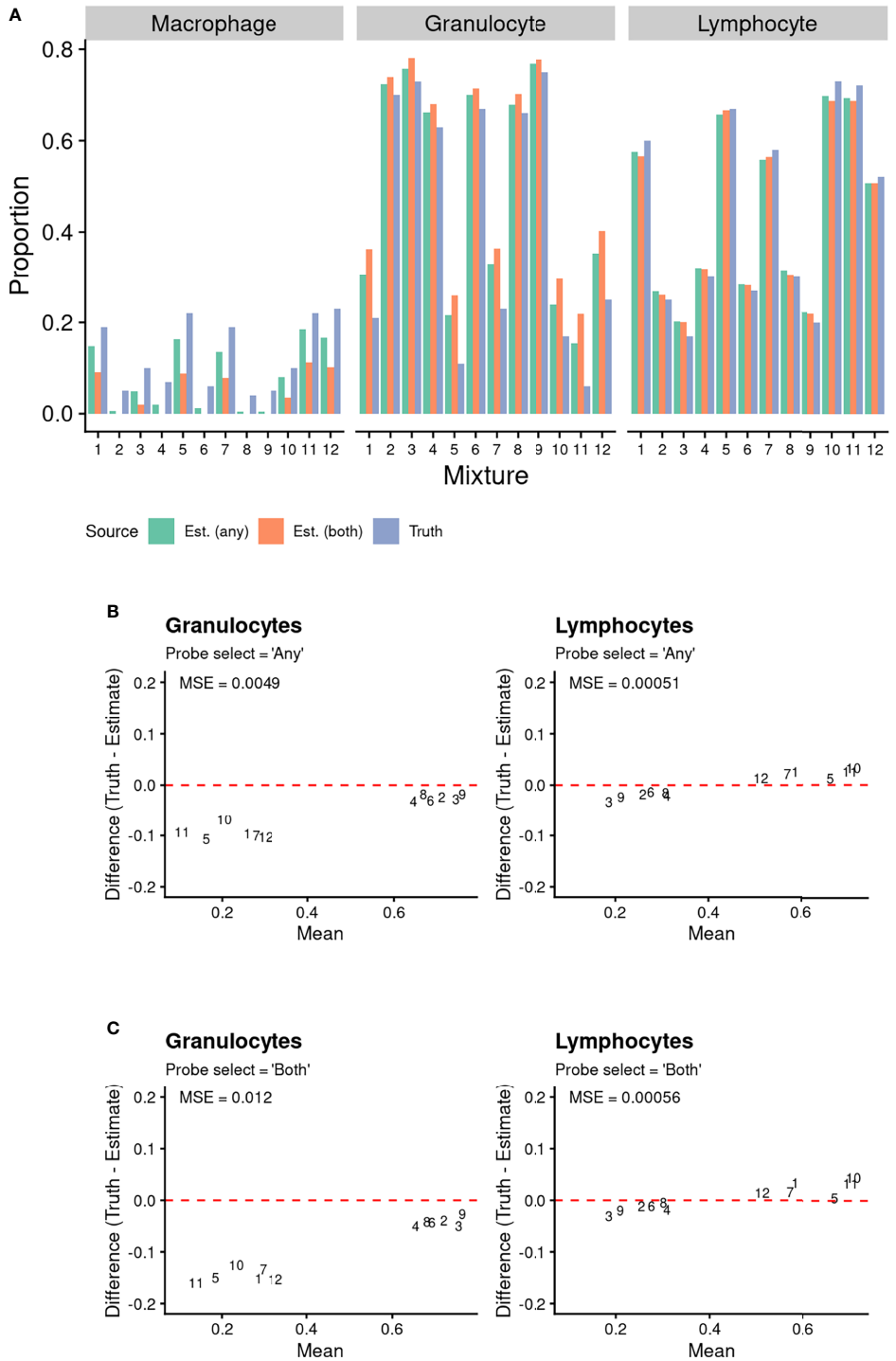

FIGURE 4 | Comparison of known proportions of artificial cell mixtures (with T Cells, B Cells, and Natural Killer cells combined into a Lymphocyte population), to methylation-based estimated cell proportions derived using BAL purified cell population data. Cell type discriminating probes were selected using "any" and "both" approaches (see methods for details). **(A)** Comparison of known proportions of artificial cell mixtures (with T Cells, B Cells, and Natural Killer cells combined into a Lymphocyte population), to methylation-based estimated cell proportions derived using BAL purified cell population data. Cell type discriminating probes were selected using "any" and "both" approaches (see methods for details). **(B, C)** Bland Altman Plots Comparing Known Artificial Cell Mixture Proportions ("Truth") and methylation-based cell proportion estimates ("Estimate"). The data point numbers represent which cell mixture the data pertains to. Cell type discriminating probes were selected using either **(B)** "any" and **(C)** "both" approaches (see *Methods* for details). The mean squared error (MSE) between the known proportion and estimated proportion was calculated for each cell type and probe selection *Method*.

TABLE 1 | Cell composition of BAL determined by both DNA methylation-based estimate and flow cytometry.

	Alveolar Macrophage			Lymphocyte			Granulocyte			Alveolar Epithelial Cell		
	Scaled Flow Cytometry	**DNAm Estimate (Any)**	**DNAm Estimate (Both)**	**Scaled Flow Cytometry**	**DNAm Estimate (Any)**	**DNAm Estimate (Both)**	**Scaled Flow Cytometry**	**DNAm Estimate (Any)**	**DNAm Estimate (Both)**	**Scaled Flow Cytometry**	**DNAm Estimate (Any)**	**DNAm Estimate (Both)**
CF1	5.2	0.7	0.5	5.5	1.6	1.8	86.1	88.8	89.8	3.2	9.2	8.7
CF2	55.7	29.9	33.7	8.9	19.7	16.3	32.5	43.1	48.0	2.9	11.2	10.5
CF3	64.6	37.3	39.3	8	22.3	20.7	23.9	22.1	25.7	3.4	21.0	20.0
CF4	72.5	66.6	68.6	7.2	11.6	10.0	19.7	13.7	15.4	0.6	9.9	9.7
CF5	63.2	50.7	52.8	7.2	11.0	9.5	29.4	34.5	35.7	0.2	5.6	5.4
Control	51.1	13.7	13.1	20.5	17.8	16.7	21.5	58.7	61.7	6.9	12.9	12.8
	Unscaled Flow Cytometry	**DNAm Estimate (Any)**	**DNAm Estimate (Both)**	**Unscaled Flow Cytometry**	**DNAm Estimate (Any)**	**DNAm Estimate (Both)**	**Unscaled Flow Cytometry**	**DNAm Estimate (Any)**	**DNAm Estimate (Both)**	**Unscaled Flow Cytometry**	**DNAm Estimate (Any)**	**DNAm Estimate (Both)**
CF1	2.4	0.7	0.5	2.5	1.6	1.8	39.7	88.8	89.8	1.5	9.2	8.7
CF2	46.1	29.9	33.7	7.4	19.7	16.3	26.9	43.1	48.0	2.4	11.2	10.5
CF3	42.5	37.3	39.3	5.3	22.3	20.7	15.8	22.1	25.7	2.3	21.0	20.0
CF4	50.2	66.6	68.6	5	11.6	10.0	13.6	13.7	15.4	0.4	9.9	9.7
CF5	31.3	50.7	52.8	3.6	11.0	9.5	14.5	34.5	35.7	0.1	5.6	5.4
Control	34.8	13.7	13.1	13.9	17.8	16.7	14.6	58.7	61.7	4.7	12.9	12.8

For DNA methylation-based estimates cell type discriminating probes were selected using "Any" and "Both" approaches (see Methods for details). Regarding flow cytometry the "scaled" proportions were calculated not including the CD45-, EpCAM – cells which are likely Red Blood Cells that do not contribute to DNA methylation data.

between the granulocyte and alveolar macrophage proportions. The discrepancy in the granulocyte estimate is likely due to the effect of cryopreservation on the BAL fraction, which is known to reduce the proportion of granulocytes in a sample due to cell lysis (10). However, the BAL fraction profiled on EPIC arrays was not cryopreserved, thus retaining a higher proportion of granulocytes. The methylation-based estimate was consistently higher than that of flow cytometry strongly suggesting that the observed difference in proportions between flow-cytometry and DNAm granulocyte proportions is best explained by the effect of cryopreservation. The variable size of the discrepancy, may be due to the fact that cryopreservation primarily reduces the CD16+ granulocyte fraction (10). Thus, samples that originally had a large CD16+ granulocyte proportion are likely to have a larger discrepancy than those with a smaller CD16+ granulocyte proportion. We have previously shown the proportion of CD16+ granulocytes in BAL ranges from 0.09%-9% indicating substantial variation (10).

The variation in the methylation-based estimates of macrophages may be a consequence of the issues with the granulocyte estimate. The sum of the cell type proportions estimated by the Houseman method is expected to be close to one (6). Thus, if one cell proportion is inaccurately estimated there will be a reciprocal effect on other cell proportions. In this case, the consistent overestimation of granulocytes (when compared to flow cytometry data), may also result in the observed underestimation of the alveolar macrophage proportion. An alternate explanation could be heterogeneity of alveolar macrophage subpopulations, potentially related to disease severity. Recently, single cell transcriptomic analysis of adult BAL has revealed 13 alveolar macrophage subpopulations (41). The composition of a patient's alveolar macrophage pool is likely related to disease severity, and each of the alveolar macrophage subpopulations will have a unique epigenetic profile. Thus, the discrepancy between the flow cytometry and methylation-based estimates of alveolar macrophage proportion seen in some subjects may be due to differences in the composition of their alveolar macrophage subtypes relative to the samples used to generate the reference epigenome. The relatively large discrepancy between the flow cytometry and methylation-based estimates of alveolar macrophage proportions for the control patient may reflect potentially altered alveolar macrophage DNA methylation profiles between control and CF patients (8).

It has been demonstrated that DNAm patterns related to exposure or disease can be confounded with differences in cell type proportions (32, 42). Furthermore, Bakulski et al (7) have shown that ensuring the DNAm reference panel used for cell proportion estimation is matched to the age of the study participants is especially important for some cell types. Adjusting using inaccurate cell proportion estimates may not completely resolve any confounding, underscoring the need to adjust for cell type proportions in BAL samples using an appropriate reference panel. The use of BAL in EWAS of pulmonary disease or exposure is appealing as it allows simultaneous assessment of methylation of local immune and epithelial cells, both of which are relevant to paediatric lung disease. Alternate biospecimens such as blood or bronchial brushings will omit cell types of interest. Our BAL-specific reference panel allows for deconvolution of multiple clinically-relevant cell types using any compatible reference-based method. While we used the Houseman method for estimating proportions, as this is a well-established and commonly used reference-based deconvolution method implemented in R, other methods could also be used in conjunction with the EPIC array data generated in this study. Furthermore, using a different probe selection strategy or varying F-statistic or beta value thresholds However, given the reference panel was derived from children with CF, it may need further validation prior to use on samples from different disease groups and ages. Although, its excellent performance when used to estimate the composition of artificial cell mixtures derived from

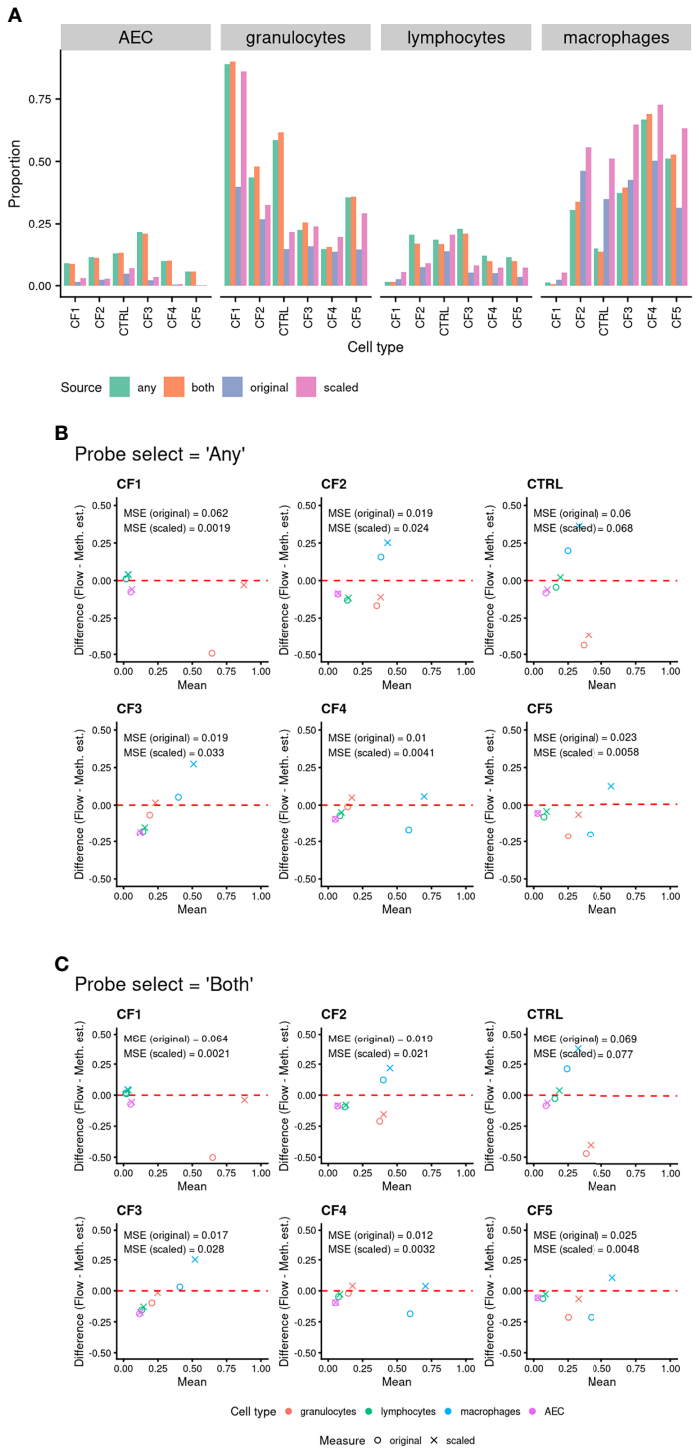

FIGURE 5 | **(A)** Comparison of cell proportions measured *via* flow cytometry to methylation-based estimated cell proportions derived using BAL purified cell population data. Cell type discriminating probes were selected using *"any"* and *"both"* approaches (see methods for details). "Original" refers to the proportion of cells from flow cytometry in the total live cell population. "Scaled" refers to the proportion of cells when limited to just the four cell types of interest. **(B, C)** Bland Altman Plots Comparing cell proportions measured by flow cytometry ("Flow") and methylation-based cell proportion estimates ("Meth. Est."). The shapes indicate use of "original" (circle) or "scaled" (cross) flow cytometry proportions. The colour indicates the cell type (see legend). Probes were selected using either **(B)** *"any"* or **(C)** *"both"* approaches (see *Methods* for details). The mean squared error (MSE) between the known proportion and estimated proportion was calculated for each cell type and probe selection *Method*.

healthy adult blood, does support that the reference panel will be suitable for broader populations.

We expect that this novel BAL-specific sorted cell type DNAm reference panel will be widely utilised by the paediatric pulmonary research community for facilitating EWAS of paediatric pulmonary diseases. Based on our findings, we would recommend the use of this reference panel on genomic DNA extracted from freshly isolated BAL samples.

DATA AVAILABILITY STATEMENT

The original contributions presented in the study are publicly available. This data can be found here: https://www.ncbi.nlm.nih.gov/geo/query/acc.cgi?acc=GSE185556.

ETHICS STATEMENT

The studies involving human participants were reviewed and approved by Royal Children's Hospital. Written informed consent to participate in this study was provided by the participants' legal guardian/next of kin.

AUTHOR CONTRIBUTIONS

All authors contributed to the design of the study. SS and SR were responsible for recruitment of participants and collection of bronchoalveolar lavage samples. SS and MN were responsible for cryopreservation and flow cytometry. SS was responsible for DNA extraction and arranging DNA methylation analysis. JM was primarily responsible for the analysis of the data with support from SS, RS and AO. All authors contributed to interpretation of the findings. SS and JM were primarily responsible for drafting the manuscript with MN, SR, AO, and RS involved in editing and revision. All authors contributed to the article and approved the submitted version.

FUNDING

This work was funded by a Vertex Pharmaceuticals Research Innovation Award (Ranganathan 2017).

ACKNOWLEDGMENTS

The authors would like to acknowledge the support of the AREST-CF team as well as the children and families who participated in this study.

SUPPLEMENTARY MATERIAL

The Supplementary Material for this article can be found online at: https://www.frontiersin.org/articles/10.3389/fimmu.2021.788705/full#supplementary-material

REFERENCES

1. Feinberg AP. The Key Role of Epigenetics in Human Disease Prevention and Mitigation. *New Engl J Med* (2018) 378(14):1323–34. doi: 10.1056/NEJMra1402513
2. Shanthikumar S, Neeland MR, Maksimovic J, Ranganathan SC, Saffery R. DNA Methylation Biomarkers of Future Health Outcomes in Children. *Mol Cell Pediatr* (2020) 7(1):7. doi: 10.1186/s40348-020-00099-0
3. Ghosh S, Yates AJ, Frühwald MC, Miecznikowski JC, Plass C, Smiraglia D. Tissue Specific DNA Methylation of Cpg Islands in Normal Human Adult Somatic Tissues Distinguishes Neural From Non-Neural Tissues. *Epigenetics* (2010) 5(6):527–38. doi: 10.4161/epi.5.6.12228
4. Michels KB, Binder AM, Dedeurwaerder S, Epstein EB, Greally JM, Gut I, et al. Recommendations for the Design and Analysis of Epigenome-Wide Association Studies. *Nat Methods* (2013) 10(10):949–55. doi: 10.1038/nmeth.2632
5. Teschendorff AE, Zheng SC. Cell-Type Deconvolution in Epigenome-Wide Association Studies: A Review and Recommendations. *Epigenomics* (2017) 9(5):757–68. doi: 10.2217/epi-2016-0153
6. Houseman EA, Accomando WP, Koestler DC, Christensen CB, Marsit CJ, Nelson HH, et al. DNA Methylation Arrays as Surrogate Measures of Cell Mixture Distribution. *BMC Bioinf* (2012) 13:86. doi: 10.1186/1471-2105-13-86
7. Bakulski KM, Feinberg JI, Andrews SV, Yang J, Brown S, McKenney SL, et al. DNA Methylation of Cord Blood Cell Types: Applications for Mixed Cell Birth Studies. *Epigenetics* (2016) 11(5):354–62. doi: 10.1080/15592294.2016.1161875
8. Chen Y, Armstrong DA, Salas LA, Hazlett HF, Nymon AB, Dessaint JA, et al. Genome-Wide DNA Methylation Profiling Shows a Distinct Epigenetic Signature Associated With Lung Macrophages in Cystic Fibrosis. *Clin Epigenetics* (2018) 10(1):152. doi: 10.1186/s13148-018-0580-2
9. Braga FAV, Kar G, Berg M, Carpaij OA, Polanski K, Simon LM, et al. A Cellular Census of Healthy Lung and Asthmatic Airway Wall Identifies Novel Cell States in Health and Disease. *bioRxiv* (2019) 2019:527408. doi: 10.1101/527408
10. Shanthikumar S, Burton M, Saffery R, Ranganathan SC, Neeland MR. Single-Cell Flow Cytometry Profiling of BAL in Children. *Am J Respir Cell Mol Biol* (2020) 63(2):152–9. doi: 10.1165/rcmb.2019-0453MA
11. Marguet C, Jouen-Boedes F, Dean TP, Warner JO. Bronchoalveolar Cell Profiles in Children With Asthma, Infantile Wheeze, Chronic Cough, or Cystic Fibrosis. *Am J Respir Crit Care Med* (1999) 159(5 Pt 1):1533–40. doi: 10.1164/ajrccm.159.5.9805028
12. Armstrong DS, Grimwood K, Carlin JB, Carzino R, Gutierrez JP, Olinsky A, et al. Lower Airway Inflammation in Infants and Young Children With Cystic Fibrosis. *Am J Respir Crit Care Med* (1997) 156(4 Pt 1):1197–204. doi: 10.1164/ajrccm.156.4.96-11058
13. Yang IV, Konigsberg I, MacPhail K, Li L, Davidson EJ, Mroz PM, et al. DNA Methylation Changes in Lung Immune Cells Are Associated With Granulomatous Lung Disease. *Am J Respir Cell Mol Biol* (2019) 60(1):96–105. doi: 10.1165/rcmb.2018-0177OC
14. Tricas L, Echeverria A, Blanco MA, Menendez M, Belda J. Flow Cytometry Counting of Bronchoalveolar Lavage Leukocytes With a New Profile of Monoclonal Antibodies Combination. *Cytom B Clin Cytom* (2012) 82(2):61–6. doi: 10.1002/cyto.b.20630
15. Hodge SJ, Hodge GL, Holmes M, Reynolds PN. Flow Cytometric Characterization of Cell Populations in Bronchoalveolar Lavage and Bronchial Brushings From Patients With Chronic Obstructive Pulmonary Disease. *Cytom B Clin Cytom* (2004) 61(1):27–34. doi: 10.1002/cyto.b.20020
16. Ringh MV, Hagemann-Jensen M, Needhamsen M, Kular L, Breeze CE, Sjoholm LK, et al. Tobacco Smoking Induces Changes in True DNA

Methylation, Hydroxymethylation and Gene Expression in Bronchoalveolar Lavage Cells. *EBioMedicine* (2019) 46:290–304. doi: 10.1016/j.ebiom.2019.07.006
17. Breeze CE, Paul DS, van Dongen J, Butcher LM, Ambrose JC, Barrett JE, et al. Eforge: A Tool for Identifying Cell Type-Specific Signal in Epigenomic Data. *Cell Rep* (2016) 17(8):2137–50. doi: 10.1016/j.celrep.2016.10.059
18. Blischak JD, Carbonetto P, Stephens M. Creating and Sharing Reproducible Research Code the Workflowr Way. *F1000Research* (2019) 8:1749. doi: 10.12688/f1000research.20843.1
19. Levy L, Juvet SC, Boonstra K, Singer LG, Azad S, Joe B, et al. Sequential Broncho-Alveolar Lavages Reflect Distinct Pulmonary Compartments: Clinical and Research Implications in Lung Transplantation. *Respir Res* (2018) 19(1):102. doi: 10.1186/s12931-018-0786-z
20. Ratjen F, Rietschel E, Griese M, Ballmann M, Kleinau I, Doring G, et al. Fractional Analysis of Bronchoalveolar Lavage Fluid Cytology in Cystic Fibrosis Patients With Normal Lung Function. Bronchoalveolar Lavage for the Evaluation of Anti-Inflammatory Treatment (BEAT) Study Group. *Eur Respir J* (2000) 15(1):141–5. doi: 10.1183/09031936.00.15114100
21. Olova N, Krueger F, Andrews S, Oxley D, Berrens RV, Branco MR, et al. Comparison of Whole-Genome Bisulfite Sequencing Library Preparation Strategies Identifies Sources of Biases Affecting DNA Methylation Data. *Genome Biol* (2018) 19(1):33. doi: 10.1186/s13059-018-1408-2
22. Bundo M, Sunaga F, Ueda J, Kasai K, Kato T, Iwamoto K. A Systematic Evaluation of Whole Genome Amplification of Bisulfite-Modified DNA. *Clin Epigenetics* (2012) 4(1):22. doi: 10.1186/1868-7083-4-22
23. Core Team R. *R: A Language and Environment for Statistical Computing* (2014). Available at: http://www.r-project.org/.
24. Maksimovic J, Phipson B, Oshlack A. A Cross-Package Bioconductor Workflow for Analysing Methylation Array Data. *F1000Research* (2016) 5:1281. doi: 10.12688/f1000research.8839.1
25. Aryee MJ, Jaffe AE, Corrada-Bravo H, Ladd-Acosta C, Feinberg AP, Hansen KD, et al. Minfi: A Flexible and Comprehensive Bioconductor Package for the Analysis of Infinium DNA Methylation Microarrays. *Bioinf (Oxford England)* (2014) 30(10):1363–9. doi: 10.1093/bioinformatics/btu049
26. Fortin JP, Triche TJJr., Hansen KD. Preprocessing, Normalization and Integration of the Illumina Humanmethylationepic Array With Minfi. *Bioinf (Oxford England)* (2017) 33(4):558–60. doi: 10.1101/065490
27. Touleimat N, Tost J. Complete Pipeline for Infinium(®) Human Methylation 450K Beadchip Data Processing Using Subset Quantile Normalization for Accurate DNA Methylation Estimation. *Epigenomics* (2012) 4(3):325–41. doi: 10.2217/epi.12.21
28. Pidsley R, Zotenko E, Peters TJ, Lawrence MG, Risbridger GP, Molloy P, et al. Critical Evaluation of the Illumina Methylationepic Beadchip Microarray for Whole-Genome DNA Methylation Profiling. *Genome Biol* (2016) 17(1):208. doi: 10.1186/s13059-016-1066-1
29. Salas LA, Koestler DC, Butler RA, Hansen HM, Wiencke JK, Kelsey KT, et al. An Optimized Library for Reference-Based Deconvolution of Whole-Blood Biospecimens Assayed Using the Illumina Humanmethylationepic Beadarray. *Genome Biol* (2018) 19(1):64. doi: 10.1186/s13059-018-1448-7
30. Phipson B, Maksimovic J, Oshlack A. Missmethyl: An R Package for Analyzing Data From Illumina's Humanmethylation450 Platform. *Bioinf (Oxford England)* (2016) 32(2):286–8. doi: 10.1093/bioinformatics/btv560
31. Maksimovic J, Oshlack A, Phipson B. Gene Set Enrichment Analysis for Genome-Wide DNA Methylation Data. *Genome Biol* (2021) 22(1):173. doi: 10.1186/s13059-021-02388-x
32. Houseman EA, Kim S, Kelsey KT, Wiencke JK. DNA Methylation in Whole Blood: Uses and Challenges. *Curr Environ Health Rep* (2015) 2(2):145–54. doi: 10.1007/s40572-015-0050-3
33. Zheng SC, Beck S, Jaffe AE, Koestler DC, Hansen KD, Houseman AE, et al. Correcting for Cell-Type Heterogeneity in Epigenome-Wide Association Studies: Revisiting Previous Analyses. *Nat Methods* (2017) 14(3):216–7. doi: 10.1038/nmeth.4187
34. Guo S, Diep D, Plongthongkum N, Fung HL, Zhang K, Zhang K. Identification of Methylation Haplotype Blocks Aids in Deconvolution of Heterogeneous Tissue Samples and Tumor Tissue-of-Origin Mapping From Plasma DNA. *Nat Genet* (2017) 49(4):635–42. doi: 10.1038/ng.3805
35. Koestler DC, Usset J, Christensen BC, Marsit CJ, Karagas MR, Kelsey KT, et al. DNA Methylation-Derived Neutrophil-to-Lymphocyte Ratio: An Epigenetic Tool to Explore Cancer Inflammation and Outcomes. *Cancer Epidemiol Biomarkers Prev Publ Am Assoc Cancer Res Cosponsored by Am Soc Prev Oncol* (2017) 26(3):328–38. doi: 10.1158/1055-9965.EPI-16-0461
36. Wiencke JK, Koestler DC, Salas LA, Wiemels JL, Roy RP, Hansen HM, et al. Immunomethylomic Approach to Explore the Blood Neutrophil Lymphocyte Ratio (NLR) in Glioma Survival. *Clin Epigenetics* (2017) 9:10. doi: 10.1186/s13148-017-0316-8
37. Dekkers KF, Neele AE, Jukema JW, Heijmans BT, de Winther MPJ. Human Monocyte-to-Macrophage Differentiation Involves Highly Localized Gain and Loss of DNA Methylation at Transcription Factor Binding Sites. *Epigenet Chromatin* (2019) 12(1):34. doi: 10.1186/s13072-019-0279-4
38. Calle-Fabregat C, Morante-Palacios O, Ballestar E. Understanding the Relevance of DNA Methylation Changes in Immune Differentiation and Disease. *Genes* (2020) 11(1) 110–35. doi: 10.3390/genes11010110
39. Blériot C, Chakarov S, Ginhoux F. Determinants of Resident Tissue Macrophage Identity and Function. *Immunity* (2020) 52(6):957–70. doi: 10.1016/j.immuni.2020.05.014
40. Tan SY, Krasnow MA. Developmental Origin of Lung Macrophage Diversity. *Development* (2016) 143(8):1318–27. doi: 10.1242/dev.129122
41. Bassler K, Fujii W, Kapellos TS, Horne A, Reiz B, Dudkin E, et al. Alterations of Multiple Alveolar Macrophage States in Chronic Obstructive Pulmonary Disease. *bioRxiv* (2020). doi: 10.1101/2020.05.28.121541
42. Jaffe AE, Irizarry RA. Accounting for Cellular Heterogeneity is Critical in Epigenome-Wide Association Studies. *Genome Biol* (2014) 15(2):R31. doi: 10.1186/gb-2014-15-2-r31

Conflict of Interest: The authors declare that the research was conducted in the absence of any commercial or financial relationships that could be construed as a potential conflict of interest.

frontiers in Immunology

ORIGINAL RESEARCH
published: 28 February 2022
doi: 10.3389/fimmu.2022.822437

Age-Related Differences in Structure and Function of Nasal Epithelial Cultures From Healthy Children and Elderly People

Anita Balázs[1,2†], Pamela Millar-Büchner[1,2†], Michael Mülleder[3], Vadim Farztdinov[3], Lukasz Szyrwiel[3,4], Annalisa Addante[1,2], Aditi Kuppe[1,2], Tihomir Rubil[1,2], Marika Drescher[1], Kathrin Seidel[1], Sebastian Stricker[1], Roland Eils[2,5], Irina Lehmann[2,6], Birgit Sawitzki[7], Jobst Röhmel[1], Markus Ralser[4,8] and Marcus A. Mall[1,2,9*]*

[1] Department of Pediatric Respiratory Medicine, Immunology and Critical Care Medicine, Chariteí - Universitaätsmedizin Berlin, Berlin, Germany, [2] German Center for Lung Research (DZL), Associated Partner Site, Berlin, Germany, [3] Charité - Universitätsmedizin Berlin, Core Facility - High-Throughput Mass Spectrometry, Berlin, Germany, [4] Charité - Universitätsmedizin Berlin, Department of Biochemistry, Berlin, Germany, [5] Center for Digital Health, Berlin Institute of Health at Charité - Universitätsmedizin Berlin, Berlin, Germany, [6] Molecular Epidemiology Unit, Berlin Institute of Health at Charité - Universitätsmedizin Berlin, Berlin, Germany, [7] Institute of Medical Immunology, Charité - Universitätsmedizin Berlin, Berlin, Germany, [8] The Francis Crick Institute, Molecular Biology of Metabolism Laboratory, London, United Kingdom, [9] Berlin Institute of Health (BIH) at Charité, Berlin, Germany

The nasal epithelium represents the first line of defense against inhaled pathogens, allergens, and irritants and plays a key role in the pathogenesis of a spectrum of acute and chronic airways diseases. Despite age-dependent clinical phenotypes triggered by these noxious stimuli, little is known about how aging affects the structure and function of the airway epithelium that is crucial for lung homeostasis and host defense. The aim of this study was therefore to determine age-related differences in structural and functional properties of primary nasal epithelial cultures from healthy children and non-smoking elderly people. To achieve this goal, highly differentiated nasal epithelial cultures were established from nasal brushes at air–liquid interface and used to study epithelial cell type composition, mucin (MUC5AC and MUC5B) expression, and ion transport properties. Furthermore, we determined age-dependent molecular signatures using global proteomic analysis. We found lower numeric densities of ciliated cells and higher levels of MUC5AC expression in cultures from children vs. elderly people. Bioelectric studies showed no differences in basal ion transport properties, ENaC-mediated sodium absorption, or CFTR-mediated chloride transport, but detected decreased calcium-activated TMEM16A-mediated chloride secretory responses in cultures from children vs. elderly people. Proteome analysis identified distinct age-dependent molecular signatures associated with ciliation and mucin biosynthesis, as well as other pathways implicated in aging. Our data identified intrinsic, age-related differences in structure and function of the nasal epithelium and provide a basis for further studies on the role of these findings in age-dependent airways disease phenotypes observed with a spectrum of respiratory infections and other noxious stimuli.

Keywords: primary nasal epithelial cultures, aging, airways disease, ion transport, proteome

OPEN ACCESS

Edited by:
Wendy W. J. Unger, Erasmus MC-Sophia Children's Hospital, Netherlands

Reviewed by:
Nicola Ivan Lorè, IRCCS San Raffaele Scientific Institute, Italy
Kenichi Okuda, University of North Carolina at Chapel Hill, United States

***Correspondence:**
Anita Balázs
anita.balazs@charite.de
Marcus A. Mall
marcus.mall@charite.de

†These authors have contributed equally to this work and share first authorship

Specialty section:
This article was submitted to Mucosal Immunity, a section of the journal Frontiers in Immunology

Received: *25 November 2021*
Accepted: *28 January 2022*
Published: *28 February 2022*

Citation:
Balázs A, Millar-Büchner P, Mülleder M, Farztdinov V, Szyrwiel L, Addante A, Kuppe A, Rubil T, Drescher M, Seidel K, Stricker S, Eils R, Lehmann I, Sawitzki B, Röhmel J, Ralser M and Mall MA (2022) Age-Related Differences in Structure and Function of Nasal Epithelial Cultures From Healthy Children and Elderly People. Front. Immunol. 13:822437. doi: 10.3389/fimmu.2022.822437

INTRODUCTION

The airway mucosa represents the first line of defense of the respiratory system against pathogens, pollutants, and irritants that are constantly inhaled during tidal breathing. At the interface with the environment, airway epithelial cells have developed specialized functions to provide host protection, such as barrier function, secretion of anti-microbial mediators, interaction with cells of the immune system, as well as elimination of potentially harmful stimuli by mucociliary clearance (MCC) (1, 2). MCC operates through the coordinated function of (i) the motile cilia, (ii) the airway surface liquid layer, and (iii) the mucus layer (3–6). Airway mucus is a viscoelastic hydrogel composed of ~97% water and ~3% solids, including the highly glycosylated polymeric mucin glycoproteins MUC5AC and MUC5B, as well as salts, lipids, and anti-microbial peptides (7). Hydration and transportability of mucus are critically dependent on ion and fluid transport across the airway epithelium, which is primarily determined by the activity of sodium absorption through the epithelial sodium channel (ENaC) and chloride secretion through the cyclic adenosine monophosphate (cAMP)-regulated chloride channel cystic fibrosis transmembrane conductance regulator (CFTR), as well as the calcium activated chloride channel transmembrane protein 16A (TMEM16A) (8, 9). In health, a well-hydrated mucus layer is continuously transported by directional beating of the cilia towards the throat, providing effective elimination of mucus entrapped particles (10, 11). Proper MCC is crucial for airway homeostasis, and mucociliary dysfunction has been implicated in the pathogenesis of acute and chronic airways diseases caused by a spectrum of pathogens, allergens, and other environmental pollutants (4, 12). Of note, the clinical airways disease phenotypes triggered by some of these noxious stimuli are strikingly age-dependent, suggesting a potential role of age-related differences in airway epithelial defense properties (13–20). However, the relationship between age and airway epithelial structure and function has not been studied.

In vitro studies utilizing highly differentiated primary human airway epithelial cell cultures grown at air–liquid interface (ALI) provided an essential contribution to our current understanding of airway epithelial innate defense (21). ALI cultures recapitulate key physiological features of the airways *in vivo* including the pseudostratified morphology, composition of relevant proportions of airway epithelial cell types, barrier function, coordinated ciliary beating, and mucus secretion (22–24). The emergence of improved cell expansion protocols enabled the generation of sufficient cell numbers to differentiate cultures from nasal brushings that can be obtained non-invasively (25). The ALI culture system has been instrumental to study genetically determined airways diseases such as cystic fibrosis or primary ciliary dyskinesia (26, 27). Furthermore, a number of studies demonstrated that ALI cultures retain donor-dependent phenotypic characteristics such as signatures of tobacco smoking, inflammation, or even aging, suggesting that epigenetic factors may remain stable even through rounds of proliferative expansion (28–31).

The aim of this study was to determine the effects of aging on the structure and function of the nasal epithelium. To achieve this goal, we generated highly differentiated nasal epithelial ALI cultures from healthy children and non-smoking elderly people and compared cell-type composition, mucin (MUC5AC and MUC5B) expression, transepithelial ion transport properties, and global proteome changes between these age groups.

MATERIALS AND METHODS

Study Population

This study was conducted in accordance with the Declaration of Helsinki and approved by the ethics committee at the Charité-Universitätsmedizin Berlin (EA2/066/20). Written informed consent was obtained from all study participants, their parents, or legal guardians. In total, our study included nasal swabs from 17 healthy children (≤10 years old) and 14 healthy non-smoking elderly people (≥60 years old). Demographics and clinical characteristics of the study population are provided in **Table 1**.

Culture of Primary Human Nasal Epithelial Cells

Primary human nasal epithelial cells were obtained by nasal brushings. Cultivation of cells was performed by the conditionally reprogrammed cell culture method as previously described (25). In brief, brushed cells were expanded in co-culture with irradiated mouse 3T3 fibroblasts in the presence of RhoA kinase inhibitor Y-27632. Epithelial cells were seeded at passage 2 or 3 on human placental type IV collagen–coated, 0.4-mm pore size Snapwell or Transwell 1.1 cm^2 supports (Corning, Glendale, NY, USA) at a density of 200,000 cells/cm^2 in UNC-ALI medium and differentiated at ALI for at least 4 weeks. Cultures were used for analysis when transepithelial electrical resistance (TEER) was ≥500 Ω^*cm^2.

Immunostaining

Cultures were first washed with PBS, then fixed by 4% paraformaldehyde for 10 min, and permeabilized with 0.1% Triton X-100 for 8 min and blocked with 5% goat serum for 30 min. The primary antibodies used were rat monoclonal anti-α-tubulin (mAb1864, Millipore, Burlington, MA, USA), mouse monoclonal anti-MUC5AC (sc-59951, Santa Cruz, Dallas, TX, USA), and rabbit polyclonal anti-KRT5 (SAB1410739, Sigma, St. Louis, MO, USA) at dilution of 1:200 for 1 h. For TMEM16A localization, rabbit polyclonal anti-TMEM16A antibody (HPA032148, Atlas Antibodies, Stockholm, Sweden) was used at a dilution of 1:50 overnight at 4°C. The secondary antibodies used

TABLE 1 | Demographics of the study population.

	Children	Elderly
Number (*n*)	17	14
Mean age (years ± SD)	4.9 ± 3.1	73.1 ± 9.4
Sex (% male)	76.5	50.0
Smoker (*n*)	0	0
Asthma (*n*)	0	0
Allergy (*n*)*	0	3

**Allergy to house dust mite or pollen.*

were Alexa Fluor 488-conjugated goat anti-rat IgG (SA5-10018, Thermo Fisher Scientific, Waltham, MA, USA), Alexa Fluor 647-conjugated goat anti-mouse IgG (A-21235, Thermo Fisher Scientific, Waltham, MA, USA), and Alexa Fluor 750-conjugated goat anti-rabbit IgG (A-21039 Thermo Fisher Scientific, Waltham, MA, USA) at 1:300 dilution for 30 min. Zonula occludens (ZO-1) antibody conjugated with Alexa Fluor 555 (MA3-39100-A555, Thermo Fisher Scientific, Waltham, MA, USA) and Hoechst 33342 (Thermo Fisher Scientific, Waltham, MA, USA) was incubated for 30 min at 1:300 and 1:5,000 dilution, respectively. Filters were cut out with a scalpel and mounted with ProLong™ Gold anti-fade reagent (Thermo Fisher Scientific, Waltham, MA, USA). All steps were performed at room temperature, unless indicated otherwise. Images were acquired using a Leica Stellaris 8 confocal laser scanning microscope equipped with Hamamatsu Orca Flash 4.0 V3 sCMOS camera for wide-field fluorescence imaging.

Quantification of Cell Types

Due to the heterogeneity of ciliated cell distribution within one filter, tile scans of the whole filter area were acquired and stitched together in a single image (~40 mm^2 filter area on average). The cultures were imaged with 10× air objective in wide-field mode (α-tubulin$^+$ cells) or in confocal mode with opened pin-hole (KRT5$^+$ or MUC5AC$^+$ cells). Images were analyzed with FIJI software (32). Cells with positive signal (α-tubulin$^+$, MUC5AC$^+$ or KRT5$^+$) were segmented by creating a binary mask with the application of an intensity threshold, where over/under-saturated pixels were adjusted based on visual control of the original image. Pixels were dilated and overlapping objects were separated by watershed command. Particles between 20 and 150 μm^2 were analyzed and cell counts per surface area were determined. Representative stacks were acquired with 20× immersion objective in confocal mode with Lightning module and maximal Z-projections are shown.

RNA Extraction and RT-PCR

Total RNA was isolated using RNeasy Micro Kit (Qiagen, Hilden, Germany) according to the manufacturer's instructions. RNA was transcribed by high-capacity cDNA reverse transcription kit (Applied Biosystems, Darmstadt, Germany). Real-time PCR was performed using Applied Biosystems 7500 Real-Time PCR system with TaqMan Universal PCR master mix and inventoried TaqMan gene expression assays (Applied Biosystems, Darmstadt, Germany) for human *CFTR* (Hs00357011_m1), *TMEM16A* (Hs00216121_M1), *MUC5AC* (Hs01365616_m1), *MUC5B* (Hs00861595_m1), and *ACTB* (4333762F). The relative expression ratios were calculated from the RT-PCR efficiencies and the crossing point deviation of target gene transcripts in comparison to the reference gene transcript *ACTB* (33).

Preparation of Cell Lysates

Filters were washed with PBS and 80 µl of RIPA buffer (Thermo Fisher Scientific, Waltham, MA, USA) containing cOmplete protease inhibitor (Merck, Darmstadt, Germany) was added; the cells were scraped and vortexed briefly. Three filters/individual were pooled, and samples from different individuals were considered as biological replicates. After 30-min incubation on ice, the lysates were cleared by centrifugation. The protein concentration of the supernatant was determined using Pierce™ BCA Protein Assay Kit (Thermo Fisher Scientific, Waltham, MA, USA), according to the manufacturer's instructions.

Mucin Agarose Gel Electrophoresis

Mucin Western blot was performed as previously described (34). In brief, 36 µg of total protein was loaded in equal volume of 30 µl. Agarose gel electrophoresis using 0.8% agarose was combined with transfer onto a nitrocellulose membrane *via* vacuum. After loading the gels, proteins were separated on 0.8% agarose gel at 80 V (1 h) with Tris-acetate-EDTA/SDS buffer. For an efficient mucin transfer, the gel was reduced for 20 min in a solution containing 10 mM dithiothreitol (DTT) and proteins were then transferred by vacuum blotting (MP Biomedicals, Irvine, CA, USA) to nitrocellulose membranes. For total protein normalization, Ponceau S (Advansta, San Jose, CA, USA) staining was used. Blots were probed with mouse monoclonal antibodies against MUC5B (sc-393952, Santa Cruz, Dallas, TX, USA) and MUC5AC (MA5-12178, Invitrogen, Waltham, MA, USA). Primary antibodies were diluted 1:250 in 1% milk-PBS. The secondary antibody was goat anti-mouse immunoglobulins/HRP (P0047, Dako, Glostrup, Denmark), diluted 1:2,000 in 1% milk-PBS. Restore™ PLUS Western Blot Stripping Buffer (Thermo Fisher Scientific, Waltham, MA, USA) was used for membrane stripping according to the manufacturer's instructions. Pierce™ ECL Western Blotting-Substrate (Thermo Fisher Scientific, Waltham, MA, USA) in combination with ChemiDoc Imaging System (Bio-Rad, Hercules, CA, USA) were used for the detection. Densitometric analysis was performed by FIJI software (32).

Ussing Chamber Experiments

Transepithelial ion transport experiments were performed in EasyMount Ussing chambers (Physiologic Instruments, San Diego, CA, USA) using voltage clamp configuration to measure the short-circuit current (I_{sc}). The I_{sc} was continuously recorded using LabChart8 (AF Instruments, Oxfordshire, UK), and transepithelial resistance was monitored by application of short voltage pulses (2 mV) every 60 s. Experiments were performed under chloride gradient conditions (basolateral 145 mM vs. apical 5 mM) to increase the electrochemical driving force for chloride secretion and augment chloride secretory responses across the epithelium as previously described (24, 35, 36). After 15–20 min equilibration, basal I_{sc} was measured and amiloride (100 µM) was added to inhibit sodium absorption *via* ENaC. Next, forskolin (Fsk, 10 µM) and 3-isobutyl-1-methylxanthin (IBMX, 100 µM) were added together, followed by CFTR-inhibitor 172 (CFTRinh172, 20 µM) to assess CFTR-mediated chloride secretion. Uridine-triphosphate (UTP, 10 µM) was added to evaluate the calcium-activated chloride secretion. In a subset of experiments, UTP was followed by small molecular weight TMEM16A inhibitor Ani9 (10 µM).

Sample Preparation for Proteomic Analysis

One hundred micrograms of protein was transferred to AFA tubes (PN 520292, 500639) and filled to 60 µl with RIPA buffer.

Proteins were extracted and DNA sheared DNA (Covaris LE220Rsc: PIP 350 W, DF 25%, CPB 200, 2 repeats, 300 s pulse, 20 C). Protein (25 µg) was used for SP3 protein preparation on a Biomek i7 workstation with single-step reduction and alkylation (37). Briefly, 16.6 µl reduction and alkylation buffer (40 mM TCEP, 160 mM CAA, and 200 mM ABC) were added, and samples were incubated for 5 min at 95°C and cooled to room temperature. Proteins were bound to 2.5 µg of paramagnetic beads (1:1 ratio of hydrophilic/hydrophobic beads) by adding acetonitrile (ACN) to 50%. Samples were washed twice with 80% ethanol and once with 100% ACN, before reconstitution in 35 µl of 100 mM ABC. Digestion was completed overnight at 37°C using a trypsin/LysC enzyme mix (Promega, Madison, WI, USA) at a protein:enzyme ratio of 50:1 (w/w) and stopped with formic acid (0.1%). The peptides were stored at −80°C until analysis by LC-MS/MS without further conditioning or clean-up.

Liquid Chromatography Mass Spectrometry

The tryptic digests were injected on the 25-cm Aurora Series with emitter column (CSI, 25 cm × 75 µm ID, 1.6 µm C18, IonOpticks), installed in the nano-electrospray source (CaptiveSpray source, Bruker Daltonics, Germany) at 50°C using UltiMate 3000 (Thermo Scientific Dionex) coupled with TIMS quadrupole time-of-flight instrument (timsTOF Pro2, Bruker Daltonics, Germany) and measured in diaPASEF mode (38). The mobile phases water/0.1% FA and ACN/0.1% FA (A and B, respectively) were applied in linear gradients starting from 2% B and increasing to 17% in 87 min, followed by an increase to 25% B in 93 min, 37% B in 98 min, and 80% B in 99 min to 104 min; the column was equilibrated in 2% B in the next 15 min. For calibration of ion mobility dimension, three ions of Agilent ESI-Low Tuning Mix ions were selected (m/z [Th], 1/K0 [Th]: 622.0289, 0.9848; 922.0097, 1.1895; 1221.9906, 1.3820). The diaPASEF windows scheme was ranging in dimension m/z from 396 to 1,103 Th and in dimension 1/K0 0.7–1.3 Vs/cm^2, with 59 × 12 Th windows). All measurements were done in low sample amount mode with ramp time 166 ms.

Protein Identification and Quantification

The raw data were processed using DIA-NN 1.8 (39) with the ion mobility module for diaPASEF (40). MS2 and MS1 mass accuracies were both set to 10 ppm, and scan window size was set to 10. DIA-NN was run in library-free mode with standard settings (fasta digest and deep learning-based spectra, RT and IMs prediction) using the uniprot human reference proteome annotations (41) (downloaded on 2019.12.20) and the match-between-runs (MBR) option.

Proteomics Data Processing, and Statistical and Functional Analysis

Peptide normalized intensities were subjected to quality control with all 27 samples passing acceptance criteria. Peptides with excessive missing values (>35% per group) were excluded from analysis. The missing values of the remaining peptides were imputed group-based using the PCA method (42). Normalization was performed with LIMMA (43) implementation of cyclic loess method (44) with option "fast" (45). To obtain a quantitative protein data matrix, the $\log_2$ intensities of peptides were filtered, and only peptides belonging to one protein group were kept and then summarized into protein log intensity by the "maxLFQ" method (46), implemented in R package iq (47). Sample protein distributions were median centered. Statistical analysis of proteomics data was carried out using internally developed R scripts based on publicly available packages. PCA exploratory analysis was carried out using the R package FactoMineR (48). Linear modeling was based on the R package LIMMA (43). The following model was applied to each tissue dataset (log(p) is $\log_2$ transformed expression of a protein): log(p) ~ 0 + Class. The categorical factor Class had two levels: old, young; reference level: young. To find regulated features, the following criteria were applied: Significance level alpha was set to guarantee the false discovery rate below ~5%. We found that alpha = 0.005 was delivering the required level of Benjamini–Hochberg FDR (49). The log fold-change criterion was applied to guarantee that the measured signal is above the average noise level. As such, we have taken median residual standard deviation of linear model: $\log_2$ (T) = median residual SD of linear modeling (= $\log_2$(1.38)). Functional analysis was carried out using the R package clusterProfiler (50) for GSEA. Log_2 fold-changes old/young of all quantified proteins were used for their ranking and calculation of the enrichment score. For selecting the most (de) regulated GO terms, we applied the following filter: 5 ≤ term size ≤ 350. Unless specified separately, analyses were carried out with Benjamini–Hochberg FDR threshold 5%. To identify epithelial cell subtypes from our proteome data, we extracted cell-type markers from the Single-cell atlas of the airway epithelium scRNAseq dataset (grch38 genes annotation) and associated the $\log_2$ fold-change proteome values (51).

Statistics

Data were analyzed with GraphPad Prism 9.1.2 for Windows (GraphPad Software, San Diego, CA, USA) and are reported as mean ± standard error of the mean (SEM). Two group comparisons were performed with Student's t-test or Mann–Whitney Rank Sum test as appropriate. $p < 0.05$ was accepted to indicate statistical significance.

RESULTS

Nasal Epithelial Cultures From Children Display Lower Numbers of Ciliated Cells, Higher Numbers of MUC5AC$^+$ Secretory Cells, and Elevated MUC5AC Expression

To investigate potential morphological differences between nasal epithelia of children and elderly people, we established highly differentiated primary cultures at ALI. Cultures were fully differentiated from week 4 onwards and displayed the expected pseudostratified morphology of the respiratory epithelium with

visible ciliary beating and mucus secretion. To characterize cell-type composition, we performed whole-mount immunohistochemistry and quantified ciliated cells (α-tubulin$^+$), secretory cells (MUC5AC$^+$), and basal cells (KRT5$^+$) (**Figures 1A–E**). We found a lower number of ciliated cells in cultures from children compared to elderly people and higher number of MUC5AC$^+$ cells, while the number of basal cells did not differ between age groups (**Figures 1C–E**). TEER values were measured as indicators of cell confluence and quality control and were comparable in both age groups (**Figure 1F**). Furthermore, we investigated the transcript and protein levels of the two major secreted mucins MUC5AC and MUC5B. We found that MUC5AC expression was higher both at the transcript and protein level in cultures from children vs. elderly people (**Figures 1G, I, J**). MUC5B expression levels were comparable between age groups, both by RT-PCR and by Western blot analysis (**Figures 1H, I, K**).

TMEM16A-Mediated Chloride Secretion Is Decreased in Nasal Epithelial Cultures From Children

To compare bioelectrical properties of cultures from healthy children and elderly people, we performed transepithelial ion transport measurements in Ussing chambers (**Figures 2A, B**). Basal I_{sc}, amiloride-insensitive I_{sc}, amiloride-sensitive I_{sc} reflecting ENaC-mediated sodium absorption, and cAMP-activated and CFTRinh172-sensitive I_{sc} reflecting CFTR-mediated chloride secretion did not differ between cultures from children and elderly people (**Figures 2C–G**). However, calcium-activated chloride secretion induced by apical stimulation of purinergic signaling by UTP showed an ~50% lower response in children compared to elderly people (**Figure 2H**). Transcript levels of *CFTR* as well as calcium-activated chloride channel *TMEM16A* did not differ in nasal cultures from children compared to elderly, although there was a trend toward higher expression of *TMEM16A* in the elderly group (**Figures 2I, J**). We also analyzed cellular localization of TMEM16A protein by immunostaining, which showed no expression in ciliated cells and low expression in MUC5AC$^+$ cells, whereas most of the TMEM16A signal was localized to other cells that do not express MUC5AC (**Supplementary Figure 1**). To assess the role of TMEM16A in the age-dependent difference in calcium-activated chloride secretion, we determined UTP-induced chloride secretory responses in the absence and presence of the TMEM16A inhibitor Ani9 (**Figures 3A–D**). Ani9 blocked 80%–100% of the UTP-induced I_{sc} in both children and elderly (**Figure 3E**).

Proteome Analysis of Nasal Epithelial Cultures From Children and Elderly People

Next, we assessed age-related proteome profiles in nasal epithelial cultures from children and elderly people by liquid

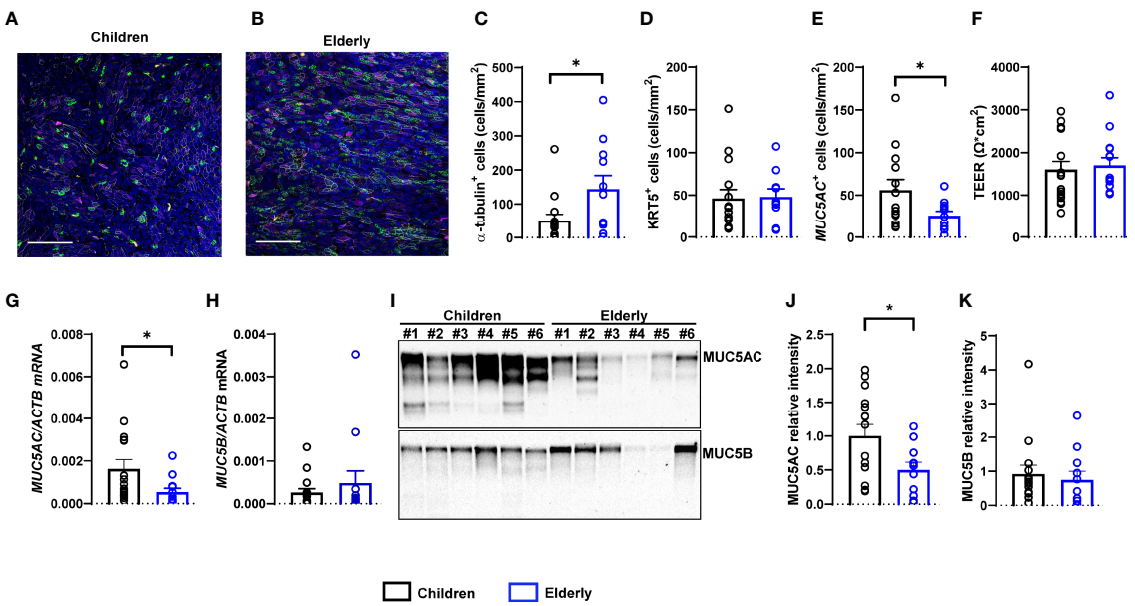

FIGURE 1 | Age-related differences in numeric densities of ciliated cells and MUC5AC expression in nasal epithelial cultures from children compared to elderly people. **(A, B)** Representative images of immunofluorescence of nasal epithelial cultures from healthy children and elderly people. Green: α-tubulin (ciliated cells), magenta: KRT5 (basal cells), yellow: MUC5AC (secretory cells), white: ZO-1 (tight junctions), and blue: Hoechst (cell nuclei). Scale bar, 100 µm. **(C–E)** Quantification of α-tubulin$^+$ (ciliated) cells **(C)**, KRT5$^+$ (basal) cells **(D)**, and MUC5AC$^+$ (secretory) cells **(E)** (n = 14 and 11 individuals per group). **(F)** Transepithelial electrical resistance (TEER) (n = 17 and 14 individuals per group). **(G, H)** Transcript levels of *MUC5AC* **(G)** and *MUC5B* **(H)** (n = 16 and 12 individuals per group). **(I)** Representative MUC5AC and MUC5B Western blot. **(J, K)** Protein quantification of MUC5AC **(J)** and MUC5B **(K)** by densitometry (n = 15 and 11 individuals per group). *$p < 0.05$ compared to children. Data are shown as mean ± S.E.M. Statistical analysis was performed with unpaired two-tailed t test in **(D-F, J)**, and with two-tailed Mann–Whitney test in **(C, G, H, K)**.

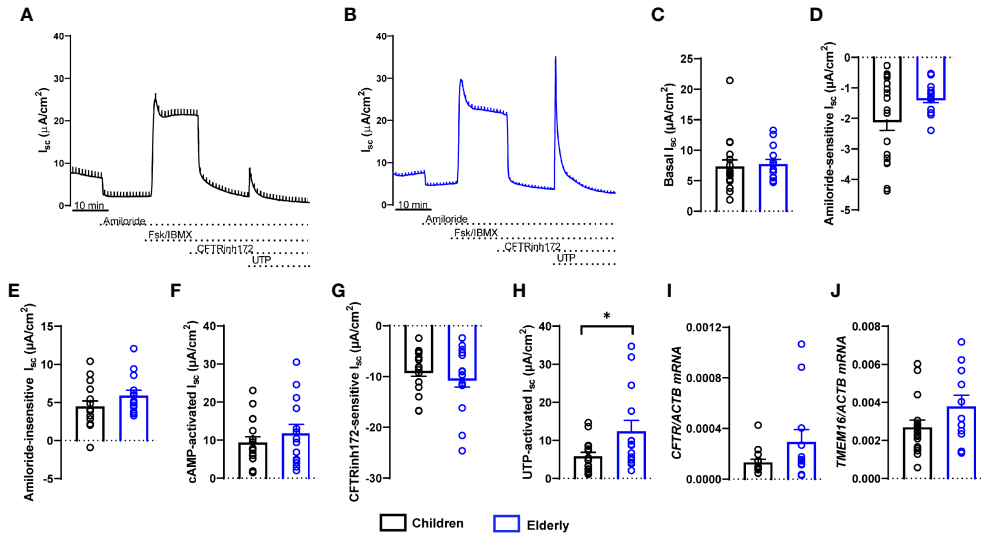

FIGURE 2 | Age-related differences in calcium-activated chloride secretion in nasal epithelial cultures from healthy children compared to elderly people. **(A, B)** Representative original recordings of transepithelial Ussing chamber measurements in primary nasal epithelial cultures from children and elderly people. **(C–G)** Summary of individual effects of basal I_{sc} **(C),** amiloride-sensitive I_{sc} **(D)**, amiloride-insensitive I_{sc} **(E)**, cAMP-activated I_{sc} **(F)**, CFTR inhibitor 172-sensitive I_{sc} **(G)**, and UTP-activated I_{sc} **(H)** (n = 17 and 14 individuals per group, data represent mean values of 2–3 filters per individual). **(I, J)** Transcript levels of *CFTR* **(I)** and *TMEM16A* **(J)** (n = 16 and 12 individuals per group). *$p < 0.05$ compared to children. Data are shown as mean ± S.E.M. Statistical analysis was performed with unpaired two-tailed t-test in **(D–G)**, and with two-tailed Mann–Whitney test in **(C, H–J)**.

chromatography tandem mass spectrometry. Overall, 7,073 proteins were detected. Principal component analysis confirmed absence of outliers and showed separation of samples according to age already using the full proteome, indicating that age is a primary source of variance (**Supplementary Figure 2**). Linear modeling revealed that among the differentially expressed proteins [alpha = 0.005 (FDR < 5%), $|\log_2(FC)|$ > median residual SD], 364 proteins were upregulated and 254 proteins were downregulated in the elderly group compared to children (**Figure 4A** and **Supplementary Table 1**). Note that increasing the stringency of feature selection to the very high level [alpha = 0.0001 (FDR < 0.7%), $|\log_2(FC)| > 1$] resulted in full separation of elderly group from children in the post-hoc PCA and hierarchical clustering (**Supplementary Figure 3**). Some of the most significantly upregulated proteins in elderly are involved in mitochondrial function (ABCB10, ATAD3B, ATP5PD, and MRPL49), while upregulated proteins in children were related to immune-epithelial cell interactions (DPP4 and ADA) and extracellular matrix organization (FN1, ITGA5, ITGB6, and ADAM9). To capture potential differences in epithelial cell populations between children and elderly, we analyzed the expression pattern of epithelial cell-type markers (51). Taking the top 20 significantly differentially expressed markers for each subtype, proteins associated with basal cells were overall decreased in elderly ($\log_2$ fold-change = −0.47 ± 0.26), accompanied by an increase in the abundance of suprabasal ($\log_2$ fold-change = 0.51 ± 0.19) markers. Secretory cell markers showed higher variability ("Secretory" cluster: $\log_2$ fold-change = −0.26 ± 0.28; "Secretory N" cluster: $\log_2$ fold-change = −0.04 ± 0.21, "Submucosal gland goblet cell" cluster: $\log_2$ fold-change = 0.02 ± 0.23), whereas genes associated with serous cells were increased in elderly samples ($\log_2$ fold-change = 0.39 ± 0.24). Ciliated cell markers were significantly upregulated in the elderly group ($\log_2$ fold-change = 0.62 ± 0.18) (**Supplementary Table 4**). To visualize protein expression patterns, a subset of known cell-type markers are showcased in **Figure 4B**. Next, we performed gene set enrichment analysis (GSEA) to understand patterns of age-dependent changes in protein expression and related biological processes. This analysis revealed an upregulation of protein sets related to mitochondria and oxidative phosphorylation, as well as cilia-related processes in the elderly. Furthermore, gene sets related to extracellular matrix were downregulated in elderly people compared to children (**Figure 4C**, **Supplementary Tables 2, 3** and **Supplementary Figure 4**).

DISCUSSION

This study provides an integrated comparison of age-related differences in the cell-type composition, mucin expression, ion transport properties, and the proteome of highly differentiated primary nasal epithelial cultures from children and elderly people. Our data show that cultures from children displayed less ciliated cells and more $MUC5AC^+$ secretory cells, as well as expressed more MUC5AC (**Figure 1**), while TMEM16A-mediated chloride secretion was lower compared to cultures from elderly people (**Figures 2**, **3**). These findings were complemented by proteome analysis, which revealed age-dependent differences in protein signatures related to cilia development and mucin secretion in addition to other pathways consistent with aging (**Figure 4**). Collectively, these

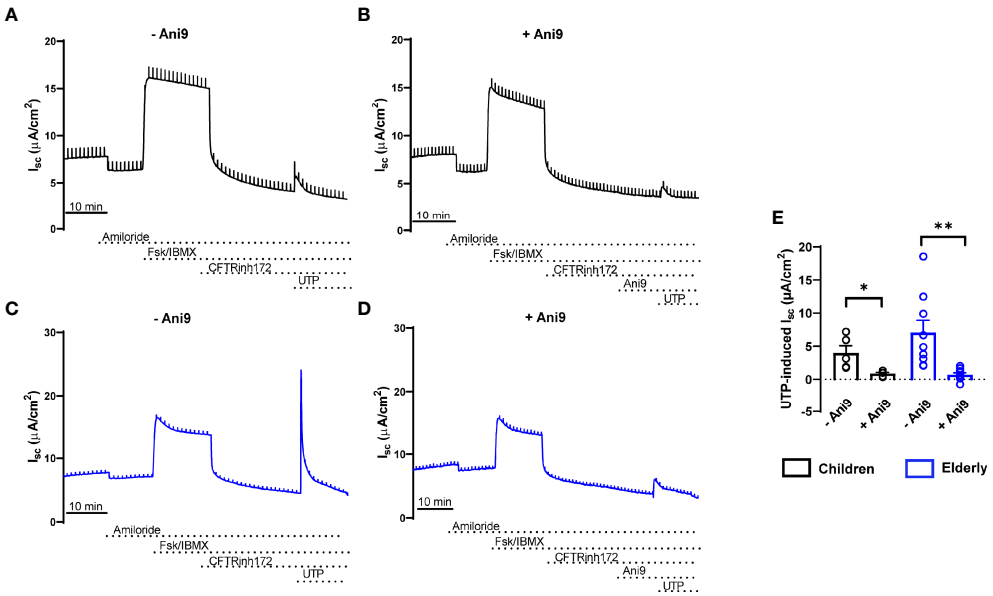

FIGURE 3 | Age-related differences in calcium-activated chloride secretion in nasal epithelial cultures are mediated by TMEM16A. **(A–E)** Representative original recordings and summary data of transepithelial Ussing chamber measurements in primary nasal epithelial cultures from healthy children **(A, B, E)** and elderly people **(C–E)** showing the effect of UTP-induced I_{SC} in the absence **(A, C, E)** and presence **(B, D, E)** of the TMEM16A inhibitor Ani9 (n = 4 and 9 individuals per group, data represent mean values of 2–3 filters per individual). *$p < 0.05$ and **$p < 0.01$ compared to Ani9- group. Data are shown as mean ± S.E.M. Statistical analysis was performed with paired two-tailed t test in **(E)**.

data provide novel insights into aging of the airway epithelium and may aid our understanding of its role in the pathogenesis of age-dependent phenotypes observed in a spectrum of acute and chronic airways diseases.

In our study, we used highly differentiated primary epithelial cultures from brushed cells collected by a non-invasive sampling technique, which enabled the comparison of healthy children and elderly people. Our morphological analysis revealed a lower number of ciliated cells and higher levels of $MUC5AC^+$ secretory cells in children, suggesting that the differentiation and cell-type composition of nasal epithelial cultures are age-dependent (**Figure 1**). These observations are in line with data from a recent single-cell RNA sequencing study that showed lower number of ciliated cells and higher amount of goblet cells in nasal brushes from children vs. adults (20). In the same report, epithelial cells from children displayed a pre-activated innate response profile, which is concordant with our findings of elevated immune cell–epithelial cell interaction signatures in children vs. elderly people by proteome analysis (**Figure 4**, **Supplementary Table 3** and **Supplementary Figure 4**). Age-related changes in airway epithelial cell lineages are further supported by another study describing a higher ciliated cell-to-club cell ratio in aged mice (52). The molecular basis of enhanced ciliary differentiation with advanced age and its role in airway homeostasis remain unknown. We speculate that a higher density of ciliated cells may help to maintain effective MCC in the aging airways. When viewed in combination, these studies indicate that our *in vitro* cultures retained age-dependent *in vivo* characteristics, supporting the relevance of this model system.

Our electrophysiological studies showed an overall similar transepithelial ion transport profile of nasal epithelial cultures from children and elderly people. Specifically, we did not find evidence of age-dependent differences in basal bioelectric properties, ENaC-mediated sodium absorption, or CFTR-mediated anion secretion across the nasal epithelium (**Figure 2**). However, we found selective upregulation of UTP-induced chloride secretory responses in the elderly group (**Figures 2**, **3**). A direct role of TMEM16A was supported by pharmacological inhibition of UTP-responses by the TMEM16A inhibitor Ani9 (**Figure 3**) (53, 54). These data suggest that calcium-activated chloride/fluid secretion and airway surface liquid regulation *via* TMEM16A may be more relevant in the airways at older age. However, the functional relevance of this finding needs to be tested in future studies.

Our proteome analysis provided independent evidence of substantial age-dependent differences in airway epithelial structure and function in children compared to elderly people. Consistent with our morphological analysis, an upregulation of ciliated cell markers (AGR3 and CAPS), axoneme components (DYNLL1, IFT43, and IFT80), and enrichment of cilia-related pathways was characteristic of the epithelial proteome of elderly people (**Figures 1**, **4**) (55). We also observed a decreased expression of basal cell markers in the elderly proteome, suggesting cellular senescence, a well-known hallmark of aging (56, 57). Furthermore, we found significantly increased expression of the cyclin-dependent kinase inhibitor CDKN1B (p27) in elderly, a known inducer of the senescence cell cycle arrest (58). While MUC5AC was below the detection limit in the

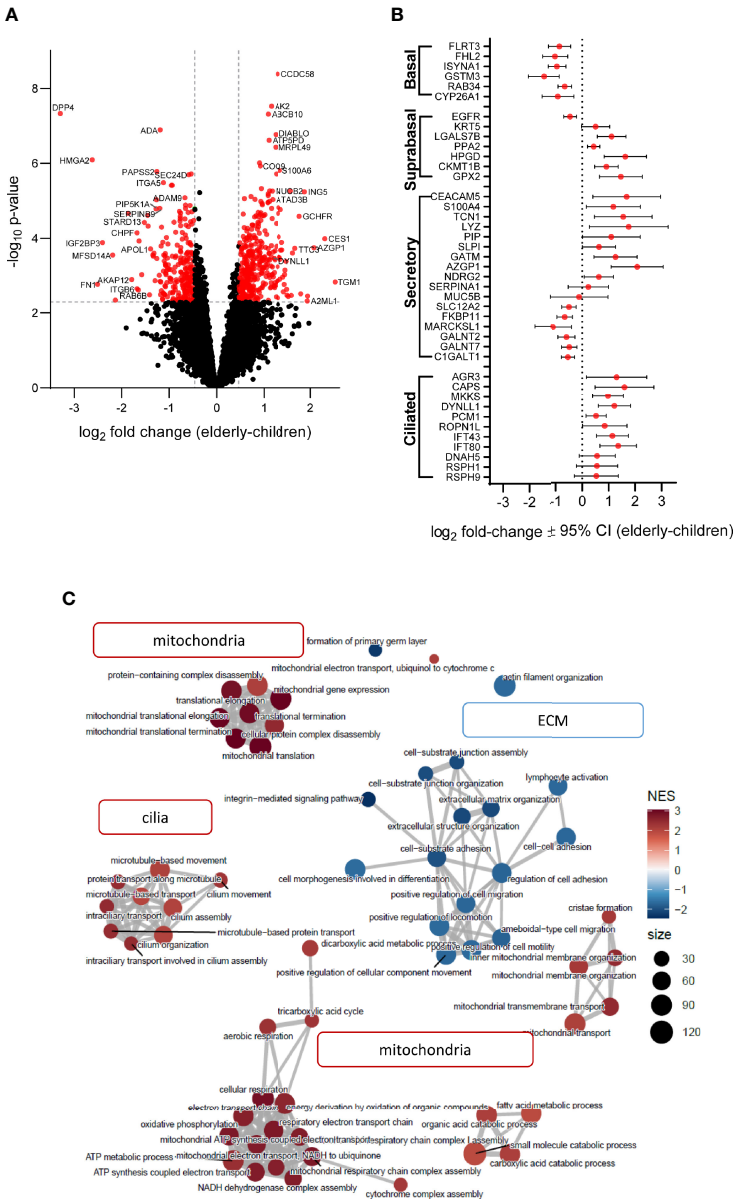

FIGURE 4 | Age-related differences in proteome signatures of nasal epithelial cultures from healthy children compared to elderly people. **(A)** Differential protein expression between age groups with reference to children (volcano plot) illustrates fold-change expression (log_2 scaling) and significance ($-log_{10}$ scaling, adjusted *p*-value). Significantly differently abundant proteins are colored red (adjusted *p*-value < 0.05 and fold-change > 1.38). **(B)** Protein expression of airway cell subtype markers. The log_2 fold-change with 95% confidence interval (CI) of detected proteins for each marker is plotted on the *x*-axis. **(C)** Enrichment map of top 60 gene ontology/biological process terms yielded by GSEA. Each node corresponds to a gene set with either high (red) or low (blue) normalized enrichment score (NES) in the elderly group. Node size correlates with number of genes that are annotated to the term.

proteome analysis, we found an upregulation of proteins related to mucin glycosylation (C1GALT1, GALNT2, and GALNT7) and mucin secretion (SLC12A2 and IL1R1) in children, in agreement with the observed increase of MUC5AC by Western blot (59, 60). Consistent with enhanced MUC5AC production, we also observed increased type-2 inflammatory response signature in children (**Supplementary Figure 4**). While mucin-related genes were elevated, markers associated with serous cells (LYZ and PIP) and anti-microbial secreted proteins (SLPI and CLU) had decreased levels in children (**Supplementary Figure 4**). To the best of our knowledge, changes in MUC5AC expression have not been reported in the context of aging. However, this finding may contribute to the age-dependent predisposition to certain muco-obstructive diseases, such as allergen-induced asthma in children where MUC5AC has been implicated in the pathogenesis of asthma severity, compared to COPD in elderly patients that is characterized predominately by an increase in MUC5B (61–63). Interestingly, we observed a

strong increase in mitochondria-related proteins and pathways in nasal cultures from elderly people. While higher abundance of ciliated cells in the elderly may be associated with higher energy expenditure (64), we also found enrichment of glycolytic pathways in children (**Supplementary Figure 4**), which may suggest a shift towards oxidative phosphorylation with aging, which would be similar to metabolic changes described in the aging brain and muscle tissue (65, 66). Increased mitochondrial mass and mitochondrial dysfunction, accompanied by increased generation of reactive oxygen species (ROS), are also markers of cellular senescence (67, 68). We found that not only mitochondrial proteins were upregulated in the elderly, but also a number of enzymes with antioxidant functions were increased, including the mitochondrial superoxide dismutase SOD1 (**Supplementary Figure 4**), suggesting an adaptive response to dampen the oxidative phenotype of cellular senescence and aging (69, 70). While we observed markers associated with increased cellular senescence in the elderly as compared to children, future studies should determine its role in the aging epithelium.

Although we could link our morphological observations with proteome data, we did not find evidence for differences in purinergic receptor activation or calcium signaling pathways that may explain our functional findings. This is likely related to the low abundance of regulatory proteins in those signaling cascades as well as the limitations of the global proteomics approach to capture post-translational modifications that govern many signaling events (71). However, mitochondria are known to play a role in the compartmentalization of calcium signals upon P2Y2-receptor stimulation in airway epithelial cells, by acting as a calcium-buffering system (72). It is possible that aging-associated mitochondrial dysfunction may disrupt the spatiotemporal fine-tuning of intracellular calcium levels, leading to enhanced calcium-activated chloride secretion by TMEM16A.

In summary, this is the first study describing age-dependent structural and functional differences in highly differentiated human primary nasal epithelial cultures, including an in-depth comparison by proteome analysis. We observed lower abundance of ciliated cells and higher expression of MUC5AC in children vs. elderly people, which correlated with age-dependent proteome signatures. Ion transport studies showed overall similarities in ENaC and CFTR function, with lower TMEM16A-mediated chloride secretion in children. These data indicate intrinsic, age-related phenotypic differences in the airway epithelium, which may help to better understand the effect of aging on innate mucosal defense and age-dependent airways disease phenotypes. Further work is needed to identify the underlying mechanisms and clinical relevance of these findings.

DATA AVAILABILITY STATEMENT

The datasets presented in this study can be found in online repositories. The names of the repository/repositories and accession number(s) can be found below: ProteomeXchange, accession no: PXD030130

ETHICS STATEMENT

The studies involving human participants were reviewed and approved by the ethics committee at the Charité-Universitätsmedizin Berlin (EA2/066/20). Written informed consent to participate in this study was provided by the participants' legal guardian/next of kin.

AUTHOR CONTRIBUTIONS

Conception and design of the study: AB, PM-B, and MaM. Acquisition, analysis, and interpretation of data: all authors. Drafting the article or revising it critically for important intellectual content: all authors. All authors contributed to the article and approved the submitted version.

FUNDING

This study was supported by grants from the German Federal Ministry of Education and Research (RECAST 01IK20337, NUM-COVID 19 Organo-Strat 01KX2021, and 82DZL009B1) and the German Research Foundation (CRC 1449–431232613 A01 and Z02 and project no. 450557679).

ACKNOWLEDGMENTS

We thank Dr. Victor M. Corman and Dr. Leif E. Sander for their contribution as principal investigators of the RECAST consortium. We are also indebted to Dr. Clara Correia-Melo for her scientific advice and editing assistance.

SUPPLEMENTARY MATERIAL

The Supplementary Material for this article can be found online at: https://www.frontiersin.org/articles/10.3389/fimmu.2022.822437/full#supplementary-material

REFERENCES

1. Whitsett JA, Alenghat T. Respiratory Epithelial Cells Orchestrate Pulmonary Innate Immunity. *Nat Immunol* (2015) 16:27–35. doi: 10.1038/ni.3045
2. Hewitt RJ, Lloyd CM. Regulation of Immune Responses by the Airway Epithelial Cell Landscape. *Nat Rev Immunol* (2021) 21:347–62. doi: 10.1038/s41577-020-00477-9
3. Knowles MR, Boucher RC. Mucus Clearance as a Primary Innate Defense Mechanism for Mammalian Airways. *J Clin Invest* (2002) 109:571–7. doi: 10.1172/JCI15217
4. Mall MA. Role of Cilia, Mucus, and Airway Surface Liquid in Mucociliary Dysfunction: Lessons From Mouse Models. *J Aerosol Med Pulm Drug Delivery* (2008) 21:13–24. doi: 10.1089/jamp.2007.0659

5. Benam KH, Vladar EK, Janssen WJ, Evans CM. Mucociliary Defense: Emerging Cellular, Molecular, and Animal Models. *Ann Am Thorac Soc* (2018) 15:S210–5. doi: 10.1513/AnnalsATS.201806-439AW
6. Boucher RC. Muco-Obstructive Lung Diseases. *N Engl J Med* (2019) 380:1941–53. doi: 10.1056/NEJMra1813799
7. Fahy JV, Dickey BF. Airway Mucus Function and Dysfunction. *N Engl J Med* (2010) 363:2233–47. doi: 10.1056/NEJMra0910061
8. Gentzsch M, Mall MA. Ion Channel Modulators in Cystic Fibrosis. *Chest* (2018) 154:383–93. doi: 10.1016/j.chest.2018.04.036
9. Webster MJ, Tarran R. Slippery When Wet: Airway Surface Liquid Homeostasis and Mucus Hydration. *Curr Top Membr* (2018) 81:293–335. doi: 10.1016/bs.ctm.2018.08.004
10. Bustamante-Marin XM, Ostrowski LE. Cilia and Mucociliary Clearance. *Cold Spring Harb Perspect Biol* (2017) 9:a028241. doi: 10.1101/cshperspect.a028241
11. Demouveaux B, Gouyer V, Gottrand F, Narita T, Desseyn J-L. Gel-Forming Mucin Interactome Drives Mucus Viscoelasticity. *Adv Colloid Interface Sci* (2018) 252:69–82. doi: 10.1016/j.cis.2017.12.005
12. Zhou-Suckow Z, Duerr J, Hagner M, Agrawal R, Mall MA. Airway Mucus, Inflammation and Remodeling: Emerging Links in the Pathogenesis of Chronic Lung Diseases. *Cell Tissue Res* (2017) 367:537–50. doi: 10.1007/s00441-016-2562-z
13. Hall CB. Respiratory Syncytial Virus and Parainfluenza Virus. *N Engl J Med* (2001) 344:1917–28. doi: 10.1056/NEJM200106213442507
14. Mall MA, Harkema JR, Trojanek JB, Treis D, Livraghi A, Schubert S, et al. Development of Chronic Bronchitis and Emphysema in Beta-Epithelial Na+ Channel-Overexpressing Mice. *Am J Respir Crit Care Med* (2008) 177:730–42. doi: 10.1164/rccm.200708-1233OC
15. Seys LJM, Verhamme FM, Dupont LL, Desauter E, Duerr J, Seyhan Agircan A, et al. Airway Surface Dehydration Aggravates Cigarette Smoke-Induced Hallmarks of COPD in Mice. *PloS One* (2015) 10:e0129897. doi: 10.1371/journal.pone.0129897
16. Jia J, Conlon TM, Ballester Lopez C, Seimetz M, Bednorz M, Zhou-Suckow Z, et al. Cigarette Smoke Causes Acute Airway Disease and Exacerbates Chronic Obstructive Lung Disease in Neonatal Mice. *Am J Physiol-Lung Cell Mol Physiol* (2016) 311:L602–10. doi: 10.1152/ajplung.00124.2016
17. Fritzsching B, Hagner M, Dai L, Christochowitz S, Agrawal R, van Bodegom C, et al. Impaired Mucus Clearance Exacerbates Allergen-Induced Type 2 Airway Inflammation in Juvenile Mice. *J Allergy Clin Immunol* (2017) 140:190–203.e5. doi: 10.1016/j.jaci.2016.09.045
18. Duerr J, Leitz DHW, Szczygiel M, Dvornikov D, Fraumann SG, Kreutz C, et al. Conditional Deletion of Nedd4-2 in Lung Epithelial Cells Causes Progressive Pulmonary Fibrosis in Adult Mice. *Nat Commun* (2020) 11:2012. doi: 10.1038/s41467-020-15743-6
19. Leitz DHW, Duerr J, Mulugeta S, Seyhan Agircan A, Zimmermann S, Kawabe H, et al. Congenital Deletion of Nedd4-2 in Lung Epithelial Cells Causes Progressive Alveolitis and Pulmonary Fibrosis in Neonatal Mice. *Int J Mol Sci* (2021) 22:6146. doi: 10.3390/ijms22116146
20. Loske J, Röhmel J, Lukassen S, Stricker S, Magalhães VG, Liebig J, et al. Pre-Activated Antiviral Innate Immunity in the Upper Airways Controls Early SARS-CoV-2 Infection in Children. *Nat Biotechnol* (2021), 1–6. doi: 10.1038/s41587-021-01037-9
21. Awatade NT, Wong SL, Hewson CK, Fawcett LK, Kicic A, Jaffe A, et al. Human Primary Epithelial Cell Models: Promising Tools in the Era of Cystic Fibrosis Personalized Medicine. *Front Pharmacol* (2018) 9:1429:1429. doi: 10.3389/fphar.2018.01429
22. Kreda SM, Mall M, Mengos A, Rochelle L, Yankaskas J, Riordan JR, et al. Characterization of Wild-Type and Deltaf508 Cystic Fibrosis Transmembrane Regulator in Human Respiratory Epithelia. *Mol Biol Cell* (2005) 16:2154–67. doi: 10.1091/mbc.e04-11-1010
23. Mall MA, Button B, Johannesson B, Zhou Z, Livraghi A, Caldwell RA, et al. Airway Surface Liquid Volume Regulation Determines Different Airway Phenotypes in Liddle Compared With Betaenac-Overexpressing Mice. *J Biol Chem* (2010) 285:26945–55. doi: 10.1074/jbc.M110.151803
24. Salomon JJ, Albrecht T, Graeber SY, Scheuermann H, Butz S, Schatterny J, et al. Chronic Rhinosinusitis With Nasal Polyps Is Associated With Impaired TMEM16A-Mediated Epithelial Chloride Secretion. *J Allergy Clin Immunol* (2021) 147:2191–2201.e2. doi: 10.1016/j.jaci.2021.02.008
25. Gentzsch M, Boyles SE, Cheluvaraju C, Chaudhry IG, Quinney NL, Cho C, et al. Pharmacological Rescue of Conditionally Reprogrammed Cystic Fibrosis Bronchial Epithelial Cells. *Am J Respir Cell Mol Biol* (2017) 56:568–74. doi: 10.1165/rcmb.2016-0276MA
26. Mall MA, Hartl D. CFTR: Cystic Fibrosis and Beyond. *Eur Respir J* (2014) 44:1042–54. doi: 10.1183/09031936.00228013
27. Mall MA, Mayer-Hamblett N, Rowe SM. Cystic Fibrosis: Emergence of Highly Effective Targeted Therapeutics and Potential Clinical Implications. *Am J Respir Crit Care Med* (2020) 201:1193–208. doi: 10.1164/rccm.201910-1943SO
28. Carson JL, Lu T-S, Brighton L, Hazucha M, Jaspers I, Zhou H. Phenotypic and Physiologic Variability in Nasal Epithelium Cultured From Smokers and non-Smokers Exposed to Secondhand Tobacco Smoke. *In Vitro Cell Dev Biol Anim* (2010) 46:606–12. doi: 10.1007/s11626-010-9310-6
29. Bai J, Smock SL, Jackson GR, MacIsaac KD, Huang Y, Mankus C, et al. Phenotypic Responses of Differentiated Asthmatic Human Airway Epithelial Cultures to Rhinovirus. *PloS One* (2015) 10:e0118286. doi: 10.1371/journal.pone.0118286
30. Chason KD, Jaspers I, Parker J, Sellers S, Brighton LE, Hunsucker SA, et al. Age-Associated Changes in the Respiratory Epithelial Response to Influenza Infection. *J Gerontol: Ser A* (2018) 73:1643–50. doi: 10.1093/gerona/gly126
31. Moheimani F, Koops J, Williams T, Reid AT, Hansbro PM, Wark PA, et al. Influenza A Virus Infection Dysregulates the Expression of microRNA-22 and its Targets; CD147 and HDAC4, in Epithelium of Asthmatics. *Respir Res* (2018) 19:145. doi: 10.1186/s12931-018-0851-7
32. Schindelin J, Arganda-Carreras I, Frise E, Kaynig V, Longair M, Pietzsch T, et al. Fiji: An Open-Source Platform for Biological-Image Analysis. *Nat Methods* (2012) 9:676–82. doi: 10.1038/nmeth.2019
33. Pfaffl MW. A New Mathematical Model for Relative Quantification in Real-Time RT–PCR. *Nucleic Acids Res* (2001) 29:e45–5. doi: 10.1093/nar/29.9.e45
34. Ramsey KA, Rushton ZL, Ehre C. Mucin Agarose Gel Electrophoresis: Western Blotting for High-Molecular-Weight Glycoproteins. *J Vis Exp* (2016):54153. doi: 10.3791/54153
35. Yankaskas JR, Cotton CU, Knowles MR, Gatzy JT, Boucher RC. Culture of Human Nasal Epithelial Cells on Collagen Matrix Supports. A Comparison of Bioelectric Properties of Normal and Cystic Fibrosis Epithelia. *Am Rev Respir Dis* (1985) 132:1281–7. doi: 10.1164/arrd.1985.132.6.1281
36. Salomon JJ, Spahn S, Wang X, Füllekrug J, Bertrand CA, Mall MA. Generation and Functional Characterization of Epithelial Cells With Stable Expression of SLC26A9 Cl- Channels. *Am J Physiol Lung Cell Mol Physiol* (2016) 310:L593–602. doi: 10.1152/ajplung.00321.2015
37. Müller T, Kalxdorf M, Longuespée R, Kazdal DN, Stenzinger A, Krijgsveld J. Automated Sample Preparation With SP3 for Low-Input Clinical Proteomics. *Mol Syst Biol* (2020) 16:e9111. doi: 10.15252/msb.20199111
38. Meier F, Brunner A-D, Frank M, Ha A, Bludau I, Voytik E, et al. diaPASEF: Parallel Accumulation–Serial Fragmentation Combined With Data-Independent Acquisition. *Nat Methods* (2020) 17:1229–36. doi: 10.1038/s41592-020-00998-0
39. Demichev V, Messner CB, Vernardis SI, Lilley KS, Ralser M. DIA-NN: Neural Networks and Interference Correction Enable Deep Proteome Coverage in High Throughput. *Nat Methods* (2020) 17:41–4. doi: 10.1038/s41592-019-0638-x
40. Demichev V, Yu F, Teo GC, Szyrwiel L, Rosenberger GA, Decker J, et al. *High Sensitivity Dia-PASEF Proteomics With DIA-NN and FragPipe* (2021). Available at: https://www.biorxiv.org/content/10.1101/2021.03.08.434385v1 (Accessed November 17, 2021).
41. UniProt Consortium. UniProt: A Worldwide Hub of Protein Knowledge. *Nucleic Acids Res* (2019) 47:D506–15. doi: 10.1093/nar/gky1049
42. Josse J, Husson F. missMDA: A Package for Handling Missing Values in Multivariate Data Analysis. *J Stat Software* (2016) 70:1–31. doi: 10.18637/jss.v070.i01
43. Ritchie ME, Phipson B, Wu D, Hu Y, Law CW, Shi W, et al. Limma Powers Differential Expression Analyses for RNA-Sequencing and Microarray Studies. *Nucleic Acids Res* (2015) 43:e47. doi: 10.1093/nar/gkv007
44. Bolstad BM, Irizarry RA, Astrand M, Speed TP. A Comparison of Normalization Methods for High Density Oligonucleotide Array Data Based on Variance and Bias. *Bioinformatics* (2003) 19:185–93. doi: 10.1093/bioinformatics/19.2.185
45. Ballman KV, Grill DE, Oberg AL, Therneau TM. Faster Cyclic Loess: Normalizing RNA Arrays *via* Linear Models. *Bioinformatics* (2004) 20:2778–86. doi: 10.1093/bioinformatics/bth327
46. Cox J, Hein MY, Luber CA, Paron I, Nagaraj N, Mann M. Accurate Proteome-Wide Label-Free Quantification by Delayed Normalization and Maximal

Peptide Ratio Extraction, Termed MaxLFQ. *Mol Cell Proteomics* (2014) 13:2513–26. doi: 10.1074/mcp.M113.031591
47. Pham TV, Henneman AA, Jimenez CR. Iq: An R Package to Estimate Relative Protein Abundances From Ion Quantification in DIA-MS-Based Proteomics. *Bioinformatics* (2020) 36:2611–3. doi: 10.1093/bioinformatics/btz961
48. Lê S, Josse J, Husson F. FactoMineR: An R Package for Multivariate Analysis. *J Stat Software* (2008) 25:1–18. doi: 10.18637/jss.v025.i01
49. Benjamini Y, Hochberg Y. Controlling the False Discovery Rate: A Practical and Powerful Approach to Multiple Testing. *J R Stat Society Ser B (Methodological)* (1995) 57:289–300. doi: 10.1111/j.2517-6161.1995.tb02031.x
50. Yu G, Wang L-G, Han Y, He Q-Y. Clusterprofiler: An R Package for Comparing Biological Themes Among Gene Clusters. *OMICS* (2012) 16:284–7. doi: 10.1089/omi.2011.0118
51. Deprez M, Zaragosi L-E, Truchi M, Becavin C, Ruiz García S, Arguel M-J, et al. A Single-Cell Atlas of the Human Healthy Airways. *Am J Respir Crit Care Med* (2020) 202:1636–45. doi: 10.1164/rccm.201911-2199OC
52. Angelidis I, Simon LM, Fernandez IE, Strunz M, Mayr CH, Greiffo FR, et al. An Atlas of the Aging Lung Mapped by Single Cell Transcriptomics and Deep Tissue Proteomics. *Nat Commun* (2019) 10:963. doi: 10.1038/s41467-019-08831-9
53. Scudieri P, Sondo E, Ferrera L, Galietta LJV. The Anoctamin Family: TMEM16A and TMEM16B as Calcium-Activated Chloride Channels. *Exp Physiol* (2012) 97:177–83. doi: 10.1113/expphysiol.2011.058198
54. Danahay HL, Lilley S, Fox R, Charlton H, Sabater J, Button B, et al. TMEM16A Potentiation: A Novel Therapeutic Approach for the Treatment of Cystic Fibrosis. *Am J Respir Crit Care Med* (2020) 201:946–54. doi: 10.1164/rccm.201908-1641OC
55. Patir A, Fraser AM, Barnett MW, McTeir L, Rainger J, Davey MG, et al. The Transcriptional Signature Associated With Human Motile Cilia. *Sci Rep* (2020) 10:10814. doi: 10.1038/s41598-020-66453-4
56. López-Otín C, Blasco MA, Partridge L, Serrano M, Kroemer G. The Hallmarks of Aging. *Cell* (2013) 153:1194–217. doi: 10.1016/j.cell.2013.05.039
57. Meiners S, Eickelberg O, Königshoff M. Hallmarks of the Ageing Lung. *Eur Respir J* (2015) 45:807–27. doi: 10.1183/09031936.00186914
58. Pruitt SC, Freeland A, Rusiniak ME, Kunnev D, Cady GK. Cdkn1b Overexpression in Adult Mice Alters the Balance Between Genome and Tissue Ageing. *Nat Commun* (2013) 4:2626. doi: 10.1038/ncomms3626
59. Wang G, Xu Z, Wang R, Al-Hijji M, Salit J, Strulovici-Barel Y, et al. Genes Associated With MUC5AC Expression in Small Airway Epithelium of Human Smokers and non-Smokers. *BMC Med Genomics* (2012) 5:21. doi: 10.1186/1755-8794-5-21
60. Chen G, Sun L, Kato T, Okuda K, Martino MB, Abzhanova A, et al. IL-1β Dominates the Promucin Secretory Cytokine Profile in Cystic Fibrosis. *J Clin Invest* (2019) 129:4433–50. doi: 10.1172/JCI125669
61. Kirkham S, Kolsum U, Rousseau K, Singh D, Vestbo J, Thornton DJ. MUC5B Is the Major Mucin in the Gel Phase of Sputum in Chronic Obstructive Pulmonary Disease. *Am J Respir Crit Care Med* (2008) 178:1033–9. doi: 10.1164/rccm.200803-391OC
62. Evans CM, Raclawska DS, Ttofali F, Liptzin DR, Fletcher AA, Harper DN, et al. The Polymeric Mucin Muc5ac Is Required for Allergic Airway Hyperreactivity. *Nat Commun* (2015) 6:6281. doi: 10.1038/ncomms7281
63. Livraghi-Butrico A, Grubb BR, Wilkinson KJ, Volmer AS, Burns KA, Evans CM, et al. Contribution of Mucus Concentration and Secreted Mucins Muc5ac and Muc5b to the Pathogenesis of Muco-Obstructive Lung Disease. *Mucosal Immunol* (2017) 10:395–407. doi: 10.1038/mi.2016.63
64. Villar PS, Vergara C, Bacigalupo J. Energy Sources That Fuel Metabolic Processes in Protruding Finger-Like Organelles. *FEBS J* (2021) 288:3799–812. doi: 10.1111/febs.15620
65. Lanza IR, Befroy DE, Kent-Braun JA. Age-Related Changes in ATP-Producing Pathways in Human Skeletal Muscle *In Vivo*. *J Appl Physiol (1985)* (2005) 99:1736–44. doi: 10.1152/japplphysiol.00566.2005
66. Goyal MS, Vlassenko AG, Blazey TM, Su Y, Couture LE, Durbin TJ, et al. Loss of Brain Aerobic Glycolysis in Normal Human Aging. *Cell Metab* (2017) 26:353–360.e3. doi: 10.1016/j.cmet.2017.07.010
67. Passos JF, Nelson G, Wang C, Richter T, Simillion C, Proctor CJ, et al. Feedback Between P21 and Reactive Oxygen Production Is Necessary for Cell Senescence. *Mol Syst Biol* (2010) 6:347. doi: 10.1038/msb.2010.5
68. Correia-Melo C, Marques FDM, Anderson R, Hewitt G, Hewitt R, Cole J, et al. Mitochondria Are Required for Pro-Ageing Features of the Senescent Phenotype. *EMBO J* (2016) 35:724–42. doi: 10.15252/embj.201592862
69. Allen RG, Tresini M, Keogh BP, Doggett DL, Cristofalo VJ. Differences in Electron Transport Potential, Antioxidant Defenses, and Oxidant Generation in Young and Senescent Fetal Lung Fibroblasts (WI-38). *J Cell Physiol* (1999) 180:114–22. doi: 10.1002/(SICI)1097-4652(199907)180:1<114::AID-JCP13>3.0.CO;2-0
70. Zhang Y, Unnikrishnan A, Deepa SS, Liu Y, Li Y, Ikeno Y, et al. A New Role for Oxidative Stress in Aging: The Accelerated Aging Phenotype in Sod1-/- Mice Is Correlated to Increased Cellular Senescence. *Redox Biol* (2017) 11:30–7. doi: 10.1016/j.redox.2016.10.014
71. Harsha HC, Pinto SM, Pandey A. Proteomic Strategies to Characterize Signaling Pathways. *Methods Mol Biol* (2013) 1007:359–77. doi: 10.1007/978-1-62703-392-3_16
72. Ribeiro CMP, Paradiso AM, Livraghi A, Boucher RC. The Mitochondrial Barriers Segregate Agonist-Induced Calcium-Dependent Functions in Human Airway Epithelia. *J Gen Physiol* (2003) 122:377–87. doi: 10.1085/jgp.200308893

Conflict of Interest: The authors declare that the research was conducted in the absence of any commercial or financial relationships that could be construed as a potential conflict of interest.

Publisher's Note: All claims expressed in this article are solely those of the authors and do not necessarily represent those of their affiliated organizations, or those of the publisher, the editors and the reviewers. Any product that may be evaluated in this article, or claim that may be made by its manufacturer, is not guaranteed or endorsed by the publisher.

frontiers in Immunology

ORIGINAL RESEARCH
published: 08 March 2022
doi: 10.3389/fimmu.2022.740513

Machine-Learning Algorithm-Based Prediction of Diagnostic Gene Biomarkers Related to Immune Infiltration in Patients With Chronic Obstructive Pulmonary Disease

Yuepeng Zhang[1], Rongyao Xia[2], Meiyu Lv[1], Zhiheng Li[3], Lingling Jin[1], Xueda Chen[1], Yaqian Han[4], Chunpeng Shi[5], Yanan Jiang[5,6] and Shoude Jin[1]**

[1] Department of Respiratory Medicine, The Fourth Hospital of Harbin Medical University, Harbin, China, [2] Department of Respiratory Medicine, The Second Hospital of Harbin Medical University, Harbin, China, [3] Department of Medical Oncology, The Fourth Hospital of Harbin Medical University, Harbin, China, [4] School of Instrumentation Science and Engineering, Harbin Institute of Technology, Harbin, China, [5] Department of Pharmacology, State-Province Key Laboratories of Biomedicine-Pharmaceutics of China, Key Laboratory of Cardiovascular Research, Ministry of Education, College of Pharmacy, Harbin Medical University, Harbin, China, [6] Translational Medicine Research and Cooperation Center of Northern China, Heilongjiang Academy of Medical Sciences, Harbin, China

OPEN ACCESS

Edited by:
Wendy W. J. Unger, Erasmus MC-Sophia Children's Hospital, Netherlands

Reviewed by:
Rosalinda Sorrentino, University of Salerno, Italy
Yogesh Singh, University of Tübingen, Germany

***Correspondence:**
Shoude Jin
jinshoude@163.com
Yanan Jiang
jiangyanan@hrbmu.edu.cn

Specialty section:
This article was submitted to Mucosal Immunity, a section of the journal Frontiers in Immunology

Received: *13 July 2021*
Accepted: *11 February 2022*
Published: *08 March 2022*

Citation:
Zhang Y, Xia R, Lv M, Li Z, Jin L, Chen X, Han Y, Shi C, Jiang Y and Jin S (2022) Machine-Learning Algorithm-Based Prediction of Diagnostic Gene Biomarkers Related to Immune Infiltration in Patients With Chronic Obstructive Pulmonary Disease. Front. Immunol. 13:740513. doi: 10.3389/fimmu.2022.740513

Objective: This study aims to identify clinically relevant diagnostic biomarkers in chronic obstructive pulmonary disease (COPD) while exploring how immune cell infiltration contributes towards COPD pathogenesis.

Methods: The GEO database provided two human COPD gene expression datasets (GSE38974 and GSE76925; n=134) along with the relevant controls (n=49) for differentially expressed gene (DEG) analyses. Candidate biomarkers were identified using the support vector machine recursive feature elimination (SVM-RFE) analysis and the LASSO regression model. The discriminatory ability was determined using the area under the receiver operating characteristic curve (AUC) values. These candidate biomarkers were characterized in the GSE106986 dataset (14 COPD patients and 5 controls) in terms of their respective diagnostic values and expression levels. The CIBERSORT program was used to estimate patterns of tissue infiltration of 22 types of immune cells. Furthermore, the *in vivo* and *in vitro* model of COPD was established using cigarette smoke extract (CSE) to validated the bioinformatics results.

Results: 80 genes were identified *via* DEG analysis that were primarily involved in cellular amino acid and metabolic processes, regulation of telomerase activity and phagocytosis, antigen processing and MHC class I-mediated peptide antigen presentation, and other biological processes. LASSO and SVM-RFE were used to further characterize the candidate diagnostic markers for COPD, SLC27A3, and STAU1. SLC27A3 and STAU1 were found to be diagnostic markers of COPD in the metadata cohort (AUC=0.734, AUC=0.745). Their relevance in COPD were validated in the GSE106986 dataset (AUC=0.900 AUC=0.971). Subsequent analysis of immune cell infiltration discovered an

association between SLC27A3 and STAU1 with resting NK cells, plasma cells, eosinophils, activated mast cells, memory B cells, CD8+, CD4+, and helper follicular T-cells. The expressions of SLC27A3 and STAU1 were upregulated in COPD models both *in vivo* and *in vitro*. Immune infiltration activation was observed in COPD models, accompanied by the enhanced expression of SLC27A3 and STAU1. Whereas, the knockdown of SLC27A3 or STAU1 attenuated the effect of CSE on BEAS-2B cells.

Conclusion: STUA1 and SLC27A3 are valuable diagnostic biomarkers of COPD. COPD pathogenesis is heavily influenced by patterns of immune cell infiltration. This study provides a molecular biology insight into COPD occurrence and in exploring new therapeutic means useful in COPD.

Keywords: COPD, LASSO, SVM-RFE, STAU1, SLC27A3, immune infiltration

INTRODUCTION

Chronic obstructive pulmonary disease (COPD) is an extremely common debilitating ailment of the modern world and represents a slowly progressive destructive pulmonary disease that involves chronic inflammation (1). COPD is currently ranked as the fourth cause of death in the world and is common in both developed and developing countries (2, 3). Early COPD diagnosis and initiation of treatment are clinically important in improving prognosis and overall survival of COPD patients. COPD is definitively diagnosed with pulmonary function testing, which offers the advantage of being a simple and easily implemented measurement that accurately gauges the severity of COPD. A wide array of imaging modalities such as chest x-rays, magnetic resonance imaging (MRI), and computed tomography (CT) have further improved COPD diagnosis (4). However, due to sensitivity and specificity limitations, current diagnostic mechanisms are not well suited in detecting early COPD. COPD develops on well-established disease drivers such as genetic factors, a history of smoking, infection, and inflammation, along with an imbalance in protease and antiprotease expression (5). COPD is indeed a complex and multifactorial entity that arises due to an amalgamation of environmental and genetic influences (6).

In recent years, the application of microarray technology and integrated bioinformatics analyses have been used to identify novel diagnostic and prognostic genes (7–11). In the realm of COPD, for example, the ROBO2 and SLIT2 genes were founded to be downregulated in COPD and inversely correlated with COPD disease stage (12, 13). FHL1 expression was associated with cigarette smoke-induced COPD (14). Additionally, increasingly evidences highlight the importance of immune cell infiltration in generation progression of various diseases (7, 15–17). However, little is known about immune cell infiltration in COPD.

This investigation involves a metadata cohort comprising of 2 COPD microarray datasets extracted from the GEO database. Differentially expressed gene (DEG) analysis was then performed between healthy samples and in COPD samples. Potentially diagnostic COPD biomarkers were discerned using machine-learning algorithms which were then validated in a separate cohort, with a logistic regression method utilizing in constructing a diagnostic prediction model. Immune cell gene expression was analyzed using CIBERSORT which successfully identified and quantified various immune cells that infiltrated into the lung parenchyma in COPD and control samples. The relationship between immune cell infiltration and identified COPD biomarkers was also characterized.

MATERIALS AND METHODS

Data Collection and Download

COPD gene expression data collected from the GEO database (https://www.ncbi.nlm.nih.gov/geo/). The GSE38974, GSE76925, and GSE106986 datasets were downloaded. The GSE106986 dataset (14 COPD samples and 5 control samples) was derived from GPL13497 platform of the Agilent-026652 Whole Human Genome Microarray 4x44K v2. The GSE76925 dataset (111 COPD samples and 40 control samples) was derived from the GPL10558 platform of Illumina HumanHT-12 V4.0 expression beadchip. GSE38974 dataset (23 COPD samples and 9 control samples) was derived from the GPL4133 platform of the Agilent-014850 Whole Human Genome Microarray 4x44K G4112F. All samples from the 3 different databases were obtained from human lung tissue.

Data Preprocessing and Differentially Expressed Genes (DEGs) Screening

Each dataset was background corrected and normalized using the "limma" package and converted to gene symbols referencing the probe annotation files of the probe names in each dataset. A metadata cohort comprising of merged GSE38974 and GSE76925 cohorts was created for further analysis. Batch variability between platforms was eliminated using the combat function of the "SVA" package (18). The GSE106986 dataset was used as the validation cohort. Similarly, 134 COPD and 49 normal samples were analyzed for DEGs using the R package "limma" with DEGs selected based on thresholds of $P < 0.05$ and $|log2\ FC| > 1$.

Functional Enrichment Analysis

The Metascape (http://metascape.org) database allowed for further understanding of the DEG biological significance using Gene Ontology enrichment analysis. The Molecular Signatures Database (MSigDB) Hallmark Gene Sets and Kyoto Encyclopedia of Genes and Genomes (KEGG) Pathway were used for pathway enrichment analysis. Meanwhile, the most significant terms which arose in statistical analysis were selected for visualization.

Screening of Candidate Diagnostic Biomarkers

Two machine-learning algorithms, the support vector machine recursive feature elimination (SVM-RFE) and least absolute shrinkage and selection operator (LASSO) were used in this study to screen for significant prognostic variables. SVM-RFE represents a widely used supervised machine-learning protocol for classification and regression that is applied using the "e1071" package. The SVM-RFE algorithm was used to identify genes with higher discriminative power (19). LASSO was performed using the "glmnet" package in R and represents a regression analysis algorithm that applies regularization for variable selection. Using LASSO, we were able to identify genes significantly associated with COPD and normal samples. We applied two algorithms in the metadata cohort and utilized the GSE106986 dataset to analyze overlapping genes from the two algorithms to further validate the expression levels of candidate diagnostic biomarkers.

Evaluation of Immune Cell Infiltration

CIBERSORT is a deconvolution algorithm that quantifies immune cell infiltration (22 various cell types) in COPD gene expression profiles (20). The "corrplot" R package was used to carry out visualization and correlation analysis of 22 types of infiltrating immune cells. Differences in infiltrating immune cells between COPD and healthy samples were visualized using boxplots drawn with the "ggplot2" package in R.

Correlation Analysis Between Diagnostic Biomarkers and Infiltrating Immune Cells

Pearson correlation analysis allowed for in-depth scrutiny of relationships between diagnostic biological markers and infiltrating immune cells. "ggplot2" of the R package was used to visualize the results of the analysis.

The Establishment of COPD Model

Six-week-old C57BL/6 mice was used to establish the COPD model. The details procedure was as described by He et al. (21). Cigarette smoke extract (CSE) was prepared by dissolving the smoke of non-filter Furong cigarette in to PBS (21). The histological changes and immune infiltration of lung tissues were then detected (21, 22). Bronchoalveolar lavage fluid (BALF) was collected. Lung tissue was cut into small pieces and digested into single cell suspension by Collagenase A (4 mg/ml in RPMI1640) for further detection.

Histological Staining

After treatment, lung tissues were collected. Paraffin embeded lung tissues were cut into slices for histological staining. HE staining was performed according to the manufacturer's instructions (Solarbio). The mean alveolar septal thickness (MAST), mean linear intercept (MLI), and destructive index (DI) were calculated. Immunohistochemistry staining was conducted using primary antibodies for SLC27A3 (Proteintech), STAU1 (Affinity), CD57 (Affinity), and CD8a (Affinity). Immunofluorescence staining was performed using primary antibodies for CD19 (Affinity) and CD27 (Santa), and secondary antibodies including Cy3-labeled goat anti-rabbit IgG (Invitrogen) and FITC-labeled goat anti-mouse IgG (Abcam).

Cell Transfection and CCK-8 Assay

BEAS-2B cells were cultured in DMEM cultural medium (Servivebio) with 10% fetal bovine serum (EVERY GREEN) in an incubator (37°C and 5% CO_2). COPD cell model was induced by 5% CSE for 24 h (23). Small interfering RNAs targeting SLC27A3 (si-SLS27A3) and STAU1 (si-STAU1), as well was negative control RNA (si-NC) were transfected into BEAS-2B cells by Lipo 3000 (Invitrogen), respectively. CCK-8 assay kit (Wanleibio) was used to detect viability of BEAS-2B cells according to the manufacturer's instructions. The optical density was measured by a microplate reader (BIOTEK).

Western Blot Assay

Total protein was extracted from lung tissues and BEAS-2B cells by protein extraction kit (Wanleibio). The concentration of protein was detected by BCA kit (Wanleibio). The protein was separated by SDS-PAGE and transferred to PVDF membrane (Millipore). The membrane was blocked by non-fat milk and then incubated with primary antibodies for SLC27A3 (Proteintech), STAU1 (Affinity), ACPL2 (Bioss), RABL4 (Biorbyt), and β-actin (Wanleibio), respectively. After 12-h of incubation at 4°C, the membrane was washed, incubated by the secondary antibody, and visualized by CEL (Wanleibio). β-actin serves as an internal control.

Real-Time PCR Assay

Total RNA was extracted from lung tissues and BEAS-2B cells by TRIpure (BioTeke). The RNA was reverse transcribed into cDNA using BeyoRT™ II M-MLV RNase H- (Beyotime). Real-time PCR assay was conducted on Exicycler 96 system (BIONEER) using SYBR Green (Solarbio). The results was calculated using $2^{-\triangle\triangle CT}$ method. The primer sequences are as follows. Mus musculus ACPL2: F, AATCGCTTCTTGGTGCTG; R, CTACGCTTGGAATGTTGC. Mus musculus RABL4: F, GAAATGCTGGATAAGTTGTG; R, GAGGGAGATG CCTGAAGT. Mus musculus SLC27A3: F, GCATT GTGGGCTGCTTGG; R, GGGCTGGTTGACGAGGTAT. Mus musculus STAU1 F, GTAAAGAAACCAGGAGACG; R, CTGCTGATGGCTAAGATAA.

Mus musculus β-actin: F, CTGTGCCCATCTACG AGGGCTAT; R, TTTGATGTCACGCACGATTTCC. Homo sapiens ACPL2: F, ATGGAGCACTTCAAGGTAA; R,

AGCAGAGTAGAGGGCAAA. Homo sapiens RABL4: F, GG AATGGATTTGGTGGTGAA; R, GAGATGCCTGGAG CCTGTGA. Homo sapiens SLC27A3: F, GTTCGGAT GGCAAATGAGG; R, TGTACCGGGCAGTTGTGAG. Homo sapiens STAU1 F, ATCCGATTAGCCGACTGG; R, AC TTGAGTGCGGGTTTGG. Homo sapiens β-actin: F, GG CACCCAGCACAATGAA; R, TAGAAGCATTTGCGGTGG.

ELISA Assay

The concentration of IL-6, IL-1β, and TNFα was measured by ELISA. ELISA kits (Wanleibio) for IL-6, IL-1β, and TNFα were used in this study and conducted according to the manufacturer's instructions. The optical density was measured by a microplate reader (BIOTEK).

Statistical Analysis

All statistical analyses were performed in R (version 3.6.1). The nonparametric Kruskal-Wallis test was used to perform intergroup comparisons of continuous variables. The degree of efficacy of each diagnostic biomarker was assessed using receiver operating characteristic (ROC) curves. Pearson correlation was used to analyze the relationship between the expression of diagnostic biomarkers and infiltrating immune cells. Comparison between two groups or among multiple groups were analyzed by student t-test or one-way ANOVA, respectively. Statistical significance was identified based on $P < 0.05$. Furthermore, bioinformatics analysis almost run for two months.

RESULTS

Screening of DEGs in COPD

Differential expression analysis between 134 COPD samples and 49 normal samples in the metadata (GSE38974 and GSE76925) cohort was carried out utilizing the "limma" R package. Of the 80 identified DEGs, 4 genes were significantly upregulated and 76 genes were significantly downregulated (**Figure 1A**). The heatmap of DEGs is depicted in **Figure 1B**.

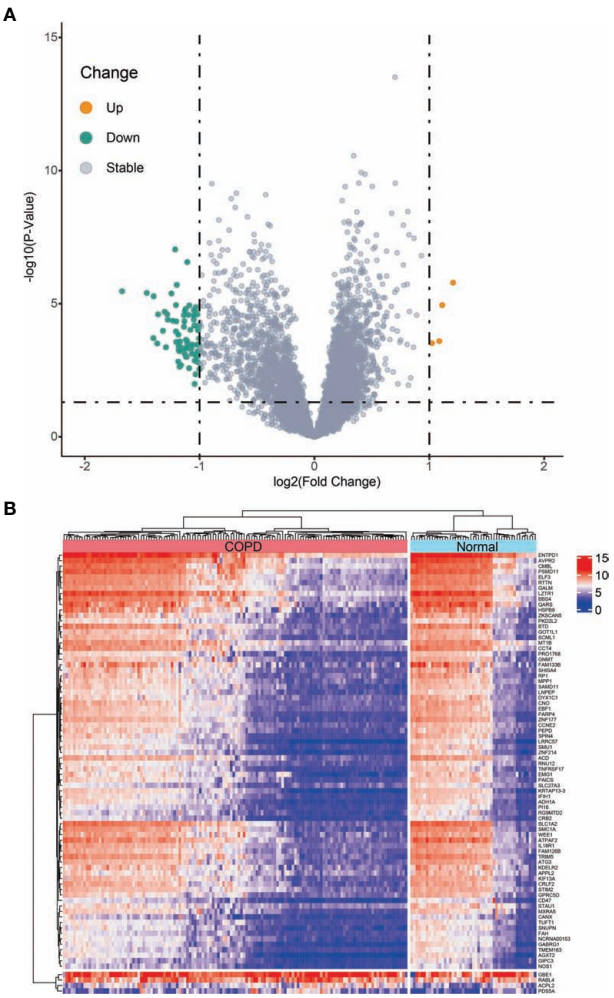

FIGURE 1 | Differentially expressed genes (DEGs) between chronic obstructive pulmonary disease tissues and normal samples in metadata (GSE38974 and GSE76925 datasets) cohort. **(A)** Volcano plot of DEGs; orange dots represent up-regulated differential genes, gray dots represent nonsignificant genes, and green dots represent down-regulated differential genes. **(B)** Heatmap plot of DEGs.

Functional Enrichment Analysis of DEGs

GO and pathway analyses were performed to identify the biological functions of DEG using the Metascape database. DEGs were primarily involved with telomerase regulation, cellular amino acid metabolic processes, multicellular organic homeostasis, MHC class I-mediated peptide antigen presentation and antigen processing in addition to various other biological processes (**Figure 2A**). Moreover, these DEGs were also mainly enriched in the S phase, TriC/CCT association with target proteins during biosynthesis and nucleotide metabolism pathways. **Figure 2B** shows the relationships between the enriched terms.

Identification and Verification of Diagnostic Biomarkers

Candidate diagnostic biomarkers were screened by two different algorithms. We utilized the LASSO logistic regression algorithm to identify and COPD related 5 feature variables from DEGs (**Figure 3A**). The SVM-RFE algorithm was used to identify a subset of 42 features in the determined DEGs (**Figure 3B**). 4 overlapping diagnostic related genes (ACPL2, RABL4, SLC27A3, and STAU1) of these two algorithms were finally selected (**Figure 3C**). The GSE106986 dataset was used to validate the accuracy of this method as well as the expression levels of the four candidate diagnostic biomarkers. ACPL2 and RABL4 expressions levels were not significantly different between COPD and normal samples (**Figures 4A, B**). However, the expression levels of SLC27A3 and STAU1 in COPD samples were notably raised in COPD samples in contrast to controls (**Figures 4C, D**; all $P < 0.05$). To further test the diagnostic efficacy of SLC27A3 and STAU1, we validated them using metadata and the GSE106986 dataset, respectively. The AUCs

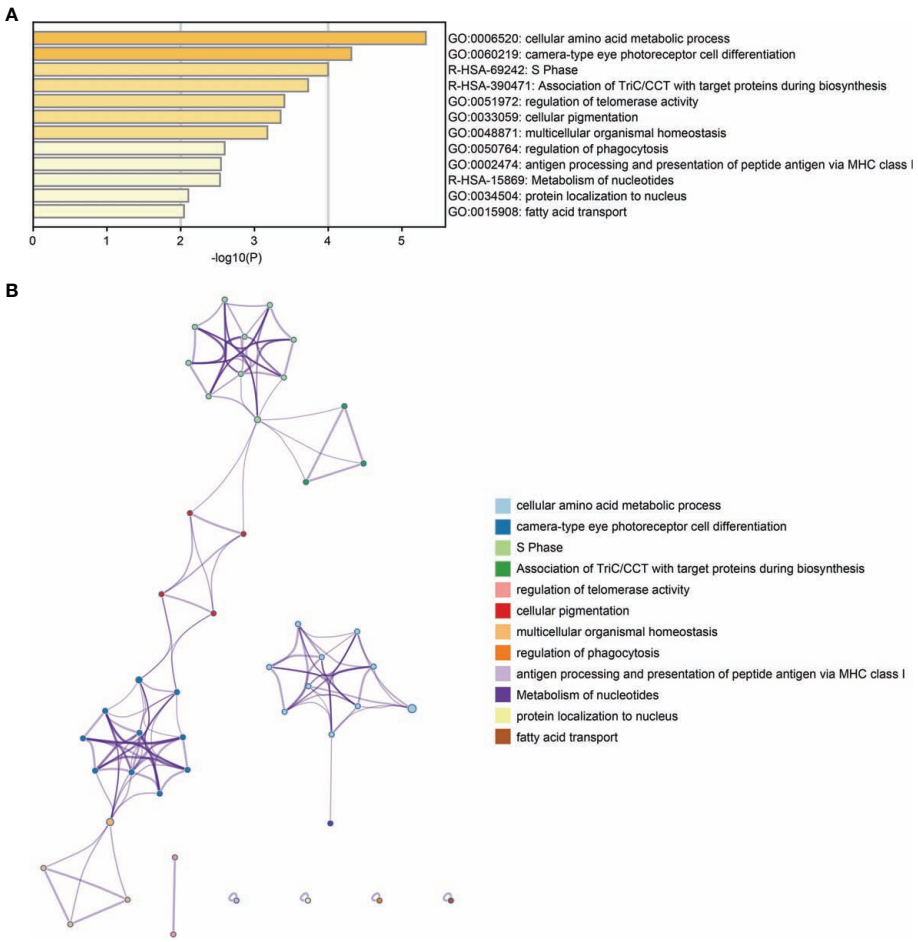

FIGURE 2 | Functional enrichment analysis of DEGs. **(A)** Bar plot of DEGs functional enrichment terms. **(B)** Network relationship plots among all terms.

of SLC27A3 and STAU1 in the metadata cohort were 0.734 and 0.745, respectively (**Figures 5A, B**). Furthermore, the AUCs of SLC27A3 and STAU1 in the GSE106986 dataset were 0.900 and 0.971, respectively (**Figures 5C, D**), indicating that both SLC27A3 and STAU1 have high diagnostic values.

Immune Cell Infiltration Landscape

With the CIBERSORT algorithm, we firstly calculated the proportion of immune cell infiltration in COPD and normal tissues. The results showed that the degree of infiltration of resting mast cells (P = 0.001), M1 macrophages (P = 0.049), and memory B cells (P = 0.020) in COPD tissues were notably raised in COPD samples in contrast to controls. Conversely, control samples demonstrated a higher proportion of infiltration of eosinophils (P = 0.002), activated mast cells (P = 0.006), resting NK cells (P = 0.004) and plasma cells (P = 0.003) compared to those found in COPD tissues (**Figure 6A**). Furthermore, we calculated the correlation between the 22 types of infiltrating immune cells (**Figure 6B**). Plasma cells and resting NK cells both individually correlated negatively with resting mast cells but positively with activated mast cells. Moreover, activated mast cells correlated positively with memory B cells.

Correlation Analysis Between SLC27A3, STAU1 and Infiltrating Immune Cells

SLC27A3 was significantly positively correlated with memory B cells (r=0.218, P=0.003), CD4 memory resting T-cells (r=0.245, P<0.001), CD8 T-cells (r=0.276, P<0.001), follicular T-helper cells (r=0.353, P<0.001), resting NK cells (r=0.406, P<0.001), eosinophils (r=0.411, P<0.001), activated mast cells (r=0.598, P<0.001) and plasma cells (r=0.619, P<0.001), and significantly negatively correlated with naive B cells (r=-0.657, P<0.001), CD4 memory activated T-cells (r=-0.578, P<0.001), resting mast cells (r=-0.388, P<0.001), resting dendritic cells (r=-0.289, P<0.001), activated NK cells (r=-0.274, P<0.001) and gamma delta T-cells (r=-0.169, P=0.022; **Figure 7A**). STAU1 was significantly positively correlated with regulatory T-cells (r=0.157, P=0.033), CD4 memory resting T-cells (r=0.174, P=0.019), CD8 T-cells (r=0.237, P=0.001), memory B cells (r=0.244, P<0.001), follicular T-helper cells (r=0.327, P<0.001), eosinophils (r=0.369, P<0.001), resting NK cells (r=0.468, P<0.001), activated mast

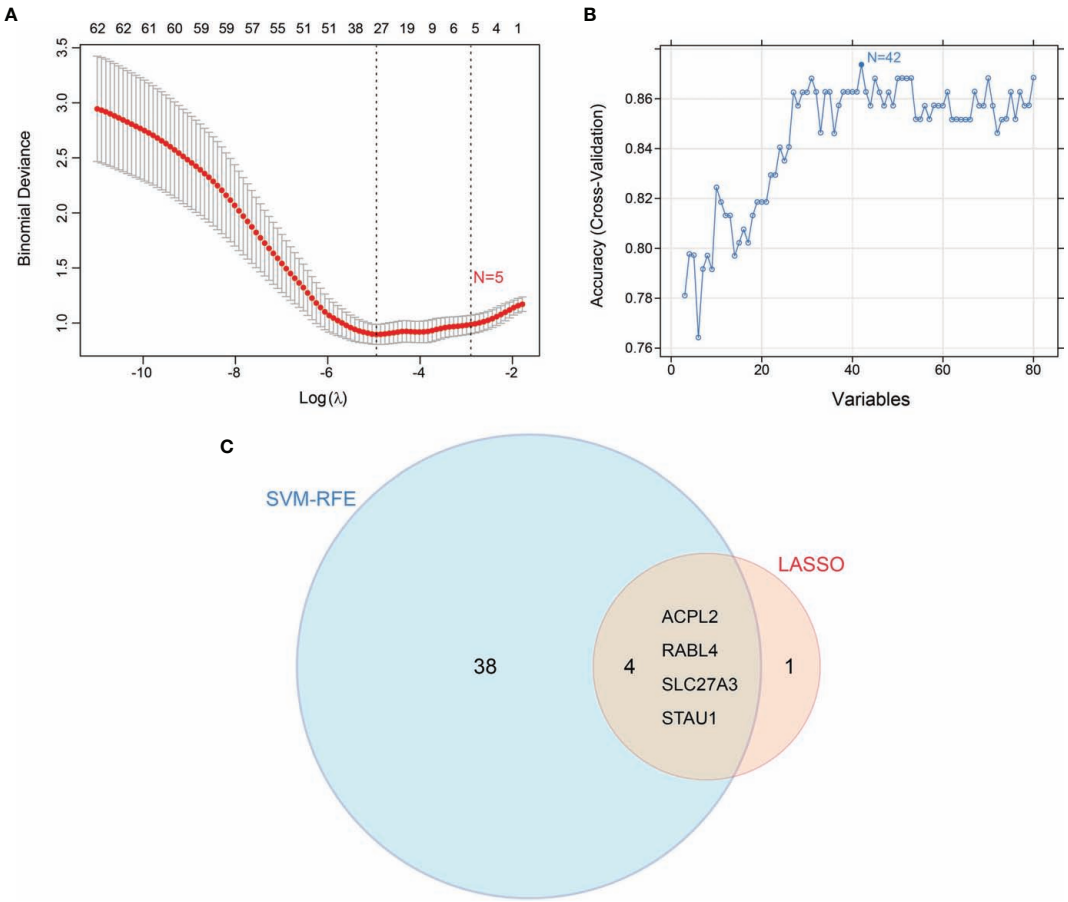

FIGURE 3 | Screening candidate diagnostic markers for chronic obstructive pulmonary disease**. (A)** Diagnostic markers were screened by the least absolute shrinkage and selection operator (LASSO) logistic regression algorithm. **(B)** Diagnostic markers were screened by a support vector machine-recursive feature elimination (SVM-RFE) algorithm. **(C)** Venn diagram of variables screened by LASSO and SVM-RFE algorithms.

cells (r=0.548, P<0.001) and plasma cells (r=0.575, P<0.001), and significantly negatively correlated with naive B cells (r=-0.590, P<0.001), CD4 memory activated T-cells (r=-0.513, P<0.001), resting mast cells (r=-0.422, P<0.001), resting dendritic cells (r=-0.230, P=0.002), activated NK cells (r=-0.299, P<0.001), gamma delta T-cells (r=-0.193, P=0.009) and M2 macrophages (r=-0.156, P=0.035; **Figure 7B**).

Immune Cell Infiltration in COPD Mouse Models

Subsequently, we established a COPD mouse model using GSE. The body weight of mouse in COPD group was significantly lower than that in control group (**Figure 8A**). HE staining showed that the MAST was shorter, and the MLI was larger in COPD group compared with that in control group (**Figures 8B–E**). We then observed the immune cell infiltrating in COPD group. The proportion of leukocyte, and the percentage of neutrophil and macrophage were larger in COPD group (**Figure 8F**). Simultaneously, the expression levels of IL-6, IL-1β, and TNF-α were all increased in bronchoalveolar lavage fluid (BRLF) and lung tissues from COPD group (**Figures 8G–I**). In addition, the expression of immune cell markers including CD8a, CD57, CD19, and CD20 were upregulated in lung tissues from mouse in COPD group (**Figures 8J, K**).

The Expression of SLC27A3 and STAU1 in COPD Models

GSE-induced COPD models were established both *in vivo* and *in vitro*. Immunohistochemistry staining, real-time PCR and western blot assay showed that the mRNA and protein levels of SLC27A3 and STAU1 were upregulated in lung tissues of mice from COPD group (**Figures 9A–F**). In accordance with these results, SLC27A3 and STAU1 were upregulated in GSE-treated BEAS-2B cells (**Figures 9G–J**). Besides, ALCPL2 was also upregulated in COPD models, while RABL4 was not significantly changed (**Figure S1**).

Knockdown of SLC27A3 and STAU1 Reversed the Effect of CSE on BEAS-2B Cells

Finally, we observed the effect of SLC27A3 and STAU1 knockdown on CSE-treated BEAS-2B cells. There siRNAs

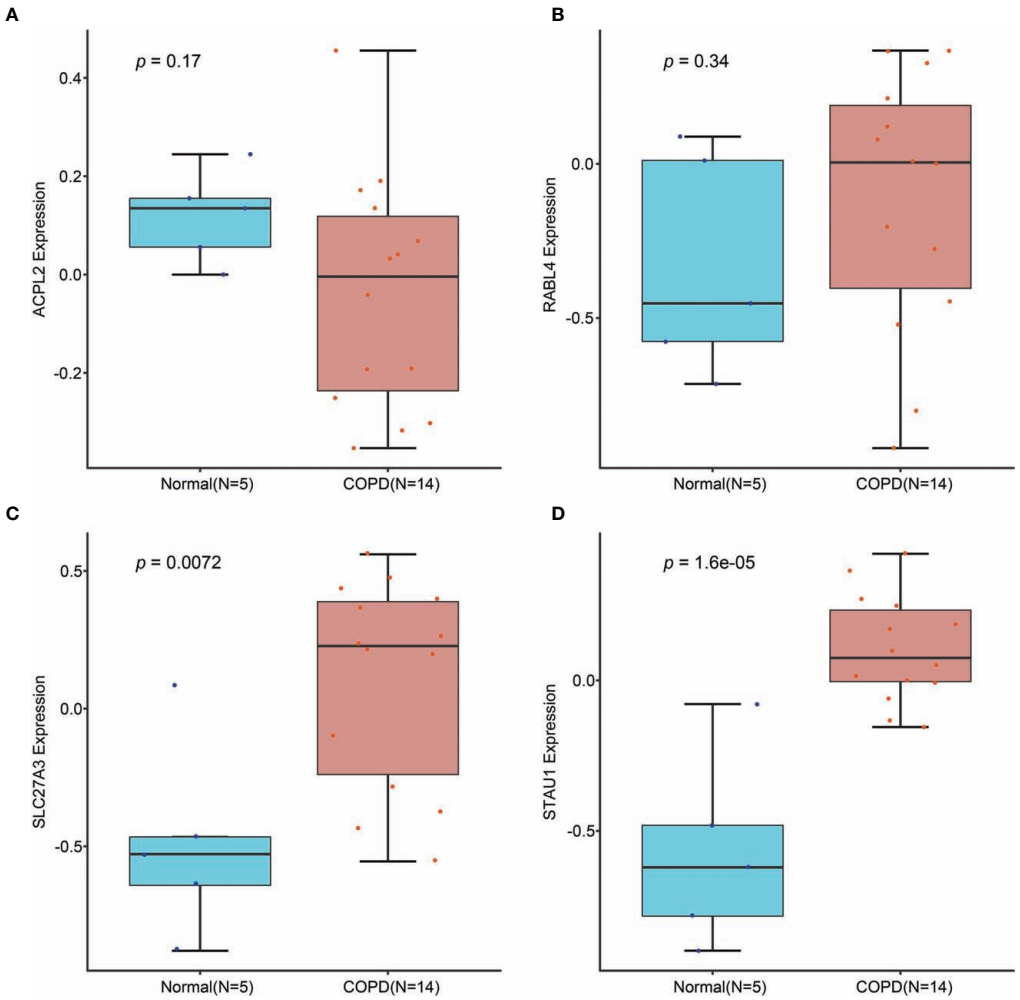

FIGURE 4 | Validation of the expression of candidate diagnostic markers in the GSE106986 dataset. **(A)** ACPL2; **(B)** RABL4; **(C)** SLC27A3; **(D)** STAU1.

sequences were designed to downregulate SLC27A3 and STAU1, respectively. The expression of SLC27A3 and STAU1 were significantly downregulated by transfection of corresponding siRNAs (**Figures 10A–D**). CSE treatment decreased the viability and increased the expression inflammatory cytokines (IL-6, IL-1β, and TNF-α) in BEAS-2B cells, which were attenuated by knockdown of SLC27A3 or STAU1 (**Figures 10E–H**).

DISCUSSION

COPD remains the third leading cause of death globally, with over three million dying annually from this debilitating disease despite significant advancements in diagnostic and therapeutic options over the last decade (24). Diagnosing COPD early is virtually impossible given the paucity of valuable biomarkers, a phenomenon that further results in poor clinical outcomes. Recent literature demonstrates that immune cell infiltration appears to be intricately involved in the occurrence and progress of COPD (25–27). Therefore, seeking for effective and novel diagnostic biomarkers for COPD amongst immune cell components is a promising avenue of research that may potentially result means of intervening early in COPD, thereby improving clinical prognosis. Recently, differentially expressed genes have been regarded as promising biomarkers in respiratory diseases, and especially in regards to COPD. For instance, HIF-1α could upregulate the expression of inflammatory factors, further aggravating the pathological process of COPD (28). In addition, FHL1 was found to be significantly modulated in CSE-treatment Beas-2B cells, providing important information on the role of inflammatory factors in COPD (14). However, there are few studies on biomarkers comprising of abnormally expressed genes associated with COPD and immune infiltration in normal tissues. Therefore, the purpose of this study is to search for candidate diagnostic biomarkers for COPD and explore how immune infiltration influences the progress of COPD.

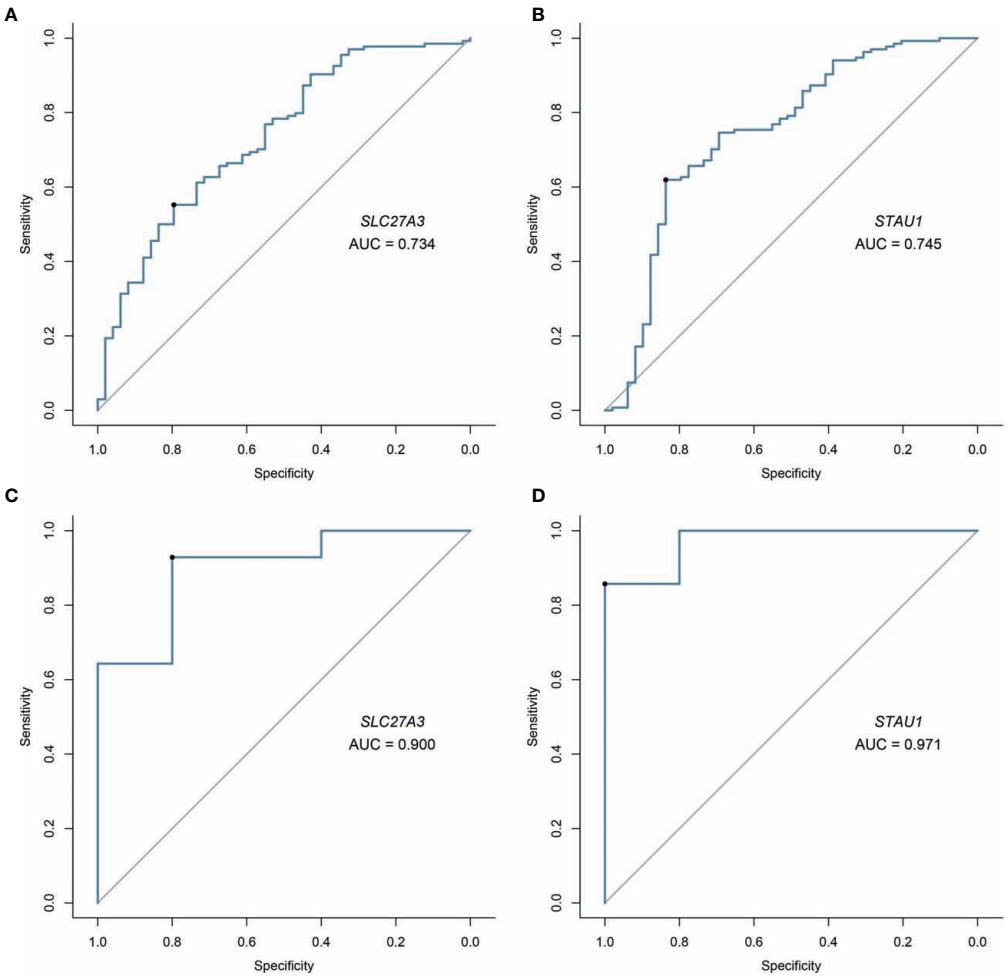

FIGURE 5 | Validation of diagnostic validity of two diagnostic markers. **(A, B)** Receiver operating characteristic (ROC) curves of SLC27A3 and STAU1 in the metadata cohort. **(C, D)** ROC curves of SLC27A3 and STAU1 in the GSE106986 dataset.

This study is a novel retrospective report that comprehensively explores GEO datasets for likely diagnostic biomarkers amongst DEGs and immune cell infiltration in COPD patients. A metadata cohort was first formed by merging two GEO datasets which was then used to identify DEGs between COPD and control samples. Our study identified 4 significantly upregulated and 76 notably downregulated genes. Subsequent enrichment analysis found that these DEGs were primarily associated with cellular amino acid metabolic process, telomerase activity, phagocytosis regulation, MHC class I-related peptide antigen presentation and antigen processing, along with other biological processes. Moreover, DEGs were also enriched in the S phase and nucleotide metabolism. These findings are consistent with previously discovered factors related to COPD. Earlier experiments have detected altered amino acid levels in patients with serve COPD which may be helpful in the diagnosis and treatment of COPD (29, 30). Chronic inflammation is a prominent feature in COPD that results to airway remodeling and lung parenchyma destruction (31). The abnormalities in telomere function contributed significantly to sustained local inflammation in the lungs as well as systemic inflammation in COPD patients (32). COPD alveolar macrophages have defective phagocytic functions with regards to the uptake and processing of respiratory pathogens and cellular debris (33). Research shows that cigarette smoke can result in an increased percentage of human fetal lung fibroblasts cells in G1 and G2/m phases in addition to a reduced percentage of cells in S phase of cell cycle. Therefore, changes in the cell cycle potentially impact COPD pathogenesis (34). Immune cells have been proven to carry out an extremely vital role in COPD, and changes in the MHC I surface expression and MHC I-mediated presentation of a specific antigen caused by cigarette smoke may lead to a distorted adaptive immune response in viral and bacterial exacerbations of COPD patients (31, 35). These findings are consistent with our experimental results, suggesting that our discoveries are accurate as well as further solidifying the critical role of the immune response in COPD. Therefore, precise control of various types of immune cells remains a promising means of developing novel COPD

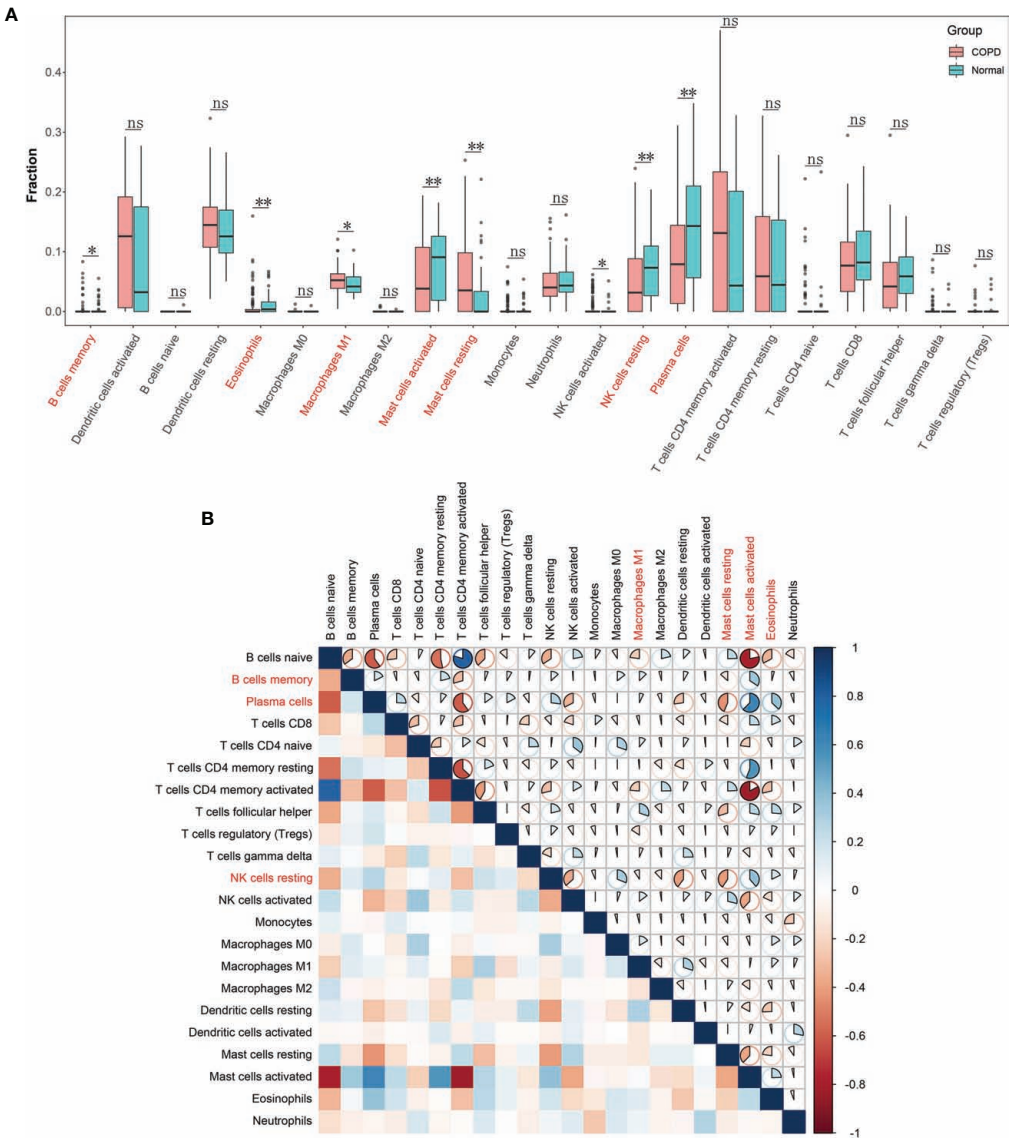

FIGURE 6 | Landscape of immune cell infiltration in chronic obstructive pulmonary disease. **(A)** Boxplot of the proportion of 22 types of immune cell infiltrates. Red in the boxes represents the chronic obstructive pulmonary disease group and blue represents the normal group. *P < 0.05; **P < 0.01; ns, not significant. **(B)** Heatmap plot of correlations among 22 types of immune cells. Blue and red indicate positive and negative correlation, respectively. The darker the color the stronger the correlation.

treatment that may offer improved clinical prognosis. Bioinformatics analysis enables identification of significant novel COPD biomarkers associated with the degree of immune cell infiltration that may be beneficial for early diagnosis and treatment of COPD.

Our study identified two diagnostic markers *via* machine-learning algorithms. Staufen 1 (STAU1) is an RNA-binding protein that is related to post transcriptional mRNA regulation and is critical in cellular defense mechanisms against stressful stimuli such as oxidative and endoplasmic reticulum (36). Dysregulated STAU1-mediated post-transcriptional genetic modulation appears to regulate apoptosis while also being a pivotal occurrence in cancer progression (37, 38). Studies have revealed that STAU1 selectively regulates genes related to inflammation and immune responses and plays a substantial role in the human immune response against the influenza virus and human immunodeficiency virus type I (HIV-1) (39–42). These facts further underscore the vital function of STAU1 in inflammation and immunity. The solute carrier 27A (SLC27A) gene belongs to a family of genes that encodes fatty acids transport proteins (FATPs). FATPs are located in the cell membrane and intracellular space and are mainly related to fatty acid activation and absorption (43). The encoding product of SLC27A3 gene (FATP3) plays an important role in long-chain fatty acids transport and very-long-chain fatty acids activation, the upregulation of which could promote lipid metabolism (44).

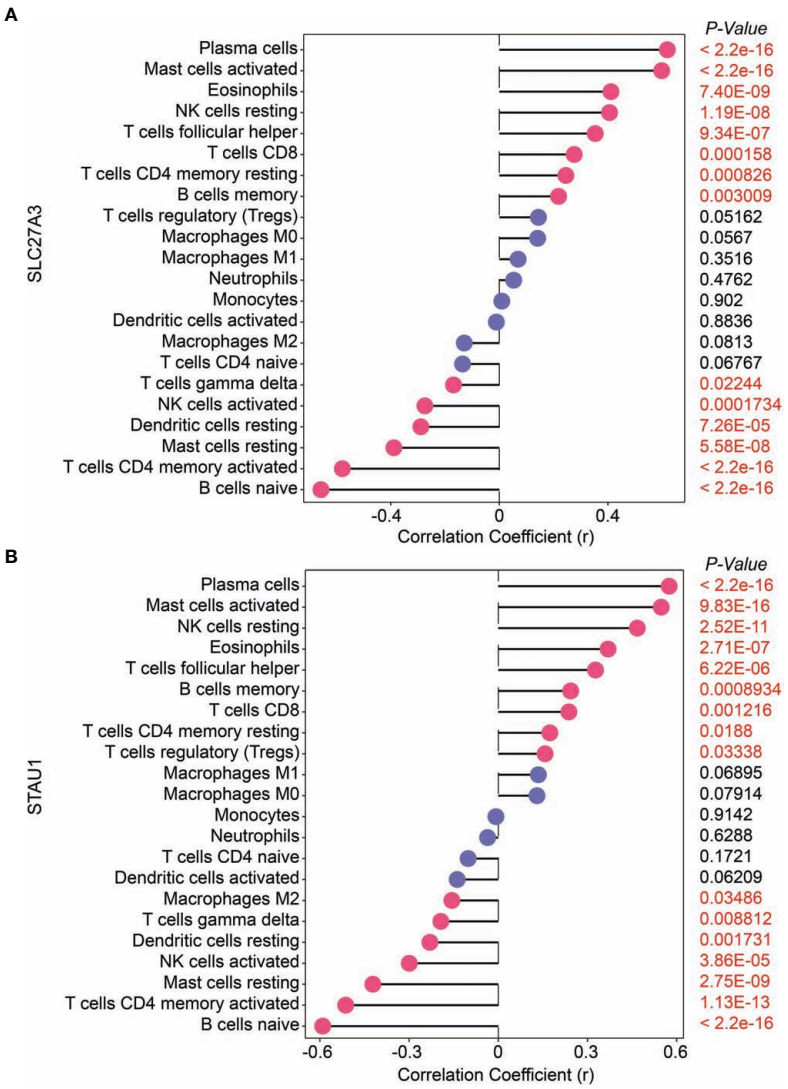

FIGURE 7 | Correlation of two diagnostic markers with 22 types of immune cell infiltration in chronic obstructive pulmonary disease. **(A)** SLC27A3; **(B)** STAU1.

COPD pathogenesis has been found to be closely related to altered lipid metabolism (45). As a result, we infer that SLC27A may function to critically modulate the initiation and progression of COPD.

The CIBERSORT assessment was used in the study to determine the profiles of immune cell infiltration in COPD subjects and in healthy controls. A myriad of immune cell subtypes has been characterized in relation to COPD. Increased infiltration of memory B cells, M1 macrophages, and resting mast cells were found in COPD in contrast to normal tissues. However, proportions of eosinophils, activated mast cells, resting NK cells, and plasma cells were found to be decreased. Furthermore, the correlation analysis of STAU1, SLC27A3, and immune cells indicated that STAU1 and SLC27A3 correlated to plasma cells, activated mast cells, eosinophils, resting NK cells, CD8+, CD4+, and helper follicular T-cells, as well as in resting memory B cells. We then established GSE-induced COPD models both *in vivo* and *in vitro*. Immune infiltration and inflammatory cytokines production were increased in COPD models. Enhanced expression of STAU1 and SLC27A3 were observed in COPD models both *in vivo* and *in vitro*. Knockdown of SLC27A3 and STAU1 reversed the effect of CSE on BEAS-2B cells. Moreover, knockdown of SLC27A3 and STAU1 reversed the effect of CSE on the viability and the expression inflammatory cytokines in BEAS-2B cells. These findings were in accordance with the bioinformatics analysis results.

Primary pathological changes of COPD mainly comprise of emphysema and chronic bronchitis. Continual airflow restriction leads to pulmonary ventilation dysfunction, which in turn leads to progressively deteriorating lung function (46). Inflammatory mechanisms lie at the core of COPD development. Various

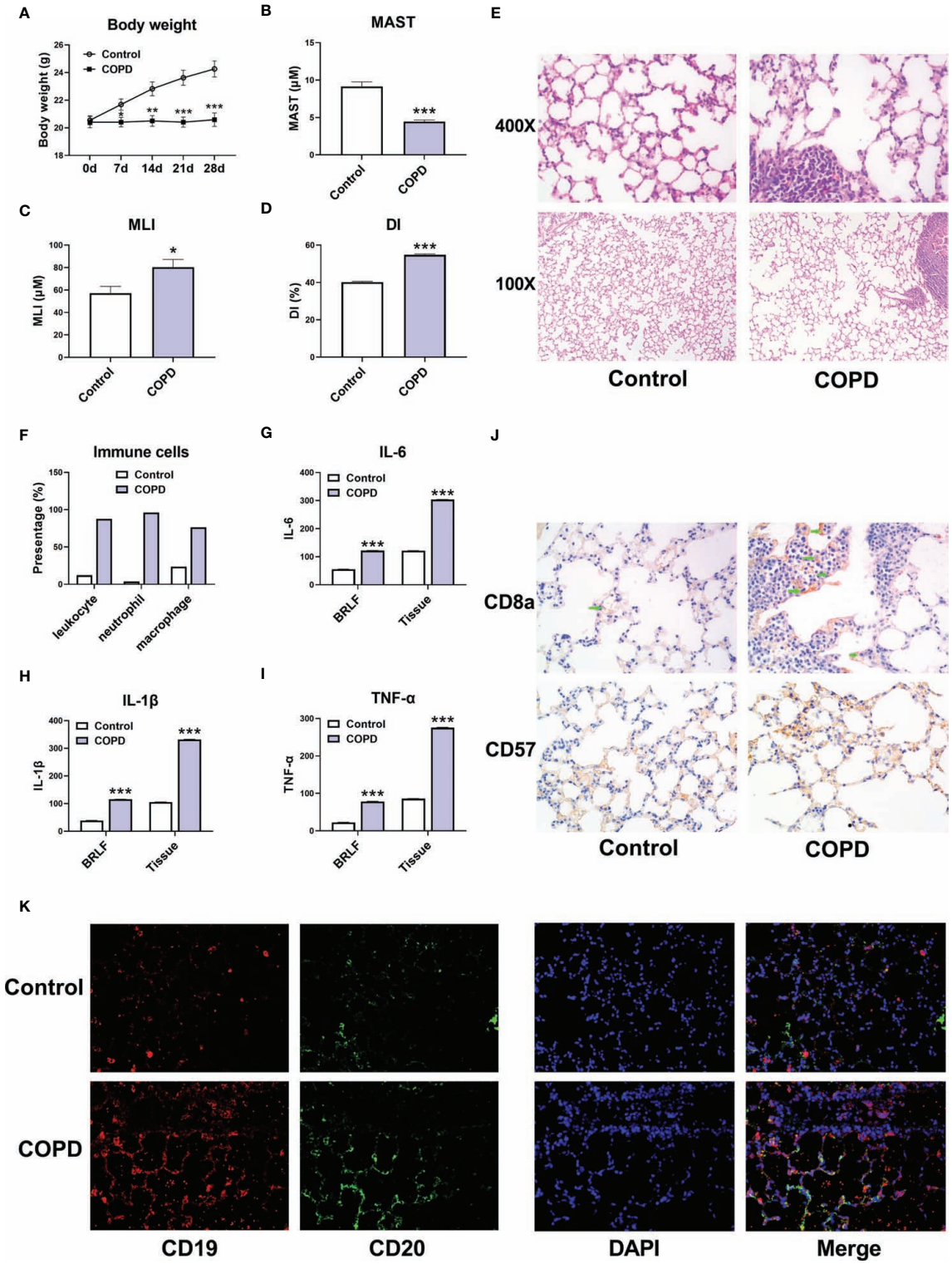

FIGURE 8 | Immune cell infiltration in COPD mouse models. **(A)** Body weight of mice. **(B)** The mean alveolar septal thickness (MAST). **(C)** Mean linear intercept (MLI). **(D)** Destructive index (DI). **(E)** Representative HE staining images (100x and 400x). **(F)** The proportion of immune cells. **(G)** The expression of IL-6 in bronchoalveolar lavage fluid (BRLF) and lung tissues of mice. **(H)** The expression of IL-1β in BRLF and lung tissues of mice. **(I)** The expression of TNF-α in BRLF and lung tissues of mice. **(J)** Representative immunohistochemistry images of CD8a and CD57 (400x). **(K)** Representative immunofluorescence images of CD19 and CD20 (400x). For panel G, H, and I, the unit for BRLF is pg/mL, and the unit for lung tissue is pg/mg. *P < 0.05, **P < 0.01, ***P < 0.001 vs. Control.

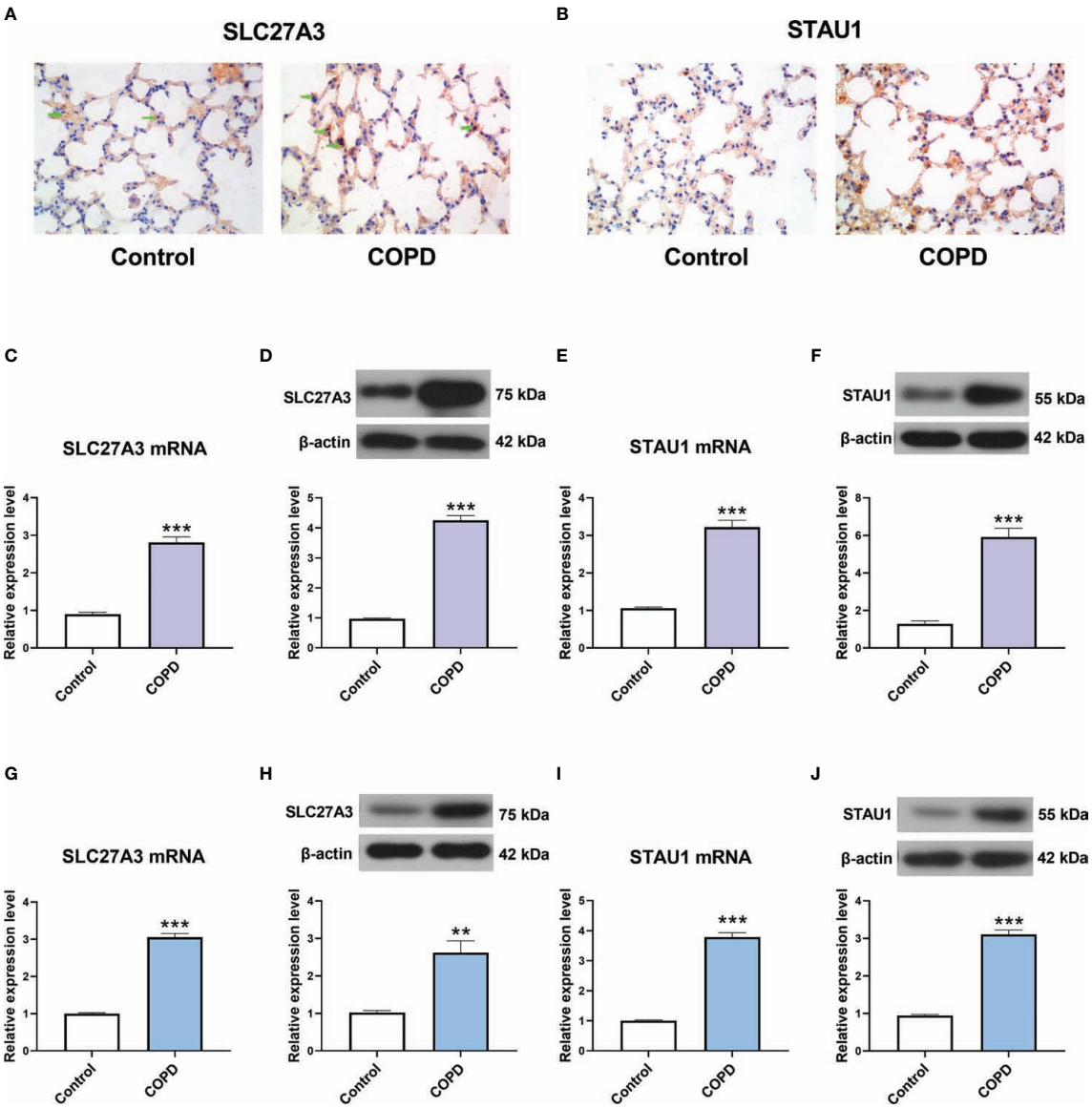

FIGURE 9 | The expression of SLC27A3 and STAU1 in COPD models. **(A)** Representative immunohistochemistry images of SLC27A3 in lung tissues of mice. **(B)** Representative immunohistochemistry images of STAU1 in lung tissues of mice. **(C)** The expression of SLC27A3 mRNA in lung tissues of mice. **(D)** The expression of SLC27A3 protein in lung tissues of mice. **(E)** The expression of STAU1 mRNA in lung tissues of mice. **(F)** The expression of STAU1 protein in lung tissues of mice. **(G)** The expression of SLC27A3 mRNA in BEAS-2B cells. **(H)** The expression of SLC27A3 protein in BEAS-2B cells. **(I)** The expression of STAU1 mRNA in BEAS-2B cells. **(J)** The expression of STAU1 protein in BEAS-2B cells. $^{**}P < 0.01$, $^{***}P < 0.001$ vs. Control.

factors can lead to inflammatory cell infiltration and release of inflammatory mediators. Inflammatory cells subsequently produce destructive enzymes that lead to the progressive destruction of lung tissue in COPD (47, 48). Studies have also found elevated expressions of CD8+T-cells in COPD lung tissues. CD8+ T-cells primarily secrete IL-4 and IL-5 cytokines, both of which are implicated in lung parenchymal tissue damage that exacerbates the development of emphysema (49). Some studies have reported that NK cells can secrete cytotoxic mediators, such as granzyme B and perforin, which may play an important role in inducing lung cell apoptosis and thereby promoting emphysema (50). There is evidence demonstrating that NK cells exert cytotoxic effects on COPD lung epithelial cells and are enhanced by the transport of IL-LS by dendritic cells of the IL-I5 receptor subUnita (LL-15RA) (51). In addition, it has been confirmed that the level of memory B cells in the peripheral blood of smokers increases, and smoking in patients is also one of the main causes of COPD (52). The wealth of evidence supporting the direct or indirect effects of inflammatory cells on COPD pathogenesis are consistent with our study findings. It is of great interest for future studies to identify potential immune targets for COPD immunotherapy.

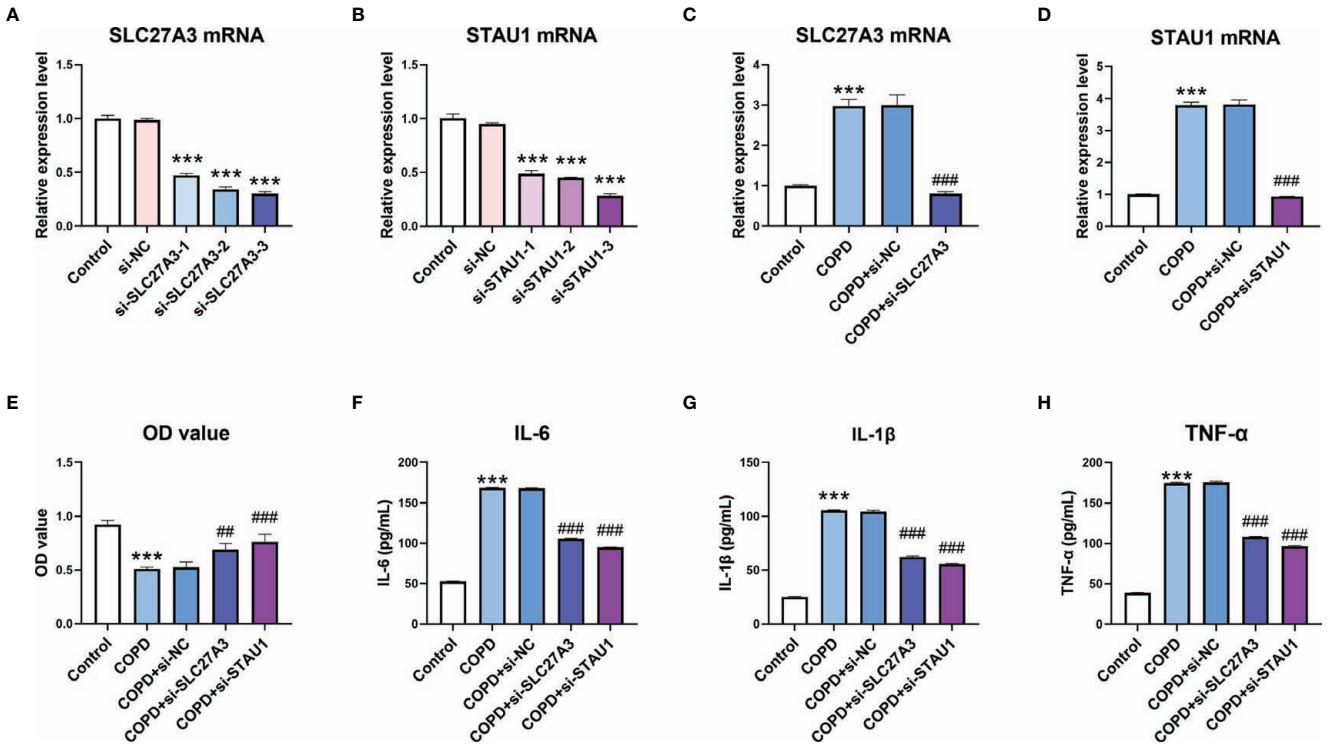

FIGURE 10 | Knockdown of SLC27A3 and STAU1 reversed the effect of cigarette smoke extract (CSE) on BEAS-2B cells. **(A)** The effect of si-SLC27A3 on SLC27A3 mRNA expression in BEAS-2B cells. **(B)** The effect of si-STAU1 on SLC27A3 mRNA expression in BEAS-2B cells. **(C)** The expression of SLC27A3 mRNA in CSE-treated BEAS-2B cells after knockdown of SLC27A3. **(D)** The expression of STAU1 mRNA in CSE-treated BEAS-2B cells after knockdown of STAU1. **(E)** The viability of CSE-treated BEAS-2B cells after knockdown of SLC27A3 or STAU1. **(F)** The expression of IL-6 in CSE-treated BEAS-2B cells after knockdown of SLC27A3 or STAU1. **(G)** The expression of IL-1β in CSE-treated BEAS-2B cells after knockdown of SLC27A3 or STAU1. **(H)** The expression of TNF-α in CSE-treated BEAS-2B cells after knockdown of SLC27A3 or STAU1. For panel A and B, ***P < 0.001 vs. si-NC; for panel C-H, ***P < 0.001 vs. Control; ##P < 0.01, ###P < 0.001 vs. COPD+si-NC.

Our study is firstly limited by its retrospective design and lack of analysis of important clinical data. Our identified upregulated genes seen to be associated with immune infiltration in COPD here require further validation in cohorts with clinical data. Secondly, the size of our GSE106986 validation cohort is small. We stress that our results should be validated in larger cohorts to determine the reproducibility of the findings. Although the functions of the two biomarkers and immune cell infiltration in COPD were assessed using bioinformatics analysis and biological experiments, larger prospective studies are needed to verify our conclusions.

CONCLUSION

To sum up, the present study strongly suggests that STAU1 and SLC27A3 are significant diagnostic biomarkers in COPD. Plasma cells, resting NK cells, activated mast cells, eosinophils, CD8+, CD4+, and helper follicular T-cells, as well as memory B-cells are important factors in COPD development. Mechanisms of immune infiltration should be focused on in the search of novel therapeutics for COPD and these immune cells are expected to be promising targets for immunotherapy in patients with COPD.

DATA AVAILABILITY STATEMENT

The datasets presented in this study can be found in online repositories. The names of the repository/repositories and accession number(s) can be found in the article/**Supplementary Material**.

AUTHOR CONTRIBUTIONS

Conceptualization, YZ and SJ. Software, RX, ML, and ZL. Writing—original draft preparation, YZ, XC, YH, and CS. Writing—review and editing, YJ and SJ. All authors contributed to the article and approved the submitted version.

FUNDING

This work was funded by the National Science Foundation of China (81670028), the Major Program of Natural Science

Foundation of Heilongjiang Province (ZD2016014), Harbin City Applied Technology Research and Development Project (2016RQXYJ116).

ACKNOWLEDGMENTS

We acknowledge the National Science Foundation of China (81670028), the Major Program of Natural Science Foundation of Heilongjiang Province (ZD2016014), Harbin City Applied Technology Research and Development Project (2016RQXYJ116). We acknowledge the support from The Fourth Hospital of Harbin Medical University.

SUPPLEMENTARY MATERIAL

The Supplementary Material for this article can be found online at: https://www.frontiersin.org/articles/10.3389/fimmu.2022.740513/full#supplementary-material

REFERENCES

1. Reid DJ, Pham NT. Emerging Therapeutic Options for the Management of COPD. *Clin Med Insights Circ Respir Pulm Med* (2013) 7:7–15. doi: 10.4137/CCRPM.S8140
2. May SM, Li JT. Burden of Chronic Obstructive Pulmonary Disease: Healthcare Costs and Beyond. *Allergy Asthma Proc* (2015) 36:4–10. doi: 10.2500/aap.2015.36.3812
3. Qureshi H, Sharafkhaneh A, Hanania NA. Chronic Obstructive Pulmonary Disease Exacerbations: Latest Evidence and Clinical Implications. *Ther Adv Chronic Dis* (2014) 5:212–27. doi: 10.1177/2040622314532862
4. Sheikh K, Coxson HO, Parraga G. This Is What COPD Looks Like. *Respirology* (2016) 21:224–36. doi: 10.1111/resp.12611
5. Fischer BM, Voynow JA, Ghio AJ. COPD: Balancing Oxidants and Antioxidants. *Int J Chron Obstruct Pulmon Dis* (2015) 10:261–76. doi: 10.2147/COPD.S42414
6. Silverman EK. Genetics of COPD. *Annu Rev Physiol* (2020) 82:413–31. doi: 10.1146/annurev-physiol-021317-121224
7. Cao Y, Tang W, Tang W. Immune Cell Infiltration Characteristics and Related Core Genes in Lupus Nephritis: Results From Bioinformatic Analysis. *BMC Immunol* (2019) 20:37. doi: 10.1186/s12865-019-0316-x
8. Qiu L, Liu X. Identification of Key Genes Involved in Myocardial Infarction. *Eur J Med Res* (2019) 24:22. doi: 10.1186/s40001-019-0381-x
9. Zhao E, Bai X. Nomogram Based on microRNA Signature Contributes to Improve Survival Prediction of Clear Cell Renal Cell Carcinoma. *BioMed Res Int* (2020) 2020:7434737. doi: 10.1155/2020/7434737
10. Zhao E, Zhou C, Chen S. Flap Endonuclease 1 (FEN1) as a Novel Diagnostic and Prognostic Biomarker for Gastric Cancer. *Clin Res Hepatol Gastroenterol* (2021) 45:101455. doi: 10.1016/j.clinre.2020.04.019
11. Zhao E, Zhou C. & Chen S. A Signature of 14 Immune-Related Gene Pairs Predicts Overall Survival in Gastric Cancer. *Clin Transl Oncol* (2021) 23:265–74. doi: 10.1007/s12094-020-02414-7
12. Keller A, Ludwig N, Fehlmann T, Kahraman M, Backes C, Kern F, et al. Low miR-150-5p and miR-320b Expression Predicts Reduced Survival of COPD Patients. *Cells* (2019) 8. doi: 10.3390/cells8101162
13. Lin YZ, Zhong XN, Chen X, Liang Y, Zhang H, Zhu DL. Roundabout Signaling Pathway Involved in the Pathogenesis of COPD by Integrative Bioinformatics Analysis. *Int J Chron Obstruct Pulmon Dis* (2019) 14:2145–62. doi: 10.2147/COPD.S216050
14. Zhong S, Chen C, Liu N, Yang L, Hu Z, Duan P, et al. Overexpression Of hsa-miR-664a-3p Is Associated With Cigarette Smoke-Induced Chronic Obstructive Pulmonary Disease *Via* Targeting Fhl1. *Int J Chron Obstruct Pulmon Dis* (2019) 14:2319–29. doi: 10.2147/COPD.S224763
15. Deng YJ, Ren EH, Yuan WH, Zhang GZ, Wu ZL, Xie QQ. GRB10 and E2F3 as Diagnostic Markers of Osteoarthritis and Their Correlation With Immune Infiltration. *Diagnostics (Basel)* (2020) 10. doi: 10.3390/diagnostics10030171
16. Nahrendorf M, Swirski FK. Innate Immune Cells in Ischaemic Heart Disease: Does Myocardial Infarction Beget Myocardial Infarction? *Eur Heart J* (2016) 37:868–72. doi: 10.1093/eurheartj/ehv453
17. Yang S, Liu T, Cheng Y, Bai Y, Liang G. Immune Cell Infiltration as a Biomarker for the Diagnosis and Prognosis of Digestive System Cancer. *Cancer Sci* (2019) 110:3639–49. doi: 10.1111/cas.14216
18. Leek JT, Johnson WE, Parker HS, Jaffe AE, Storey JD. The Sva Package for Removing Batch Effects and Other Unwanted Variation in High-Throughput Experiments. *Bioinformatics* (2012) 28:882–3. doi: 10.1093/bioinformatics/bts034
19. Huang S, Cai N, Pacheco PP, Narrandes S, Wang Y, Xu W. Applications of Support Vector Machine (SVM) Learning in Cancer Genomics. *Cancer Genomics Proteomics* (2018) 15:41–51. doi: 10.21873/cgp.20063
20. Newman AM, Liu CL, Green MR, Gentles AJ, Feng W, Xu Y, et al. Robust Enumeration of Cell Subsets From Tissue Expression Profiles. *Nat Methods* (2015) 12:453–7. doi: 10.1038/nmeth.3337
21. He S, Xie L, Lu J, Sun S. Characteristics and Potential Role of M2 Macrophages in COPD. *Int J Chron Obstruct Pulmon Dis* (2017) 12:3029–39. doi: 10.2147/COPD.S147144
22. Spond J, Billah MM, Chapman RW, Egan RW, Hey JA, House A, et al. The Role of Neutrophils in LPS-Induced Changes in Pulmonary Function in Conscious Rats. *Pulm Pharmacol Ther* (2004) 17:133–40. doi: 10.1016/j.pupt.2004.01.003
23. Araya J, Tsubouchi K, Sato N, Ito S, Minagawa S, Hara H, et al. PRKN-Regulated Mitophagy and Cellular Senescence During COPD Pathogenesis. *Autophagy* (2019) 15:510–26. doi: 10.1080/15548627.2018.1532259
24. Terzikhan N, Verhamme KM, Hofman A, Stricker BH, Brusselle GG, Lahousse L. Prevalence and Incidence of COPD in Smokers and non-Smokers: The Rotterdam Study. *Eur J Epidemiol* (2016) 31:785–92. doi: 10.1007/s10654-016-0132-z
25. Bu T, Wang LF, Yin YQ. How Do Innate Immune Cells Contribute to Airway Remodeling in COPD Progression? *Int J Chron Obstruct Pulmon Dis* (2020) 15:107–16. doi: 10.2147/COPD.S235054
26. Caramori G, Ruggeri P, Di Stefano A, Mumby S, Girbino G, Adcock IM, et al. Autoimmunity and COPD: Clinical Implications. *Chest* (2018) 153:1424–31. doi: 10.1016/j.chest.2017.10.033
27. Cruz T, Lopez-Giraldo A, Noell G, Casas-Recasens S, Garcia T, Molins L, et al. Multi-Level Immune Response Network in Mild-Moderate Chronic Obstructive Pulmonary Disease (COPD). *Respir Res* (2019) 20:152. doi: 10.1186/s12931-019-1105-z
28. Zhang HX, Yang JJ, Zhang SA, Zhang SM, Wang JX, Xu ZY, et al. HIF-1alpha Promotes Inflammatory Response of Chronic Obstructive Pulmonary Disease by Activating EGFR/PI3K/AKT Pathway. *Eur Rev Med Pharmacol Sci* (2018) 22:6077–84. doi: 10.26355/eurrev_201809_15946
29. Kuo WK, Liu YC, Chu CM, Hua CC, Huang CY, Liu MH, et al. Amino Acid-Based Metabolic Indexes Identify Patients With Chronic Obstructive Pulmonary Disease And Further Discriminates Patients In Advanced BODE Stages. *Int J Chron Obstruct Pulmon Dis* (2019) 14:2257–66. doi: 10.2147/COPD.S220557
30. Ubhi BK, Cheng KK, Dong J, Janowitz T, Jodrell D, Tal-Singer R, et al. Targeted Metabolomics Identifies Perturbations in Amino Acid Metabolism That Sub-Classify Patients With COPD. *Mol Biosyst* (2012) 8:3125–33. doi: 10.1039/c2mb25194a
31. Alter P, Baker JR, Dauletbaev N, Donnelly LE, Pistenmaa C, Schmeck B, et al. Update in Chronic Obstructive Pulmonary Disease 2019. *Am J Respir Crit Care Med* (2020) 202:348–55. doi: 10.1164/rccm.202002-0370UP
32. Amsellem V, Gary-Bobo G, Marcos E, Maitre B, Chaar V, Validire P, et al. Telomere Dysfunction Causes Sustained Inflammation in Chronic Obstructive Pulmonary Disease. *Am J Respir Crit Care Med* (2011) 184:1358–66. doi: 10.1164/rccm.201105-0802OC
33. Jubrail J, Kurian N, Niedergang F. Macrophage Phagocytosis Cracking the Defect Code in COPD. *BioMed J* (2017) 40:305–12. doi: 10.1016/j.bj.2017.09.004

34. D'Anna C, Cigna D, Costanzo G, Ferraro M, Siena L, Vitulo P, et al. Cigarette Smoke Alters Cell Cycle and Induces Inflammation in Lung Fibroblasts. *Life Sci* (2015) 126:10–8. doi: 10.1016/j.lfs.2015.01.017
35. Kammerl IE, Dann A, Mossina A, Brech D, Lukas C, Vosyka O, et al. Impairment of Immunoproteasome Function by Cigarette Smoke and in Chronic Obstructive Pulmonary Disease. *Am J Respir Crit Care Med* (2016) 193:1230–41. doi: 10.1164/rccm.201506-1122OC
36. Bonnet-Magnaval F, Philippe C, Van Den Berghe L, Prats H, Touriol C, Lacazette E. Hypoxia and ER Stress Promote Staufen1 Expression Through an Alternative Translation Mechanism. *Biochem Biophys Res Commun* (2016) 479:365–71. doi: 10.1016/j.bbrc.2016.09.082
37. Liu Z, Chen Z, Fan R, Jiang B, Chen X, Chen Q, et al. Over-Expressed Long Noncoding RNA HOXA11-AS Promotes Cell Cycle Progression and Metastasis in Gastric Cancer. *Mol Cancer* (2017) 16:82. doi: 10.1186/s12943-017-0651-6
38. Xu TP, Wang YF, Xiong WL, Ma P, Wang WY, Chen WM, et al. E2F1 Induces TINCR Transcriptional Activity and Accelerates Gastric Cancer Progression *via* Activation of TINCR/STAU1/CDKN2B Signaling Axis. *Cell Death Dis* (2017) 8:e2837. doi: 10.1038/cddis.2017.205
39. de Lucas S, Peredo J, Marion RM, Sanchez C, Ortin J. Human Staufen1 Protein Interacts With Influenza Virus Ribonucleoproteins and Is Required for Efficient Virus Multiplication. *J Virol* (2010) 84:7603–12. doi: 10.1128/JVI.00504-10
40. Lee JH, Oh JY, Pascua PN, Kim EG, Choi YK, Kim HK. Impairment of the Staufen1-NS1 Interaction Reduces Influenza Viral Replication. *Biochem Biophys Res Commun* (2011) 414:153–8. doi: 10.1016/j.bbrc.2011.09.042
41. Rao S, Hassine S, Monette A, Amorim R, DesGroseillers L, Mouland AJ. HIV-1 Requires Staufen1 to Dissociate Stress Granules and to Produce Infectious Viral Particles. *RNA* (2019) 25:727–36. doi: 10.1261/rna.069351.118
42. Zhong Y, Hu Z, Wu J, Dai F, Lee F, Xu Y. STAU1 Selectively Regulates the Expression of Inflammatory and Immune Response Genes and Alternative Splicing of the Nerve Growth Factor Receptor Signaling Pathway. *Oncol Rep* (2020) 44:1863–74. doi: 10.3892/or.2020.7769
43. Anderson CM, Stahl A. SLC27 Fatty Acid Transport Proteins. *Mol Aspects Med* (2013) 34:516–28. doi: 10.1016/j.mam.2012.07.010
44. Pecka-Kielb E, Kowalewska-Luczak I, Czerniawska-Piatkowska E, Zielak-Steciwko AE. Effects of Single Nucleotide Polymorphisms in the SLC27A3 Gene on the Nutritional Value of Sheep Milk. *Anim (Basel)* (2020) 10. doi: 10.3390/ani10040562
45. Chen H, Li Z, Dong L, Wu Y, Shen H, Chen Z. Lipid Metabolism in Chronic Obstructive Pulmonary Disease. *Int J Chron Obstruct Pulmon Dis* (2019) 14:1009–18. doi: 10.2147/COPD.S196210
46. Vestbo J, Hurd SS, Agusti AG, Jones PW, Vogelmeier C, Anzueto A, et al. Global Strategy for the Diagnosis, Management, and Prevention of Chronic Obstructive Pulmonary Disease: GOLD Executive Summary. *Am J Respir Crit Care Med* (2013) 187:347–65. doi: 10.1164/rccm.201204-0596PP
47. Polosukhin VV, Richmond BW, Du RH, Cates JM, Wu P, Nian H, et al. Secretory IgA Deficiency in Individual Small Airways Is Associated With Persistent Inflammation and Remodeling. *Am J Respir Crit Care Med* (2017) 195:1010–21. doi: 10.1164/rccm.201604-0759OC
48. Richmond BW, Du RH, Han W, Benjamin JT, van der Meer R, Gleaves L, et al. Bacterial-Derived Neutrophilic Inflammation Drives Lung Remodeling in a Mouse Model of Chronic Obstructive Pulmonary Disease. *Am J Respir Cell Mol Biol* (2018) 58:736–44. doi: 10.1165/rcmb.2017-0329OC
49. Barczyk A, Pierzchala W, Kon OM, Cosio B, Adcock IM, Barnes PJ. Cytokine Production by Bronchoalveolar Lavage T Lymphocytes in Chronic Obstructive Pulmonary Disease. *J Allergy Clin Immunol* (2006) 117:1484–92. doi: 10.1016/j.jaci.2006.02.013
50. Suzuki M, Sze MA, Campbell JD, Brothers JF2nd, Lenburg ME, McDonough JE, et al. The Cellular and Molecular Determinants of Emphysematous Destruction in COPD. *Sci Rep* (2017) 7:9562. doi: 10.1038/s41598-017-10126-2
51. Finch DK, Stolberg VR, Ferguson J, Alikaj H, Kady MR, Richmond BW, et al. Lung Dendritic Cells Drive Natural Killer Cytotoxicity in Chronic Obstructive Pulmonary Disease *via* IL-15ralpha. *Am J Respir Crit Care Med* (2018) 198:1140–50. doi: 10.1164/rccm.201712-2513OC
52. Brandsma CA, Hylkema MN, Geerlings M, van Geffen WH, Postma DS, Timens W, et al. Increased Levels of (Class Switched) Memory B Cells in Peripheral Blood of Current Smokers. *Respir Res* (2009) 10:108. doi: 10.1186/1465-9921-10-108

Conflict of Interest: The authors declare that the research was conducted in the absence of any commercial or financial relationships that could be construed as a potential conflict of interest.

frontiers in Immunology

ORIGINAL RESEARCH
published: 31 March 2022
doi: 10.3389/fimmu.2022.737968

Eosinophil Progenitors in Patients With Non-Asthmatic Eosinophilic Bronchitis, Eosinophilic Asthma, and Normal Controls

Chen Zhan[1†], Rong Xu[1†], Bizhou Li[1,2†], Jiaxing Liu[1], Wanqin Liang[1], Shengfang Zhang[1], Liman Fang[1], Shuxin Zhong[1], S. Dushinka Shaniya Helen de Silva[1,3], Dhinesan Sivapalan[1,3], Wei Luo[1], Jing Li[1], Kefang Lai[1], Nanshan Zhong[1], Roma Sehmi[4], Paul M. O'Byrne[4*] and Ruchong Chen[1*‡]*

[1] Department of Allergy and Clinical Immunology, State Key Laboratory of Respiratory Disease, National Clinical Research Center for Respiratory Disease, Guangzhou Institute of Respiratory Health, the First Affiliated Hospital of Guangzhou Medical University, Guangzhou, China, [2] School of Basic Medical Sciences, Guangzhou Medical University, Guangzhou, China, [3] International College of Education, Guangzhou Medical University, Guangzhou, China, [4] Department of Medicine, Firestone Institute for Respiratory Health, St. Joseph's Healthcare and McMaster University, Hamilton, ON, Canada

Objective: This study aims to explore the potential of *in situ* airway differentiation of eosinophil progenitors (EoPs) and hematopoietic progenitor cells (HPCs) in sputum and peripheral blood from patients with non-asthmatic eosinophilic bronchitis (NAEB), eosinophilic asthma (EA), and healthy controls (HC).

Methods: Using flow cytometry, we enumerated sputum and blood HPCs and EoPs in patients with NAEB (n=15), EA (n=15), and HC (n=14) at baseline. Patients with NAEB and EA were then treated for 1 month with budesonide (200 μg, bid) or budesonide and formoterol (200/6 μg, bid), respectively. HPCs and EoPs in both compartments were re-evaluated.

Results: At baseline, NAEB and EA both had significantly greater numbers of sputum but not blood HPCs and EoPs ($p<0.05$) compared to HC. There were no differences between NAEB and EA. After 1 month of inhaled corticosteroid (ICS) treatment, NAEB patients showed a significant improvement in cough symptoms, but the attenuation of sputum HPC and EoP levels was not significant.

Conclusions: NAEB patients have increased airway levels of HPCs and EoPs. One-month treatment with ICS did not fully suppress the level of EoPs in NAEB. Controlling *in situ* airway differentiation of EoPs may control airway eosinophilia and provide long-term resolution of symptoms in NAEB.

Keywords: non-asthmatic eosinophilic bronchitis, hematopoietic progenitor cells, eosinophil progenitors, airway inflammation, eosinophil

OPEN ACCESS

Edited by:
Wendy W. J. Unger, Erasmus MC-Sophia Children's Hospital, Netherlands

Reviewed by:
Selma Van Staveren, Erasmus University Medical Center, Netherlands
Lili Chen, Icahn School of Medicine at Mount Sinai, United States

***Correspondence:**
Ruchong Chen
chen_rch@163.com
Roma Sehmi
sehmir@mcmaster.ca
Paul M. O'Byrne
obyrnep@mcmaster.ca

[†]These authors have contributed equally to this work and share first authorship

[‡]Lead contact

Specialty section:
This article was submitted to Mucosal Immunity, a section of the journal Frontiers in Immunology

Received: *08 July 2021*
Accepted: *03 March 2022*
Published: *31 March 2022*

Citation:
Zhan C, Xu R, Li B, Liu J, Liang W, Zhang S, Fang L, Zhong S, de Silva SDSH, Sivapalan D, Luo W, Li J, Lai K, Zhong N, Sehmi R, O'Byrne PM and Chen R (2022) Eosinophil Progenitors in Patients With Non-Asthmatic Eosinophilic Bronchitis, Eosinophilic Asthma, and Normal Controls. Front. Immunol. 13:737968. doi: 10.3389/fimmu.2022.737968

INTRODUCTION

Non-asthmatic eosinophilic bronchitis (NAEB) is a common cause of chronic cough (1, 2). It is characterized by persistent troublesome cough and airway eosinophilia but lack of airway hyper-responsiveness (3). NAEB patients often respond well to inhaled corticosteroids but frequently relapse (4).

Previous studies have shown that NAEB is a T-helper 2 (Th2)-driven disease. In addition to airway eosinophilia, it was reported that, like asthmatics, NAEB patients have raised levels of inflammatory mediators and cytokines, such as histamine, cysteinyl-leukotrienes, interleukin (IL)-5, and eosinophilic cationic protein (5–7). Persistent sputum eosinophilia is a risk factor for relapse (8), suggesting that airway eosinophilia may be one major pathogenic mechanism in NAEB. Investigating the immunological processes that promote eosinophilic inflammation in the airways is important for the development of novel NAEB therapies.

Mature eosinophils differentiate from eosinophil-lineage committed progenitor cells (EoPs), which arise from bone-marrow-derived CD34+ hematopoietic progenitor cells (HPCs) (9). The differentiation and maturation of EoPs was originally thought to be restricted to the bone marrow (10, 11). However, increased numbers of HPCs and EoPs have been detected in the peripheral blood and tissue compartments from atopic subjects (12–15). It has now been proposed that *in situ* differentiation of EoPs can rapidly increase mucosal numbers of mature eosinophils during an inflammatory response, an element that may drive airway eosinophilia (16, 17). This suggests an important role of *in situ* eosinophil differentiation in the pathology of allergic diseases including asthma and allergic rhinitis.

We hypothesized that *in situ* differentiation of EoPs play a potential role in the pathogenesis of airway eosinophilia in NAEB. In the current study, we enumerated levels of HPCs and EoPs in induced sputum and peripheral blood from NAEB patients compared to eosinophilic asthmatics (EAs) and normal healthy controls (HCs). In addition, we repeated these measurements in NAEB and EA patients after 1 month of treatment with inhaled corticosteroids (ICS) or ICS plus long-acting beta-agonists (LABA), respectively.

MATERIALS AND METHODS

Study Design and Participants

Fifteen patients with NAEB were recruited in the First Affiliated Hospital of Guangzhou Medical University between June 2016 and May 2017. Fifteen patients with EA and 14 HCs were included as disease and health controls. Pulmonary function, fractional exhaled nitric oxide, sputum differential counts, complete blood counts (CBC), serum IgE, symptom scores, and questionnaires including Asthma Control Test (ACT), Leicester Cough Questionnaires (LCQ), and Visual Analogue Scale (VAS) were recorded. Levels of sputum and blood HPCs and EoPs were enumerated by flow cytometry in all participants. NAEB patients were prescribed budesonide (200 μg, bid), and EA patients were prescribed budesonide/formoterol (200/6 μg, bid) for 1 month. Following this, FeNO, sputum differential count, CBC, and flow cytometric assessments of progenitor cells were re-evaluated in both patient groups.

NAEB was diagnosed according to the Chinese cough guidelines (18). The subjects had (1) persistent cough for more than 8 weeks; (2) a normal chest radiograph; (3) sputum eosinophilia (sputum Eos% ≥ 2.5%); and (4) normal spirometry and normal methacholine airway responsiveness. The subjects with EA were diagnosed according to the GINA 2015 criteria (19). All patients with EA had characteristic symptoms (such as wheezing, shortness of breath, chest tightness, or cough); increased sputum eosinophilia (sputum Eos% ≥ 3%), and >12% forced expiratory volume in 1 s (FEV1) reversibility after short-acting bronchodilator or a positive methacholine provocative test. All patients with NAEB or EA were not currently on any steroid therapy. The healthy controls (n=14) had normal spirometry, negative methacholine provocative test, and no history of respiratory disease, allergies, or systemic disease. All subjects were non-smokers. Subjects were excluded if they had experienced a respiratory infection in the past 4 weeks or had a history of bronchiectasis, chronic obstructive pulmonary disease, or other chronic pulmonary diseases.

Sputum Induction and Cell Isolation

Sputum was induced by inhalation of an aerosol of hypertonic saline as previously described (20). Sputum samples were processed by selecting the mucus plugs, mixing with 4 parts 0.1% dithiothreitol, then filtered through a 48-mm nylon mesh and centrifuged at 3,000 rpm for 10 min at 4°C. The cell pellet was re-suspended in phosphate-buffered saline (PBS). The sputum supernatants were stored at −80°C. The cell smear was prepared and stained with hematoxylin–eosin stain. The differential cell counts of sputum samples were obtained by counting 400 non-squamous cells. The remaining cells were subjected to immunofluorescence staining and enumeration by flow cytometry.

PBMC Isolation

Peripheral blood mononuclear cells (PBMCs) were isolated from venous blood by Ficoll density gradient centrifugation. In brief, whole blood was diluted 1:1 with PBS and layered onto Ficoll-PAQUE Plus (GE Healthcare, Marlborough, MA, USA), centrifuged at 1,200*g* and 4°C for 25 min with the brake off. The buffy coat was collected and washed twice (500*g* for 5 min) with PBS. Cell count and viability were quantified in a Neubauer's chamber with 0.4% Trypan Blue Solution.

Flow Cytometry

Freshly isolated blood-derived mononuclear cells and sputum-extracted cells were immediately incubated with fluorescence-labeled antibodies to define cell subpopulations. Antibodies (BD Biosciences) used for flow cytometry were FITC-CD45, PE-Cy5-CD34, and PE-CD125. Cells were analyzed by FACSVerse analytical flow cytometry (BD Company, San Diego, CA, USA). The percentage of HPCs ($FSC^{medium}SSC^{low}CD45^{dull}CD34^{+}$) and

EoPs ($FSC^{medium}SSC^{low}CD45^{dull}CD34^{+}CD125^{+}$) were determined using FlowJo software (BD Biosciences). The absolute numbers of HPCs or EoPs were calculated by multiplying percentage of HPCs or EoPs within R2 (singlets with medium FSC and low SSC) in flow cytometry with the absolute number of lymphocytes in blood routine test or sputum cell counts. The gating strategy is shown in **Supplementary Figure S1**.

Statistical Analysis

Statistical analysis was performed by using SPSS Version23.0 (SPSS Inc., Chicago, IL, USA). Age, body mass index (BMI), FEV1pred, MMEFpred, FEV1/forced vital capacity (FEV1/FVC), and blood eosinophil were presented as mean ± SD and analyzed by one-way ANOVA followed by the Tukey post-test for multiple comparisons. Sputum differential counts, FeNO, serum total IgE, HPCs, and EoPs levels were presented as median (IQR) and analyzed by Kruskal–Wallis test and Dunn's *post-hoc* analyses for multiple comparisons. Comparisons of LCQ, VAS, ACT, FeNO, sputum and blood eosinophils, HPCs, and EoPs before and after treatment were calculated using a paired t-test or Wilcoxon matched-pairs sign rank test. Correlations among clinical parameters were computed using a Spearman test. Differences were considered to be statistically significant when $p<0.05$.

RESULTS

Demographics and Clinical Characteristics at Baseline

Baseline characteristics of participants in the study are shown in **Table 1**. NAEB and EA patients were significantly older and had a higher BMI than HC controls (all $p<0.01$). Similar to EA, NAEB showed higher levels of FeNO, sputum eosinophils, and blood eosinophils compared with HC ($p<0.05$). No differences of FeNO, sputum, and blood eosinophils were found between NAEB and EA.

Airway HPCs and EoPs Are Increased in Patients With NAEB

PBMCs were successful obtained from all subjects for flow cytometry detection. Sputum samples for flow cytometry were obtained from 14 patients with NAEB, 11 patients with EA, and 9 subjects with HC.

In the airway, sputum HPCs levels in NAEB [770 (8,219) cells/ml] and EA [742 (1,322) cells/ml] were significantly higher than in the HC group [135 (343) cells/ml] (both $p<0.05$, **Figure 1A**). In addition, sputum EoPs levels were significantly higher in patients with NAEB [91 (219) cells/ml] and EA [69 (199) cells/ml] compared to the HC group [17 (26) cells/ml] (both $p<0.05$, **Figure 1B**). In contrast, there were no significant differences in sputum HPCs or EoPs levels between NAEB and EA. Overall, there was a strong correlation between sputum HPCs and EoPs levels (r=0.778, $p<0.001$, **Supplementary Figure S2**) and a moderate association between sputum EoPs and eosinophils levels (r=0.378, $p<0.05$, **Supplementary Figure S2**).

In the blood, there was no significant difference in HPCs or EoPs levels in NAEB [HPCs, 1,123 (650)/ml; EoPs, 71 (110)/ml] compared with the HC [HPCs, 952 (1,246)/ml; EoPs, 118 (117)/ml] or EA group [HPCs, 1,498 (1,109)/ml; EoPs, 121 (156)] (**Figures 1C, D**). Neither blood HPCs levels nor EoPs levels correlated with blood eosinophil, sputum HPCs, or EoPs levels (**Supplementary Figure S1**).

HPCs and EoPs Levels Following Treatment With ICS for NAEB or ICS/LABA for EA

After 1-month ICS treatment, patients with NAEB presented an improvement in cough symptoms as reflected by a significant

TABLE 1 | Demographics and clinical characteristics at baseline.

	HC n=14	NAEB n=15	EA n=15
Sex, F/M	8/6	5/10	9/6
Age, y	29.2 ± 6.4	46.7 ± 14.6#	44.5 ± 10.9#
BMI	20.1 ± 2.5	23.5 ± 2.9*	23.9 ± 3.9*
FeNO. ppb	16.0 (9.0, 23.0)	34.0 (23.0, 61.0) #	50.0 (36.0, 79.0) #
FEV1, pred%	95.6 ± 8.2	100.8 ± 12.8‡	81.6 ± 22.3
FEV1/FVC, %	87.7 ± 8.0	83.4 ± 6.6‡	69.8 ± 12.1#
MMEF, pred%	84.0 ± 24.6	88.7 ± 25.5‡	44.0 ± 21.9#
Induced Sputum			
TCC, $x10^6$/mL	2.3 (0.8-5.8)	2.8 (1.4-13.2)	2.3 (0.9-11.2)
Neutrophils, %	60.2 (40.5, 65.5)	59.0 (26.0, 77.5)	49.0 (21.5, 78.0)
Macrophage, %	37.5 (23.8, 58.5)	21.0 (8.5, 47.0)	11.8 (1.5, 53.5)
Eosinophils, %	0.2 (0.0, 1.0)	4.5 (3.5, 18.5)#	16.0 (8.2, 37.8)#
Lymphocyte, %	1.5 (0.8, 2.2)	1.5 (1.0, 11.5)	2.0 (1.0, 2.5)
Blood			
Eosinophils, %	2.2 ± 1.6	5.2 ± 3.2*	6.4 ± 3.2#
Eosinophils, (10^9/L)	0.1 ± 0.1	0.3 ± 0.2*	0.4 ± 0.2#
Total IgE (KU/L)	55.7 (27.4, 89.9)	98.7 (50.6, 180.0)	107.2 (67.2, 327.0)

*Age, BMI, FeNO, FEV1pred, FEV1/FVC, MMEFpred and blood eosinophil are presented as mean ± SD and analyzed by one-way ANOVA. Sputum different counts and Total IgE are presented as median (IQR); sputum TCC is presented as median (min–max) and calculated by Kruskal–Wallis test. The distribution of sex was calculated by chi-square test. Compared with EA: ‡p < 0.01; compared with healthy control: *p < 0.05, #p < 0.01.*

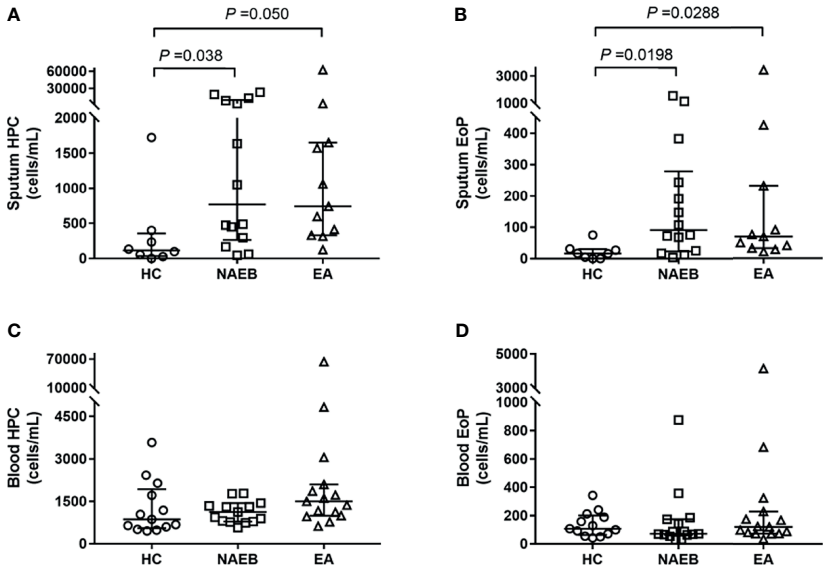

FIGURE 1 | Absolute numbers of hematopoietic progenitor cells (HPC) and eosinophilic progenitor cells (EoPs) in three groups at baseline. Absolute numbers of sputum HPC cells **(A)** and EoP cells **(B)**, and the peripheral blood HPC cells **(C)** and EoP cells **(D)**. Absolute cell numbers enumerated by flow cytometry are presented as cells/ml, and data are presented as median (IQR) values. HC, healthy control group; NAEB, non-asthmatic eosinophilic bronchitis group; EA, eosinophilic asthmatics group.

improvement of LCQ [16.2 ± 2.4 vs. 20.4 ± 3.5] and VAS [50 (30) vs. 10 (5)] (all $p<0.05$). One patient reported complete resolution of symptoms. In addition, the NAEB group displayed decreased levels of FeNO [59 (53) vs. 25 (11)] and blood eosinophils [0.3 (0.2) vs. 0.2 (0.1)] (all $p<0.05$). There was reduction in the level of sputum HPCs, EoPs, and eosinophils [HPCs, 1,345(11,476) vs. 887(1,370); EoPs, 169(275) vs. 7(200), cells/ml; Eos, 5.0(37.8) vs. 3.8(10.3), %], although this change did not achieve significance (**Figure 2** and **Table 2**).

In patients with EA, an improvement in symptoms was observed as reflected by an increasing ACT score (19.4 ± 3.7 vs. 23.3 ± 1.7) ($p<0.05$). A significant reduction was found in blood HPCs and EoPs levels [HPCs, 1,553(1,697) vs. 775(1,160); EoPs, 145(328) vs. 84 (90), cells/ml] (all $p<0.05$) but not mature eosinophils. In contrast, no differences were found in FeNO levels or sputum eosinophils, HPCs, or EoPs after treatment in these patients (**Figure 2** and **Table 2**). For the follow-up time point, when data from EA and NAEB patients were combined, the sputum EoPs level did not correlate with sputum HPCs nor eosinophils levels (**Supplementary Figure S2B**).

DISCUSSION

The current study has demonstrated, for the first time, that NAEB patients have significantly increased levels of EoPs and HPC in the airways when compared to healthy controls. One-month ICS therapy improved symptoms in NAEB patients; however, the reduction in inflammatory indices including airway EoPs, HPCs, and mature eosinophils was not significant. The results suggest that *in situ* airway differentiation of EoPs may be one of the possible pathways mediating the airway eosinophilia in NAEB. In addition, longer treatment strategies may be required to investigate whether normalization of lung inflammatory cells may further improve symptoms of NAEB and chances of future relapse.

Immune cells that contribute to airway eosinophilia in NAEB are not clearly defined. Brightling et al. (6) previously reported that the proportion of BALF IL-4+CD4+ T cells and the number of IL-4+ and IL-5+ cells in bronchial submucosa are significantly higher in NAEB compared to HC controls, suggesting that the Th2 cell may drive airway eosinophilia in these patients. In addition to the traffic of mature eosinophils from the periphery, *in situ* eosinophilopoiesis has been proposed as an additional process that may drive airway eosinophilia in allergic asthma and rhinitis. It can rapidly increase mucosal levels of mature eosinophils during an inflammatory response. Studies have shown that the increase in numbers of sputum EoPs precedes the development of airway eosinophilia after allergen inhalational challenge in asthmatics (21). Cameron et al. (16) found that local IL-5-dependent differentiation of EoPs was observed when nasal biopsies were cultured *ex vivo* with IL-5 or ragweed allergen resulting in a reduction in CD34 immunopositive/IL-5Rα mRNA+ cells and a concurrent increase in the number of MBP immunoreactive cells, likely mature eosinophils. Our data showed increased levels of sputum HPCs, EoPs in NAEB, and a moderate association between sputum EoPs and sputum eosinophilia indicating, that *in situ* differentiation may mediate local increases in mature eosinophil levels in NAEB. Consistent with this hypothesis, NAEB patients had increased concentrations of IL-5 and granulocyte-macrophage colony-stimulating factor (GM-CSF), which could induce HPCs and EoPs differentiation into

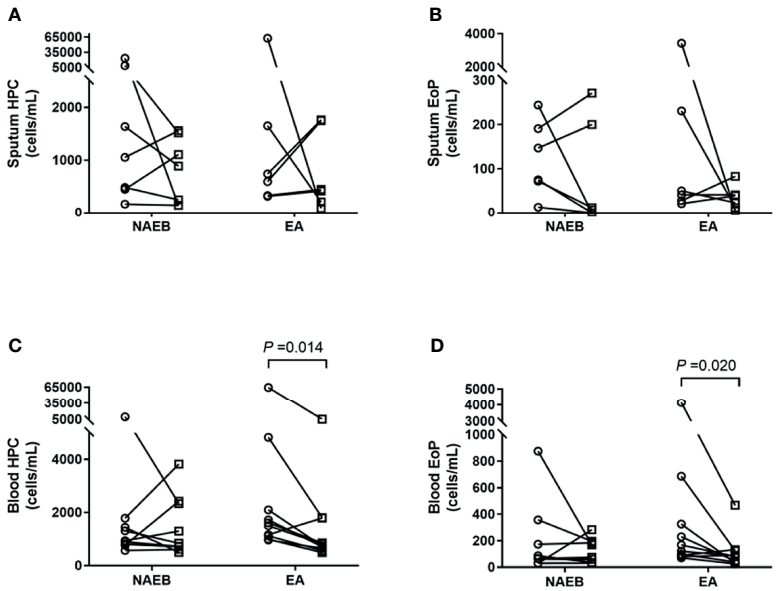

FIGURE 2 | Enumeration of hematopoietic progenitor cells (HPC) and eosinophilic progenitor cells (EoPs) in sputum and peripheral blood after 1 month of ICS treatment in NAEB and ICS/LABA treatment in EA. The changes in sputum HPC counts **(A)** and EoP counts **(B)**, and blood HPC counts **(C)** and EoP counts **(D)** before (open circle) and after (open square) therapy. NAEB, Non-asthmatic eosinophilic bronchitis group. EA, eosinophilic asthmatics group.

TABLE 2 | Changes of biomarkers after one-month treatment in NAEB and EA Group.

	NAEB (n=9)			EA (n=10)		
	Baseline	**Follow-up**	***p*-value**	**Baseline**	**Follow-up**	***p*-value**
FeNO, ppb	59(53)	25(11)*	0.020	46.5(57.3)	28.5(51.7)	0.416
LCQ	16.2 ± 2.4	20.4 ± 3.5*	0.049	NA	NA	NA
VAS	50(30)	10(5)#	<0.001	NA	NA	NA
ACT	NA	NA	NA	19.4 ± 3.7	23.3 ± 1.7*	0.014
Sputum Eos, %	5.0(37.8)	3.8(10.3)	0.148	16.4(36)	5(41.6)	0.734
Sputum Eos (10^9/L)	0.20(0.80)	0.18(0.40)	0.461	0.41(1.70)	0.10(0.70)	0.160
Blood Eos (10^9/L)	0.3(0.2)	0.2(0.1)*	0.050	0.4(0.2)	0.3(0.2)	0.456
Blood HPC (cells/ml)	939(822)	843(1,726)	0.820	1553(1,697)	775(1,160)*	0.014
Blood EoP (cells/ml)	68(229)	76(143)	0.637	145(328)	84 (90)*	0.020
	NAEB (n=7)			**EA (n=6)**		
Sputum HPC (cells/ml)	1345(11476)	887(1370)	0.297	742(2051)	432(1574)	0.900
Sputum EoP (cells/ml)	169(275)	7(200)	0.297	69(294)	31(41)	0.438

*FeNO, LCQ, VAS, and ACT were presented as mean ± SD and analyzed by pair t-test. Other variables were presented as median (IQR) calculated by Wilcoxon matched-pairs sign rank test. Absolute cell numbers enumerated by means of flow cytometry are presented as cells per milliliter. Compared with baseline: *p < 0.05, #p < 0.01*

eosinophils within the airways (6, 22, 23). In addition, recent studies have suggested that HPCs and EoPs may act as pro-inflammatory effector cells following activation by epithelial cell-derived alarmin cytokines (24). Upon stimulation with thymic stomal lymphopoietin (TSLP) and/or interleukin-33 (IL-33), HPCs shown to express TSLPR and ST2 (25) release high levels of IL-5, IL-13, and GM-CSF (26). Whether NAEB has higher levels of alarmin cytokines in the airways and whether sputum HPC and EoP express greater amounts of type 2 cytokines compared to healthy controls remains to be investigated.

In line with previous studies (17, 21), we found that asthmatic patients showed elevated levels of airway HPCs and EoPs. However, no differences in blood EoPs were observed. This might be related to the severity of the asthmatic patients enrolled, as blood and sputum EoPs in severe asthma are significantly higher than in mild asthma (17). In the current study, the asthmatic patients were mild and steroid naive. Our previous data (17) found a 10-fold greater number of sputum EoPs in prednisone-dependent severe asthmatics compared to mild asthmatics, while these cells were comparable in the PB of both subject groups, suggesting that an enhanced eosinophilopoietic environment exits in the airways of severe asthmatics with persistent eosinophilia.

In contrast to the EA group, neither blood HPCs nor blood EoPs in the NAEB group were different when compared to HC controls. We speculated that there may be systemic component

involving mobilization of progenitor cells from bone marrow in EA compared to NAEB where the inflammatory responses appear to be localized to the airways. Eotaxin/CCR3 and SDF-1/CXCR4 axes are reported to play a role promoting progenitors release from the bone marrow in EA and might be less prominent or involved in progenitor cell trafficking to the airways in NAEB (27, 28). This is supported by our previous findings where we found no difference in serum levels of eotaxin or IL-5 in NAEB compared to HC, suggesting that NAEB displayed only mild systemic inflammation (21).

After 1 month of treatment with ICS in NAEB, or ICS/LABA in EA, we found an inconsistent relationship between the improvement of symptoms and relief of inflammation. Despite a significant reduction in blood eosinophils, sputum levels of HPCs, EoPs, and mature eosinophil only showed a trend of not a significant decline in NAEB. In addition, a moderate correlation was found between sputum EoPs and eosinophils in these patients; this might fit out with the hypothesis that that local airway levels of EoP may contribute to the airway eosinophilia. Despite that the attenuation of sputum HPC and EoP levels in EA patients after ICS treatment was not significant, ICS treatment may still have a suppression role on local airway eosinophil differentiation to mature cells. The reasons are as follows: first, the weaker correlation between sputum EOS and HPC or EoP might provide indirect evidence that ICS treatment suppresses differentiation of EoPs into mature eosinophils (**Supplementary Figure S2B**). Second, Kim et al. reported that an increase in CD34+ mononuclear cells occurs in steroid-treated nasal polyps (29). A possible mechanism that they proposed is that inhibition of the differentiation of mature cells from progenitors may cause more residing CD34+ progenitor cells in the local tissue. Since we have previously reported a higher rate of recurring episodes after 1 month of ICS treatment compared to 3 months treatment, during a 1-year follow-up in NAEB (30), our current data suggest that a longer treatment strategy may be required to fully investigate whether reduction in local eosinophilopoietic processes may reduce airway eosinophilia and further improve the management of NAEB.

Some limitations of the study should be noted. First, we measured the total numbers of HPCs and EoPs, and the numbers of activated or cytokine-producing HPCs and EoPs were not determined. Second, our current study is an initial observational, small group study that is hypothesis generating, which provides indirect evidence of the existence of *in situ* airway differentiation in NAEB as reflected by the increased sputum EoPs in NAEB and its moderate correlation with sputum eosinophils. The significance of *in situ* airway differentiation of EoPs leading to airway eosinophilia in NAEB needs to be further investigated.

In summary, this study demonstrated that increases in HPCs and EoPs in NAEB are predominantly found in the airways and that these cells may contribute to the airway eosinophilia. One-month ICS treatment improved the symptoms in NAEB but did not fully suppress the airway inflammatory responses.

DATA AVAILABILITY STATEMENT

The datasets generated for this study can be obtained from the corresponding author upon reasonable request. Requests to access the datasets should be directed to chen_rch@163.com.

ETHICS STATEMENT

The studies involving human participants were reviewed and approved by the Ethic Committee of the First Affiliated Hospital of Guangzhou Medical University. The IRB number of the ethic approval is 2016-52. The patients/participants provided their written informed consent to participate in this study.

AUTHOR CONTRIBUTIONS

RS, PB, and RC planned the study and designed the experiments. JXL, WQL, SZ, LF, SXZ, DSHS, DS, and WL cared for the patients and provided clinical information. CZ, RX, and BL performed the experiments. CZ, RX, and BL performed the statistical analysis and wrote the manuscript. JL, KL, NZ, RS, PB, and RC contributed to made critical revision of the manuscript. RS, PB, and RC supervised the work. All authors contributed to the article and approved the submitted version.

FUNDING

This study was supported by grants from the National Natural Science Foundation of China (81870079), State Key Laboratory of Respiratory Disease (SKLRD-QN-201702), Guangzhou Science and Technology Project/Nanshan Medical Foundation (202102010349), Incubation Project for Innovation Team of GMU (Grant 2017-159), and Incubation Program of National Science Found for Distinguished Young Scholars (GMU2020-207).

SUPPLEMENTARY MATERIAL

The Supplementary Material for this article can be found online at: https://www.frontiersin.org/articles/10.3389/fimmu.2022.737968/full#supplementary-material

REFERENCES

1. Brightling CE, Ward R, Goh KL, Wardlaw AJ, Pavord ID. Eosinophilic Bronchitis Is an Important Cause of Chronic Cough. *Am J Resp Crit Care* (1999) 160:406–10. doi: 10.1164/ajrccm.160.2.9810100
2. Lai K, Chen R, Lin J, Huang K, Shen H, Kong L, et al. A Prospective, Multicenter Survey on Causes of Chronic Cough in China. *Chest* (2013) 143:613–20. doi: 10.1378/chest.12-0441
3. Gibson PG, Dolovich J, Denburg J, Ramsdale EH, Hargreave FE. Chronic Cough: Eosinophilic Bronchitis Without Asthma. *Lancet*

(London England) (1989) 1:1346–8. doi: 10.1016/s0140-6736(89)92801-8
4. Gibson PG, Hargreave FE, Girgis-Gabardo A, Morris M, Denburg JA, Dolovich J. Chronic Cough With Eosinophilic Bronchitis: Examination for Variable Airflow Obstruction and Response to Corticosteroid. *Clin Exp Allergy* (1995) 25:127–32. doi: 10.1111/j.1365-2222.1995.tb01017.x
5. Brightling CE, Symon FA, Birring SS, Bradding P, Wardlaw AJ, Pavord ID. Comparison of Airway Immunopathology of Eosinophilic Bronchitis and Asthma. *Thorax* (2003) 58(6):528–32. doi: 10.1136/thorax.58.6.528
6. Brightling CE, Symon FA, Birring SS, Bradding P, Pavord ID, Wardlaw AJ. TH2 Cytokine Expression in Bronchoalveolar Lavage Fluid T Lymphocytes and Bronchial Submucosa Is a Feature of Asthma and Eosinophilic Bronchitis. *J Allergy Clin Immunol* (2002) 110:899–905. doi: 10.1067/mai.2002.129698
7. Brightling CE, Ward R, Woltmann G, Bradding P, Sheller JR, Dworski R, et al. Induced Sputum Inflammatory Mediator Concentrations in Eosinophilic Bronchitis and Asthma. *Am J Resp Crit Care* (2000) 162:878–82. doi: 10.1164/ajrccm.162.3.9909064
8. Lai K, Liu B, Xu D, Han L, Lin L, Xi Y, et al. Will Nonasthmatic Eosinophilic Bronchitis Develop Into Chronic Airway Obstruction?: A Prospective, Observational Study. *Chest* (2015) 148:887–94. doi: 10.1378/chest.14-2351
9. Sehmi R, Denburg JA. Differentiation of Human Eosinophils. Role in Allergic Inflammation. *Chem Immunol* (2000) 76:29–44. doi: 10.1159/000058788
10. Sanderson CJ. Interleukin-5, Eosinophils, and Disease. *BLOOD* (1992) 79:3101–9. doi: 10.1182/blood.V79.12.3101.bloodjournal79123101
11. Clutterbuck EJ, Hirst EM, Sanderson CJ. Human Interleukin-5 (IL-5) Regulates the Production of Eosinophils in Human Bone Marrow Cultures: Comparison and Interaction With IL-1, IL-3, IL-6, and GMCSF. *Blood* (1989) 73:1504–12. doi: 10.1182/blood.V73.6.1504.bloodjournal7361504
12. Gibson PG, Dolovich J, Girgis-Gabardo A, Morris MM, Anderson M, Hargreave FE, et al. The Inflammatory Response in Asthma Exacerbation: Changes in Circulating Eosinophils, Basophils and Their Progenitors. *Clin Exp Allergy* (1990) 20:661–8. doi: 10.1111/j.1365-2222.1990.tb02705.x
13. Gibson PG, Manning PJ, O'Byrne PM, Girgis-Gabardo A, Dolovich J, Denburg JA, et al. Allergen-Induced Asthmatic Responses. Relationship Between Increases in Airway Responsiveness and Increases in Circulating Eosinophils, Basophils, and Their Progenitors. *Am Rev Respir Dis* (1991) 143:331–5. doi: 10.1164/ajrccm/143.2.331
14. Sehmi R, Howie K, Sutherland DR, Schragge W, O'Byrne PM, Denburg JA. Increased Levels of CD34+ Hemopoietic Progenitor Cells in Atopic Subjects. *Am J Resp Cell Mol* (1996) 15:645–55. doi: 10.1165/ajrcmb.15.5.8918371
15. Dorman SC, Babirad I, Post J, Watson RM, Foley R, Jones GL, et al. Progenitor Egress From the Bone Marrow After Allergen Challenge: Role of Stromal Cell-Derived Factor 1alpha and Eotaxin. *J Allergy Clin Immunol* (2005) 115:501–7. doi: 10.1016/j.jaci.2004.11.017
16. Cameron L, Christodoulopoulos P, Lavigne F, Nakamura Y, Eidelman D, McEuen A, et al. Evidence for Local Eosinophil Differentiation Within Allergic Nasal Mucosa: Inhibition With Soluble IL-5 Receptor. *J Immunol (Baltimore Md.: 1950)* (2000) 164:1538–45. doi: 10.4049/jimmunol.164.3.1538
17. Sehmi R, Smith SG, Kjarsgaard M, Radford K, Boulet L, Lemiere C, et al. Role of Local Eosinophilopoietic Processes in the Development of Airway Eosinophilia in Prednisone-Dependent Severe Asthma. *Clin Exp Allergy* (2016) 46:793–802. doi: 10.1111/cea.12695
18. The Asthma Workgroup of Chinese Society of Respiratory Diseases (CSRD), Chinese Medical Association. The Chinese National Guidelines on Diagnosis and Management of Cough (December 2010). *Chin Med J-PEKING* (2011) 124:3207–19. doi: 10.3760/cma.j.issn.0366-6999.2011.20.002
19. *Global Strategy for Asthma Management and Prevention* (2015). Available at: http://guide.medlive.cn/guideline/12751.
20. Pizzichini E, Pizzichini MM, Efthimiadis A, Evans S, Morris MM, Squillace D, et al. Indices of Airway Inflammation in Induced Sputum: Reproducibility and Validity of Cell and Fluid-Phase Measurements. *Am J Respir Crit Care Med* (1996) 154(2 Pt 1):308–17. doi: 10.1164/ajrccm.154.2.8756799
21. Dorman SC, Efthimiadis A, Babirad I, Watson RM, Denburg JA, Hargreave FE, et al. Sputum CD34+IL-5Ralpha+ Cells Increase After Allergen: Evidence for *In Situ* Eosinophilopoiesis. *Am J Resp Crit Care* (2004) 169:573–7. doi: 10.1164/rccm.200307-1004OC
22. Zhan C, Xu R, Liu J, Zhang S, Luo W, Chen R, et al. Increased Sputum IL-17a Level in Non-Asthmatic Eosinophilic Bronchitis. *Lung* (2018) 196:699–705. doi: 10.1007/s00408-018-0166-y
23. Zhang R, Luo W, Liang Z, Tan Y, Chen R, Lu W, et al. Eotaxin and IL-4 Levels Are Increased in Induced Sputum and Correlate With Sputum Eosinophils in Patients With Nonasthmatic Eosinophilic Bronchitis. *Medicine* (2017) 96:e6492. doi: 10.1097/MD.0000000000006492
24. Allakhverdi Z, Comeau MR, Smith DE, Toy D, Endam LM, Desrosiers M, et al. CD34+ Hemopoietic Progenitor Cells Are Potent Effectors of Allergic Inflammation. *J Allergy Clin Immunol* (2009) 123:472–8. doi: 10.1016/j.jaci.2008.10.022
25. Hui CCK, Rusta-Sallehy S, Asher I, Heroux D, Denburg JA. The Effects of Thymic Stromal Lymphopoietin and IL-3 on Human Eosinophil-Basophil Lineage Commitment: Relevance to Atopic Sensitization. *Immunity Inflamm Dis* (2014) 2:44–55. doi: 10.1002/iid3.20
26. Smith SG, Gugilla A, Mukherjee M, Merim K, Irshad A, Tang W, et al. Thymic Stromal Lymphopoietin and IL-33 Modulate Migration of Hematopoietic Progenitor Cells in Patients With Allergic Asthma. *J Allergy Clin Immunol* (2015) 135:1594–602. doi: 10.1016/j.jaci.2014.12.1918
27. Wright DE, Bowman EP, Wagers AJ, Butcher EC, Weissman IL. Hematopoietic Stem Cells Are Uniquely Selective in Their Migratory Response to Chemokines. *J Exp Med* (2002) 195:1145–54. doi: 10.1084/jem.20011284
28. Lévesque J, Hendy J, Takamatsu Y, Simmons PJ, Bendall LJ. Disruption of the CXCR4/CXCL12 Chemotactic Interaction During Hematopoietic Stem Cell Mobilization Induced by GCSF or Cyclophosphamide. *J Clin Invest* (2003) 111:187–96. doi: 10.1172/JCI15994
29. Kim YK, Uno M, Hamilos DL, Beck L, Bochner B, Schleimer R, et al. Immunolocalization of CD34 in Nasal Polyposis. Effect of Topical Corticosteroids. *Am J Resp Cell Mol* (1999) 20:388–97. doi: 10.1165/ajrcmb.20.3.3060
30. Zhan W, Tang J, Chen X, Yi F, Han L, Liu B, et al. Duration of Treatment With Inhaled Corticosteroids in Nonasthmatic Eosinophilic Bronchitis: A Randomized Open Label Trial. *Ther Adv Respir Dis* (2019) 13:1023340736. doi: 10.1177/1753466619891520

Conflict of Interest: RS reports grants and personal fees from Genentech Inc, grants and personal fees from Astra Zeneca, grants and personal fees from Teva Pharmaceuticals, personal fees from GSK, all outside the scope of this work; PO'B has grants in aid and speaker's fees from AstraZeneca, grants in aid from Bayer, Genentech, Merck, and Novartis, and has received speaker's fees from GSK, Chiesi and Covis, all outside the scope of this work. RC reports grants and speaker's fees from AstraZeneca GSK, Sanofi and Novartis, all outside the scope of this work.

The remaining authors declare that the research was conducted in the absence of any commercial or financial relationships that could be construed as a potential conflict of interest.

Publisher's Note: All claims expressed in this article are solely those of the authors and do not necessarily represent those of their affiliated organizations, or those of the publisher, the editors and the reviewers. Any product that may be evaluated in this article, or claim that may be made by its manufacturer, is not guaranteed or endorsed by the publisher.

frontiers | Frontiers in Immunology

ORIGINAL RESEARCH
published: 14 June 2022
doi: 10.3389/fimmu.2022.803362

Increased Expression of *LASI* lncRNA Regulates the Cigarette Smoke and COPD Associated Airway Inflammation and Mucous Cell Hyperplasia

*Marko Manevski[1], Dinesh Devadoss[1], Christopher Long[1], Shashi P. Singh[2], Mohd Wasim Nasser[3], Glen M. Borchert[4], Madhavan N. Nair[1], Irfan Rahman[5], Mohan Sopori[2] and Hitendra S. Chand[1]**

[1] Department of Immunology and Nano-Medicine, Herbert Wertheim College of Medicine, Florida International University, Miami, FL, United States, [2] Respiratory Immunology Program, Lovelace Respiratory Research Institute, Albuquerque, NM, United States, [3] Department of Biochemistry and Molecular Biology, University of Nebraska Medical Center, Omaha, NE, United States, [4] Department of Pharmacology, University of South Alabama, Mobile, AL, United States, [5] Department of Environmental Medicine, University of Rochester Medical Center, Rochester, NY, United States

OPEN ACCESS

Edited by:
Wendy W. J. Unger,
Erasmus MC-Sophia Children's Hospital, Netherlands

Reviewed by:
Venkataramana Sidhaye,
Johns Hopkins University, United States
Dhyan Chandra,
University at Buffalo, United States

***Correspondence:**
Hitendra S. Chand
hchand@fiu.edu

Specialty section:
This article was submitted to Mucosal Immunity, a section of the journal Frontiers in Immunology

Received: 27 October 2021
Accepted: 09 May 2022
Published: 14 June 2022

Citation:
Manevski M, Devadoss D, Long C, Singh SP, Nasser MW, Borchert GM, Nair MN, Rahman I, Sopori M and Chand HS (2022) Increased Expression of LASI lncRNA Regulates the Cigarette Smoke and COPD Associated Airway Inflammation and Mucous Cell Hyperplasia. Front. Immunol. 13:803362. doi: 10.3389/fimmu.2022.803362

Research Impact: Cigarette smoke (CS) exposure is strongly associated with chronic obstructive pulmonary disease (COPD). In respiratory airways, CS exposure disrupts airway barrier functions, mucous/phlegm production, and basic immune responses of airway epithelial cells. Based on our recent identification of a specific immunomodulatory long noncoding RNA (lncRNA), we investigated its role in CS-induced responses in bronchial airways of cynomolgus macaque model of CS-induced COPD and in former smokers with and without COPD. The lncRNA was significantly upregulated in CS-induced macaque airways and in COPD airways that exhibited higher mucus expression and goblet cell hyperplasia. Experimental models of cells derived from COPD subjects recapitulated the augmented inflammation and mucus expression following the smoke challenge. Blocking of lncRNA expression in cell culture setting suppressed the smoke-induced and COPD-associated dysregulated mucoinflammatory response suggesting that this airway specific immunomodulatory lncRNA may represent a novel target to mitigate the smoke-mediated inflammation and mucus hyperexpression.

Rationale: In conducting airways, CS disrupts airway epithelial functions, mucociliary clearances, and innate immune responses that are primarily orchestrated by human bronchial epithelial cells (HBECs). Mucus hypersecretion and dysregulated immune response are the hallmarks of chronic bronchitis (CB) that is often exacerbated by CS. Notably, we recently identified a long noncoding RNA (lncRNA) antisense to ICAM-1 (*LASI*) that mediates airway epithelial responses.

Objective: To investigate the role of *LASI* lncRNA in CS-induced airway inflammation and mucin hyperexpression in an animal model of COPD, and in HBECs and lung tissues from

former smokers with and without COPD. To interrogate *LASI* lncRNA role in CS-mediated airway mucoinflammatory responses by targeted gene editing.

Methods: Small airway tissue sections from cynomolgus macaques exposed to long-term mainstream CS, and those from former smokers with and without COPD were analyzed. The structured-illumination imaging, RNA fluorescence *in-situ* hybridization (FISH), and qRT-PCR were used to characterize lncRNA expression and the expression of inflammatory factors and airway mucins in a cell culture model of CS extract (CSE) exposure using HBECs from COPD (CHBEs) in comparison with cells from normal control (NHBEs) subjects. The protein levels of mucin MUC5AC, and inflammatory factors ICAM-1, and IL-6 were determined using specific ELISAs. RNA silencing was used to block *LASI* lncRNA expression and lentivirus encoding *LASI* lncRNA was used to achieve *LASI* overexpression (LASI-OE).

Results: Compared to controls, *LASI* lncRNA was upregulated in CS-exposed macaques and in COPD smoker airways, correlating with mucus hyperexpression and mucus cell hyperplasia in severe COPD airways. At baseline, the unstimulated CHBEs showed increased *LASI* lncRNA expression with higher expression of secretory mucin MUC5AC, and inflammatory factors, ICAM-1, and IL-6 compared to NHBEs. CSE exposure of CHBEs resulted in augmented inflammation and mucus expression compared to controls. While RNA silencing-mediated *LASI* knockdown suppressed the mucoinflammatory response, cells overexpressing *LASI* lncRNA showed elevated mRNA levels of inflammatory factors.

Conclusions: Altogether, *LASI* lncRNA may represent a novel target to control the smoke-mediated dysregulation in airway responses and COPD exacerbations.

Keywords: bronchial epithelial cells, cigarette smoke (CS), chronic obstructive pulmonary disease (COPD), long noncoding RNA (lncRNA), mucus hyperexpression, lncRNA antisense to ICAM-1 (LASI)

INTRODUCTION

COPD is the third leading cause of death globally, with over 300 million diagnosed cases and over 3 million COPD-related fatalities annually (1, 2). Environmental exposure to toxins or allergens exacerbates the disease and are associated with a very high (55%) 5-year mortality rate among COPD patients (3). COPD is an aging-associated condition characterized by progressive and irreversible airway obstruction and tissue remodeling which presents as chronic bronchitis (CB) and alveolar tissue destruction (4). CB patients often suffer from dyspnea, cough and sputum production leading to increased rates of exacerbation, accelerated lung tissue aging and decline in lung function, reduced quality of life, and increased mortality (4, 5). CB is more prevalent among COPD patients, with approximately 74% patients reportedly affected with CB (5).

Among the environmental factors, cigarette smoke (CS) is the primary risk factor associated with COPD development. CS exposure induces inflammatory pathways and epithelial tissue remodeling in conducting airways through goblet cell hyperplasia and the loss of ciliary cells (2). CS exposure induces epigenetic events such as DNA methylation, histone modifications and notably, changes in expression of noncoding transcripts such as microRNAs (miRNAs) and long noncoding RNAs (lncRNAs) (6, 7). LncRNAs are noncoding transcripts over 200 bases in length and may interact with proteins, DNA, chromatin, and other RNAs to induce epigenetic and transcriptomic changes, affecting cell and tissue functions (8). A growing number of lncRNAs have been implicated in chronic pulmonary conditions, including CS-related immune responses, and inflammatory dysregulation (6, 9, 10). LncRNA-mediated regulation of immune responses is potentially central to the

Abbreviations: AB, Alcian Blue; AB-H&E, Alcian Blue Hematoxylin and Eosin; AB-PAS, Alcian Blue and Periodic Acid Schiff's reagent; ALI, Air-liquid interface; BL, Basal Lamina; CB, Chronic Bronchitis; CHBEs, COPD human bronchial epithelial cells; COPD, Chronic Obstructive Pulmonary Disease; CS, Cigarette Smoke; CSE, Cigarette Smoke Extract; CXCL8, C-X-C Motif Chemokine 8 or interleukin (IL)-8; FISH, Fluorescent *In-Situ* Hybridization; HBECs, Human Bronchial Epithelial Cells; ICAM-1, Intracellular Adhesion Molecule-1; *ICR*: ICAM-1-related long noncoding RNA; IL-6, Interleukin 6; *LASI*, lncRNA antisense to ICAM-1; lncRNA, Long Noncoding RNA; *MALAT1*, Metastasis Associated Lung Adenocarcinoma Transcript 1; miRNA, micro-RNA; MOI, multiplicity of infection; *NEAT1*, Nuclear Enriched Assembly Transcript 1; NHBEs, normal human bronchial epithelial cells; qRT-PCR, Quantitative Real-Time PCR; SPDEF, Sam-Pointed Domain Containing ETS Transcription Factor; TFG-β, Transforming Growth Factor β; *WAKMAR2*, Wound and Keratinocyte Migration Associated Long Noncoding RNA.

establishment of innate mucosal immunity, and dysregulated expressions may promote hyperactive immune responses like those observed in COPD subjects, following exacerbations. To understand the molecular mechanisms through which lncRNA regulate innate immune responses, we recently identified novel lncRNAs that impact lung pathology. Specifically, we identified a specific immunomodulatory lncRNA referred to as *LASI*, a lncRNA antisense to ICAM-1, and confirmed its direct involvement in modulating airway inflammatory and mucus hyperexpression responses (11).

We recently observed that long-term mainstream CS exposure results in airway remodeling in cynomologus macaques (*Macaca fascicularis*) with augmented chronic bronchitis (CB) and reduction in lung functions similar to those observed in smoke-associated COPD (12). Based on the important role of lncRNAs in COPD (6) and specifically *LASI* lncRNA in airway epithelial cells (11), we hypothesized that *LASI* lncRNA affected the CS-induced airway inflammation and mucus hypersecretion in COPD. Herein, using the structured-illumination imaging and RNA FISH, we found that *LASI* lncRNA was upregulated in the small airway epithelium of an animal model of chronic CS exposure as well as in former smokers with COPD, and its expression correlates with aggravated inflammatory and mucus secretory responses. In addition, unstimulated airway cells from COPD subjects showed strong association of higher *LASI* expression with upregulated expression of mucin and other inflammatory factors. Most importantly, we find blocking *LASI* expression rescues impaired airway responses due to CS-mediated dysregulations in COPD bronchial epithelial cells and the ectopic overexpression of LASI lncRNA resulted in increased expression of airway epithelial inflammatory factors.

MATERIALS AND METHODS

Human Lung Tissue Samples

Lung tissue samples were obtained from the Lung Tissue Research Consortium (LTRC) from the National Institutes of Health (NIH). The COPD patient cohorts are defined as patients with a post-bronchodilator FEV1/FVC <0.7, currently the most widely accepted and robust test for COPD. Although reports have shown that early-stage COPD may present with emphysematous or other pathologic changes prior to a presentation of an FEV1/FVC <0.7, this test remains the standard confirmation of COPD diagnosis. COPD patient samples were compared to samples from GOLD stage 0 patients, which are defined as having normal spirometry results, however, may have chronic symptoms such as cough and sputum product, and may present with risk factors for COPD such as smoking behavior (13). GOLD 0 individuals may or may not progress to active COPD status and are classified as pre-COPD (14). Both male and female subjects in each GOLD stage were grouped together and all groups include both active and former smokers. GOLD stage determination was made by spirometry testing and assigned to the appropriate GOLD stage group, per the protocols described by the National Heart, Lung, and Blood Institute and World Health Organization (13). In this report, GOLD stages I and II were defined as patients with mild COPD status and GOLD stages III and IV were defined as patients with severe COPD status. Each group had a minimum n=6 with a mean age between 59.7 and 65.2 years old. All COPD patients had a smoking history with average packs per year (PY) ranging between 22.4 and 41.5 and former smokers had not been smoking for an average of 13.2 and 22.9 years. Smoking history was self-reported for all patients. Lung tissue homogenates include epithelial tissue as well as other tissues and cell types. Samples were obtained from varying anatomical regions of the lungs, however all samples contained bronchial epithelial cells as confirmed by expression of pan-cytokeratin (pan-CK) from epithelial cells and MUC5AC mucin from secretory goblet cells.

M. fascicularis Cigarette Smoke Exposure

Female cynomolgus macaques (*M. fascicularis*) were exposed to mainstream CS in H2000 whole body exposure chambers at 250 mg/m^3 total suspended particulate matter (TPM) for 6 hours per day, 5 days per week, corresponding to 4 packs of cigarettes per day as described previously (12). At these concentrations C. macaques develop observable changes in lung physiology within three months of exposure. Lung resections and tissue sections were obtained as described previously (12).

Human Bronchial Epithelial Cell Culture and CSE Treatment

The primary HBECs from COPD and non-COPD donors were obtained from the commercial suppliers (Lonza Inc. or MatTek Corp). All primary cell lines were grown and treated in bronchial epithelial cell growth media (BEGM from Lonza or UNC MLI Tissue Procurement and Cell Culture Core). Air-liquid interface (ALI) cultures of primary cells were grown in BEGM and differentiated in bronchial ALI (B-ALI) differentiation media (Lonza or UNC MLI Tissue Procurement and Cell Culture Core), as described previously (11). ALI cultures were seeded at a density of 5 x 10^5 cells/cm^2 on collagen IV-coated Costar® 6.5 mm Transwells with 0.4 μm pore polyester membranes (Corning Costar Corporation). Cells were differentiated for a minimum of 21 days before treatments. Epithelial differentiation was confirmed by live cell imaging of ciliary beatings and mucus glycoprotein expression. For CSE preparation, CS particulate matter collected on the filter membranes from mainstream smoke of 3RF4 research cigarettes (courtesy Philip Kuehl, Lovelace Biomedical) were used and final treatments at 20 μg/ml CSE were used. Apical side epithelial cells were exposed to treatments for 30 minutes at each treatment point. In addition, paraffin-embedded tissue sections human COPD and healthy control lungs were obtained from the LTRC.

Quantitative Real-Time PCR With Reverse Transcription (qRT-PCR)

For all RT-qPCR analysis, total RNA extraction was performed using the RNeasy Mini kit (Qiagen) according to manufacturer's instructions. RNA concentration was quantified using the

Synergy HTX reader (BioTek, VT). Complementary (c)DNA was synthesized using the iScript Advanced cDNA synthesis kit (Bio-Rad), per manufacturer's instructions. FAM-based and SYBR Green primers were used. The *LASI, ICR, WAKMAR-2, NEAT1, MALAT1* lncRNAs and *MUC5AC* and *SPDEF* mRNA levels were quantified using FAM-based primer/probe sets and TaqMan gene expression kit or the SsoFast qPCR master mix (Applied Biosystems, Thermo Fisher). *ICAM-1*, *IL6*, and *CXCL8* mRNA levels were quantified using SYBR Green-based primers and the iTaq master mix (Bio-Rad). qRT-PCR was conducted using the Bio-Rad CFX Real-Time PCR detection system. Quantification of the results was performed using the delta-delta (ΔΔ)Ct method and U6 noncoding small nuclear RNA (snRNA) was used as a reference gene for lncRNA expression levels and *beta-actin* and *GAPDH* were used for mRNA expression levels as described recently (15).

RNA Fluorescence *In-Situ* Hybridization (FISH)

The RNAScope® 2.5 HD duplex assay and reagent kit (Advanced Cell Diagnostics, Biotechne) was used for RNA FISH as per the manufacturer's instructions. A double-Z probe set against *LASI* was designed containing 20 dual probes targeting various segments across the *LASI* lncRNA. RNA FISH was conducted on paraffin-embedded 5 μm tissue sections obtained from the LTRC of the NIH. Deparaffinization was conducted in consecutive xylene, graded ethanol, and deionized water. Pretreatment was conducted with hydrogen peroxide solution and the RNAScope® target retrieval buffer and protease plus solutions were used to exposure the antigen. Probe hybridization was conducted for 2 hours at 40°C in the HybEZ® II oven. The signal was amplified using the Amp1, Amp2, Amp3 and the HRP probe at 40°C in the HybEZ® II oven. The signal was detected using the tyramide signal amplification (TSA) reaction with an Alexa fluor labeled TSA kit (Perkin Elmer). Sections were then processed for immunohistochemistry or directly mounted with the 4',6-diamidino-2-phenylindole (DAPI)-containing Fluormount-G (Southern Biotechnology). Images were captured using the Keyence BZ-X700 structured illumination fluorescent microscope. Analysis was conducted with the Keyence BZ-X analysis software and using the ImageJ software (NIH). RNA FISH quantification was conducted according the RNAScope® histo (H)-score methodology. In each image, probe signals were counted for each cell, both in the nuclear and cytosolic region and assigned to appropriate bins: bin 0 (no signals), bin 1 (1-3 signals/cell), bin 2 (4-9 signals/cell), bin 3 (10-15 signals/cell) and bin 4 (>15 signals/cell). The H-score was calculated as follows: H-score was the sum of each bin multiplied by the percentage of cells that fall into that bin. H-score = (0 x % cells in bin 0) + (1 x % cells in bin 1) + (2 x % cells in bin 2) + (3 x % cells in bin 3) + (4 x % cells in bin 4). Final H-scores ranged from 0 to 400 per group.

Immunohistochemistry

Tissue sections or fixed cells were washed in 0.05% V Brij-35 in PBS+. Antigen retrieval was performed using 10 mM citrate buffer (pH 6.0). Blocking solution (1% NDS, 3% BSA, 1% gel, 0.2% TX-1000 and 0.2% saponin in PBS+) incubation was conducted for 1 hour at room temperature followed by incubation at 4°C overnight with primary antibodies against mucin MUC5AC (Millipore Sigma) and pan-cytokeratin (pan-CK, Santa Cruz Biotechnology). Appropriate DyLight® fluorescently-conjugated secondary antibodies (Abcam) were used, and sections were incubated for 1 hour at room temperature. Sections were mounted with DAPI-containing Fluormount-G. Immunofluorescent images were captured using the Keyence BZ-X700 microscope and image analysis was conducted using the ImageJ software (NIH). Mean fluorescence intensity per number of epithelial cells was used to compare mucin MUC5AC expression levels. Pan-CK was used as a confirmation of epithelial cell identity.

Histochemical Analyses

Tissue sections were deparaffinized and hydrated in graded ethanol and deionized water. Histochemical staining was conducted with Alcian blue-period acid Schiff (AB-PAS) or AB followed by hematoxylin and eosin (H&E) or AB-H&E staining as described (16). The mucus secretory cells (goblet/mucous cells) were quantified as a total number of AB-PAS+ or just AB+ cells per mm basal lamina for each image.

Enzyme-Linked Immunosorbent Assays (ELISAs)

Culture media and apical cell culture washes from NHBEs and CHBEs differentiated in 3D ALI culture for 28 days was collected prior to CSE treatment and every two days after treatment. Final apical washes and culture media supernatant were collected prior to the termination of the experiment and was either stored at -80°CC or processed for analysis. The protein levels of MUC5AC, ICAM-1, and IL-6 were determined using human ELISA kits against MUC5AC (MyBioSource Inc., San Diego, CA), ICAM-1 (LifeSpan Biosciences Inc., Seattle, WA), and IL-6 (BioLegend Inc., San Diego, CA), respectively, as per manufacturers' instructions.

Immunofluorescent Cytometry

For immunostaining analyses, cell cultures grown in Nunc™ Lab-Tek™ II 8-chamber slide system were washed using 0.05% v Brij-35 in PBS(+) and immunostained as described previously (11). Cells were stained with antibodies to mucin MUC5AC (Millipore, Inc.), ICAM-1 (Cell Signaling Technology, Inc.) and pan cytokeratin (Cell Signaling Technology, Inc.). Immunostained cells were detected using respective secondary fluor-conjugated antibodies (Thermo Fisher Scientific, Inc) and mounted with DAPI-containing mounting media. Immunofluorescent images were captured using a Keyence BZ-X710 all-in-one fluorescence microscopy system and were analyzed using Keyence analysis software and Image J software (National Institutes of Health). Labtech slides of NHBEs and CHBEs treated with or without CSE were immunostained for MUC5AC or ICAM-1 separately. Labtech slides stained for either MUC5AC or ICAM-1 were imaged, three random images per well were captured with 2 wells per treatment and a total of 200

cellswere counted per treatment group and the percent positive cells were calculated, as described earlier (11).

lncRNA *LASI* Overexpression

A full-length *LASI* lncRNA sequence was cloned into a pLenti-GIII-CMV-GFP-2A-Puro vector and a high titer lentivirus preparation was obtained from Applied Biological Materials Inc. (Richmond, Canada). Primary HBECs cultured overnight in 6-well plates were transduced with *LASI*-overexpression (LASI-OE) lentiviral preparation at 0.5 and 2 MOI (multiplicity of infection) using a culture media containing 8 µg/ml of polybrene (Sigma). Set of control cells were also transduced similarly with empty vector lentiviral preparation (Lenti-EV) at 0.5 and 2 MOI. The GFP-tag fluorescence was followed to assess the transduction efficiency. Forty-eight-hour post-transfection, cells were harvested, and qPCR was performed for expression analysis of *LASI* lncRNA and other transcripts. Mock-transduced cells (or cells with 0 MOI) were used as controls to analyze the expression levels.

Statistical Analysis

Grouped results were expressed as mean ± SEM and $p<0.05$ was considered significant. Data were analyzed using GraphPad Prism Software (GraphPad Software Inc.) using one-way analysis of variance (ANOVA) with and Tukey's multiple comparison test or using a two-tailed t test for comparison between two groups. When significant main effects were detected ($p<0.05$), student's t test was used to determine differences between the groups. All *in-vitro* studies were performed following 3 separate experiments. NHBEs and CHBEs were obtained from three different donors for the baseline and the CSE-treatment analysis.

RESULTS

Chronic CS Exposure Results in Goblet/Mucous Cell Hyperplasia and Increased *LASI* lncRNA Expression in Bronchial Airway Epithelium

We recently analyzed the effects of long-term CS exposure in a large animal model where cynomologus macaques (*M. fascicularis*) were exposed to mainstream CS for twenty-seven weeks, where CS-exposed macaques showed COPD-like respiratory phenotypes (12). Here, we specifically analyzed the bronchial epithelial responses in archived lung tissues of CS-exposed macaques and filtered room-air (FA) exposed control macaques (n=4 each). Compared to FA group, CS-exposed macaque lungs showed significant bronchial airway epithelial remodeling with augmented goblet/mucous cell hyperplasia (**Figure 1A**) as analyzed by histochemical staining using AB-PAS reagent. There were 2.6-fold higher number of AB-PAS+ goblet/mucous cells per mm basal lamina (BL) in CS-exposed macaques compared to FA group (**Figure 1B**). The expression levels of secretory mucin *MUC5AC* mRNA were 3-fold higher in CS group compared to FA macaques (**Figure 1C**) as determined by qRT-PCR. CS-induced MUC5AC expression was also corroborated by immunostaining of bronchial tissue sections

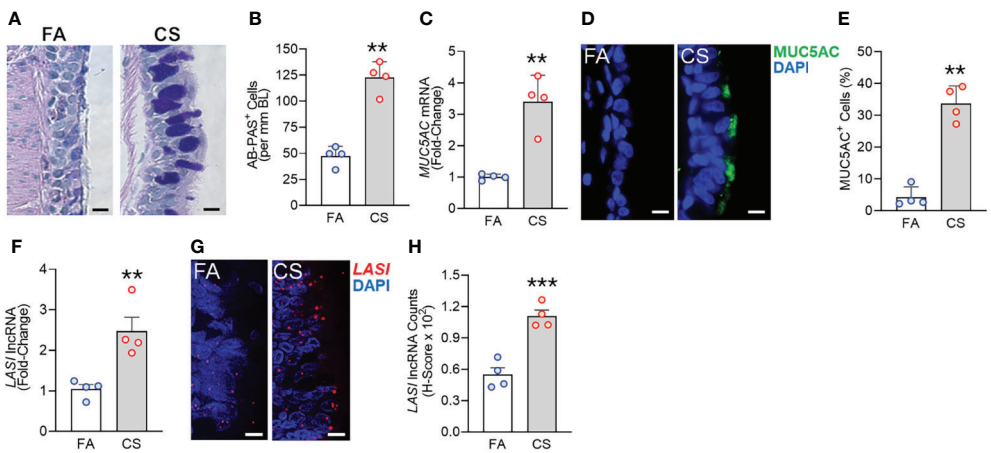

FIGURE 1 | Chronic cigarette smoke (CS) exposure of cynomolgus macaques results in goblet/mucous cell hyperplasia that is strongly associated with increased *LASI* lncRNA expression in bronchial airways. Bronchial airway tissues from C. macaques exposed to mainstream CS or control filtered-air (FA) for 27 weeks as reported recently (12) were analyzed. **(A)** Representative histomicrographs of bronchial tissue sections showing AB-PAS-stained goblet/mucous cells in CS- and FA-exposed macaques, scale – 10 µm. **(B)** Number of AB-PAS+ cells quantified per mm of basal lamina (BL) in each group. **(C)** Relative quantity of secretory mucin *MUC5AC* mRNA in CS-exposed macaques compared to FA-controls as determined by qPCR. **(D)** Representative micrographs of bronchial tissue sections showing MUC5AC immunopositivity in CS- and FA-exposed macaques, scale – 5 µm. **(E)** Percentage of MUC5AC+ cells over the total epithelial cells quantified for each group. **(F)** Relative quantity of *LASI* lncRNA in CS-exposed macaques versus FA-controls as determined by qPCR. **(G)** Representative micrographs showing *LASI* lncRNA expression in FA and CS macaques as determined by FISH, scale – 5 µm. **(H)** Quantification of LASI lncRNA expression in bronchial epithelial cells of each group as determined by H-score analysis described earlier (11). Data shown as mean ± SEM; n=4/gp and analyzed by student's t-test; $^{**}p<0.01$; $^{***}p<0.001$.

(**Figure 1D**) with 7.9-fold higher percentage of MUC5AC-positive ($MUC5AC^+$) cells observed in CS macaques over FA group (**Figure 1E**). Thus, chronic CS exposure results in goblet cell hyperplasia with increased expression of MUC5AC mucin.

LncRNAs are essential regulators of smoke mediated inflammatory responses (6, 7) and based on the critical role of *LASI* lncRNA in airway inflammatory and mucus hyperexpression (11), we analyzed the effects of CS on bronchial epithelial *LASI* lncRNA expression. Compared to the FA group, we observed a 2.4-fold increase in *LASI* transcript levels in CS-exposed macaques (**Figure 1F**). Cellular *LASI* expression levels were further analyzed by performing RNA-FISH as described previously (11), which allowed for single RNA molecule-level resolution and subcellular localization evaluation (**Figure 1G**). We found that the number of *LASI* lncRNA transcripts per cell was significantly upregulated upon CS treatment (**Figure 1H**). Overall, in a large animal model of chronic CS exposure, bronchial epithelial cells show a strong correlative increase in *LASI* lncRNA levels and MUC5AC mucin expression.

Disease Severity Associated Increased Mucin Expression, Inflammation, and Mucous Cell Hyperplasia in COPD Airways

Next, we analyzed the archived lung tissue samples obtained from 14 COPD patients and 6 control donors with no-COPD (**Table 1**). All the samples were from former smokers with or without COPD were stratified based on the NIH and WHO's Global Initiative for Chronic Obstructive Lung Disease (GOLD) criteria (17). According to these criteria, six donor patients had mild (GOLD stage 1 or 2) COPD, and eight donor patients had severe (GOLD stage 3 or 4) COPD. To evaluate airway mucoglycoproteins (mucins) and mucous/goblet cells, tissue sections were stained with AB-H&E as described (11). Among the severe COPD patients, the small airways had disproportionately prominent mucus masses or plugs (**Figure 2A**). Based on the number of AB+ mucous cells in each group, there was a significant increase in mucus expressing cells in severe COPD tissue samples (**Figure 2B**). Specifically, there were 31.6, 82.9, and 113.4 mucous cells per mm BL in no-COPD, mild-COPD, and severe-COPD samples, respectively. Mucus hypersecretion is a driving factor of COPD pathology and CS exposure induces the of secretory mucin MUC5AC levels (17–21). We also found that *MUC5AC* mRNA levels were significantly upregulated in mild and severe COPD tissue samples, with 44- and 30-fold higher expression, respectively, compared to no-COPD control tissues (**Figure 2C**). In addition, we immunoprobed the tissue samples for MUC5AC protein expression and both mild and severe COPD samples showed higher MUC5AC immunopositivity (**Figure 2D**). Compared to no-COPD controls, there was a 4.2-fold and 6.8-fold increase in the percentage of MUC5AC+ cells in mild and severe COPD samples, respectively (**Figure 2E**). However, there was no significant change in the expression levels of a master transcriptional regulator of mucus response, *SPDEF* (**Supplementary Figure S1A**). Among inflammatory factors, mRNA levels of *IL-6* were upregulated in mild COPD samples only (**Supplementary Figure S1B**) and *ICAM-1* mRNAs showed a trend towards upregulated expression in mild and severe COPD tissue samples, as compared to no-COPD controls (**Supplementary Figure S1C**). These data corroborate the association of small airway tissue pathology with clinically defined COPD disease status and increased mucoinflammatory responses among COPD subjects.

TABLE 1 | Demographics of the study cohort of COPD patients with clinically-defined GOLD stage severity and self-reported smoking history.

	No COPD	Mild COPD	Severe COPD
Age*	54.2±3.2	69.2±3.9	65.1±2.7
Gender, M/F	3M/3F	4M/2F	3M/5F
Smoking in PY*	54.0±12.6 (2)	29.9±10.7 (3)	35.0±2.8 (3)
Stop Smoking (Y)*	6.6 ± 1.6	21.4±12.8	11.9±2.5

**Mean±SEM; M, Male; F, Female; PY, Packs per Year; Y, Years.*

LASI lncRNA Levels Are Upregulated in COPD Airway Epithelium

We next investigated the correlation between the airway epithelial *LASI* lncRNA expression and the mucoinflammatory phenotype of COPD tissue samples. The transcript expression levels in lung tissue homogenates of COPD and no COPD control samples were evaluated by qRT-PCR. *LASI* transcript levels were 4-fold and 6-fold higher in the mild COPD (n=6) and severe COPD tissue samples, (n=8), respectively, compared to no-COPD control tissues (n=6) (**Figure 2F**). We also investigated of the expression of other lncRNAs such as, ICAM-1-related lncRNA (*ICR*), which regulates ICAM-1 expression by mRNA stabilization *via* direct interaction and duplex formation (22), but there was no significant change in ICR levels among COPD tissue samples (**Supplementary Figure S1D**). Similarly, there was no change in the expression levels of highly prevalent lncRNA *NEAT1* or nuclear enriched assembly transcript 1 (**Supplementary Figure S1E**) and *MALAT1* or metastasis associated lung adenocarcinoma transcript 1 (**Supplementary Figure S1F**). *NEAT1* lncRNA has been implicated as a potential prognostic marker of COPD exacerbations where its expression level correlated with disease severity (23). Similarly, *MALAT1* lncRNA has been proposed as a potential therapeutic target because silencing its expression blocked the COPD-associated lung remodeling (10). We also analyzed the expression levels of lncRNA called *WAKMAR2* or a wound and keratinocyte migration-associated lncRNA, which regulates the proinflammatory responses in keratinocytes (24) and there were no significant changes among COPD subjects (**Supplementary Figure S1G**).

To further corroborate the COPD-associated *LASI* lncRNA expression levels and to evaluate airway epithelium specific expression, we conducted RNA-FISH to examine *LASI* expression at a single RNA molecule resolution and evaluate the *LASI* subcellular localization (**Figure 2G**). We found that in small airways, both mild and severe COPD tissue samples present with significantly upregulated *LASI* expression as compared to non-COPD controls. There was 1.4- and 1.6-fold higher *LASI* expression

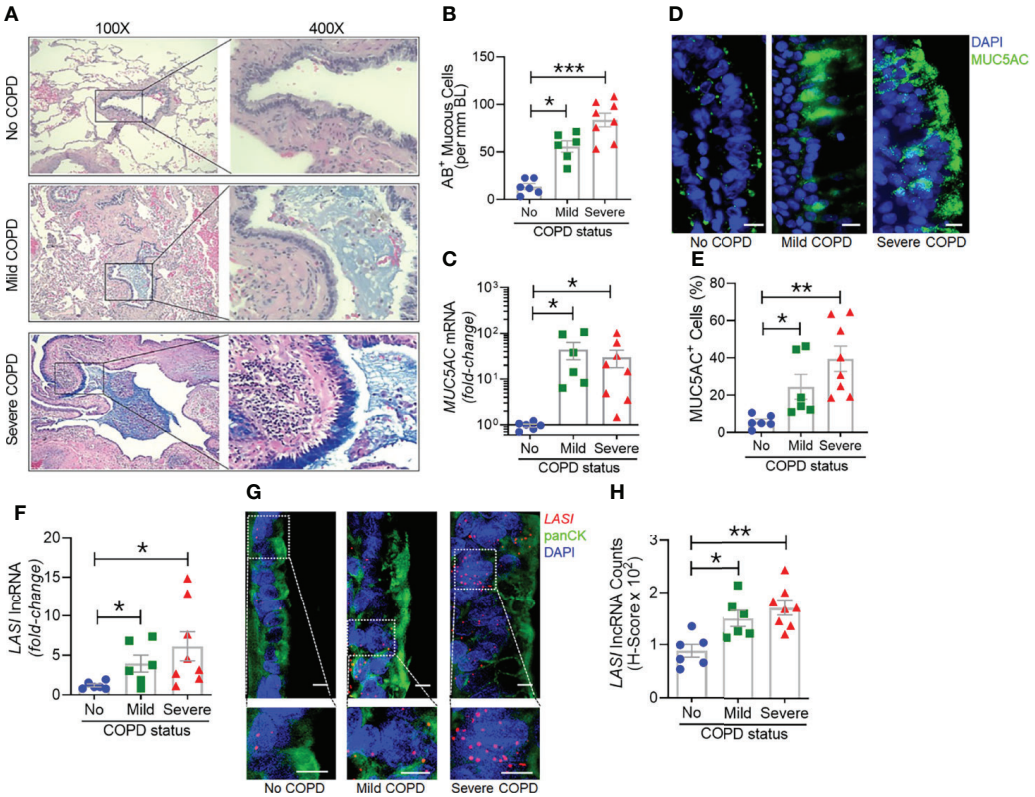

FIGURE 2 | Archived airway sections of COPD patients show increased mucus expression and goblet cell hyperplasia along with increased *LASI* lncRNA expression in epithelial cells. **(A)** Representative histomicrographs of airway tissue sections from subjects with No, Mild, or Severe COPD stained with alcian blue (AB). Images are shown at 100x magnification and inset images are magnified 400x in the right panels. **(B)** Quantification of AB+ mucous/goblet cells per mm of basal lamina (BL). **(C)** Relative quantities of *MUC5AC* mRNA levels in tissues from mild and severe COPD subjects compared to control subjects with no COPD, analyzed by qRT-PCR. **(D)** Micrographs showing MUC5AC mucin immunopositivity (green) in tissue sections and counterstained with DAPI (shown in blue) to identify nuclei, scale – 10 µm. **(E)** Quantification of MUC5AC+ cells per mm BL in each group. **(F)** Quantitation of *LASI* lncRNA levels in mild and severe COPD subjects compared to control subjects with No COPD. **(G)** Micrographs showing *LASI* lncRNA levels in airway epithelial cells of patient bronchial tissues. *LASI* lncRNAs were detected by RNA-FISH (shown in red) and epithelial cells were immunostained by pan-cytokeratin (panCK, shown in green) antibody, and nuclei (shown in blue) were stained by DAPI. Lower panels show magnified images of the insets drawn in upper panels (scale – 5µm). **(H)** Quantitation for *LASI* lncRNAs per epithelial cell as measured by H-score analysis. Data shown as mean ± SEM; n=6-8/gp; data analyzed by ANOVA with multiple comparisons; *$p<0.05$; **$p<0.01$; ***$p<0.001$.

in pan-cytokeratin+ epithelial cells of mild and severe COPD tissues, respectively (**Figure 2H**). *LASI* transcripts were found both in the perinuclear and the cytosolic regions of bronchial epithelial cells. Collectively, these data suggest a strong correlation between *LASI* lncRNA expression and mucus hypersecretion, mucous cell hyperplasia, and COPD pathogenesis.

Primary HBECs From COPD Patients Show Higher Transcript Levels of *LASI* lncRNA and Mucoinflammatory Factors

To assess epithelial cell-specific responses, we next cultured primary differentiated human bronchial epithelial cells (HBECs) obtained from COPD donors (CHBEs) and compared with HBECs from control donors with no-COPD (NHBEs). Primary NHBEs and CHBEs were differentiated on air-liquid interface (ALI), as 3D airway cultures. We first compared the baseline differences between differentiated NHBEs and CHBEs, without any treatment or stimulation. Among the lncRNAs analyzed, expression levels of ICAM-1 loci associated lncRNAs, *LASI* (**Figure 3A**) and *ICR* (**Figure 3B**) were 6.2- and 8.0-fold higher in unstimulated CHBEs compared to NHBEs, respectively. Expression levels of other lncRNAs were also higher in CHBEs with *NEAT1*, *MALAT1*, and *WAKMAR-2* lncRNAs expressed at 3.3-, 1.6-, and 3.2-fold higher in CHBEs compared to NHBEs, respectively (**Supplementary Figures S2A–C**).

Next, we examined the baseline expression of epithelial inflammatory factors and secretory mucins in NHBEs and CHBEs. Compared to NHBEs, the *MUC5AC* mucin (**Figure 3C**), *ICAM-1* (**Figure 3D**), and *IL-6* (**Figure 3E**) mRNA levels were 3.0-, 4.6-, and 6.0-fold higher in CHBEs. In order to determine whether the changes in transcript levels recapitulate the secretory protein levels, we analyzed the MUC5AC protein levels in apical wash samples and found that MUC5AC levels were approximately 39.1 ng/ml and 152.2 ng/ml

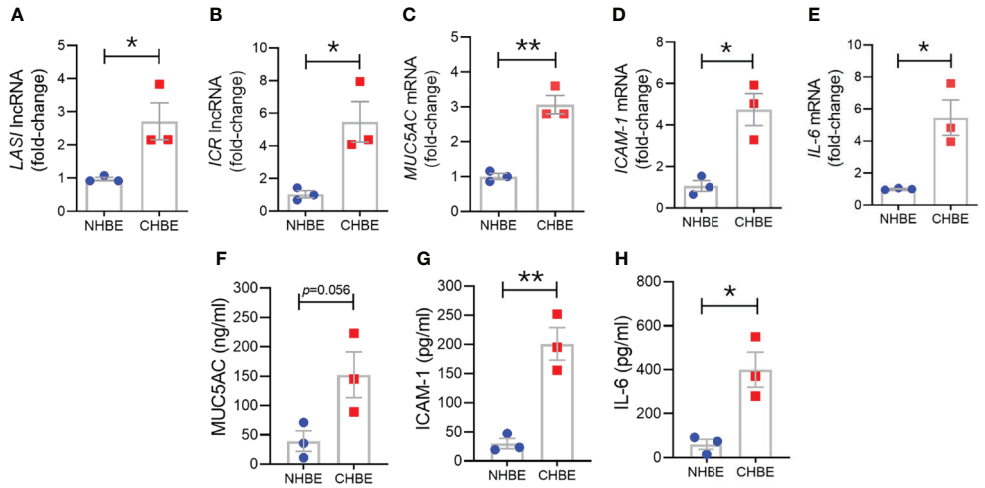

FIGURE 3 | Differentiated bronchial epithelial cells from COPD subjects show increased expression of immunomodulatory lncRNAs, MUC5AC mucin, and IL-6 and ICAM-1 compared to control cells from non-COPD donors. Relative transcript levels for lncRNA *LASI* **(A)**, and *ICR* **(B)** in 3D cultured and unstimulated NHBE and CHBE cells as determined by qRT-PCR. Relative mRNA levels of *MUC5AC* **(C)**, *ICAM-1* **(D)**, and *IL-6* **(E)** inflammatory factors. Quantification of secretory MUC5AC mucin levels **(F)** in the apical washes, and the secreted ICAM-1 **(G)**, and IL-6 **(H)** levels in basal media supernatant as analyzed by specific sandwich ELISA assays. Data shown as mean ± SEM as fold-change over NHBEs; n = 3/gp; data analyzed by student's t-test; *$p<0.05$; **$p<0.01$.

in NHBEs and CHBEs, respectively (**Figure 3F**). Protein levels of ICAM-1 and IL-6 were analyzed in NHBE and CHBE basal culture media supernatants. Secreted ICAM-1 levels were approximately 29.9 pg/ml and 200.8 pg/ml in NHBE and CHBE culture media, respectively (**Figure 3G**), with a 6.7-fold increase in CHBEs. Similarly, average secreted IL-6 level in NHBE culture media was 60.6 pg/ml whereas in CHBE culture media was 399.8 pg/ml (**Figure 3H**). Collectively, these data suggest a strong dysregulation of inflammatory responses in the bronchial epithelial cells in COPD with coordinated changes in lncRNA, mRNA, and protein expression.

CS Exposure Results in an Augmented Inflammatory Response in COPD HBECs

To evaluate the CS-induced response, CHBEs and NHBEs were treated with 20 µg/ml CSE for 48h as described previously (25), and total cell RNA was evaluated for changes in lncRNAs and inflammatory factors' expression. Interestingly, both ICAM-loci associated lncRNAs, *LASI* (**Figure 4A**) and *ICR* (**Figure 4B**) were significantly upregulated with 3.3-fold and 1.9-fold upregulation in CSE-treated CHBEs, respectively, as compared to CSE-treated NHBEs. However, expression levels of *NEAT1* and *MALAT1* lncRNAs failed to show any significant change following CSE treatment (**Supplementary Figures S3A, B**), but the *WAKMAR-2* lncRNA levels were 2.8-fold higher following CSE-treatment of CHBEs over NHBEs (**Supplementary Figure S3C**). This change in CSE-induced lncRNAs directly correlated with expression of *ICAM-1* mRNA, which was 2.0-fold upregulated in CSE-treated CHBEs than NHBEs (**Figure 4C**). No significant changes were observed in CSE-induced *IL-6* and *CXCL-8* mRNA expression between CHBEs and NHBEs (**Figures 4D, E**). These data suggest that the CSE induces a dysregulated response in NHBEs, and the

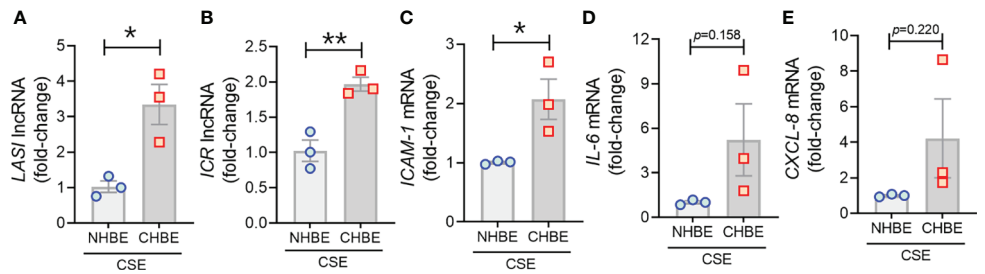

FIGURE 4 | Cigarette smoke exposure of COPD bronchial epithelial cells induces higher levels of immunomodulatory lncRNAs, and inflammatory factor mRNAs compared to non-COPD control cells. Primary NHBEs and CHBEs grown in submerged culture setting were treated with a 20 µg/ml cigarette smoke extract (CSE) and forty-eight hours after treatment cells were harvested and qRT-PCR was performed. Relative transcript levels for lncRNA *LASI* **(A)**, and *ICR* **(B)** in CSE-treated NHBE and CHBE cells as determined by qRT-PCR. Relative mRNA levels of *ICAM-1* **(C)**, *IL-6* **(D)**, and *CXCL-8* **(E)** inflammatory factors. Data shown as mean ± SEM as fold-change over NHBEs; n=3/gp; data analyzed by student's t-test; *$p<0.05$; **$p<0.01$.

responses are further potentiated in CHBEs; and that there is a potential direct regulatory relationship between *LASI* and *ICR* lncRNAs and ICAM-1 expression.

To further substantiate these findings, we additionally performed cytometric analysis of MUC5AC and ICAM-1 protein expression in NHBEs and CHBEs grown on Labtech® slides and treated with 20μg/ml CSE for 48h. The cells showing immunopositivity for MUC5AC (MUC5AC+) and ICAM-1 (ICAM-1+) were quantified and there was a 2.3-fold increase in MUC5AC+ cells in CSE-treated NHBEs, and a 15.4-fold increase in CSE-treated CHBEs (**Figures 5A, B**). Similarly, NHBEs showed a 2.3-fold increase in ICAM-1+ cells, while CHBEs showed a 2.9-fold increase in ICAM-1+ cells upon CSE treatment (**Figures 5C, D**). These data further suggest that CS insult causes CHBEs to respond with a significantly more severe, dysregulated mucus secretory and inflammatory response.

Knocking Down *LASI* Expression Suppresses the Smoke-Induced Inflammation, Mucin Expression, and Mucus Cell Hyperplasia

In order to determine whether the correlation between *LASI* lncRNA with *MUC5AC* and *ICAM-1* expression is functionally significant, we genetically silenced *LASI* lncRNA expression using siRNAs targeting *LASI* (siLASI), as described previously (11), in differentiated CHBEs then challenged with 20 μg/ml CSE for 48h. CHBEs transfected with negative control siRNA (siCTRL) followed by 48 h 20 μg/ml CSE treatment served as controls. Compared to siCTRL, the siLASI-transfected CHBEs showed a 37.5% reduction in *LASI* lncRNA expression (**Figure 6A**). Interestingly, even with this moderate reduction in *LASI* expression, there was a 63.9% reduction in CSE-induced *MUC5AC* mRNA levels in siLASI-transfected CHBEs (**Figure 6B**), suggesting that functional availability of *LASI* lncRNA is necessary for CSE-mediated induction of *MUC5AC* expression in CHBEs. Notably, we found no change in *SPDEF* transcription factor levels (**Supplementary Figure S4A**), suggesting that a CSE-induced and *LASI*-mediated MUC5AC expression may not be dependent on SPDEF-mediated transcriptional upregulation. Expression levels of another airway secretory mucin, *MUC5B* mRNA were not changed in siLASI-transfected CHBEs (**Supplementary Figure S4B**). We also evaluated the changes in the CSE-mediated inflammatory responses in siLASI-transfected CHBEs. Notably, we found that siLASI induced a significant 36.2% reduction in *ICAM-1* mRNA levels (**Figure 6C**) and a 66% reduction in *IL-6* mRNA levels

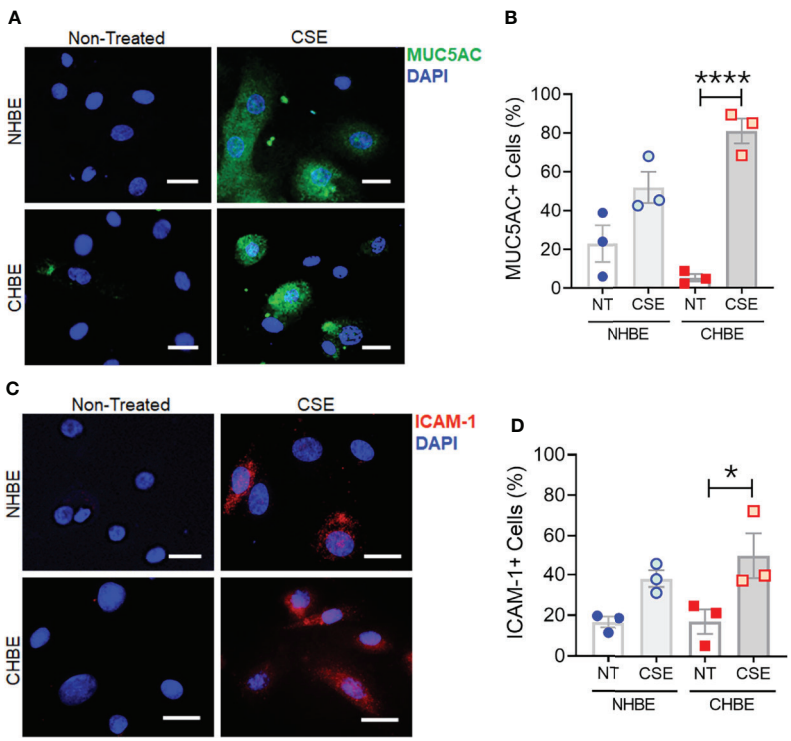

FIGURE 5 | Cigarette smoke treatment augments mucous cell hyperplasia in CHBEs with higher ICAM-1 protein expression compared to non-COPD control cells. Primary NHBEs and CHBEs grown in LabTek-II® slides were treated with a 20 μg/ml CSE and forty-eight hours after treatment cells were fixed with 4% paraformaldehyde (PFA) and processed for staining with antibodies against MUC5AC and ICAM-1. **(A)** Representative micrographs showing MUC5AC immunopositivity (shown in green) in NHBEs and CHBEs treated with CSE or left non-treated (NT), and nuclei were stained by DAPI (shown in blue), scale – 10μm. **(B)** Quantification of MUC5AC-positive (+) cells in NHBEs and CHBEs treated with CSE compared to NT cells. **(C)** Representative micrographs showing ICAM-1 immunopositivity (shown in red) in NHBEs and CHBEs treated with or without CSE, scale – 10 μm. **(D)** Quantification of ICAM-1-positive (+) cells in NHBEs and CHBEs treated with CSE compared to NT controls. Data shown as mean ± SEM as fold-change compared to NT cells; n=3/gp; data analyzed by ANOVA; *p<0.05; ****p<0.0001.

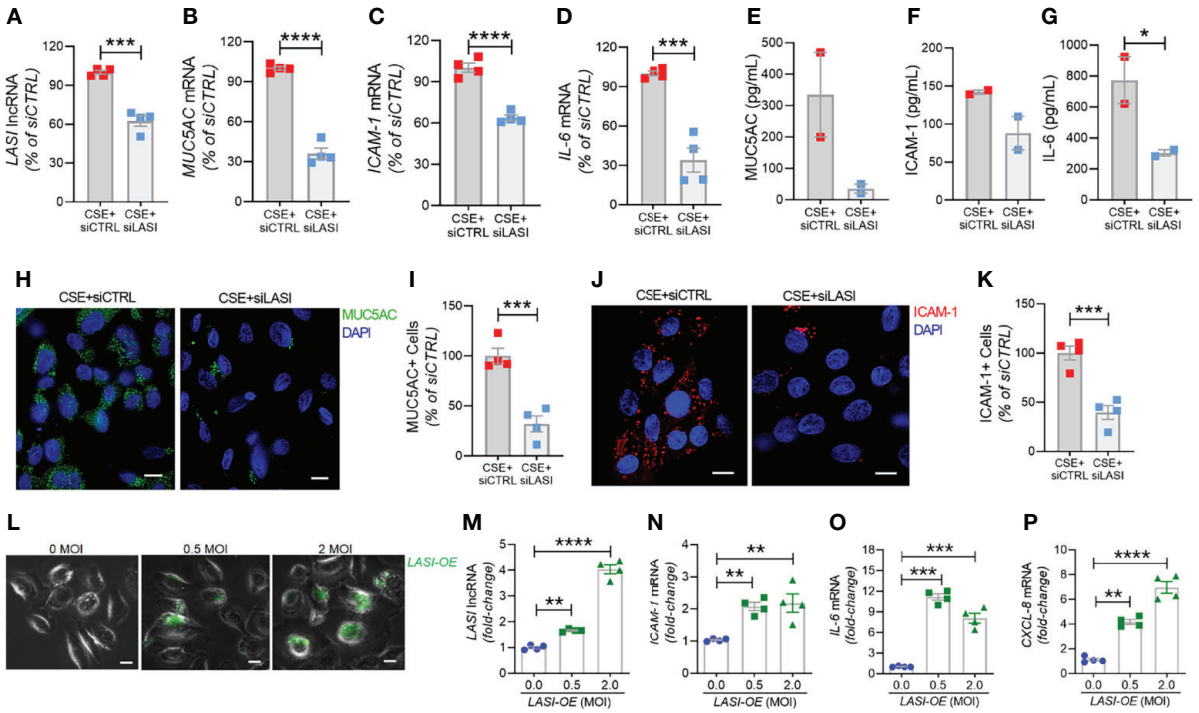

FIGURE 6 | Silencing *LASI* lncRNA suppresses the CSE-induced mucoinflammatory responses whereas *LASI* overexpression augments the expression of inflammatory factors. CHBEs grown in 3D ALI tissue culture conditions were transfected with either siRNA targeting *LASI* (siLASI) or scrambled control siRNA (siCTRL), and cells were treated with 20 µg/ml CSE to obtain CSE+siLASI and CSE+siCTRL cells, respectively. Cells harvested forty-eight hours post CSE-treatment were analyzed for the expression levels of *LASI* lncRNA **(A)**, and mRNA levels of *MUC5AC* **(B)**, *ICAM-1* **(C)**, and *IL-6* **(D)** by qRT-PCR. Apical washes from 3D tissue cultures were analyzed for MUC5AC mucin **(E)** by ELISA, and the basal media supernatants were analyzed for ICAM-1 **(F)**, and IL-6 **(G)** protein levels by specific ELISA assays. **(H)** Representative micrographs of CHBEs transfected with siCTRL or siLASI and treated with CSE showing MUC5AC mucin immunopositivity (shown in green) and nuclei were stained by DAPI (shown in blue), scale – 5µm. **(I)** Quantification of MUC5AC+ cells among CSE+siLASI CHBEs, shown as percentage of CSE+siCTRL cells. **(J)** Micrographs of CHBEs showing ICAM-1 immunopositivity (shown in red), scale – 5 µm. **(K)** Quantification of ICAM-1+ CHBEs. Data shown as mean ± SEM compared to CSE+siCTRL cells (n=4); data analyzed by student's t-test; *p<0.05; ***p<0.001; ****p<0.0001. **(L)** Representative micrographs of cells transduced with 0, 0.5, and 2 MOI of LASI-OE lentiviral preparation showing GFP reporter fluorescence (shown in green) and phase contrast images of cells, scale – 5µm. Cells harvested forty-eight hours post-transduction were analyzed for expression levels of *LASI* lncRNA **(M)**, and mRNA levels of *ICAM-1* **(N)**, *IL-6* **(O)**, and *CXCL-8* **(P)** by qRT-PCR. Data shown as mean ± SEM compared to mock-transduced cells (0 MOI); data analyzed by ANOVA with multiple comparisons; **p<0.01; ***p<0.001; ****p<0.0001.

(**Figure 6D**), suggesting that *LASI* lncRNA may contribute to the expression of these inflammatory factors. However, expression levels of inflammatory factor CXCL-8 mRNAs were not changed in siLASI-transfected CHBEs (**Supplementary Figure S4C**).

Next, we used sandwich ELISA to measure the secreted protein levels of mucin MUC5AC, and cytokines ICAM-1 and IL-6 in siLASI-transfected CHBEs followed by 48h CSE treatment. Interestingly, apical wash from siCTRL-transfected CHBEs had 236.6 ng/ml of mucin MUC5AC while the siLASI-transfected CHBEs had 73.9 ng/ml (**Figure 6E**). Furthermore, the culture media supernatants from the siLASI-transfected CHBEs had 298.2 pg/ml IL-6 levels compared to the 765.8 pg/ml in siCTRL-transfected CHBEs (**Figure 6F**), Similarly, siLASI-transfected CHBEs secreted 105.3 pg/ml ICAM-1 levels whereas the siCTRL-treated CHBEs secreted 138.3 pg/ml (**Figure 6G**). Overall, siLASI-transfected CHBEs showed a 2.6-fold reduction in IL-6 and a 1.3-fold reduction in ICAM-1 secretory levels following CSE treatment over siCTRL-transfected CHBEs. Notably, CSE-induced MUC5AC mucin secretion was reduced by 3.2-fold in siLASI-transfected CHBEs compared to the siCTRL-transfected CHBEs.

We further corroborated the data by immunoprobing the siCTRL- and siLASI- transfected CHBEs for MUC5AC and ICAM-1 protein expression following 48 h CSE treatment (**Figures 6H, J**). We found that silencing LASI expression by siLASI resulted in a 3.1-reduction in MUC5AC-expressing (MUC5AC+) cells (**Figure 6I**) and a 2.5-fold reduction in cell expressing ICAM-1 protein (**Figure 6K**). These data strongly suggest lncRNA *LASI* represents an important regulatory mediator in the CS-induced pathophysiological changes observed in COPD airways, including dysregulated immune response and chronic mucus hypersecretion.

Ectopic *LASI* lncRNA Expression Results in Increased Expression of Inflammatory Factors

To determine whether *LASI* lncRNA directly mediates the expression of inflammatory factors, a lentiviral preparation

encoding *LASI* lncRNA was used to transduce airway epithelial cells, and the ectopic *LASI* overexpression (LASI-OE) was followed by assessing GFP-tag fluorescence (**Figure 6L**). Compared to mock-transduced (0 MOI) controls, cells transduced with 0.5 and 2.0 MOI of lentivirus-*LASI* resulted in 1.7- and 4.0-fold increased expression of *LASI* lncRNA, respectively (**Figure 6M**). Set of control cells transduced with empty vector lentiviral preparation (Lenti-EV) showed no change in the expression of airway *LASI* lncRNA or associated inflammatory factor mRNAs (**Supplementary Figure S5**). Interestingly, LASI-OE cells showed two-fold or higher levels of *ICAM-1* mRNA expression (**Figure 6N**) and expression levels of *IL-6* (**Figure 6O**) and *CXCL-8* (**Figure 6P**) mRNAs were also increased by as much as eight- and four-fold, respectively. Thus, ectopic overexpression of *LASI* lncRNA directly upregulates the airway epithelial inflammatory factor mRNA levels.

DISCUSSION

CS exposure is the most important and the best-studied risk factor associated with COPD. That said, studies are needed to unravel novel underlying molecular pathways for improved diagnostic and therapeutic interventions for CS-induced pathologies and COPD-related comorbidities. The newly discovered lncRNA molecular species are now being proposed as novel cellular entities that play an important role in physiology and pathophysiology (6, 26). We have recently identified novel immunomodulatory lncRNAs that may play a crucial role in airway inflammatory responses. In the present study, we find a strong association of immunomodulatory *LASI* lncRNA expression with CS-induced airway mucus hyperexpression and inflammatory responses as summarized in **Figure 7**. The correlation was observed both in a large animal model of CS-induced COPD, and in lung tissue samples from former smokers with COPD in comparison with tissues from former smokers with no COPD. We found that lung tissue samples of CS-exposed macaques and those of COPD patients (with mild and severe COPD) presented with an increased *LASI* lncRNA expression in bronchial airway epithelial cells. *LASI* lncRNA expression correlated to the increased expression of secretory mucin MUC5AC, and innate airway inflammatory factors, IL-6, and ICAM-1, which were all upregulated in COPD tissue samples and in macaques exposed to mainstream CS. These data suggested that *LASI* lncRNA may play a role in smoke-associated bronchial epithelial remodeling and COPD. To validate the airway epithelial specific significance of *LASI* lncRNA in CS-induced responses, we utilized a 3D airway tissue culture model of primary HBECs from COPD and compared the baseline and CSE-induced responses to that of control cells from donors with no COPD. We found that unstimulated CHBEs, show a baseline upregulation of *LASI* lncRNA, along with other immunomodulatory lncRNAs such as *ICR*, *NEAT1*, *MALAT1*, and *WAKMAR2*. However, none of these lncRNAs were responsive to CSE-treatment except for *LASI* and *ICR* lncRNAs. This led us to explore the responses to CS exposure and *LASI* was the only lncRNA explored in this report which showed a potentiated dysregulated response to CSE treatment in CHBEs as compared to NHBEs. *LASI* lncRNA further showed a strong correlation with expression levels of ICAM-1, as well as IL-6 and CXCL-8, suggesting a functional importance in COPD pathogenesis. Accordingly, we knocked

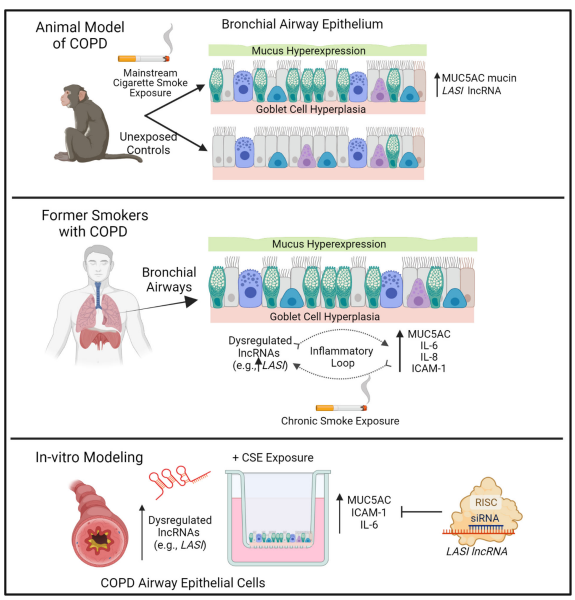

FIGURE 7 | Schematic representation on the potential role of bronchial epithelial LASI lncRNA in CS-induced and COPD-associated airway mucus hyperexpression and inflammatory responses.

down *LASI* lncRNA expression in CHBEs and discovered that a reduction in *LASI* lncRNA expression resulted in a significant reduction in CSE-induced mucoinflammatory response by reducing the expression of MUC5AC, IL-6, and ICAM-1 levels both at mRNA and protein levels. These data thus collectively implicate *LASI* lncRNA as a novel mediator of CS-induced and COPD-associated airway pathophysiologies. Moreover, even in the absence of any external stimulation, the ectopic overexpression of *LASI* lncRNA directly upregulated the transcript levels of airway inflammatory factors, suggesting that *LASI* lncRNA may be directly involved in the transcriptional upregulation or mRNA stability of these inflammatory factors.

Cigarette smoking is strongly associated with COPD where more than 50% of COPD patients are active smokers and over 70% have a history of smoking. Notably, over 50% of COPD mortality is attributable to active smoking (27). Patients who are exposed to CS present with exacerbated mucus secretory and airway inflammatory conditions. As such, the dysregulated response to smoke exposure may provide the most useful insight into the severe COPD pathology and potentially fatal exacerbations (28, 29). However, due to limitation of the longitudinal sampling from human COPD subjects and the other genetic and environmental heterogeneity, animal models of COPD following chronic CS exposure are widely studied to understand the smoke-mediated disease pathogenesis. Small animal models of CS exposure do not recapitulate all aspects of human COPD specifically in bronchial airway remodeling and therefore, we recently performed a study using the cynomologus macaque model of chronic CS exposure. Following 27-weeks of mainstream CS exposure, these animals show reduced lung functions and chronic bronchitis similar to that observed in COPD smokers compared to control macaques kept in room air. Thus, we were able to employ the archived lung tissues from these well-characterized macaques to establish the correlation of CS-induced airway inflammatory responses with airway lncRNA expression. Due to the labor- and time-intensive nature of these large animal model studies, we are currently analyzing whether there is a murine homolog of *LASI* lncRNA or if there is any other airway-specific lncRNA of rodent airways involved in CS-mediated inflammation. Accordingly, future studies will be planned to test the *in-vivo* efficacy of targeting lncRNAs in suppressing CS-mediated airway remodeling and mucoinflammatory responses.

Airway mucus hypersecretion is the hallmark of COPD pathogenesis, enabling the compounding cascade of inflammation, ROS generation, and airborne pathogen retention in airways due to compromised mucociliary clearance, distal airway occlusion and inability to effectively clear the airways (4). Airway mucins MUC5AC and MUC5B are the predominant gel-forming mucins in COPD, and CS exposure and frequent bacterial or viral infection synergistically amplify MUC5AC levels (17–21). Several other inflammatory biomarkers have been implicated with COPD and smoke-associated exacerbations (26). Among the most prominent factors are the ICAM-family proteins, specifically ICAM-1, and an innate inflammatory cytokine, IL-6 which have shown strong association to decreased lung function in COPD, both in active and former smokers with varying degree of severity (30). Airway epithelial cells play a vital role in the secretion of ICAM-1 and IL-6, and could serve as drivers of the chronic changes observed in COPD (31).

Till date, thousands of lncRNAs have been discovered, however, studies on the functional significance of the changes in lncRNA expression are lacking. The structural flexibility and 3D-conformation enables lncRNAs to interact with large number of cellular macromolecules including proteins, DNA, RNA, and chromatin to modulate epigenetic and transcriptomic changes and associated cellular responses (8). Large number of lncRNAs have been implicated in pathology, including chronic pulmonary conditions, CS-related immune responses, and inflammatory regulation (6, 9, 10). LncRNA-mediated regulation of innate immune responses is potentially central for the establishment of host-beneficial trained immunity (32), but these responses could be dysregulated in case of chronic pulmonary disease resulting in hyperactive inflammatory responses. Microarray analysis has shown over 39,000 lncRNAs are differentially expressed in COPD patients, stratified by smoking status (33). Numerous lncRNAs have been experimentally characterized and shown to affect the inflammatory responses of airway epithelium *via* epigenetic and/or transcriptomic mechanisms and induce an accelerated aging of lung epithelium associated with COPD (6).

Goblet cell hyperplasia is a salient feature of COPD pathology where the 33% of distal conducting airway epithelium is comprised of goblet cells in COPD lungs, versus less than 5% observed in the distal airways of non-COPD lungs (34). We also report a disease severity associated increase in goblet cell hyperplasia in COPD tissue samples, with a 2.1- to 3.0-fold increase in goblet cell numbers per mm BL in mild and severe COPD tissues, respectively. This suggests accurate modeling of molecular level changes in COPD epithelium. We found that the lncRNA *LASI* correlates with disease severity, while other lncRNAs do not, suggesting a potential regulatory role which we further explored using an *in vitro* COPD model. Our panel of lncRNAs showed the *NEAT1*, *MALAT1* and *WAKMAR2* were not upregulated following CSE- treatments. Interestingly, Hu and colleagues (2020) reported increased expression of MALAT1 in COPD lung tissue specimens, however we found that there was no change in MALAT1 expression in correlation with disease severity (10). However, to evaluate whether the effects observed were specifically driven by CS exposure, we relied on the archived tissue samples from C. macaques that were exposed to CS chronically and the data strongly suggests that long-term CS exposure is a driving factor behind the airway pathology observed. Importantly, we used primary HBECs from controls with no COPD and with COPD i.e., NHBEs and CHBEs for *in-vitro* validation of our ex-vivo findings. Recent reports have shown that the pathologic changes in epithelial histology, goblet cell numbers, and mucus hypersecretion are preserved in differentiated COPD subject-derived lung epithelial cells in ALI culture settings, and transcriptomic analysis showed over 200 differentially expressed transcripts (35). The ciliary beating

impairment has also been found to be reflected in differentiated CHBEs versus NHBEs. Here, we report a significant higher baseline expression, of MUC5AC, ICAM-1, and IL-6 in CHBEs, as compared to NHBEs without any treatment or stimulation. Thus, our *in-vitro* model do recapitulates the differences observed in COPD subjects thus suggesting of epigenetic and transcriptomic transformations that are preserved in bronchial epithelial cells. Further, CHBEs also showed a significantly increased baseline levels of *LASI* lncRNA as compared to NHBEs. In addition, there was an increased expression of *ICR*, *NEAT1*, *MALAT1*, and *WAKMAR2* lncRNAs in cultured CHBEs, however, we did not observe any significant change in these lncRNAs in lung tissue homogenates of COPD subjects. This suggests that these lncRNAs may respond in cell/tissue-context manner, and the epithelial expression of these lncRNA may not play a direct role in COPD pathogenesis.

Also of note, we found that blocking *LASI* lncRNA expression in CHBEs led to a suppressed induction of MUC5AC mucin expression with no change in transcription factor SPDEF expression, suggesting that CSE-mediated mucin expression may not directly involve the previously observed *LASI* lncRNA-and SPDEF-mediated mucin upregulation observed in allergic asthma studies (11). CSE exposure induces SPDEF *via* NOTCH3 signaling, suggesting that *LASI*-mediated dysregulation is not dependent on NOTCH3, and further suggests a need to evaluate the role of *LASI* lncRNA on other signaling pathways involved in CS-mediated mucoinflammatory responses such as epithelial growth factor receptor (EGFR)-mediated inflammation (36). EGFR-mediated signaling is likely to be the predominant driver of airway remodeling and mucus cell hyperplasia in CS-induced COPD pathogenesis, and this pathway may not involve SPDEF-mediated mucous responses (11, 37). In terms of molecular regulation of other inflammatory factors' expression, lncRNAs are shown to act as molecular sponges/scaffolds for miRNAs as reported recently in COPD (38–40). For example, lncRNA TUG1 promotes airway remodeling *via* suppressing the miR-145-5p in CS-induced COPD models. The lncRNA NNT-AS1 was shown to regulate COPD associated airway cell proliferation/cell death, inflammation, and remodeling *via* the miR-582-5p and FBXO11 pathways. Interestingly, high levels of IL-6 and lncRNA IL6-AS1 were reported in COPD subjects with concurrent upregulation of miR-149-5p and early B-cell factor 1. Similar studies are underway to determine possible *LASI* lncRNA binding partners using the LASI-OE approach described in the present study to identify the molecular mechanisms responsible for plausible increased transcriptional activity or mRNA stability that augments the airway inflammatory responses.

LncRNAs modulate gene expression at multiple levels to alter the cell functions/responses. They are known to modulate chromatin structure or bind to directly to DNA. They can also bind to and suppress the expression of miRNAs or pre-miRNAs (8, 41). LncRNAs can directly enhance or suppress the expression of many mRNAs or functional transcripts. In our studies, knockdown of *LASI* lncRNA led to a suppressed expression of CSE-induced *ICAM-1* and *IL-6* mRNAs suggesting that there is no direct interaction between *LASI* lncRNA and *ICAM-1* or *IL-6* mRNAs. Instead, *LASI* lncRNA may be indirectly affecting the transcription of ICAM-1 and IL-6, whereby *LASI* lncRNA may be regulating the other intermediary immunoregulatory elements such as miRNAs or promoters upstream of ICAM-1 and IL-6. Accordingly, our data posit that *LASI* lncRNA may not be directly interacting with ICAM-1 protein, mRNA, or pre-mRNA, but experimental validation are needed. In a separate study we have observed that silencing ICAM-1 expression does not affect the *LASI* lncRNA levels (data not shown), thus implicating that the expression levels of these transcripts are driven independently *via* possible mutually exclusive transcriptional regulation of the opposite strands. The data further suggests that at the transcription level, a direct induction of *LASI* lncRNA by CSE treatment may be one of the drivers for the COPD-associated mucoinflammatory responses. Furthermore, we observed that *LASI* lncRNA was expressed in perinuclear region and cytosolic regions of bronchial airway epithelial cells of both macaques and human tissues. RNA-interference based silencing works primarily in the cytosolic region and even with only 37.5% suppression of *LASI* lncRNA levels, we observed a highly significant reduction in CSE-induced MUC5AC, ICAM-1, and IL-6 expression. This data does suggest that cytosolic *LASI* lncRNA may be important mediator of mucoinflammatory response, but further cell fractionation studies are needed to determine the subcellular location specific role of *LASI* lncRNAs in driving the CSE-treatment and COPD associated inflammatory responses.

The present study has several limitations as outlined here and should be strongly considered for drawing the inferences. Firstly, the archived lung tissues from the large animal model study are from female macaques only as human epidemiological studies suggest that female smokers show higher prevalence of COPD than males but the data presented here should be interpreted accordingly. Secondly, human lung tissue samples were provided by LTRC (NIH), but the COPD patient cohort data collection relies on self-reported smoking history and lacks accuracy. Thirdly, the *in-vitro* modeling studies used NHBEs and CHBEs from three separate donors only and are from a commercial supplier with no information provided on the race, age, gender, or smoking history. Moreover, the *in-vitro* modeling used bronchial airway epithelial cells only and responses in other epithelial and submucosal cells are not investigated that could drive smoke- and COPD-associated airway remodeling. Additionally, this study is focused on *LASI* lncRNA only, which may act synergistically with additional lncRNAs, specifically with *ICR* lncRNA. Furthermore, the studies reported here used acute model of CS exposure using CS extract instead of direct mainstream smoke exposure. However, with data presented from animal model of CS exposure, and from COPD tissue and airway epithelial cells, this study does corroborate the strong association of *LASI* lncRNA with CS-induced transcriptional modulation of airway mucoinflammatory responses.

In conclusion, this study elucidates *LASI* lncRNA as a novel regulator of CSE-induced and COPD-associated airway epithelial dysregulation and further suggests that targeting *LASI* lncRNA expression could present a novel therapeutic intervention modality to treat COPD phenotypes of upper airways. Specifically, the currently available therapies have limited success in treating COPD pathophysiologies creating an unmet need in discovery of novel therapeutic avenues (42–44). Recent epidemiological and pathological studies have shown that mucus hypersecretion is a prime target of COPD treatment avenues (45). Thus, airway epithelial expressed *LASI* lncRNA may provide additional novel method of controlling mucous responses specifically when noncoding RNA-based therapeutics are shown to be promising treatment modalities (46). Present study also suggests that the lncRNA *ICR* may play a similarly important role in CHBE dysregulation and requires further investigation. Future experiments will investigate the mechanism of action of *LASI* lncRNA to identify its binding partners and potential interactions that regulate airway innate immune responses.

DATA AVAILABILITY STATEMENT

The original contributions presented in the study are included in the article/**Supplementary Material**. Further inquiries can be directed to the corresponding author.

ETHICS STATEMENT

The animal study was reviewed and approved by Institutional Animal Care and Use Committee of Lovelace Respiratory Research Institute, Albuquerque, NM.

AUTHOR CONTRIBUTIONS

MM and DD designed and conducted the experiments. MM and HC wrote, edited, and/or revised the manuscript. MM, DD, and CL was responsible for data curation. HC conceptually de-signed the overall experiments and manuscript, and acquired funding. SS, MWN, GB, MNN, IR, and MS provided the oversight on the study design and edited the manuscript. All authors contributed to the article and approved the submitted version.

FUNDING

The National Institutes of Health (NIH) AI159237, AI144374, HL149898, and CA241752 supported this work.

ACKNOWLEDGMENTS

The authors would like to acknowledge Alejandro Perez and Natalia Orso for their assistance in optimization of study protocols. Authors would also like to acknowledge, Dr. Philip Kuehl of Lovelace Biomedical for providing the filter membranes with mainstream cigarette smoke particulate matters, Dr. Binoy Appukuttan of Flinders University, Adelaide, Australia for ICR lncRNA primer-probe sequences, and Dr. Madepalli Lakshmana of Florida International University, Miami, FL for providing the empty vector lentiviral preparation.

SUPPLEMENTARY MATERIAL

The Supplementary Material for this article can be found online at: https://www.frontiersin.org/articles/10.3389/fimmu.2022.803362/full#supplementary-material

REFERENCES

1. James SL, Abate D, Abate KH, Abay SM, Abbafati C, Abbasi N, et al. Global, Regional, and National Incidence, Prevalence, and Years Lived With Disability for 354 Diseases and Injuries for 195 Countries and Territories, 1990-2017: A Systematic Analysis for the Global Burden of Disease Study 2017. *Lancet* (2018) 392(10159):1789–858. doi: 10.1016/s0140-6736(18)32279-7
2. Rabe KF, Watz H. Chronic Obstructive Pulmonary Disease. *Lancet* (2017) 389(10082):1931–40. doi: 10.1016/s0140-6736(17)31222-9
3. Wong AWM, Gan WQ, Burns J, Sin DD, van Eeden SF. Acute Exacerbation of Chronic Obstructive Pulmonary Disease: Influence of Social Factors in Determining Length of Hospital Stay and Readmission Rates. *Can Respir J* (2008) 15(7):361–4. doi: 10.1155/2008/569496
4. Kim V, Criner GJ. Chronic Bronchitis and Chronic Obstructive Pulmonary Disease. *Am J Respir Crit Care Med* (2013) 187(3):228–37. doi: 10.1164/rccm.201210-1843CI
5. Vogelmeier CF, Román-Rodríguez M, Singh D, Han MK, Rodríguez-Roisin R, Ferguson GT. Goals of COPD Treatment: Focus on Symptoms and Exacerbations. *Respir Med* (2020) 166:105938. doi: 10.1016/j.rmed.2020.105938
6. Devadoss D, Long C, Langley RJ, Manevski M, Nair M, Campos MA, et al. Long Noncoding Transcriptome in Chronic Obstructive Pulmonary Disease. *Am J Respir Cell Mol Biol* (2019) 61(6):678–88. doi: 10.1165/rcmb.2019-0184TR
7. Sundar IK, Rahman I. Gene Expression Profiling of Epigenetic Chromatin Modification Enzymes and Histone Marks by Cigarette Smoke: Implications for COPD and Lung Cancer. *Am J Physiol Lung Cell Mol Physiol* (2016) 311(6):L1245–l1258. doi: 10.1152/ajplung.00253.2016
8. Schmitz SU, Grote P, Herrmann BG. Mechanisms of Long Noncoding RNA Function in Development and Disease. *Cell Mol Life Sci* (2016) 73(13):2491–509. doi: 10.1007/s00018-016-2174-5
9. Faiz A, Steiling K, Roffel MP, Postma DS, Spira A, Lenburg ME, et al. Effect of Long-Term Corticosteroid Treatment on microRNA and Gene-Expression Profiles in COPD. *Eur Respir J* (2019) 53(4):1801202. doi: 10.1183/13993003.01202-2018
10. Hu TJ, Huang HB, Shen HB, Chen W, Yang ZH. Role of Long Non-Coding RNA MALAT1 in Chronic Obstructive Pulmonary Disease. *Exp Ther Med* (2020) 20(3):2691–7. doi: 10.3892/etm.2020.8996
11. Devadoss D, Daly G, Manevski M, Houserova D, Hussain SS, Baumlin N, et al. A Long Noncoding RNA Antisense to ICAM-1 Is Involved in Allergic Asthma Associated Hyperreactive Response of Airway Epithelial Cells. *Mucosal Immunol* (2021) 14(3):630–9. doi: 10.1038/s41385-020-00352-9
12. Chand HS, Vazquez-Guillamet R, Royer C, Rudolph K, Mishra N, Singh SP, et al. Cigarette Smoke and HIV Synergistically Affect Lung Pathology in Cynomolgus Macaques. *J Clin Invest* (2018) 128(12):5428–33. doi: 10.1172/JCI121935
13. Pauwels RA, Buist AS, Calverley PM, Jenkins CR, Hurd SS. Global Strategy for the Diagnosis, Management, and Prevention of Chronic Obstructive Pulmonary Disease. NHLBI/WHO Global Initiative for Chronic Obstructive

Lung Disease (GOLD) Workshop Summary. *Am J Respir Crit Care Med* (2001) 163(5):1256–76. doi: 10.1164/ajrccm.163.5.2101039
14. Han MK, Agusti A, Celli BR, Criner GJ, Halpin DMG, Roche N, et al. From GOLD 0 to Pre-COPD. *Am J Respir Crit Care Med* (2021) 203(4):414–23. doi: 10.1164/rccm.202008-3328PP
15. Singh SP, Devadoss D, Manevski M, Sheybani A, Ivanciuc T, Exil V, et al. Gestational Exposure to Cigarette Smoke Suppresses the Gasotransmitter H (2)S Biogenesis and the Effects Are Transmitted Transgenerationally. *Front Immunol* (2020) 11:1628. doi: 10.3389/fimmu.2020.01628
16. Chand HS, Mebratu YA, Kuehl PJ, Tesfaigzi Y. Blocking Bcl-2 Resolves IL-13-Mediated Mucous Cell Hyperplasia in a Bik-Dependent Manner. *J Allergy Clin Immunol* (2017) 140(5):1456-59.e9. doi: 10.1016/j.jaci.2017.05.038
17. Radicioni G, Ceppe A, Ford AA, Alexis NE, Barr RG, Bleecker ER, et al. Airway Mucin MUC5AC and MUC5B Concentrations and the Initiation and Progression of Chronic Obstructive Pulmonary Disease: An Analysis of the SPIROMICS Cohort. *Lancet Respir Med* (2021) 9(11):1241–54. doi: 10.1016/S2213-2600(21)00079-5
18. Baginski TK, Dabbagh K, Satjawatcharaphong C, Swinney DC. Cigarette Smoke Synergistically Enhances Respiratory Mucin Induction by Proinflammatory Stimuli. *Am J Respir Cell Mol Biol* (2006) 35(2):165–74. doi: 10.1165/rcmb.2005-0259OC
19. Caramori G, Casolari P, Di Gregorio C, Saetta M, Baraldo S, Boschetto P, et al. MUC5AC Expression Is Increased in Bronchial Submucosal Glands of Stable COPD Patients. *Histopathology* (2009) 55(3):321–31. doi: 10.1111/j.1365-2559.2009.03377.x
20. Kesimer M, Ford AA, Ceppe A, Radicioni G, Cao R, Davis CW, et al. Airway Mucin Concentration as a Marker of Chronic Bronchitis. *N Engl J Med* (2017) 377(10):911–22. doi: 10.1056/NEJMoa1701632
21. Okuda K, Chen G, Subramani DB, Wolf M, Gilmore RC, Kato T, et al. Localization of Secretory Mucins MUC5AC and MUC5B in Normal/Healthy Human Airways. *Am J Respir Crit Care Med* (2019) 199(6):715–27. doi: 10.1164/rccm.201804-0734OC
22. Guo W, Liu S, Cheng Y, Lu L, Shi J, Xu G, et al. ICAM-1-Related Noncoding RNA in Cancer Stem Cells Maintains ICAM-1 Expression in Hepatocellular Carcinoma. *Clin Cancer Res* (2016) 22(8):2041–50. doi: 10.1158/1078-0432.CCR-14-3106
23. Ming X, Duan W, Yi W. Long Non-Coding RNA NEAT1 Predicts Elevated Chronic Obstructive Pulmonary Disease (COPD) Susceptibility and Acute Exacerbation Risk, and Correlates With Higher Disease Severity, Inflammation, and Lower miR-193a in COPD Patients. *Int J Clin Exp Pathol* (2019) 12(8):2837–48.
24. Herter EK, Li D, Toma MA, Vij M, Li X, Visscher D, et al. WAKMAR2, a Long Noncoding RNA Downregulated in Human Chronic Wounds, Modulates Keratinocyte Motility and Production of Inflammatory Chemokines. *J Invest Dermatol* (2019) 139(6):1373–84. doi: 10.1016/j.jid.2018.11.033
25. Hussain SS, George S, Singh S, Jayant R, Hu CA, Sopori M, et al. A Small Molecule BH3-Mimetic Suppresses Cigarette Smoke-Induced Mucous Expression in Airway Epithelial Cells. *Sci Rep* (2018) 8(1):13796. doi: 10.1038/s41598-018-32114-w
26. Nyunoya T, Mebratu Y, Contreras A, Delgado M, Chand HS, Tesfaigzi Y. Molecular Processes That Drive Cigarette Smoke-Induced Epithelial Cell Fate of the Lung. *Am J Respir Cell Mol Biol* (2014) 50(3):471–82. doi: 10.1165/rcmb.2013-0348TR
27. Eisner MD, Anthonisen N, Coultas D, Kuenzli N, Perez-Padilla R, Postma D, et al. An Official American Thoracic Society Public Policy Statement: Novel Risk Factors and the Global Burden of Chronic Obstructive Pulmonary Disease. *Am J Respir Crit Care Med* (2010) 182(5):693–718. doi: 10.1164/rccm.200811-1757ST
28. Christenson SA, van den Berge M, Faiz A, Inkamp K, Bhakta N, Bonser LR, et al. An Airway Epithelial IL-17A Response Signature Identifies a Steroid-Unresponsive COPD Patient Subgroup. *J Clin Invest* (2019) 129(1):169–81. doi: 10.1172/jci121087
29. Decramer M, Janssens W, Miravitlles M. Chronic Obstructive Pulmonary Disease. *Lancet* (2012) 379(9823):1341–51. doi: 10.1016/s0140-6736(11)60968-9
30. Walter RE, Wilk JB, Larson MG, Vasan RS, Keaney JFJr., Lipinska I, et al. Systemic Inflammation and COPD: The Framingham Heart Study. *Chest* (2008) 133(1):19–25. doi: 10.1378/chest.07-0058
31. Manevski M, Muthumalage T, Devadoss D, Sundar IK, Wang Q, Singh KP, et al. Cellular Stress Responses and Dysfunctional Mitochondrial-Cellular Senescence, and Therapeutics in Chronic Respiratory Diseases. *Redox Biol* (2020) 33:101443. doi: 10.1016/j.redox.2020.101443
32. Fanucchi S, Fok ET, Dalla E, Shibayama Y, Borner K, Chang EY, et al. Immune Genes Are Primed for Robust Transcription by Proximal Long Noncoding RNAs Located in Nuclear Compartments. *Nat Genet* (2019) 51(1):138–50. doi: 10.1038/s41588-018-0298-2
33. Wang H, Chen L, Li D, Zeng N, Wu Y, Wang T, et al. Microarray Analysis of Lung Long Non-Coding RNAs in Cigarette Smoke-Exposed Mouse Model. *Oncotarget* (2017) 8(70):115647–56. doi: 10.18632/oncotarget.23362
34. Rao W, Wang S, Duleba M, Niroula S, Goller K, Xie J, et al. Regenerative Metaplastic Clones in COPD Lung Drive Inflammation and Fibrosis. *Cell* (2020) 181(4):848–864.e18. doi: 10.1016/j.cell.2020.03.047
35. Gindele JA, Kiechle T, Benediktus K, Birk G, Brendel M, Heinemann F, et al. Intermittent Exposure to Whole Cigarette Smoke Alters the Differentiation of Primary Small Airway Epithelial Cells in the Air-Liquid Interface Culture. *Sci Rep* (2020) 10(1):6257. doi: 10.1038/s41598-020-63345-5
36. Bodas M, Moore AR, Subramaniyan B, Georgescu C, Wren JD, Freeman WM, et al. Cigarette Smoke Activates NOTCH3 to Promote Goblet Cell Differentiation in Human Airway Epithelial Cells. *Am J Respir Cell Mol Biol* (2021) 64(4):426–40. doi: 10.1165/rcmb.2020-0302OC
37. Shaykhiev R. Emerging Biology of Persistent Mucous Cell Hyperplasia in COPD. *Thorax* (2019) 74(1):4–6. doi: 10.1136/thoraxjnl-2018-212271
38. Gu W, Yuan Y, Wang L, Yang H, Li S, Tang Z, et al. Long non-Coding RNA TUG1 Promotes Airway Remodelling by Suppressing the miR-145-5p/DUSP6 Axis in Cigarette Smoke-Induced COPD. *J Cell Mol Med* (2019) 23(11):7200–9. doi: 10.1111/jcmm.14389
39. Mei J, Zhang Y, Lu S, Wang J. Long Non-Coding RNA NNT-AS1 Regulates Proliferation, Apoptosis, Inflammation and Airway Remodeling of Chronic Obstructive Pulmonary Disease *via* Targeting miR-582-5p/FBXO11 Axis. *BioMed Pharmacother* (2020) 129:110326. doi: 10.1016/j.biopha.2020.110326
40. Yi E, Zhang J, Zheng M, Zhang Y, Liang C, Hao B, et al. Long Noncoding RNA IL6-AS1 Is Highly Expressed in Chronic Obstructive Pulmonary Disease and is Associated With Interleukin 6 by Targeting miR-149-5p and Early B-Cell Factor 1. *Clin Transl Med* (2021) 11(7):e479. doi: 10.1002/ctm2.479
41. Statello L, Guo CJ, Chen LL, Huarte M. Gene Regulation by Long Non-Coding RNAs and Its Biological Functions. *Nat Rev Mol Cell Biol* (2021) 22(2):96–118. doi: 10.1038/s41580-020-00315-9
42. Caobi A, Dutta RK, Garbinski LD, Esteban-Lopez M, Ceyhan Y, Andre M, et al. The Impact of CRISPR-Cas9 on Age-Related Disorders: From Pathology to Therapy. *Aging Dis* (2020) 11(4):895–915. doi: 10.14336/ad.2019.0927
43. Manevski M, Devadoss D, Castro R, Delatorre L, Yndart A, Jayant RD, et al. Development and Challenges of Nanotherapeutic Formulations for Targeting Mitochondrial Cell Death Pathways in Lung and Brain Degenerative Diseases. *Crit Rev BioMed Eng* (2020) 48(3):137–52. doi: 10.1615/CritRevBiomedEng.2020034546
44. Rogers DF, Barnes PJ. Treatment of Airway Mucus Hypersecretion. *Ann Med* (2006) 38(2):116–25. doi: 10.1080/07853890600585795
45. Cerveri I, Brusasco V. Revisited Role for Mucus Hypersecretion in the Pathogenesis of COPD. *Eur Respir Rev* (2010) 19(116):109–12. doi: 10.1183/09059180.00002710
46. Winkle M, El-Daly SM, Fabbri M, Calin GA. Noncoding RNA Therapeutics - Challenges and Potential Solutions. *Nat Rev Drug Discov* (2021) 20(8):629–51. doi: 10.1038/s41573-021-00219-z

Conflict of Interest: The authors declare that the research was conducted in the absence of any commercial or financial relationships that could be construed as a potential conflict of interest.

this article, or claim that may be made by its manufacturer, is not guaranteed or endorsed by the publisher.

frontiers | Frontiers in Immunology

TYPE Correction
PUBLISHED 08 August 2022
DOI 10.3389/fimmu.2022.988069

OPEN ACCESS

EDITED AND REVIEWED BY
Nils Yngve Lycke,
University of Gothenburg, Sweden

*CORRESPONDENCE
Hitendra S. Chand
hchand@fiu.edu

SPECIALTY SECTION
This article was submitted to Mucosal Immunity, a section of the journal Frontiers in Immunology

RECEIVED 06 July 2022
ACCEPTED 25 July 2022
PUBLISHED 08 August 2022

CITATION
Manevski M, Devadoss D, Long C, Singh SP, Nasser MW, Borchert GM, Nair MN, Rahman I, Sopori M and Chand HS (2022) Corrigendum: Increased expression of *LASI* LncRNA regulates the cigarette smoke and COPD associated airway inflammation and mucous cell hyperplasia. *Front. Immunol.* 13:988069. doi: 10.3389/fimmu.2022.988069

Corrigendum: Increased expression of *LASI* LncRNA regulates the cigarette smoke and COPD associated airway inflammation and mucous cell hyperplasia

Marko Manevski[1], Dinesh Devadoss[1], Christopher Long[1], Shashi P. Singh[2], Mohd Wasim Nasser[3], Glen M. Borchert[4], Madhavan N. Nair[1], Irfan Rahman[5], Mohan Sopori[2] and Hitendra S. Chand[1]*

[1]Department of Immunology and Nano-Medicine, Herbert Wertheim College of Medicine, Florida International University, Miami, FL, United States, [2]Respiratory Immunology Program, Lovelace Respiratory Research Institute, Albuquerque, NM, United States, [3]Department of Biochemistry and Molecular Biology, University of Nebraska Medical Center, Omaha, NE, United States, [4]Department of Pharmacology, University of South Alabama, Mobile, AL, United States, [5]Department of Environmental Medicine, University of Rochester Medical Center, Rochester, NY, United States

KEYWORDS

bronchial epithelial cells, cigarette smoke (CS), chronic obstructive pulmonary disease (COPD), long noncoding RNA (lncRNA), mucus hyperexpression, lncRNA antisense to ICAM-1 (LASI)

A corrigendum on

Increased expression of LASI LncRNA regulates the cigarette smoke and COPD associated airway inflammation and mucous cell hyperplasia

by Manevski M, Devadoss D, Long C, Singh SP, Nasser MW, Borchert GM, Nair MN, Rahman I, Sopori M, Chand HS (2022). *Front. in Immunol.* 2022 Jun 14; 13:803362. doi: 10.3389/fimmu.2022.803362

In the published article, there was an error in Table 1 as published. The information about the smoking history (Stop Smoking) for the subjects with 'No COPD' was duplicated. The corrected Table 1 and its caption appear below.

The authors state that this does not change the scientific conclusions of the article in any way. The original article has been updated.

10.3389/fimmu.2022.988069

TABLE 1 Demographics of the study cohort of COPD patients with clinically-defined GOLD stage severity and self-reported smoking history.

	No COPD	Mild COPD	Severe COPD
Age*	54.2 ± 3.2	69.2 ± 3.9	65.1 ± 2.7
Gender, M/F	3M/3F	4M/2F	3M/5F
Smoking in PY*	54.0 ± 12.6 (2)	29.9 ± 10.7 (3)	35.0 ± 2.8 (3)
Stop Smoking (Y)*	6.6 ± 1.6	21.4 ± 12.8	11.9 ± 2.5

*Mean, ± SEM; M, Male; F, Female; PY, Packs per Year; Y, Years.

Publisher's note

frontiers | Frontiers in Immunology

TYPE Original Research
PUBLISHED 18 August 2022
DOI 10.3389/fimmu.2022.935114

OPEN ACCESS

EDITED BY
Rabindra Tirouvanziam,
Emory University, United States

REVIEWED BY
Soumya Panigrahi,
Case Western Reserve University, United States
Kushagra Bansal,
Jawaharlal Nehru Centre for Advanced Scientific Research, India

*CORRESPONDENCE
Junko Nishio
junko.nishio@med.toho-u.ac.jp
Toshihiro Nanki
toshihiro.nanki@med.toho-u.ac.jp

SPECIALTY SECTION
This article was submitted to Mucosal Immunity, a section of the journal Frontiers in Immunology

RECEIVED 03 May 2022
ACCEPTED 18 July 2022
PUBLISHED 18 August 2022

CITATION
Yamada Z, Nishio J, Motomura K, Mizutani S, Yamada S, Mikami T and Nanki T (2022) Senescence of alveolar epithelial cells impacts initiation and chronic phases of murine fibrosing interstitial lung disease. *Front. Immunol.* 13:935114. doi: 10.3389/fimmu.2022.935114

Senescence of alveolar epithelial cells impacts initiation and chronic phases of murine fibrosing interstitial lung disease

Zento Yamada[1,2], Junko Nishio[2,3]*, Kaori Motomura[2], Satoshi Mizutani[2], Soichi Yamada[2], Tetuo Mikami[4] and Toshihiro Nanki[1,2]*

[1]Department of Internal Medicine, Toho University Graduate School of Medicine, Tokyo, Japan, [2]Division of Rheumatology, Department of Internal Medicine, Toho University School of Medicine, Tokyo, Japan, [3]Department of Immunopathology and Immunoregulation, Toho University School of Medicine, Tokyo, Japan, [4]Department of Pathology, Toho University School of Medicine, Tokyo, Japan

Fibrosing interstitial lung disease (ILD) develops due to the impaired reparative processes following lung tissue damage. Cellular senescence has been reported to contribute to the progression of fibrosis. However, the mechanisms by which these senescent cells initiate and/or drive the progression of lung tissue fibrosis are not yet fully understood. We demonstrated that $p21^{WAF1/CIP1}$- and $p16^{INK4A}$-pathway-dependent senescence in type 2 alveolar epithelial cells (AEC2) were both involved in the initiation and progression of lung fibrosis in murine bleomycin (BLM)-induced ILD. $p21^{WAF1/CIP1}$-senescent AEC2 emerged rapidly, as early as 1 day after the intratracheal instillation of BLM. Their number subsequently increased and persisted until the later fibrosis phase. Very few $p16^{INK4A}$-senescent AEC2 emerged upon the instillation of BLM, and their increase was slower and milder than that of $p21^{WAF1/CIP1+}$ AEC2. AEC2 enriched with senescent cells sorted from BLM-ILD lungs expressed senescence-associated secretory phenotype (SASP)-related genes, including *Il6*, *Serpin1*, *Tnfa*, *Ccl2*, *Tgfb*, and *Pdgfa*, at the initiation and chronic phases of fibrosis, exhibiting distinct expression patterns of magnitude that were dependent on the disease phase. $Ly6C^+$ inflammatory monocytes increased in the lungs immediately after the instillation of BLM and interstitial macrophages increased from day 3. The expression of *Acta2* and *Col1a1* was upregulated as early as day 1, indicating the activation of fibroblasts. We speculated that IL-6, plasminogen activator inhibitor-1 (PAI-1), and TGF-β contributed to the accumulation of senescent cells during the progression of fibrosis in an autocrine and paracrine manner. In addition, CCL2, produced in large amounts by senescent AEC2, may have induced the infiltration of $Ly6C^+$ inflammatory monocytes in the early phase, and TGF-β and PDGFa from senescent AEC2 may contribute to the activation of fibroblasts in the very early phases. Our study indicated that senescent AEC2 plays a role in the pathogenesis of fibrosing ILD throughout the course of the disease and

provides insights into its pathogenesis, which may lead to the development of new therapeutic methods targeting senescent cells or SASP molecules.

KEYWORDS

interstitial lung disease, p21, p16, senescence-associated secretary phenotype, type 2 alveolar epithelial cell, IL-6, interstitial macrophages

Introduction

Fibrosing interstitial lung diseases (ILDs) are a group of diseases in which excessive extracellular matrix proteins are produced by persistently activated fibroblasts causing the destruction of the alveolar architecture (1). Fibrosis occurs in the normal wound healing process and resolves over time. However, continuous inflammation and unresolved cellular damage impair reparative processes, leading to the progression of fibrosis and tissue remodeling (2). While smoking (3) and the inhalation of silica (4) are well-known environmental factors that cause idiopathic pulmonary fibrosis (IPF), several genetic variants for surfactant protein-C, surfactant protein-A2, telomerase reverse transcriptase, telomerase RNA component, and MUC5B have been identified as factors associated with IPF or familial interstitial pulmonary fibrosis (5–8). Autoimmune reactions are also triggering factors that initiate tissue injury in fibrosing ILD in association with connective tissue diseases, including rheumatoid arthritis, systemic scleroderma, polymyositis, and dermatomyositis (9). Regardless of the triggers and/or causative genetic variants, the molecular mechanisms underlying tissue/cellular damage and resultant fibrosis are not fully understood, and they involve complex interactions between immune cells, epithelial cells, fibroblasts, and endothelial cells (9).

The paradigm that the damage of alveolar epithelial cells (AECs) and impaired reparative processes drive lung fibrosis has recently become prominent in the pathogenesis of ILD (10). AECs are classified as type 1 (AEC1) and type 2 (AEC2). AEC2 are progenitor cells that self-renew and transdifferentiate into AEC1, and are also producers of surfactant phospholipids and proteins, which reduce surface tension at the alveolar air-liquid interface (10). Continuous environmental stimuli from airways have been suggested to cause AEC2 dysfunction, such as a hyper-activated state, apoptosis, or senescence, leading to inflammatory cell infiltration and parenchymal fibrosis in the lungs.

Cellular senescence is a state of permanent cell cycle arrest induced by various types of extrinsic or intrinsic stresses, including DNA damage by telomere shortening, genotoxic stress, reactive oxidative stress, mitochondrial dysfunction, and oncogene activation (11, 12). These stressors activate the p53-$p21^{WAF1/CIP1}$ and/or the $p16^{INK4A}$-pRB pathways. $p21^{WAF1/CIP1}$ and $p16^{INK4A}$ are both cyclin-dependent kinase (CDK) inhibitors that inhibit the kinase activity of cyclin–CDK complexes, which are required for cell cycle progression (13). The prolonged activation of either pathway, p53-$p21^{WAF1/CIP1}$ or $p16^{INK4A}$-pRB, is sufficient to induce senescence (13). Although $p21^{WAF1/CIP1}$ is more relevant for the initiation of senescence, the expression of $p16^{INK4A}$ is critical for persistent senescence (14).

Cell cycle markers, typically $p21^{WAF1/CIP1}$, $p16^{INK4A}$, p53, phospho-p53, a decrease in pRB, and the absence of proliferation, are used to detect cellular senescence. However, these are not universal markers because they are also expressed in non-senescent cells (15). Moreover, whereas p53-$p21^{WAF1/CIP1}$ is transiently activated and more relevant for the initiation of senescence, the expression of $p16^{INK4A}$ is critical for persistent senescence (14). Therefore, additional hallmarks are used in combination to conclusively identify senescence: structural changes associated with senescence, such as an increased lysosomal mass detected by a morphologically enlarged cell size; senescence-associated β-galactosidase (SA-βgal) activity; changes in organelle structures represented by the downregulation of Lamin B1; and nuclear alterations detected by DNA damage response-associated proteins or phosphorylated H2A histone family member X (γ-H2AX) (15).

Although cell growth is arrested, senescent cells remain metabolically active and acquire a senescence-associated secretory phenotype (SASP), by which senescent cells produce a wide array of soluble molecules, including cytokines, chemokines, matrix remodeling proteases, extracellular matrix components, and growth modulators (11, 13). These mediators alter the state of the surrounding cells. In addition, SASP promotes senescence in an autocrine manner and that of neighboring cells in a paracrine manner, thereby spreading senescent cells throughout the entire tissue (12, 13, 16).

Cellular senescence was recently reported to contribute to various age-related inflammatory diseases, including obesity, atherosclerosis, osteoarthritis, Alzheimer's disease, and lung diseases, such as IPF (17). Since senescent cells are resistant to apoptosis, they accumulate in aged organs, leading to these inflammatory diseases due to SASP (17). SA-βgal, $p16^{INK4A}$, p53, or $p21^{WAF1/CIP1}$ and disease-dependent SASP are present at inflamed sites. In murine disease models, these diseases are ameliorated by the elimination of senescent cells using genetically engineered mice or senolytics (18–21).

Previous studies have shown that in human IPF, DNA damage and expressions of SA-βgal, $p16^{INK4A}$, p53, or $p21^{WAF1/CIP1}$ have been observed in lung fibroblasts and/or epithelial cells (22–28). Similar to human IPF, senescence markers or SASP have been detected in AEC and/or fibroblasts in bleomycin-induced ILD (BLM-ILD) (29–33). Since BLM elicits DNA damage in cell lines and primary cells, including epithelial cells and fibroblasts (34), its intratracheal instillation is considered to induce DNA damage and resultant senescence in the lung cells of BLM-ILD. However, these studies have stressed the importance of the senescence of different cell types, including AECs, fibroblasts, and endothelial cells, in BLM-ILD.

Although the emergence of senescent cells has been demonstrated in human IPF as well as in its murine model, the mechanisms by which these senescent cells initiate and/or promote the progression of lung tissue fibrosis are not yet fully understood. Furthermore, most studies on murine BLM-ILD have analyzed SASP-associated mediators in the chronic phase of lung fibrosis on day 14 or 28 after the instillation of BLM. No studies have focused on the role of senescence at the initiation phase. Furthermore, the link between SASP and pathogenesis, such as immune cell infiltration and fibroblast activation, remains unknown.

To investigate how cellular senescence and SASP contribute to the development and progression of fibrosing ILD, we investigated the dynamics of $p21^{WAF1/CIP1}$- and $p16^{INK4A}$-dependent senescence from disease initiation to the established fibrosis phase in murine BLM-ILD. We found that type 2 AEC (AEC2) expressed both $p21^{WAF1/CIP1}$ and $p16^{INK4A}$ proteins upon the BLM instillation with a distinct pattern of expression dynamics. Senescent cell-enriched AEC2 subsets highly expressed a set of inflammatory SASP-related genes at both the initiation and fibrosis phases. These inflammatory mediators may promote the infiltration of monocytes and activation of fibroblasts from the early phase of the progression of fibrosis. These results suggest a critical role for senescent AEC2 throughout the course of fibrosing ILD and provide insights into its pathogenesis, which may lead to the development of new therapeutic methods targeting senescent cells or SASP molecules.

Results

$p21^{WAF1/CIP1}$-expressing cells in the early phase in BLM-ILD

Although the emergence of senescent cells in BLM-ILD has been demonstrated, most studies detected these cells in the late phase of fibrosis. To elucidate the dynamics of the emergence of senescent cells, we first examined the expression of $p21^{WAF1/CIP1}$, a cell cycle arrest marker, in lung tissue by immunohistochemistry in parallel with an evaluation of histological fibrosis during the progression of BLM-ILD. Lung tissue stained with hematoxylin and eosin (HE) and Masson's trichrome (MT) exhibited normal alveolar wall thickness and very limited infiltration in a small area at day 3 post-BLM instillation (Figure 1A). The infiltration and thickening of alveolar septa appeared on day 7. The accumulation of collagen became evident and gradually increased after day 7. The extensive formation of fibrotic loci was observed after day 10. Mice intratracheally instilled with saline did not show any cell infiltration or septal collagen fibers, even on day 14 (Figure 1A). The Ashcroft score (35), a semi-quantitative method to score lung fibrosis based on cell infiltration and the accumulation of collagen, showed that the area of cell infiltration with accumulated collagen gradually increased (Figure 1C). The quantitative analysis of MT-stained sections revealed a gradual increase in collagen deposition from the early phase to the fibrosis phase on day 14 (Figure 1D). Cells expressing the senescence marker $p21^{WAF1/CIP1}$ appeared in some alveoli and were scattered throughout the lungs on day 3 post-BLM instillation, when fibrosis was not evident by HE or MT staining (Figure 1B). The number of $p21^{WAF1/CIP1+}$ cells increased after day 3 and were more concentrated in fibrotic loci on days 10 and 14. Most $p21^{WAF1/CIP1+}$ cells were morphologically enlarged, which is a characteristic of senescent cells. The quantitative analysis revealed that the number of $p21^{WAF1/CIP1+}$ cells was increased as early as on day 1. After day 3, the number of $p21^{WAF1/CIP1+}$ cells was significantly higher than on day 0, and gradually increased, persisting after day 10 (Figure 1E). In contrast, the expression of *Cdkn1a*, encoding $p21^{WAF1/CIP1}$, was strongly induced as early as day 1 after the instillation of BLM. However, it decreased from day 7 (Figure 1F). The divergence of expression dynamics between $p21^{WAF1/CIP1}$ and *Cdkn1a* might be attributed to the transient expression of $p21^{WAF1/CIP1}$ in some cells upon the BLM stimulation and the post-translational regulation of $p21^{WAF1/CIP1}$ (see *Discussion*). Thus, these results suggested that the cellular senescence of alveolar cells was induced immediately upon the BLM instillation and preceded the histological formation of fibrosis.

We speculated that most $p21^{WAF1/CIP1+}$ cells were AEC2 based on their spherical shape and relatively large round nuclei, as shown in Figure 1B. As expected, double color immunofluorescence of $p21^{WAF1/CIP1}$ and prosurfactant protein C (proSP-C), a marker of AEC2, showed that $p21^{WAF1/CIP1}$ was stained on the nuclei of proSP-C-positive AEC2 (Figure 2). Approximately 30% of AEC2 were positive for $p21^{WAF1/CIP1}$ (Supplementary Table 1). Taken together, these results indicated that AEC2 highly expressed $p21^{WAF1/CIP1}$ from the initiation phase of BLM-ILD and that $p21^{WAF1/CIP1+}$ AEC2 increased and persisted until the later fibrosis phase.

Distinct expression dynamics of $p16^{INK4A}$ in the progression of lung fibrosis in BLM-ILD

Since there are no highly sensitive and specific markers of cellular senescence (15, 36), we examined the expression of another cell cycle arrest marker, $p16^{INK4A}$, in the lungs throughout the progression of BLM-ILD. We observed the

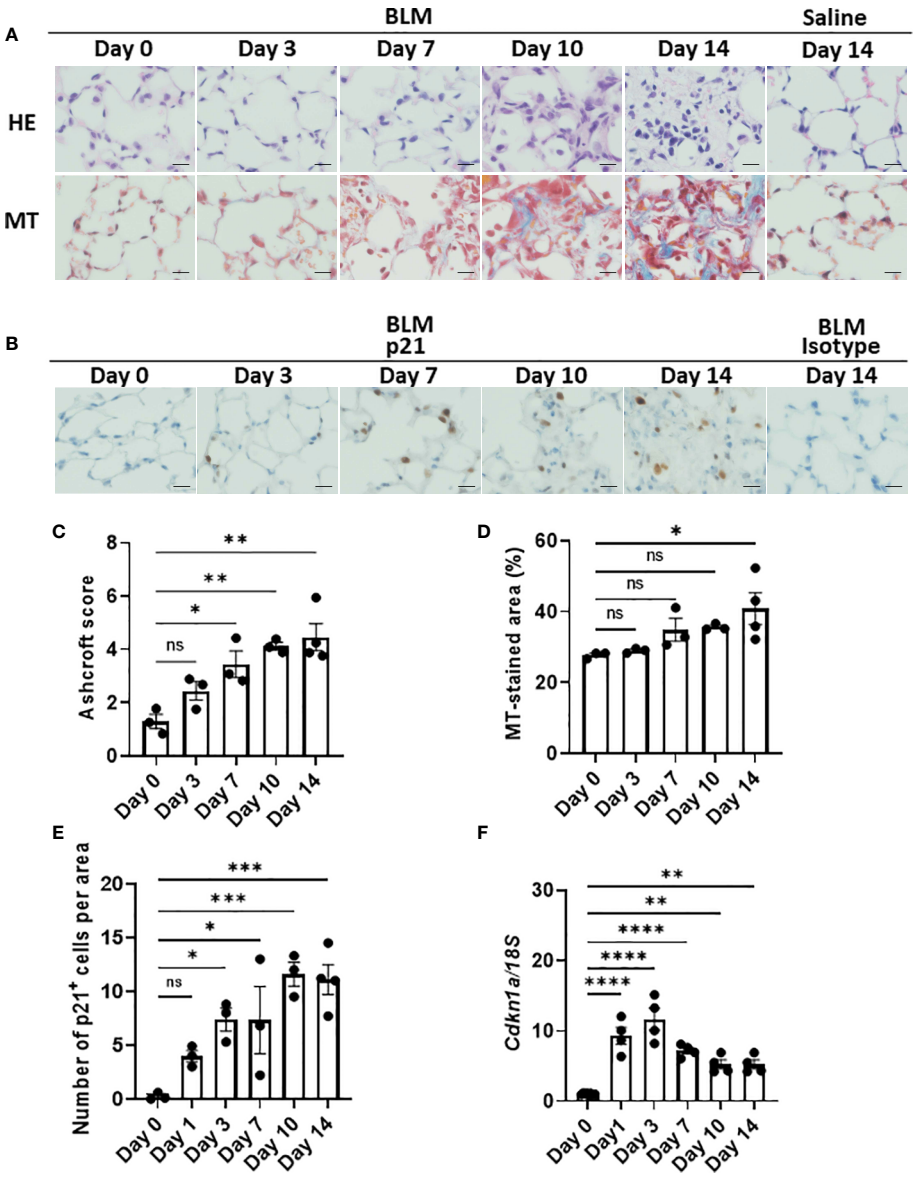

FIGURE 1
Emergence of p21WAF1/CIP1+ cells in lungs in the early phase of bleomycin-induced ILD (BLM-ILD).C57BL/6 mice were intratracheally instilled with BLM to induce BLM-ILD. Control mice were intratracheally instilled with saline. The lungs were obtained before and 1, 3, 7, 10, and 14 days after the instillation of BLM and 14 days after the instillation of saline. **(A)** Representative images of hematoxylin and eosin (HE) and Masson's trichrome (MT) staining of paraffin-embedded lung tissue on the indicated days. **(B)** Representative images of the immunohistochemical staining of p21WAF1/CIP1 of lung tissue from mice on the indicated days. **(C)** The Ashcroft scale using MT-stained lung tissue from pooled mice. **(D)** Percentage of the collagen fiber area in MT-stained lung tissue. The MT-stained area was measured by ImageJ in 20 randomly selected areas (360 × 240 μm) and the average was plotted. **(E)** Number of p21WAF1/CIP1+ cells per area of the right lung from pooled mice. p21WAF1/CIP1+ cells were counted in 10 randomly selected areas (180 × 120 μm) and the average was plotted. **(F)** Cdkn1a expression relative to 18S rRNA (18S) of the lung by quantitative RT-PCR (qRT-PCR). Scale bars indicate 5 μm. n = 3–4 per day **(C–E)**; n = 4 per day **(F)**. Data are presented as the mean ± SEM. Statistics show p-values from a one-way ANOVA with Dunnett's multiple comparisons test as a post-hoc test comparing values on day 0. ns, not significant. *p < 0.05; **p < 0.01; ***p < 0.001; ****p < 0.0001.

expression of $p16^{INK4A}$ in the nuclei of a very small number of AEC as early as on day 1, and $p16^{INK4A+}$ cells increased as the disease progressed (Figures 3A, B), but were not detected on day 0. Most $p16^{INK4A+}$ cells had a spherical shape, suggesting AEC2. They were also enlarged, similar to $p21^{WAF1/CIP1+}$ cells. It is important to note that increases in the number of $p16^{INK4A+}$ AEC2 were milder and slower in the early phase (Figure 3B) than those in $p21^{WAF1/CIP1+}$ AEC2 (Figure 1E). $p16^{INK4A+}$ AEC2 exhibited a marked increase after day 7 (Figure 3B). The expression of *Cdkn2a* encoding $p16^{INK4A}$ gradually increased

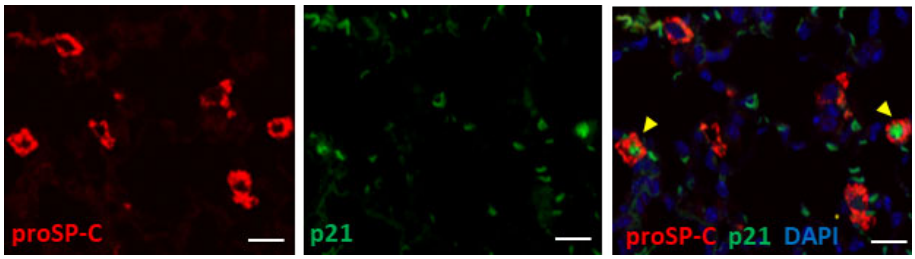

FIGURE 2
Type 2 alveolar epithelial cells (AEC2) undergo senescence in BLM-ILD.Paraffin-embedded lung tissue sections from mice 14 days after the instillation of BLM were used for double immunofluorescence staining for prosurfactant protein C (proSP-C) (red) and p21WAF1/CIP1 (p21) (green) with 4,6-diamidino-2-phenylindole (DAPI) (blue) counterstaining for nuclei. Yellow arrows indicate double-positive cells. The scale bar indicates 20 μm.

upon the BLM instillation, with a significant increase being observed on day 14 (Figure 3C). These results showed that the slight increase in $p16^{INK4A+}$ AEC2 in the early phase was in contrast to the sudden emergence of a relatively large number of $p21^{WAF1/CIP1+}$ AEC2 upon the BLM instillation. Moreover, $p16^{INK4A}$ and $p21^{WAF1/CIP1}$ were both persistently expressed in AEC2 in the later fibrosis phase, indicating that senescence dependent on both pathways continued to exist in AEC2 of fibrotic lung tissue. Therefore, $p16^{INK4A}$ expression may be more strongly affected by tissue environmental changes induced after the BLM instillation rather than by the direct effects of BLM.

AEC2 in BLM-ILD lungs show senescent cell characteristics

As described above, a combination of markers is used to prove the cellular senescence of AEC2. Although SA-βgal is a common marker for identifying senescent cells, it was not possible to measure its enzyme activity in the paraffinized sections used in this study. AEC2 did not express Ki-67 in fibrotic areas in the later phases (Figure 3D), supporting the lack of proliferation, which is also a characteristic of senescence. In contrast, Ki-67^{+} cells from the same lung section were localized in the area with cell infiltration, in which senescent cells were absent (Figure 3D). We also examined γ-H2AX, indicating DNA damage, which is another hallmark of senescent cells, in BLM-ILD on day 3 (Figure 3E). We found that γ-H2AX-stained cells were morphologically identified as enlarged AEC2, indicating that double-stranded DNA damage was induced in these cells by BLM (Figures 3E, F). On the other hand, its expression decreased on day 14 (Figures 3E, F). Since DNA damage may lead to apoptosis, we also examined cleaved caspase 3 (CC-3). Although a subset of cells with the shape of AEC2 expressed CC-3 on day 3, very few cells expressed it on day 14 (Figures 3G, H). These results suggested that the majority of $p21^{WAF1/CIP1}$-expressing AEC2 cells had acquired senescence, but that a small subset of $p21^{WAF1/CIP1+}$ AEC2 cells underwent apoptosis due to BLM-induced double-stranded DNA breaks in the early phase of BLM-ILD. These results also indicated that the persistent expression of $p21^{WAF1/CIP1}$ in the later fibrosis phase was not driven by DNA damage. Collectively, enlarged AEC2 were positive with another cell cycle arrest marker, $p16^{INK4A}$, and did not proliferate, indicating that a subset of AEC2 were senescent cells. Furthermore, the senescence of AEC2 occurred due to DNA breakage through the direct effects of BLM in the early phase; however, persistent senescence in the fibrosis phase may be driven by other factors. This senescence appeared to be dependent on environmental alterations caused by tissue damage.

AEC2 acquired SASP in BLM-ILD

Previous studies reported the senescence of fibroblasts, AEC, and/or endothelial cells in human IPF (22–28) as well as in murine BLM-ILD (29–33). However, which senescent cells exhibit the SASP-mediated production of inflammatory mediators and contribute to the development of lung fibrosis has not been clarified. Since we found a robust senescence phenotype in AEC2 from the early phase to the fibrosis phase, we hypothesized a critical role for the cellular senescence of AEC2 in fibrosing ILD. Therefore, we examined the gene expression of SASP-related mediators of AEC2 in the early phase before the accumulation of collagen as well as in the later phases of fibrosis, and investigated whether senescent AEC2 acquire SASP and contributes to the initiation/progression of fibrosing ILD. It was challenging to collect live AEC2 because of the limited availability of surface markers. We confirmed that proSP-C, an intracellular marker of AEC2, was expressed in the limited population highly expressing EpCAM ($EpCAM^{hi}$ cells) by a flow cytometric analysis (Figure 4A). Therefore, we isolated $EpCAM^{hi}$ cells as an AEC2 subset by flow cytometric sorting on days 3 and 14 after the BLM instillation (Figure 4B) and examined their expression of canonical pro-inflammatory cytokines, chemokines, and growth factors associated with SASP by qRT-PCR (Figure 4C). We confirmed that *Cdkn1a* was more highly expressed in BLM-

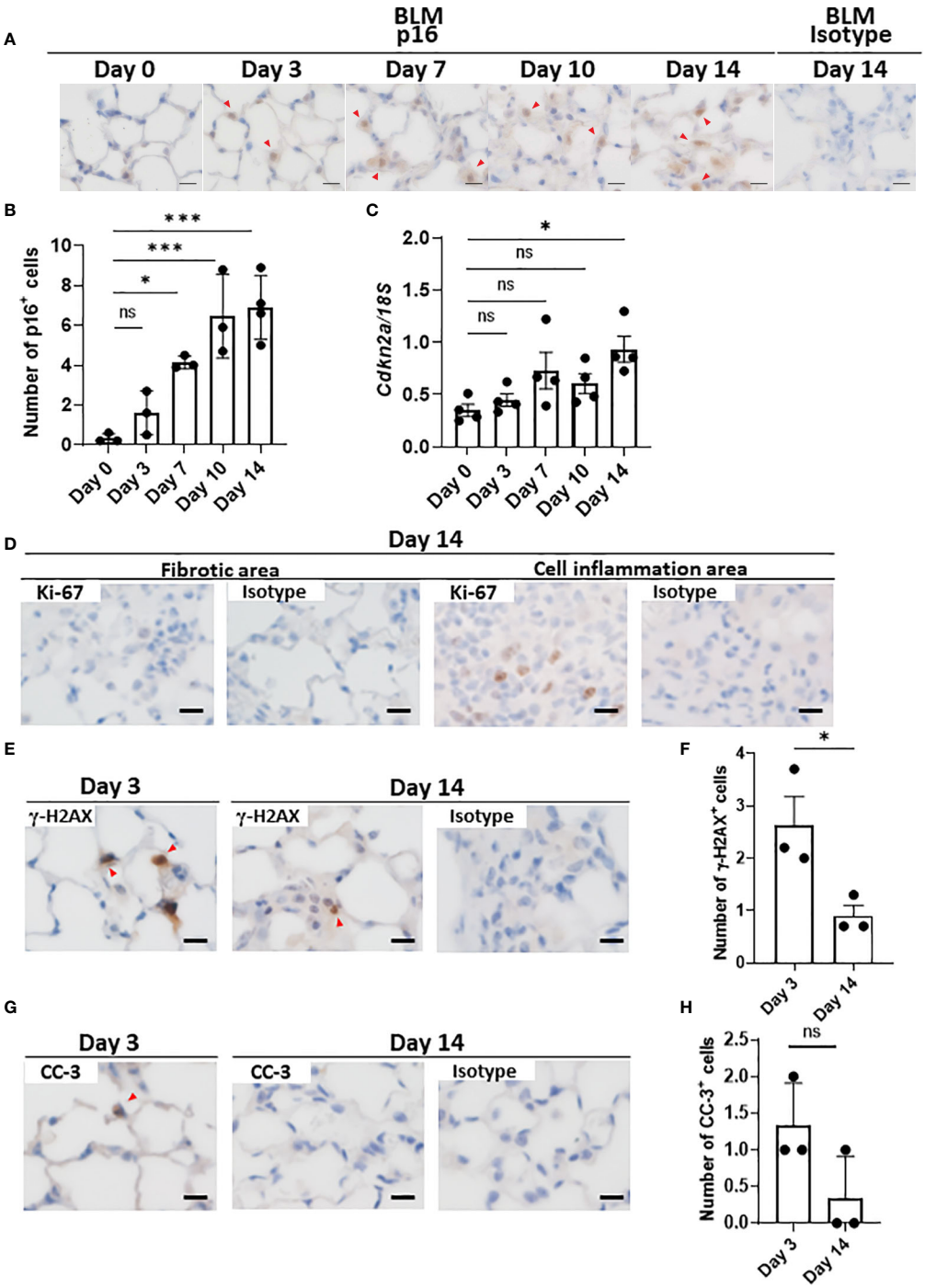

FIGURE 3
AEC2 in BLM-ILD express other cellular senescence markers.Paraffin-embedded lung tissue was prepared as described in Figure 1. **(A)** Representative images of immunohistochemical staining for p16INK4A on the indicated days. **(B)** Numbers of p16INK4A+ cells per area of the right lung from pooled mice. p16INK4A+ cells were counted in 10 randomly selected areas (180 × 120 μm) and the average was plotted. n = 3–4 per day. **(C)** Cdkn2a expression relative to 18S rRNA in the lungs of pooled mice by qRT-PCR. n = 4 per day. **(D–H)** Immunohistochemical analysis of Ki-67 **(D)**, γ-H2AX **(E, F)**, and cleaved caspase-3 (CC-3, **G, H**) in the lungs of mice 3 and/or 14 days after the instillation of BLM. The numbers of γ-H2AX+ **(F)** cells per area or the total number of CC-3+ **(H)** cells in 10 areas were plotted as described in Figure 1E. Red arrows indicate positive cells. Scale bars indicate 5 μm. Data are presented as the mean ± SEM. A one-way ANOVA with Dunnett's multiple comparisons test was used as a post-hoc test comparing values on day 0 **(B, C)**. Unpaired t-tests were used for two-group comparisons **(F, H)**. ns, not significant. *p < 0.05; ***p < 0.001.

instilled lungs than in saline-instilled lungs on days 3 and 14. Of note, *Cdkn1a* expression levels were >10-fold higher than in saline-instilled lungs on day 3. Although its expression level was decreased on day 14, it was still fourfold higher than in saline-instilled mice. These results are consistent with those shown in Figure 1F. We were unable to quantify *Cdkn2a* from 10,000 to 20,000 sorted AEC2, which was the maximum number of cells obtained with high purity from the lungs of a mouse. The canonical SASP-related genes, *Il6* and *Serpine1* encoding plasminogen activator 1 (PAI-1), were expressed at levels that were >5-fold higher than those in control mice on days 3 and 14. Since IL-6 and PAI-1 were previously demonstrated to promote and transmit the senescence of self and neighboring cells (13, 37, 38), these molecules may have contributed to the persistence and augmentation of senescent AEC2 during the progression of BLM-ILD. We also examined inflammatory mediators associated with the migration and activation of monocytes/macrophages because they play pivotal roles in fibrosing ILD (39). The expression levels of *Ccl2*, which chemoattracts circulating monocytes, were 20- and 5-fold higher on days 3 and 14, respectively, than in saline-instilled mice. The expression of *Tnfa*, which activates macrophages, was slightly increased throughout the disease. Fibroblast growth factor genes, including *Tgfb*, *Pdgfa*, and *Pdgfb*, were also examined. High expression levels of *Tgfb* were continuously observed throughout BLM-ILD. On the other hand, significantly high expression levels of *Pdgfa* were detected in the early phase, whereas those in the late phase were similar to those in the control lung. We found no significant increase in *Pdgfb* expression in the early phase and only a slight increase in the late phase. Therefore, AEC2 in BLM-ILD lungs expressed various SASP-related genes, including mediators to promote and transmit senescence and to activate monocytes/macrophages or fibroblasts with temporal differences in the magnitude of each component, suggesting the contribution of senescent AEC2 to the initiation and progression of BLM-ILD in different context-dependent manners.

Cytokines and chemokines derived from senescent AEC2 contribute to the initiation of lung fibrosis in BLM-ILD

Activated macrophages play a critical role in the development of lung fibrosis (39). $Ly6C^+$ monocytes, which are derived from the circulation and express CCR2, migrate to inflamed tissue through the CCL2–CCR2 interaction (40, 41). As shown in Figures 5A, C, $Ly6C^+$ monocytes immediately increased in the lungs by approximately threefold within 24 h of the BLM instillation, whereas the frequency of $Ly6C^+$ monocytes ($CD45^+CD11b^+MHCII^-Ly6C^+$) gradually decreased after day 3. The dynamics of monocyte migration appeared to correlate with the expression of *Ccl2* by AEC2 (Figures 4C, 5C). Furthermore, we found that interstitial macrophages ($CD45^+CD11b^+MHCII^+CD64^+$) increased from day 3, which was after monocyte migration (Figures 5B, D). Since $Ly6C^+$ monocytes differentiate into activated interstitial macrophages that express MHCII under proinflammatory cytokines, including TNFα (42), TNFα produced by senescent AEC2 may have contributed to the increase in interstitial macrophages.

The expression of *Acta2*, encoding α-smooth muscle actin, and *Col1a1*, encoding pro-α1 chains of type I collagen, was increased as early as day 3, indicating that the activation of fibroblasts and production of collagen had already been initiated as early as day 3 (Figures 6A, B). Therefore, the production of TGFβ and PDGFa by senescent AEC2 in the early phase (Figure 4C) may directly promote the activation of fibroblasts and resultant collagen production from the early phase of BLM-ILD.

Discussion

In this study, we examined the dynamics of the emergence of senescent cells and the characteristics of SASP during the progression of murine BLM-ILD to clarify how cellular senescence and SASP are involved in the pathogenesis of fibrosing ILD. We found that the $p21^{WAF1/CIP1}$ protein was induced in AEC2 as early as day 1 post-BLM instillation, and that $p21^{WAF1/CIP1}$-expressing AEC2 gradually increased and persisted until the later fibrosis phase in BLM-ILD. Its mRNA *Cdkn1a* was transiently and highly expressed in the early phase and then decreased to a certain level that was maintained until the later phase. This initial $p21^{WAF1/CIP1}$-dependent senescence in AEC2 was speculated to be attributed to BLM-induced DNA damage through the activated p53-$p21^{WAF1/CIP1}$ pathway, as previously demonstrated (30). This is consistent with the observation of γ-H2AX expression in a subset of AEC2 in the early phase. AEC2 also expressed another senescent marker, $p16^{INK4A}$, which was expressed as early as day 1 in a small number of AEC2, and increases in $p16^{INK4A+}$ AEC2 numbers were slower and milder than those in $p21^{WAF1/CIP1+}$ AEC2, suggesting that $p16^{INK4A}$-dependent senescence in AEC2 was affected not only by the direct effects of BLM, but also by alterations in the tissue microenvironment caused by inflammatory cell infiltration and the resultant inflammation, apoptosis, and senescence themselves. AEC2 sorted from BLM-ILD lungs in the early phase expressed various inflammatory or profibrotic genes associated with SASP, including *Il6*, *Tnfa*, *Ccl2*, *Serpin1*, *Tgfb*, and *Pdgfa*. We speculated that these inflammatory mediators contributed to the initiation and progression of the disease: IL-6, PAI-1 encoded by *Serpin1*, and TGFβ promoted senescent cells and/or amplified senescence; CCL2 attracted circulating $Ly6C^+$ monocytes into the lungs; and infiltrated $Ly6C^+$ monocytes were activated by TNFα and differentiated into MHCII-expressing interstitial macrophages. The activation of fibroblasts, as shown by early increases in *Acta2* and *Col1a* immediately upon the BLM instillation, may reflect the

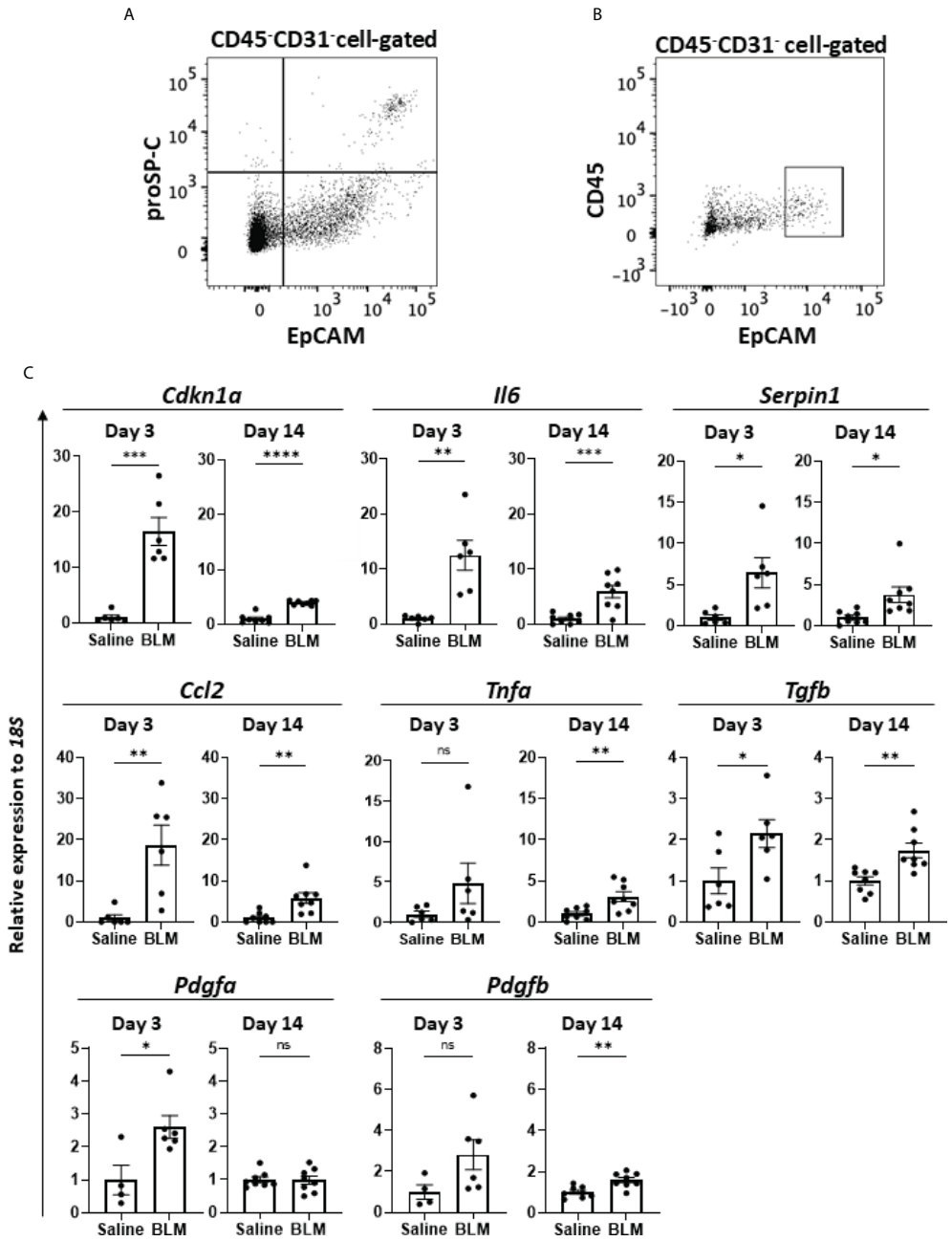

FIGURE 4
SASP-acquired AEC2 express multiple inflammatory mediators in BLM-ILD lungs. A cell suspension was obtained from the lungs of mice 14 days after the instillation of BLM and stained with fluorochrome-conjugated antibodies for a flow cytometric analysis. **(A)** After surface staining with monoclonal antibodies (mAbs) for CD31, CD45, and EpCAM, intracellular staining with an anti-proSP-C polyclonal antibody and Alexa-Fluor 555-conjugated secondary antibody was performed. **(B)** Gating of the CD45-CD31-EpCAMhi cell population sorted as AEC2. **(C)** Relative expression of the indicated SASP-related genes in sorted CD45-CD31-EpCAMhi cells from BLM-ILD lungs 3 and 14 days after the instillation of BLM. n = 6 on day 3; n = 8 on day 14. Data are presented as the mean ± SEM. Statistics show p-values from the unpaired t-test. ns, not significant. *p < 0.05; **p < 0.01; ***p < 0.001; ****p < 0.0001.

production of TGFβ and PDGFa by senescent AEC2 in the early phase.

Several studies have suggested pathological roles for cellular senescence in fibrosing ILD. However, most studies were performed using *in vitro* or *ex vivo* experiments in the chronic phase of fibrosis in human IPF lung samples. Furthermore, only senescent cells and/or SASP in the later phase of fibrosis were investigated in most *in vivo* animal studies, including those involving the depletion of

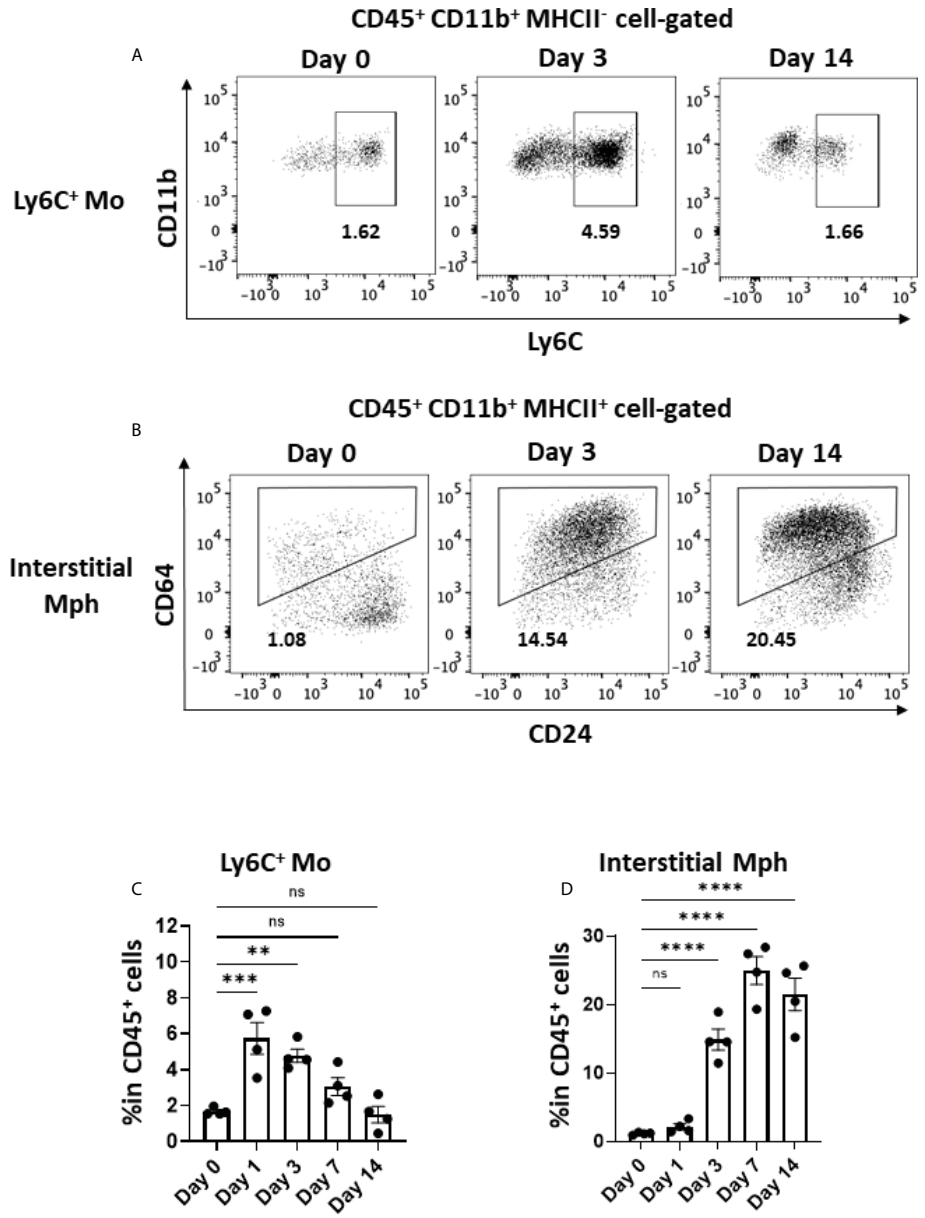

FIGURE 5
Monocyte migration and accumulated interstitial macrophages in the early phase in BLM-ILD. A lung cell suspension was obtained from mice before and 3 and 14 days after the instillation of BLM and stained with fluorochrome-conjugated antibodies for CD45, CD11b, I-Ab CD24, and CD64. **(A, B)** Representative cytograms showing Ly6C+ monocytes (Mo) **(A)** and interstitial macrophages (Mph) **(B)** on the indicated days. The number indicates the percentage in CD45+ cells. **(C, D)** Frequencies of Ly6C+ monocytes **(C)** and interstitial macrophages **(D)** in CD45+ cells in the lungs from pooled mice. n = 4 per day. Data are presented as the mean ± SEM. Statistics show p-values from a one-way ANOVA with Dunnett's multiple comparisons test as the post-hoc test comparing values on day 0. ns, not significant. **p < 0.01; ***p < 0.001; ****p < 0.0001.

senescent cells using genetically mutated mice or senolytics (31). Therefore, it is important to note that our study demonstrated that $p21^{WAF1/CIP1}$- and p16-dependent senescent cells were involved in both the initiation and progression of chronic fibrosis by clarifying the dynamics of the accumulation of senescent cells dependent on both pathways.

The $p21^{WAF1/CIP1}$ protein was expressed in a large number of AEC2 as early as 1 day after the BLM instillation. DNA damage by BLM activates the p53-$p21^{WAF1/CIP1}$ pathway. If DNA is normally repaired, the replication ability of cells is restored; otherwise, cells undergo senescence or apoptosis (43). We found a divergence in dynamics between the $p21^{WAF1/CIP1}$ protein and

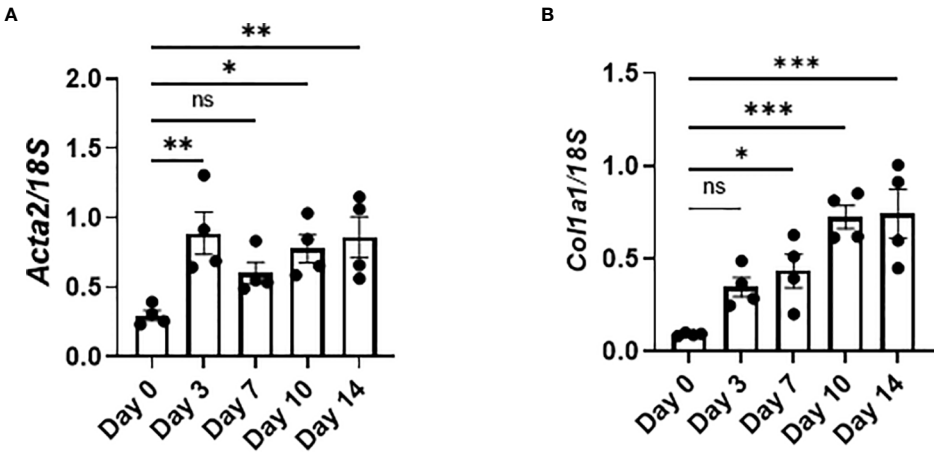

FIGURE 6
Activated fibroblasts produce collagen from the early phase in BLM-ILD. Lungs were obtained before and 3, 7, 10, and 14 days after the BLM instillation and subjected to qRT-PCR. The expression of Col1a1 **(A)** and Acta2 **(B)** in the lungs on the indicated days. n = 4 per day. Data are presented as the mean ± SEM. Statistics show p-values from a one-way ANOVA with Dunnett's multiple comparisons test as the post-hoc test comparing values on day 0. ns, not significant. *p < 0.05; **p < 0.01; ***p < 0.001.

its gene expression: with higher levels in the early phase, its gene expression decreased and was maintained at a certain level in the later phase, whereas its protein expression, with lower levels in the early phase, gradually increased as fibrosis progressed. After the onset of DNA damage by BLM and the resultant induction of $p21^{WAF1/CIP1}$, DNA was repaired and $p21^{WAF1/CIP1}$ expression was suppressed in some AEC2. However, DNA damage was not repaired and $p21^{WAF1/CIP1}$ expression persisted in other AEC2, leading to the induction of senescence. Moreover, the $p21^{WAF1/CIP1}$ protein was stabilized post-transcriptionally (44). We speculated that the divergence of the accumulation of the $p21^{WAF1/CIP1}$ protein and the lower expression of *Cdkn1a* in the late stage is attributed to the post-transcriptional regulation of $p21^{WAF1/CIP1}$.

The mechanisms by which senescent AEC2 persisted and increased after the initial stimulus with BLM are unclear. We observed high expression levels of the canonical SASP factors IL-6 and PAI-1 in AEC2 both in the early and late phases of BLM-ILD. Since IL-6 has been reported to promote senescence through the activation of NF-κB in an autocrine manner (16), the BLM-induced senescence of AEC2 may persist by self-produced IL-6. Another canonical SASP factor, PAI-1, was shown to activate the p52-$p21^{WAF1/CIP1}$ pathway and promote the senescence of AEC2 in both autocrine and paracrine manners (37, 38). TGFβ, which was detected in AEC2 from the early phase and throughout the progression of BLM-ILD in this study, has also been reported to induce the senescence of neighboring cells in a paracrine manner (16). Therefore, the persistent expression of IL-6, PAI-1, and TGFβ may amplify senescence across lung tissue by reinforcing senescence, inducing senescence in other cells, and contributing to the accumulation of $p21^{WAF1/CIP1}$-dependent and $p16^{INK4A}$-dependent senescent cells from the early phase throughout BLM-ILD. Therefore, inhibitors of senescent cells and SASP-related mediators have potential as a treatment for ILD.

The present study has several limitations. Although 85% of sorted $EpCAM^{hi}$ cells expressed proSP-C indicating AEC2, SASP-related mediators expressed in $EpCAM^{hi}$ cells may be influenced by those produced by contaminated type 1 AEC. In addition, apoptotic cells produce proinflammatory cytokines, such as IL-1β and TNFα, which overlap with SASP-related cytokines. Therefore, the extent to which apoptotic AEC2 contributed to the expression of some mediators produced by senescent AEC2 in the early phase remains unclear. However, since apoptotic cells do not produce IL-6 (45, 46), most of this cytokine was considered to be derived from senescent AEC2. Another point is that we found differences in the magnitude and components of SASP between the early and late phases of BLM-ILD by examining several genes of SASP-related mediators expressed in AEC2. However, it is important to perform comprehensive analyses of SASP-related mediators expressed in senescent AEC2, such as a single-cell analysis, to understand their roles in diseases and to identify therapeutic targets. Loss-of-function experiments, such as the depletion of $p21^{WAF1/CIP1}$-dependent senescent AEC2 or the inhibition of SASP-related mediators, are required to demonstrate that the accumulation of interstitial macrophages and the initiation of fibrosis at early time points are dependent on the senescence of AEC2.

In summary, we demonstrated that $p21^{WAF1/CIP1}$-dependent and $p16^{INK4A}$-dependent senescent cells emerged from the

initiation phase with different dynamics and persisted during the fibrosis phase in murine BLM-ILD. We also showed that SASP-related genes derived from AEC2 were expressed at different magnitudes in the early phase and later fibrosis phase. These results may contribute to a better understanding of the mechanisms involved in cellular senescence as well as useful information for the development of senescent cell- or SASP mediator-targeted therapy.

Materials and methods

Mice

Male C57BL/6J mice aged 5–6 weeks were purchased from CLEA Japan Inc. (Tokyo, Japan) and maintained at the animal facility of Toho University. Mice were randomly assigned by a third party and housed in plastic cages (n = 3–4 mice per cage) with *ad libitum* water and food under controlled temperature and humidity with a 12-h light/dark cycle. They were housed for 2 to 3 weeks to acclimate them to the environment after shipping. All experimental procedures were conducted in the SPF animal laboratory of Toho University. Animal experiments were performed according to the animal experiment guidelines approved by Toho University Animal Experiment User Committee (Approval numbers: 19-41-432, 20-42-432 and 21-43-432).

BLM-ILD

Male C57BL/6J mice aged 8–10 weeks were intratracheally instilled with 80 µl of saline containing 3.2 mg/kg body weight of bleomycin sulfate (Nippon Kayaku Co., Ltd., UK) to induce BLM-ILD or 80 µl of saline alone as the control. Mice were anesthetized with an intraperitoneal injection of 0.75 mg/kg of medetomidine (Nippon Zenyaku Kogyo, Fukushima, Japan), 4.0 mg/kg of midazolam (Sandoz, Tokyo, Japan), and 5.0 mg/kg of vetorphale (Meiji Seika Pharma, Tokyo, Japan) before the procedure, and medetomidine was antagonized by a peritoneal injection of 0.75 mg/kg of atipamezole (Nippon Zenyaku Kogyo, Fukushima, Japan) after the procedure. The lungs were dissected under the anesthesia described above before or on day 1, 3, 7, 10, or 14 after the administration of BLM.

Histological procedure

Lung tissue was fixed with 4% paraformaldehyde and embedded in paraffin. Sections with a thickness of 3 µm were used for HE, MT, and immunohistochemical staining. In the immunohistochemical analysis, sections were deparaffinized and antigen retrieval was performed in antigen retrieval buffer pH 9 (Nichirei Biochemicals Inc., Tokyo, Japan) using a pressure cooker. After the inactivation of endogenous peroxidase activity with 3% H_2O_2 for 5 min and subsequent blocking for 30 min, sections were stained with primary antibodies. Information on primary antibodies and horseradish peroxidase-conjugated secondary antibodies are listed with incubation times and dilutions in Supplementary Table 2. Histological images of HE or MT staining and immunohistochemical analyses were captured using a BX-63 microscope (Olympus, Tokyo, Japan). Immunofluorescence images were captured using a Nikon ECLIPSE Ti2 Microscope (Nikon, Tokyo, Japan) with the Andor DragonFly Spinning Disk Confocal System (Oxford Instruments, Abington, UK).

Quantitative histological analysis

An image of the total left lobe area with MT and immunohistochemical staining was divided into grid areas of 240 × 360 µm and 120 × 180 µm, respectively. Pulmonary fibrosis was scored in 20 randomly selected grid areas (240 × 360 µm) by the Ashcroft scale (47) using MT-stained slides, and the average score of each section was calculated. Regarding the quantification of collagen, the MT-stained area and total area of 20 randomly selected grid areas (120 × 180 µm) were measured by ImageJ (NIH, USA) and the average of the percentage of MT areas in the total area was calculated. To quantify $p21^{WAF1/CIP1+}$ AEC2 cells in immunofluorescent images, cells were counted in 20 randomly selected areas (300 × 300 µm).

Flow cytometric analysis and sorting

Lungs were cut into fine pieces (1 mm^3) in RPMI1640 containing 2.5 mg/ml collagenase (FUJIFILM Wako Pure Chemical Corporation, Osaka, Japan), 1 mg/ml of dispase II (Roche, Basel Switzerland), and 0.02 mg/ml of DNase I (Millipore, Barrington, USA). The cell suspension was incubated at 37°C for 21 min with pipetting every 7 min and passed through a 70-µm cell strainer. After washing, red blood cells were lysed and Fc receptors were blocked. Cells were stained with fluorescence-conjugated monoclonal antibodies for surface molecules shown in Supplementary Table 3 and incubated on ice for 15 min. After washing, cells were ready for the flow cytometric analysis of surface molecules. Regarding staining with prosurfactant protein C (proSP-C), cells were further fixed and permeabilized with eBioscience Intracellular Fixation/Permeabilization buffer (Thermo Fisher Scientific, Waltham, USA), and then stained with anti-proSP-C polyclonal Ab (pAb) (Abcam, Cambridge, UK) followed by staining with Alexa Fluor 555-conjugated anti-rabbit pAb (Abcam). The flow cytometric analysis was performed using BD LSRFortessa TM (BD Biosciences, San Jose, USA), and

data analyses were conducted using FlowJo software ver. 10.7.1 (BD Biosciences). BD FACS Aria™ III (BD Biosciences) was used for flow cytometric sorting.

Quantitative RT-PCR

Dissected lungs were soaked in RNA Protect Tissue Reagent (QIAGEN, Hilden, Germany) at 4°C for a few days and subsequently stored at −80°C until the extraction of RNA. Frozen lung tissue immersed in RNA extraction buffer RA1 from NucleoSpin RNA (TAKARA) was homogenized using TissueLyser LT (QIAGEN) and total RNA was extracted following the manufacturer's protocol. Sorted cells were lysed after adding Trizol LS (Thermo Fisher Scientific) and total RNA was extracted according to the manufacturer's protocol. Total RNA was reverse-transcribed using the PrimeScript™ RT reagent Kit with the gDNA Eraser (TAKARA) following the manufacturer's protocol. qRT-PCR was performed on QuantStudio 3 (Thermo Fisher Scientific) using TB Green® *Premix Ex Taq*™ II (TAKARA) and values were normalized to the expression of *18S* ribosomal RNA. Primer sequences are listed in Supplementary Table 4.

Statistical analysis

Statistical analyses were performed using Prism ver. 7.0 software (GraphPad Software, San Diego, USA). A one-way ANOVA was used for multiple-group comparisons. Dunnett's multiple comparison test was employed as a post-hoc test. An unpaired *t*-test was used for two-group comparisons. *p*-values less than 0.05 were considered to be significant. All data were expressed as the mean ± standard error of the mean (SEM).

Data availability statement

The raw data supporting the conclusions of this article will be made available by the authors, without undue reservation.

Ethics statement

The animal study was reviewed and approved by Toho University Animal Care and User Committee.

Author contributions

ZY, JN, and TN contributed to conception and design of the study. ZY, KM, SM, SY and TM performed experiments. ZY, JN, and KM performed the statistical analysis. ZY, JN, and TN wrote the manuscript. All authors contributed to manuscript revision, read, and approved the submitted version.

Funding

This work was supported in part by Japan Society for the Promotion of Science (18K07166 and 21K08482); the Private University Research Branding Project from the Ministry of Education, Culture, Sports, Science, and Technology, Japan; the Science Research Promotion Fund from the Promotion and Mutual Aid Corporation for Private Schools of Japan; Takeda Science Foundation; Research Promotion Grant from the Toho University Graduate School of Medicine (17-01, 20-01); and Project Research Grant from the Toho University School of Medicine (20-20).

Acknowledgments

We thank Kanoh Kondo at the Division of Rheumatology, Department of Internal Medicine, Toho University School of Medicine and Yuichi Tsuchiya at the Department of Biochemistry, Toho University School of Medicine for their technical advice on the immunohistological analysis; Tatsuya Tsukui at the Lung Biology Center, Department of Medicine, University of California for his technical advice on the isolation of mouse lung cells; and Marii Ise at the Department of Molecular Immunology, Toho University for her assistance with the flow cytometric analysis and flow cytometric cell sorting.

Conflict of interest

The authors declare that the research was conducted in the absence of any commercial or financial relationships that could be construed as a potential conflict of interest.

Publisher's note

Supplementary material

The Supplementary Material for this article can be found online at: https://www.frontiersin.org/articles/10.3389/fimmu.2022.935114/full#supplementary-material

References

1. Wuyts WA, Agostini C, Antoniou KM, Bouros D, Chambers RC, Cottin V, et al. The pathogenesis of pulmonary fibrosis: A moving target. *Eur Respir J* (2013) 41(5):1207–18. doi: 10.1183/09031936.00073012

2. Bignold R, Johnson JR. Effects of cytokine signaling inhibition on inflammation-driven tissue remodeling. *Curr Res Pharmacol Drug Discov* (2021) 2:100023. doi: 10.1016/j.crphar.2021.100023

3. Baumgartner KB, Samet JM, Stidley CA, Colby TV, Waldron JA. Cigarette smoking: A risk factor for idiopathic pulmonary fibrosis. *Am J Respir Crit Care Med* (1997) 155(1):242–8. doi: 10.1164/ajrccm.155.1.9001319

4. Li N, Shi F, Wang X, Yang P, Sun K, Zhang L, et al. Silica dust exposure induces pulmonary fibrosis through autophagy signaling. *Environ Toxicol* (2021) 36(7):1269–77. doi: 10.1002/tox.23124

5. Maitra M, Wang Y, Gerard RD, Mendelson CR, Garcia CK. Surfactant protein A2 mutations associated with pulmonary fibrosis lead to protein instability and endoplasmic reticulum stress. *J Biol Chem* (2010) 285(29):22103–13. doi: 10.1074/jbc.M110.121467

6. Armanios MY, Chen JJ, Cogan JD, Alder JK, Ingersoll RG, Markin C, et al. Telomerase mutations in families with idiopathic pulmonary fibrosis. *N Engl J Med* (2007) 356(13):1317–26. doi: 10.1056/NEJMoa066157

7. Seibold MA, Wise AL, Speer MC, Steele MP, Brown KK, Loyd JE, et al. A common Muc5b promoter polymorphism and pulmonary fibrosis. *N Engl J Med* (2011) 364(16):1503–12. doi: 10.1056/NEJMoa1013660

8. Zhang Y, Noth I, Garcia JG, Kaminski N. A variant in the promoter of Muc5b and idiopathic pulmonary fibrosis. *New Engl J Med* (2011) 364(16):1576–7. doi: 10.1056/NEJMc1013504

9. Spagnolo P, Distler O, Ryerson CJ, Tzouvelekis A, Lee JS, Bonella F, et al. Mechanisms of progressive fibrosis in connective tissue disease (Ctd)-associated interstitial lung diseases (Ilds). *Ann Rheumatic Dis* (2021) 80(2):143–50. doi: 10.1136/annrheumdis-2020-217230

10. Katzen J, Beers MF. Contributions of alveolar epithelial cell quality control to pulmonary fibrosis. *J Clin Invest* (2020) 130(10):5088–99. doi: 10.1172/JCI139519

11. Munoz-Espin D, Serrano M. Cellular senescence: From physiology to pathology. *Nat Rev Mol Cell Biol* (2014) 15(7):482–96. doi: 10.1038/nrm3823

12. Gonzalez-Meljem JM, Apps JR, Fraser HC, Martinez-Barbera JP. Paracrine roles of cellular senescence in promoting tumourigenesis. *Br J Cancer* (2018) 118 (10):1283–8. doi: 10.1038/s41416-018-0066-1

13. Kumari R, Jat P. Mechanisms of cellular senescence: Cell cycle arrest and senescence associated secretory phenotype. *Front Cell Dev Biol* (2021) 9:645593. doi: 10.3389/fcell.2021.645593

14. Herranz N, Gil J. Mechanisms and functions of cellular senescence. *J Clin Invest* (2018) 128(4):1238–46. doi: 10.1172/JCI95148

15. Gonzalez-Gualda E, Baker AG, Fruk L, Munoz-Espin D. A guide to assessing cellular senescence in vitro and in vivo. *FEBS J* (2020) 288(1):56–80. doi: 10.1111/febs.15570

16. Acosta JC, Banito A, Wuestefeld T, Georgilis A, Janich P, Morton JP, et al. A complex secretory program orchestrated by the inflammasome controls paracrine senescence. *Nat Cell Biol* (2013) 15(8):978–90. doi: 10.1038/ncb2784

17. Childs BG, Gluscevic M, Baker DJ, Laberge RM, Marquess D, Dananberg J, et al. Senescent cells: An emerging target for diseases of ageing. *Nat Rev* (2017) 16 (10):718–35. doi: 10.1038/nrd.2017.116

18. Childs BG, Baker DJ, Wijshake T, Conover CA, Campisi J, van Deursen JM. Senescent intimal foam cells are deleterious at all stages of atherosclerosis. *Sci (New York NY* (2016) 354(6311):472–7. doi: 10.1126/science.aaf6659

19. Farr JN, Xu M, Weivoda MM, Monroe DG, Fraser DG, Onken JL, et al. Targeting cellular senescence prevents age-related bone loss in mice. *Nat Med* (2017) 23(9):1072–9. doi: 10.1038/nm.4385

20. Ogrodnik M, Zhu Y, Langhi LGP, Tchkonia T, Kruger P, Fielder E, et al. Obesity-induced cellular senescence drives anxiety and impairs neurogenesis. *Cell Metab* (2019) 29(5):1061–77.e8. doi: 10.1016/j.cmet.2018.12.008

21. Bussian TJ, Aziz A, Meyer CF, Swenson BL, van Deursen JM, Baker DJ. Clearance of senescent glial cells prevents tau-dependent pathology and cognitive decline. *Nature* (2018) 562(7728):578–82. doi: 10.1038/s41586-018-0543-y

22. Kuwano K, Kunitake R, Kawasaki M, Nomoto Y, Hagimoto N, Nakanishi Y, et al. P21waf1/Cip1/Sdi1 and P53 expression in association with DNA strand breaks in idiopathic pulmonary fibrosis. *Am J Respir Crit Care Med* (1996) 154(2 Pt 1):477–83. doi: 10.1164/ajrccm.154.2.8756825

23. Minagawa S, Araya J, Numata T, Nojiri S, Hara H, Yumino Y, et al. Accelerated epithelial cell senescence in ipf and the inhibitory role of Sirt6 in tgf-Beta-Induced senescence of human bronchial epithelial cells. *Am J Physiol* (2011) 300(3):L391–401. doi: 10.1152/ajplung.00097.2010

24. Alvarez D, Cardenes N, Sellares J, Bueno M, Corey C, Hanumanthu VS, et al. Ipf lung fibroblasts have a senescent phenotype. *Am J Physiol* (2017) 313(6): L1164–73. doi: 10.1152/ajplung.00220.2017

25. Lomas NJ, Watts KL, Akram KM, Forsyth NR, Spiteri MA. Idiopathic pulmonary fibrosis: Immunohistochemical analysis provides fresh insights into lung tissue remodelling with implications for novel prognostic markers. *Int J Clin Exp Pathol* (2012) 5(1):58–71.

26. Disayabutr S, Kim EK, Cha SI, Green G, Naikawadi RP, Jones KD, et al. Mir-34 mirnas regulate cellular senescence in type ii alveolar epithelial cells of patients with idiopathic pulmonary fibrosis. *PloS One* (2016) 11(6):e0158367. doi: 10.1371/journal.pone.0158367

27. Lehmann M, Korfei M, Mutze K, Klee S, Skronska-Wasek W, Alsafadi HN, et al. Senolytic drugs target alveolar epithelial cell function and attenuate experimental lung fibrosis ex vivo. *Eur Respir J* (2017) 50(2):1602367. doi: 10.1183/13993003.02367-2016

28. Waters DW, Blokland KEC, Pathinayake PS, Burgess JK, Mutsaers SE, Prele CM, et al. Fibroblast senescence in the pathology of idiopathic pulmonary fibrosis. *Am J Physiol* (2018) 315(2):L162–72. doi: 10.1152/ajplung.00037.2018

29. Aoshiba K, Tsuji T, Nagai A. Bleomycin induces cellular senescence in alveolar epithelial cells. *Eur Respir J* (2003) 22(3):436–43. doi: 10.1183/09031936.03.00011903

30. Aoshiba K, Tsuji T, Kameyama S, Itoh M, Semba S, Yamaguchi K, et al. Senescence-associated secretory phenotype in a mouse model of bleomycin-induced lung injury. *Exp Toxicol Pathol* (2013) 65(7-8):1053–62. doi: 10.1016/j.etp.2013.04.001

31. Schafer MJ, White TA, Iijima K, Haak AJ, Ligresti G, Atkinson EJ, et al. Cellular senescence mediates fibrotic pulmonary disease. *Nat Commun* (2017) 8:14532. doi: 10.1038/ncomms14532

32. Tian Y, Li H, Qiu T, Dai J, Zhang Y, Chen J, et al. Loss of pten induces lung fibrosis *Via* alveolar epithelial cell senescence depending on nf-kappab activation. *Aging Cell* (2019) 18(1):e12858. doi: 10.1111/acel.12858

33. Muthuramalingam K, Cho M, Kim Y. Cellular senescence and emt crosstalk in bleomycin-induced pathogenesis of pulmonary fibrosis-an in vitro analysis. *Cell Biol Int* (2020) 44(2):477–87. doi: 10.1002/cbin.11248

34. Petrova NV, Velichko AK, Razin SV, Kantidze OL. Small molecule compounds that induce cellular senescence. *Aging Cell* (2016) 15(6):999–1017. doi: 10.1111/acel.12518

35. Hubner RH, Gitter W, El Mokhtari NE, Mathiak M, Both M, Bolte H, et al. Standardized quantification of pulmonary fibrosis in histological samples. *BioTechniques* (2008) 44(4):507–11, 14-7. doi: 10.2144/000112729

36. Kirkland JL, Tchkonia T. Senolytic drugs: From discovery to translation. *J Internal Med* (2020) 288(5):518–36. doi: 10.1111/joim.13141

37. Jiang C, Liu G, Luckhardt T, Antony V, Zhou Y, Carter AB, et al. Serpine 1 induces alveolar type ii cell senescence through activating P53-P21-Rb pathway in fibrotic lung disease. *Aging Cell* (2017) 16(5):1114–24. doi: 10.1111/acel.12643

38. Kortlever RM, Higgins PJ, Bernards R. Plasminogen activator inhibitor-1 is a critical downstream target of P53 in the induction of replicative senescence. *Nat Cell Biol* (2006) 8(8):877–84. doi: 10.1038/ncb1448

39. Wynn TA. Integrating mechanisms of pulmonary fibrosis. *J Exp Med* (2011) 208(7):1339–50. doi: 10.1084/jem.20110551

40. Hashimoto M, Asai A, Kawagishi H, Mikawa R, Iwashita Y, Kanayama K, et al. Elimination of P19(Arf)-expressing cells enhances pulmonary function in mice. *JCI Insight* (2016) 1(12):e87732. doi: 10.1172/jci.insight.87732

41. Shi T, Denney L, An H, Ho LP, Zheng Y. Alveolar and lung interstitial macrophages: Definitions, functions, and roles in lung fibrosis. *J Leukoc Biol* (2021) 110(1):107–14. doi: 10.1002/JLB.3RU0720-418R

42. Smigiel KS, Parks WC. Macrophages, wound healing, and fibrosis: Recent insights. *Curr Rheumatol Rep* (2018) 20(4):17. doi: 10.1007/s11926-018-0725-5

43. Georgakilas AG, Martin OA, Bonner WM. P21: A two-faced genome guardian. *Trends Mol Med* (2017) 23(4):310–9. doi: 10.1016/j.molmed.2017.02.001

44. Jascur T, Brickner H, Salles-Passador I, Barbier V, El Khissiin A, Smith B, et al. Regulation of P21(Waf1/Cip1) stability by Wisp39, a Hsp90 binding tpr protein. *Mol Cell* (2005) 17(2):237–49. doi: 10.1016/j.molcel.2004.11.049

45. Place DE, Kanneganti TD. Cell death-mediated cytokine release and its therapeutic implications. *J Exp Med* (2019) 216(7):1474–86. doi: 10.1084/jem.20181892

46. Vanden Berghe T, Kalai M, Denecker G, Meeus A, Saelens X, Vandenabeele P. Necrosis is associated with il-6 production but apoptosis is not. *Cell signalling* (2006) 18(3):328–35. doi: 10.1016/j.cellsig.2005.05.003

47. Ashcroft T, Simpson JM, Timbrell V. Simple method of estimating severity of pulmonary fibrosis on a numerical scale. *J Clin Pathol* (1988) 41(4):467–70. doi: 10.1136/jcp.41.4.467

Frontiers in Immunology

Explores novel approaches and diagnoses to treat immune disorders.

The official journal of the International Union of Immunological Societies (IUIS) and the most cited in its field, leading the way for research across basic, translational and clinical immunology.

Discover the latest Research Topics

See more →

Frontiers

Avenue du Tribunal-Fédéral 34
1005 Lausanne, Switzerland
frontiersin.org

Contact us

+41 (0)21 510 17 00
frontiersin.org/about/contact